

DOUTORAMENTO
CIÊNCIAS BIOMÉDICAS

Bioprinting of cell-responsive bioinks for skin tissue engineering

Rúben Filipe Pereira

D
2018



**Bioprinting of cell-responsive
bioinks for skin tissue engineering**
Rúben Filipe Pereira



Rúben Filipe Brás Pereira

Bioprinting of cell-responsive bioinks for skin tissue engineering

Tese de Candidatura ao grau de Doutor em Ciências Biomédicas submetida ao Instituto de Ciências Biomédicas Abel Salazar da Universidade do Porto

Orientador:

Professor Doutor Paulo Jorge da Silva Bártolo

Categoria – Professor Catedrático

Afiliação – School of Mechanical, Aerospace and Civil Engineering & Manchester Institute of Biotechnology, University of Manchester

Co-orientador:

Doutor Pedro Lopes Granja

Categoria – Investigador Principal/Professor Associado

Afiliação – i3S - Instituto de Investigação e Inovação em Saúde, INEB - Instituto de Engenharia Biomédica & ICBAS - Instituto de Ciências Biomédicas Abel Salazar, Universidade do Porto

Aos meus pais.

The work presented in this thesis was developed at:

Biomaterials for Multistage Drug & Cell Delivery Group
i3S - Instituto de Investigação e Inovação em Saúde and
INEB - Instituto de Engenharia Biomédica
Universidade do Porto, Porto, Portugal
Rua Alfredo Allen, 208
4200-135 Porto, Portugal
www.i3s.up.pt | www.ineb.up.pt



Financial Support

Rúben Filipe Brás Pereira was supported by a PhD grant (SFRH/BD/91151/2012) from Fundação para a Ciência e Tecnologia (FCT).

This work was financed by FEDER - Fundo Europeu de Desenvolvimento Regional funds through the COMPETE 2020 - Operational Programme for Competitiveness and Internationalisation (POCI), Portugal 2020, and by Portuguese funds through FCT/Ministério da Ciência, Tecnologia e Inovação in the framework of the project " In situ skin tissue engineering" (Ref. PTDC/BBB-ECT/2145/2014).



ACKNOWLEDGEMENTS

Após quatro anos de intensa dedicação, por vezes exclusiva, à realização deste trabalho de investigação chegou o momento de expressar os meus mais sinceros agradecimentos a todos aqueles que sempre me apoiaram, encorajaram e incentivaram durante este percurso. Apesar de, na grande maioria dos momentos, não ter sido um percurso fácil, todos vocês de uma forma ou de outra, contribuíram para que este momento se torne uma realidade.

As minhas primeiras palavras vão para o meu orientador, o professor Paulo Bárto. Todas as palavras são poucas para expressar a minha gratidão por sempre ter acreditado em mim desde o momento que me recebeu no CDRSP em 2009. Ao longo destes nove anos sempre me proporcionou as condições necessárias para evoluir cientificamente e me deu total liberdade para expor e colocar em prática as minhas ideias, mesmo aquelas que estavam desde logo destinadas ao insucesso. Admiro-o muito pela sua capacidade de trabalho incansável, persistência, visão e capacidade de liderança. Um sentido agradecimento pela amizade e por sempre me ter apoiado e incentivado ao longo deste percurso.

Agradeço também ao meu co-orientador, o professor Pedro Granja, por me ter recebido no INEB e me ter proporcionado a possibilidade de realizar este trabalho de investigação no seu laboratório. A forma como me recebeu e sempre me fez sentir em casa tornou tudo mais fácil. O entusiasmo que sempre me transmitiu e a confiança que em mim depositou desde cedo foram também fundamentais para este percurso. Agradeço a amizade, o companheirismo e a oportunidade que me concedeu para participar na implementação de uma nova área de investigação. A sua resiliência, determinação e força de vontade são para mim um exemplo.

À professora Cristina Barrias quero agradecer por sempre me ter recebido para as nossas discussões de trabalho e por ter estado sempre disponível desde o primeiro momento. A sua visão crítica foi, sem dúvida, uma importante ajuda neste trabalho.

Não posso deixar de agradecer à professora Ausenda Mendes por toda a amizade, apoio e incentivo desde os tempos de licenciatura. Obrigado por sempre acreditar em mim e me encorajar a evoluir.

ACKNOWLEDGEMENTS

À professora Daniela Vaz um agradecimento pelo companheirismo e apoio mesmo à distância ao longo destes últimos anos.

Obrigado à Mariana Andrade do Centro de Materiais da Universidade do Porto pela disponibilidade e apoio nas análises de ressonância magnética nuclear indispensáveis à realização deste trabalho. Agradeço também ao Frederico Silva do B2Tech (Biochemical and Biophysical Technologies) do i3S pela ajuda nas experiências de HPLC e explicações concedidas. Quero deixar também um agradecimento à Cláudia Machado do i3S pela disponibilidade e ajuda na histologia.

Agradeço também ao CDRSP, em particular ao professor Nuno Alves, por disponibilizar o equipamento de fotopolimerização essencial na realização deste trabalho.

Um agradecimento aos colegas e amigos do INEB por partilharem comigo muitos dos momentos passados no laboratório e fora dele. Um agradecimento especial à Ana Silva, Andreia Silva, Catarina Pereira, Daniela Vasconcelos, Estrela Neto, Flávia Castro e Vasco Pinto. Agradeço também à Filipa Lourenço por toda ajuda e apoio.

Quero agradecer em especial a todos os colegas e amigos do grupo Biocarrier pelas discussões científicas, ajuda nas experiências ou simplesmente pela pausa para café. Um agradecimento especial à Sílvia Bidarra pela ajuda nas experiências de zimografia, ao Tiago Santos pelos momentos descontraídos, à Filipa Sousa pela ajuda nas culturas celulares e ao Marco Araújo pelas discussões químicas. Uma palavra especial à Lu pela amizade, boa disposição e apoio ao longo desta etapa.

Não posso deixar de agradecer a todos os estudantes que comigo colaboraram por todas as discussões e bons momentos. Um agradecimento especial ao Bojidar Rangelov pelo companheirismo e trabalho produtivo – *Thanks Bojidar!*

Um obrigado especial aos “amigos das saídas”, Rui Ribeiro e Marta Ribeiro, pela amizade e pelos momentos descontraídos e bem passados. Ao José Teixeira um agradecimento pelo apoio e amizade.

Agradeço à minha amiga Maria João Gomes pelos momentos que partilhámos no laboratório e por toda amizade e apoio mesmo à distância.

Um agradecimento especial à querida Bianca por me ter recebido com um enorme sorriso desde o primeiro dia. Obrigado por acreditares em mim, pelo teu apoio, amizade e companheirismo incondicionais. A tua boa disposição e pensamento positivo foram e são fundamentais para ultrapassar os dias menos bons e aproveitar melhor os dias bons. Muito

obrigado pela companhia fora de horas, pela “AMP” e ajuda fundamentais para que este momento se concretize.

Por último mas não em último, agradeço à minha família que é o pilar de tudo.

Aos meus queridos pais, Carlos Pereira e Lurdes Brás, as palavras não chegam para expressar a minha gratidão por sempre estarem presentes e me apoiarem incondicionalmente nas minhas escolhas, mas fazendo sempre questão de darem os seus sábios conselhos. Muito obrigado pelos valores que sempre me transmitiram de união, companheirismo, humildade, amizade e amor. Muito obrigado por tudo.

Uma palavra especial para a minha família, Armando Reis, Rosa Pereira, José Pereira, Dulce Ferreira, Telmo Reis e Bruno Pereira por sempre me apoiarem.

ABSTRACT

The limited reparative capacity of the skin after injury and the drawbacks of current therapeutic approaches represent the major challenges in the treatment of cutaneous wounds. Despite the advances on the development of novel biomaterials for wound dressings and bioengineered skin substitutes, key limitations such as poor vascularization, delayed cell infiltration, scarring, and poor mechanical properties still persist. Bioprinting holds the promise to overcome these challenges by the automated deposition of material formulations loadable with cells and/or bioactive molecules, termed as bioinks, into multilayer three-dimensional (3D) skin constructs both *in vitro* and *in vivo*. Although several hydrogels have been adapted as bioinks, a major bottleneck in skin bioprinting is the limited number of bioinks exhibiting suitable printability, fast crosslinking and cell-instructive properties. Thus, the main aim of this doctoral thesis was to develop novel photocrosslinkable pectin hydrogels as cell-responsive bioinks for the extrusion bioprinting of cellularized 3D constructs for skin tissue engineering. Optimal bioink properties were based on the ability to print 3D constructs with high shape fidelity, supporting the functions of embedded cells, the deposition of extracellular matrix (ECM) components and the *in vitro* skin formation.

The first part of the work focused on the synthesis and formulation of a dual-crosslinked pectin hydrogel bioink for the bioprinting of dermal 3D constructs. Pectin was modified with methacrylate groups via reaction with methacrylic anhydride (MA) to form chemical hydrogels through ultraviolet (UV) photopolymerization. Pectin methacrylate (PECMA) with different degrees of modification (21.7–50.2 %) was synthesized without compromising the ionic gelation ability. A base-catalysed thiol-Michael addition reaction was applied to conjugate a thiolated cell-adhesive peptide (CGGGGRGDSP) to the methacrylate groups in pectin backbone, promoting the attachment of dermal fibroblasts embedded within the gel network. Suitable printability and rheological properties were obtained through the ionic gelation of a low concentration PECMA solution (1.5 wt%) using 5 mM calcium chloride. The physically crosslinked bioink loaded with dermal fibroblasts was printed into 3D constructs that supported viable and metabolically active cells throughout 14 days of culture, providing a suitable cell microenvironment that stimulated the deposition of dermal ECM components, including fibronectin and type-I collagen.

To develop bioinks with controllable cell-degradation properties, in the second part, novel photocrosslinkable pectin macromers were synthesized to form protease-degradable hydrogels through UV photoinitiated thiol-norbornene click chemistry. Pectin was firstly

ABSTRACT

converted to its tetrabutylammonium (TBA) salt for solubilization in dimethyl sulfoxide (DMSO) and then modified with carbic anhydride (CA), yielding norbornene-modified pectin (NorPEC). To mimic both cell-adhesion and cell-mediated remodelling properties of the skin, enzymatically-degradable hydrogels were formed by reaction between a peptide crosslinker sensitive to cell-secreted proteases (CGPQGIWGQC) flanked with biscysteine and the norbornene groups in pectin backbone upon exposure to UV light (20 s) in the presence of VA-086 as photoinitiator. The thiolated cell-adhesive peptide (CGGGGRGDSP) was also tethered to the norbornene groups during the photopolymerization, promoting the adhesion and spreading of embedded fibroblasts. Mechanical properties of hydrogels (2.5 wt%) were tailored in a broad range (70.03 ± 10.39 Pa to 446.75 ± 35.66 Pa) by varying the bulk concentration of the peptide crosslinker (4–6 mM). Fibroblasts embedded within these hydrogels displayed spread morphology and secreted matrix metalloproteinases (MMP-2 and MMP-9) involved in the cutaneous wound healing. Histological and immunofluorescence analysis showed the ability of the developed hydrogels to support the *in vitro* formation of skin consisting of a dermal compartment containing elongated fibroblasts surrounded by ECM proteins (fibronectin and type-I collagen) and a well-defined epidermal compartment with thickness (120 μ m) within the range of the human epidermis (60–150 μ m).

To develop advanced bioinks with tuneable biochemical and biophysical properties, in the third part of the work, NorPEC macromer was converted into a protease-degradable bioink through calcium (Ca^{2+})- or barium (Ba^{2+})-mediated ionic crosslinking and applied for the bioprinting of ECM-like microenvironments. Rheological characterization revealed that a higher concentration of Ba^{2+} (15 mM) is needed to achieve suitable bioink printability compared to Ca^{2+} (13 mM). Bioinks displayed a shear thinning behaviour and fast recovery post-printing, regardless the cation used for ionic gelation. The response of fibroblasts within the developed bioinks was evaluated by the printing of cell-laden 3D constructs with low (30 s UV curing) and high (90 s UV curing) elastic modulus. Extensive cell spreading and fibronectin deposition were observed in all constructs with exception to the stiffer Ba^{2+} -crosslinked bioink, in which lower metabolic activity, DNA content, and ECM deposition were verified probably due to the mechanical constraints imposed by the hydrogel.

Overall, in this research work, novel photocrosslinkable and cell-responsive pectin bioinks were developed for skin bioprinting as a result of an original combination of chemical modification strategies, crosslinking reactions and bioprinting approaches. Both PECMA and NorPEC bioinks showed suitable printability and cytocompatible gelation mechanisms, allowing the printing of cellularized 3D constructs that support the deposition of ECM components of the native skin. The proposed bioinks address important limitations in the field and show promising properties for applications in skin tissue engineering as 3D constructs for cutaneous wound healing, *in vitro* testing models and bioinks for *in situ* skin bioprinting.

RESUMO

A limitada capacidade de reparação da pele após lesão e as desvantagens das atuais abordagens terapêuticas representam os principais desafios no tratamento de lesões cutâneas. Apesar dos avanços no desenvolvimento de novos biomateriais para curativos e substitutos biológicos de pele, importantes limitações ainda persistem, tais como a limitada vascularização, infiltração celular tardia, formação de tecido fibroso e fracas propriedades mecânicas. A bioimpressão 3D assume-se como uma alternativa promissora para ultrapassar estas limitações através da deposição automática de materiais contendo células e/ou moléculas bioativas, designados de *bioinks*, em estruturas tridimensionais (3D) multicamada de pele quer *in vitro* quer *in vivo*. Apesar de vários hidrogéis terem vindo a ser adotados para utilização como *bioinks*, um dos principais desafios em bioimpressão 3D de pele consiste no limitado número de *bioinks* apresentando propriedades reológicas adequadas, rápida gelificação e capacidade de estimular as células a desempenhar as suas funções. Deste modo, o principal objetivo desta tese de doutoramento consistiu no desenvolvimento de novos hidrogéis fotopolimerizáveis baseados em pectina para a bioimpressão por extrusão de estruturas 3D celulares para a engenharia de tecidos da pele. As propriedades ótimas das *bioinks* tiveram como base a possibilidade de criar estruturas 3D com elevada definição geométrica capazes de estimular as funções das células incorporadas, a deposição de componentes da matriz extracelular (ECM) e a formação de pele *in vitro*.

A primeira parte do trabalho incidiu na síntese e desenvolvimento de uma *bioink* baseada em pectina para a bioimpressão de estruturas 3D da derme. Para tal, a pectina foi modificada com grupos metacrilato através da reação com metacrilato anidrido (MA) de forma a permitir a formação de géis químicos através da fotopolimerização por radiação ultravioleta (UV). Pectina funcionalizada com grupos metacrilato (PECMA) foi sintetizada com diferentes graus de substituição (21,7–50,2 %) sem comprometer a capacidade de gelificação iónica. A reação de adição de Michael catalisada por uma base foi utilizada para conjugar uma sequência peptídica (CGGGGRGDSP) aos grupos metacrilato na pectina através de uma cisteína terminal, promovendo a adesão de fibroblastos da derme no interior do gel. Propriedades reológicas adequadas para bioimpressão foram obtidas através da reticulação iónica de soluções de PECMA a baixa concentração (1,5 m/v%) na presença de 5 mM de cloreto de cálcio. A *bioink* contendo fibroblastos da derme foi utilizada na bioimpressão de estruturas 3D capazes de suportar a viabilidade celular durante os 14 dias

RESUMO

de cultura celular, fornecendo um microambiente celular adequado e capaz de estimular a produção de componentes da ECM, incluindo fibronectina e colagénio tipo-I.

Com o objetivo de desenvolver *bioinks* com propriedades de degradação controladas, na segunda parte do trabalho de investigação, novos derivados fotopolimerizáveis de pectina foram sintetizados para a formação de hidrogéis degradáveis por ação de proteases secretadas pelas células através de uma reação de tiol-norborneno iniciada por fotopolimerização por radiação UV. A pectina foi inicialmente convertida no seu sal de tetrabutilamónio (TBA) para solubilização em dimetilsulfóxido (DMSO) e modificada por reação com *carbic anhydride* (CA), resultando em derivados de pectina funcionalizados com grupos norborneno (NorPEC). De forma a mimetizar a adesão e remodelação celulares características da pele, hidrogéis degradáveis através de processos enzimáticos foram obtidos através da reação de tiol-norborneno entre um péptido como agente reticulante susceptível à degradação por parte de proteases (CGPQGIWGQC) contendo dois grupos sulfidrilo terminais e os grupos norborneno na pectina, após irradiação UV (20 s) e na presença de VA-086 como fotoiniciador. Um péptido capaz de promover a adesão celular e contendo um grupo sulfidrilo terminal (CGGGGRGDSP) foi também conjugado aos grupos norborneno durante a fotopolimerização, promovendo a adesão e alongamento dos fibroblastos no interior do gel. As propriedades mecânicas dos hidrogéis (2,5 %m/v) foram manipuladas numa ampla gama ($70,03 \pm 10,39$ Pa to $446,75 \pm 35,66$ Pa) através da variação da concentração do péptido reticulante (4–6 mM). Fibroblastos incorporados no interior destes hidrogéis apresentaram uma morfologia alongada com secreção de metaloproteinases de matriz, MMP-2 e MMP-9, envolvidas no processo de cicatrização da pele. Análises histológicas e de imunofluorescência mostraram a capacidade dos hidrogéis desenvolvidos em suportar a formação de pele *in vitro*, constituída por uma camada equivalente à derme contendo fibroblastos com uma morfologia alongada envoltos numa ECM rica em proteínas (fibronectina e colagénio tipo-I) e uma camada bem definida equivalente à epiderme com uma espessura (120 μ m) compreendida no intervalo de valores da pele humana (60–150 μ m).

De forma a desenvolver *bioinks* com propriedades bioquímicas e biofísicas definidas, na terceira parte do trabalho de investigação, a solução de NorPEC foi convertida numa *bioink* degradável pela ação de metaloproteinases de matriz através de gelificação iónica mediada por iões cálcio (Ca^{2+}) ou bário (Ba^{2+}) e utilizada na bioimpressão de microambientes que mimetizam as propriedades da ECM. A caracterização reológica revelou a necessidade de se utilizar uma concentração superior de Ba^{2+} (15 mM) para obter níveis similares de consistência do filamento comparativamente ao Ca^{2+} (13 mM). Independentemente do tipo e concentração do catião utilizado na reticulação iónica, as *bioink* apresentaram comportamento reológico similar. A resposta dos fibroblastos no interior

das *bioink* desenvolvidas foi avaliada através da bioimpressão de estruturas 3D celulares reticuladas com luz UV de forma a apresentarem baixo (30 s de irradiação UV) ou elevado (90 s de irradiação UV) módulo de elasticidade. Foi possível observar que as células no interior dos hidrogéis apresentaram extenso alongamento e deposição de fibronectina com exceção da *bioink* reticulada com Ba^{2+} , na qual se verificou uma redução na atividade metabólica, teor em DNA e deposição de ECM, provavelmente devido aos constrangimentos físicos impostos pela rigidez do hidrogel.

De uma forma sucinta, neste trabalho de investigação foram desenvolvidas novas *bioink* fotopolimerizáveis baseadas em pectina para a bioimpressão de pele através de uma combinação original de estratégias de modificação química, reações de reticulação e abordagens de bioimpressão. Ambas as *bioink* desenvolvidas com base PECMA e NorPEC demonstraram propriedades reológicas adequadas e mecanismos de reticulação biocompatíveis, permitindo a bioimpressão de estruturas 3D celulares que estimularam a deposição de componentes da ECM da pele. As *bioink* propostas resolvem importantes limitações na área e apresentam propriedades promissoras para aplicações em engenharia de tecidos da pele como estruturas 3D para a reparação de lesões cutâneas, modelos de teste *in vitro* e bioinks para a bioimpressão de pele *in situ*.

TABLE OF CONTENTS

ACKNOWLEDGEMENTS	V
ABSTRACT.....	IX
RESUMO	XI
LIST OF ABBREVIATIONS	XIX
LIST OF PUBLICATIONS AND COMMUNICATIONS	XXIII
CHAPTER I - AIMS AND THESIS OUTLINE	1
1.1. OVERVIEW	3
1.1.1. Skin wound care: facts and numbers.....	3
1.1.2. Hydrogels in wound healing	5
1.1.3. Biofabrication of hydrogels for skin reconstruction.....	6
1.2. MOTIVATION	7
1.3. OBJECTIVE AND SPECIFIC AIMS.....	8
1.4. THESIS OUTLINE	9
1.5. REFERENCES.....	10
CHAPTER II - GENERAL INTRODUCTION.....	15
ABSTRACT.....	17
2.1. INTRODUCTION	18
2.2. SKIN STRUCTURE AND COMPOSITION	19
2.3. WOUND HEALING PROCESS.....	22
2.3.1. Acute wound healing	23
2.3.1.1. Haemostasis	23
2.3.1.2. Inflammation.....	24
2.3.1.3. Proliferation.....	24
2.3.1.4. Remodelling	25
2.3.2. Chronic wound healing.....	26
2.4. THERAPEUTIC OPTIONS FOR SKIN RECONSTRUCTION	28
2.4.1. Conventional therapies.....	28
2.4.1.1. Autografts and allografts	29
2.4.1.2. Herbal-derived compounds	30
2.4.1.3. Animal-derived products	30
2.4.1.4. Living organisms	31
2.4.1.5. Solutions, creams and ointments	32
2.4.1.6. Traditional dressings	32
2.4.2. Advanced therapies.....	32
2.4.2.1. Modern wound dressings	33

TABLE OF CONTENTS

2.4.2.2.	Bioengineered skin substitutes.....	35
2.4.2.3.	Growth factor therapy.....	38
2.4.2.4.	Biophysical agents.....	39
2.5.	BIOFABRICATION TECHNOLOGIES.....	39
2.5.1.	Light-based technologies.....	40
2.5.1.1.	Vat photopolymerization.....	40
2.5.1.2.	Laser-assisted bioprinting.....	42
2.5.2.	Inkjet bioprinting.....	43
2.5.3.	Extrusion bioprinting.....	45
2.6.	BIOPRINTING OF PHOTOCROSSLINKABLE HYDROGEL BIOINKS.....	47
2.6.1.	Hydrogels as ECM mimics.....	47
2.6.2.	Photopolymerization Reactions.....	52
2.6.3.	Cytocompatible photoinitiators.....	55
2.6.4.	Photocrosslinkable bioinks.....	59
2.7.	BIOPRINTING HYDROGELS FOR SKIN TISSUE ENGINEERING.....	62
2.7.1.	Requirements of printed skin.....	63
2.7.1.1.	Cellular composition.....	63
2.7.1.2.	Biochemical composition.....	63
2.7.1.3.	Zonal organization and material composition.....	63
2.7.1.4.	Tissue architecture and shape.....	64
2.7.1.5.	Barrier function.....	64
2.7.1.6.	Appendages and pigmentation.....	64
2.7.1.7.	Vascularization.....	65
2.7.2.	Hydrogel bioinks for skin bioprinting.....	65
2.7.3.	Bioprinted constructs for skin repair.....	69
2.7.4.	Bioprinted constructs as in vitro skin models.....	70
2.7.5.	Bioprinted constructs with skin appendages and pigmentation.....	73
2.7.6.	Bioprinted vascularized skin constructs.....	75
2.7.7.	In situ bioprinting of skin substitutes.....	77
2.8.	CONCLUSIONS.....	79
2.9.	REFERENCES.....	81
CHAPTER III - A SINGLE-COMPONENT HYDROGEL BIOINK FOR BIOPRINTING OF BIOENGINEERED 3D CONSTRUCTS FOR DERMAL TISSUE ENGINEERING.....		105
ABSTRACT.....		107
3.1.	INTRODUCTION.....	108
3.2.	MATERIALS AND METHODS.....	110
3.2.1.	Synthesis of methacrylate-functionalized pectin.....	110
3.2.2.	Conjugation of cell-adhesive peptide.....	110
3.2.3.	Preparation of pectin hydrogels.....	111

3.2.4.	Characterization of gel fraction, swelling ratio, microstructure and in vitro degradation	111
3.2.5.	Characterization of hydrogel stiffness.....	112
3.2.6.	Assessment of hydrogel's biological behaviour	112
3.2.7.	Bioink preparation, assessment of rheological properties and bioprinting	113
3.2.8.	Determination of metabolic activity and cell viability	113
3.2.9.	Bioprinted cell morphology and ECM synthesis.....	114
3.2.10.	Statistical Analysis.....	114
3.3.	RESULTS AND DISCUSSION.....	114
3.3.1.	Synthesis of pectin methacrylate and hydrogel design	114
3.3.2.	Photopolymerization of pectin hydrogels with tuneable properties.....	116
3.3.3.	Biofunctionalized hydrogels support the viability and spreading of embedded dermal fibroblasts	119
3.3.4.	Bioprinting cell-laden 3D constructs using a dual-crosslinked, single-component hydrogel bioink	122
3.3.5.	Bioprinted 3D constructs provide a cell-instructive microenvironment for the deposition of endogenous dermal ECM components.....	126
3.4.	CONCLUSIONS	131
3.5.	ACKNOWLEDGEMENTS.....	131
3.6.	REFERENCES.....	132
3.7.	SUPPLEMENTARY INFORMATION.....	136
CHAPTER IV - CELL-INSTRUCTIVE PECTIN HYDROGELS CROSSLINKED VIA THIOL-NORBORNENE PHOTO-CLICK CHEMISTRY FOR SKIN TISSUE ENGINEERING		147
	ABSTRACT.....	149
4.1.	INTRODUCTION	150
4.2.	MATERIALS AND METHODS	152
4.2.1.	Synthesis of norbornene functionalized pectin.....	152
4.2.2.	Formation and characterization of photocrosslinked hydrogels.....	152
4.2.3.	3D cell embedding within hydrogels, cell viability and morphology analysis...	154
4.2.4.	Matrix metalloproteinases secretion by gelatin zymography	155
4.2.5.	Formation of full-thickness skin using cell-instructive pectin hydrogels	155
4.2.6.	Histological and immunofluorescence analysis.....	155
4.2.7.	Statistical analysis	156
4.3.	RESULTS AND DISCUSSION	156
4.3.1.	Synthesis of norbornene-functionalized pectin macromers for thiol-ene photopolymerization	156

TABLE OF CONTENTS

4.3.2.	Formation and characterization of thiol-ene click pectin hydrogels	158
4.3.3.	Chemically defined cell-instructive pectin hydrogels promote 3D cell attachment and spreading.....	163
4.3.4.	Thiol-ene click pectin hydrogels support full-thickness skin formation.....	168
4.4.	CONCLUSIONS	171
4.5.	ACKNOWLEDGEMENTS.....	171
4.6.	REFERENCES.....	172
4.7.	SUPPLEMENTARY INFORMATION.....	177
CHAPTER V - BIOORTHOGONAL PECTIN BIOINK FOR BIOPRINTING OF PROTEASE-DEGRADABLE 3D CELLULAR MICROENVIRONMENTS		189
	ABSTRACT.....	191
5.1.	INTRODUCTION	192
5.2.	MATERIALS AND METHODS	194
5.2.1.	Bioink synthesis and preparation.....	194
5.2.2.	Rheological measurements	195
5.2.3.	Mechanical properties of hydrogels	195
5.2.4.	Bioprinting of cellularized 3D constructs	195
5.2.5.	Characterization of bioprinted 3D constructs	196
5.2.6.	Statistical analysis	197
5.3.	RESULTS AND DISCUSSION	197
5.3.1.	Design of a modular bioink crosslinked by thiol-norbornene click chemistry ..	197
5.3.2.	Tuning the bioink printability via ionic crosslinking.....	200
5.3.3.	Modulating the viscoelastic properties of thiol-ene bioinks.....	205
5.3.4.	Bioprinted cell-responsive 3D microenvironments support cell spreading and ECM deposition	207
5.4.	CONCLUSIONS	212
5.5.	ACKNOWLEDGEMENTS.....	212
5.6.	REFERENCES.....	212
CHAPTER VI - GENERAL DISCUSSION AND FUTURE PERSPECTIVES		215
6.1.	GENERAL DISCUSSION.....	217
6.2.	FUTURE PERSPECTIVES.....	221
6.3.	REFERENCES.....	223

LIST OF ABBREVIATIONS

AFSs	Amniotic Fluid-derived Stem Cells
ALI	Air–liquid Interface
ANOVA	One-way Analysis of Variance
ASCs	Adipose-derived Stem Cells
Ba²⁺	Barium Ion
bFGF	Basic Fibroblast Growth Factor
BMP-4	Bone Morphogenetic Protein 4
BSA	Bovine Serum Albumin
CA	Carbic Anhydride
Ca²⁺	Calcium Ion
CaCl₂	Calcium Chloride
CEAs	Cultured Epithelial Autografts
CM	Complementary Medicine
DAPI	4',6-diamidino-2-phenylindole dihydrochloride
DE	Degree of Esterification
DM	Degree of Methacrylation
DMDs	Digital Micromirror Devices
DMEM	Dulbecco's Modified Eagle's Medium
DMSO	Dimethyl Sulfoxide
DNA	Deoxyribonucleic Acid
DOD	Drop-On-Demand
dsDNA	Double-stranded Deoxyribonucleic Acid
DTT	Dithiothreitol
ECM	Extracellular Matrix
EDTA	Ethylenediamine Tetraacetic Acid
EGF	Epidermal Growth Factor
e.g.	<i>Exempli gratia</i>

ACRONYMS AND ABBREVIATIONS LIST

em.	Emission
EPCs	Endothelial Progenitor Cells
ex.	Excitation
FBS	Fetal Bovine Serum
FDA	Food and Drug Administration
FGF	Fibroblast Growth Factor
FITC	Fluorescein isothiocyanate
g	G force
GAGs	Glycosaminoglycans
GalA	Galacturonic Acid
GM-CSF	Granulocyte Macrophage-colony Stimulating Factor
H&E	Hematoxylin and Eosin Stain
HA-HP	Heparin-conjugated Hyaluronic Acid
HBSS	Hanks' Balanced Salt Solution
HEPES	4-(2-hydroxyethyl)-1-piperazineethanesulfonic acid
HGF	Hepatocyte Growth Factor
HMVECs	Human Dermal Microvascular Endothelial Cells
hNDFs	Human Neonatal Dermal Fibroblasts
HUVECs	Human Umbilical Vein Endothelial Cells
i.e.	<i>Id est</i>
iECs	Induced Pluripotent Stem Cell-derived Endothelial Cells
IFN	Interferon
IGF-1	Insulin-like Growth Factor-one
IL-1	Interleukin-1
IL-6	Interleukin-6
iPSCs	Induced Pluripotent Stem Cell
I2959	1-[4-(2-hydroxyethoxy)-phenyl]-2-hydroxy-2-methyl-1-propane-1-one
KGF	Keratinocyte Growth Factor
LAB	Laser-Assisted Bioprinting
LAP	Lithium phenyl-2,4,6-trimethylbenzoylphosphinate

μSTLG	Micro Stereo-Thermal-Lithography
MA	Methacrylic Anhydride
MMP	Matrix Metalloproteinase
MSCs	Mesenchymal Stem Cells
MWCO	Molecular Weight Cut Off
NaCl	Sodium Chloride
Near-IR	Near-infrared light
NMR	Nuclear Magnetic Resonance
NorPEC	Norbornene-modified Pectin
NPWT	Negative Pressure Wound Therapy
PECMA	Pectin Methacrylate
PEC-TBA	Tetrabutylammonium Salt of Pectin
PBS	Phosphate Buffered Saline
PCL	Poly(ε-caprolactone)
PDGF	Platelet-derived Growth Factor
PDLLA	Poly(D,L-lactide)
PEO/PBT	Poly(ethylene oxide)–poly(butylene terephthalate)
PEG	Polyethylene Glycol
PFA	Paraformaldehyde
PGA/PLA	Polyglycolic acid/Poly(lactic acid)
PPF	Propylene Fumarate
ppm	Parts per million
PTMC	Poly(trimethylene carbonate)
RGD	Arginyl-glycyl-aspartic acid
RG-I	Rhamnogalacturonan-I
RG-II	Rhamnogalacturonan-II
Rh-GM-CSF	Recombinant Human-Granulocyte Macrophage-colony Stimulating Factor
Rh-VEGF	Recombinant Human-Vascular Endothelial Growth Factor
ROS	Reactive Oxygen Species
rpm	Rotation per minute

ACRONYMS AND ABBREVIATIONS LIST

SEM	Scanning Electron Microscopy
T&CM	Traditional and Complementary Medicine
TBA	Tetrabutylammonium
TBSA	Total Body Surface Area
TGF-α	Transforming Growth Factor Alpha
TGF-β	Transforming Growth Factor Beta
TIMPs	Tissue Inhibitors of Metalloproteinases
TM	Traditional Medicine
TNF-α	Tumour Necrosis Factor Alpha
UK	United Kingdom
UV	Ultraviolet
US	United States
VA-086	2,2'-azobis[2-methyl-N-(2-hydroxyethyl)propionamide]
VEGF	Vascular Endothelial Growth Factor
VEGF-A	Vascular Endothelial Growth Factor-A
WHO	World Health Organization
2D	Two-Dimensional
2PP	Two-photon Polymerization
3D	Three-Dimensional

LIST OF PUBLICATIONS AND COMMUNICATIONS

The work performed under the scope of this PhD thesis resulted in the publications and communications listed below.

Original papers in peer-reviewed journals

1. **Pereira, R.F.**, Sousa, A., Barrias, C.C., Bártolo, P.J., Granja, P.L. "A single-component hydrogel bioink for bioprinting of bioengineered 3D constructs for dermal tissue engineering" *Materials Horizons*, 5, 1100-1111, 2018.
2. **Pereira, R.F.**, Barrias, C.C., Bártolo, P.J., Granja, P.L. "Cell-instructive pectin hydrogels crosslinked via thiol-norbornene photo-click chemistry for skin tissue engineering", *Acta Biomaterialia*, 66, 282-293, 2018.
3. **Pereira, R.F.**, Lourenço, B.N., Bártolo, P.J., Granja, P.L. "Bioorthogonal pectin bioink for bioprinting of protease-degradable 3D cellular microenvironments". (in preparation)

Review papers in peer-reviewed journals

1. **Pereira, R.F.**, Sousa, A., Barrias, C.C., Bayat, A., Granja, P.L., Bártolo, P.J. "Advances in bioprinted cell-laden hydrogels for skin tissue engineering", *Biomanufacturing Reviews*, 2, 1-26, 2017.
2. **Pereira, R.F.**, Bártolo, P.J. "Traditional therapies for skin wound healing", *Advances in Wound Care (New Rochelle)*, 5, 208-229, 2016.
3. **Pereira, R.F.**, Bártolo, P.J. "3D bioprinting of photocrosslinkable hydrogel constructs" *Journal of Applied Polymer Science*, 132, 42458, 2015.
4. **Pereira, R.F.**, Bártolo, P.J. "3D Photo-Fabrication for Tissue Engineering and Drug Delivery", *Engineering*, 1, 90-112, 2015.
5. **Pereira, R.F.**, Barrias, C.C., Granja, P.L., Bártolo, P.J. "Advanced biofabrication strategies for skin regeneration and repair", *Nanomedicine*, 8, 603-621, 2013.

Books

1. P.J. Bártolo, **R.F. Pereira**. "Biomanufacturing: materials, processes and applications", Springer. (in preparation)

PUBLICATIONS

Book Chapters

1. Neves, S., **Pereira, R.F.**, Araújo, M., Barrias, C.C. "Bioengineered peptide-functionalized hydrogels for tissue regeneration and repair", In: Peptides and proteins as biomaterials for tissue regeneration and repair, edited by M. Barbosa and C. Martins, Elsevier, pp. 101-125, 2018 (ISBN: 9780081008034).
2. **Pereira, R.F.**, Bártolo, P.J. "Recent Advances in Additive Biomanufacturing", In: Comprehensive Materials Processing, edited by S. Hashmi, Elsevier, pp. 265-284, 2014 (ISBN: 9780080965338).
3. **Pereira, R.F.**, Bártolo, P.J. "Photopolymerizable hydrogels in regenerative medicine and drug delivery", In: Hot topics in biomaterials for healthcare, Future Science, pp. 6-28, 2014 (ISBN: 978-1-909453-70-8).
4. **Pereira, R.F.**, Bártolo, P.J. "Photocrosslinkable materials for the fabrication of tissue-engineered constructs by stereolithography", In: Tissue Engineering: Computer Modelling, Biofabrication and Cell Behavior, Edited by P.J. Bártolo and P. Fernandes, Springer, pp. 149-178, 2014 (ISBN: 978-94-007-7073-7).
5. **Pereira, R.F.**, Almeida, H.A., Bártolo, P.J. "Biofabrication of hydrogel constructs", In: Drug Delivery Systems: Advanced Technologies Potentially Applicable in Personalized Treatments (Volume 4), Edited by J.F.J. Coelho, Springer, pp. 225-254, 2013 (ISBN: 978-94-007-6009-7).

Conference abstracts published in international scientific journals

1. **Pereira, R.**, Sousa, A., Barrias, C., Bártolo, P.J., Granja, P.L. "A cell-responsive, photocrosslinkable bioink for extrusion bioprinting of 3D hydrogel constructs", European Cells and Materials Vol. 33 Suppl. 2, 2017.

Invited oral communications

1. **Pereira, R.**, Granja, P.L. "Materiais biofuncionais para a bioimpressão de tecidos", II Jornadas de Metalurgia e Materiais, Faculdade de Engenharia da Universidade do Porto, Portugal, 2017.
2. **Pereira, R.** "Estratégias avançadas de biofabricação para a regeneração de tecidos e órgãos", III Jornadas de Biomecânica, Escola Superior de Tecnologia e Gestão de Leiria, Leiria, Portugal, 2013.

Oral communications

1. **Pereira, R.F.**, Sousa, A., Barrias, C.C., Bártolo, P.J., Granja, P.L. "Photocrosslinkable pectin hydrogels as cell carriers for biofabrication", 6th China-Europe Symposium on Biomaterials in Regenerative Medicine, Porto, Portugal, 2017.
2. **Pereira, R.F.**, Sousa, A., Barrias, C.C., Bártolo, P.J., Granja, P.L. "A dual-crosslinking strategy to design biofunctional pectin hydrogels for extrusion bioprinting", International Symposium on Materials "Materiais 2017", Aveiro, Portugal, 2017.
3. **Pereira, R.**, Sousa, A., Barrias, C., Granja, P., Bártolo, P. "Effect of physicochemical properties and peptide ligands on fibroblasts embedded in dual crosslinked pectin hydrogels for skin repair", International Conference on New Advances in Probing Cell-Extracellular Matrix Interactions (CellMatrix), Berlin, Germany, 2016.
4. **Pereira, R.F.**, Sousa, A., Barrias, C.C., Granja, P., Bártolo, P.J. "Synthesis of naturally derived hydrogels for tissue engineering", The Second CIRP Conference on Biomanufacturing, Manchester Conference Centre, UK, 2015.

Poster communications

1. **Pereira, R.**, Sousa, A., Barrias, C., Bártolo, P.J., Granja, P.L. "Design a single-component bioink for the bioprinting of skin tissue constructs", 28th European Conference on Biomaterials, Athens, Greece, 2017.
2. **Pereira, R.**, Sousa, A., Barrias, C., Bártolo, P.J., Granja, P.L. "A cell-responsive, photocrosslinkable bioink for extrusion bioprinting of 3D hydrogel constructs", TERMIS-EU 2017, Davos, Switzerland, 2017.
3. **Pereira, R.**, Sousa, A., Barrias, C., Granja, P., Bártolo, P. "Effect of physicochemical properties and peptide ligands on fibroblasts embedded in dual crosslinked pectin hydrogels for skin repair", International Conference on New Advances in Probing Cell-Extracellular Matrix Interactions (CellMatrix), Berlin, Germany, 2016.

CHAPTER I

AIMS AND THESIS OUTLINE

1.1. Overview

1.1.1. Skin wound care: facts and numbers

The skin is the largest organ of the human body, located at the interface between the internal organs and the external environment, performing protective, sensory, metabolic and aesthetic functions. It encompasses a surface area of 1.8 m² and comprises approximately 16% of the total body weight [1]. Skin acts as an efficient barrier that prevents dehydration and the entrance of exogenous organisms into the body. Anatomically, it is a multilayered organ composed by three functional layers of epidermis, dermis and hypodermis, containing distinct cell populations (e.g., stem cells, fibroblasts, keratinocytes, adipocytes) surrounded by an intricate extracellular matrix (ECM). The interplay between resident cell populations and their niches ensures tissue homeostasis, barrier properties and wound repair [2, 3].

As the outermost organ of the human body, skin is under permanent interaction with the outside environment, which can result in different types of damage caused by injury or disease. Skin damage causes a disruption in tissue organization, leading to wound formation and initiating the process of wound healing to restore the tissue function. Depending on the underlying cause, wounds can be classified into acute (e.g., surgical wounds, burns, abrasions) and chronic (e.g., diabetic foot ulcers, pressure ulcers, leg ulcers). Acute wounds proceed orderly and timely throughout the cascade of the healing phases until repair, while in chronic wounds the excessive protease activity and reactive oxygen species (ROS) production, unbalanced ECM turnover, and wound colonization and infection have been identified as major biological events [4-6]. These events, together with the underlying pathophysiology (e.g., venous insufficiency, diabetes mellitus, arterial occlusion), are responsible for the wound healing arrest, often in the inflammatory phase, resulting in a failure of granulation tissue formation and subsequent re-epithelialization for a period longer than three months [7]. While most of the acute wounds (e.g., surgical wounds, abrasions) often heal without major complications, extensive burn injuries and chronic wounds are often associated with expensive treatments and eventually long hospitalization times, increasing the total health expenditure.

For small areas of full-thickness skin loss (<1 cm), wound closure spontaneously occurs through contraction and cell ingrowth. However, in larger or difficult-to-heal wounds, the innate self-healing ability of the skin is insufficient to restore its native architecture, composition and functions [8]. In these cases, immediate wound covering is needed to

prevent local and systemic infections. Conventional full-thickness or split-thickness autografting are the 'gold standard' treatment for full skin reconstruction, though they present several drawbacks such as the limited availability, patient morbidity, scarring at the donor sites and lengthy hospitalization times [9]. Although the application of meshing technique maximizes the wound area covered by the grafts [10], in patients with extensive injury (e.g., burns), difficult-to-heal acute wounds or chronic wounds, advanced wound care products and therapies are required. In order to address these needs, researchers have explored interdisciplinary approaches to develop alternative therapeutic options, including advanced dressings (e.g., foams, hydrogels, films, alginate), genetically modified grafts, bioengineered skin substitutes (e.g., epidermal and/or dermal), active wound care (e.g., growth factors, protease inhibitors), and therapy devices (e.g., electrical stimulation therapy, negative wound pressure therapy) [11-14]. Despite the fact that dressings provide a temporary solution for wound coverage and can maintain a moist environment in the wound bed, some wounds require a more permanent form of coverage. Bioengineered skin substitutes refers to wound care products manufactured based on cells, ECM-like biomaterials or their combination. These products are composed of dermal and/or epidermal components, providing a solution to the reconstruction of both epidermal and dermal skin layers. They are mostly manufactured from collagen and glycosaminoglycans (GAGs), being available as either acellular or cellular products. Skin substitutes are the most advanced wound care products available in the market, but they still present important limitations such as the inability of complete regeneration of functional skin (e.g., adnexal structures, pigmentation, vascularization), lack of underlying connective tissue (dermal and subcutaneous), peripheral scarring and high cost [15, 16].

Wound treatment represents a substantial economic burden to the healthcare system of a country due to increased health care costs, aging population, and higher incidence of diabetes and obesity. In the United States (US), it was estimated that the total direct cost of skin disease was about \$75 billion in 2013, compared to \$29 billion in 2004. Nearly \$40 billion were devoted to the top 10 skin disease categories with the largest economic burden, including wounds, burns, ulcers and cutaneous infections [17]. According to data from the United Kingdom (UK), annual costs with wound treatment accounts for approximately £5 billion, corresponding to hospital stay (~50%), nursing time (~35%) and dressing materials (~15%) [18]. In US, it is estimated that each year 35.2 million cases of significant skin loss require major therapeutic intervention, while about 6.5 million of these wounds become chronic [18]. Every year there are about 3 million cases of pressure and leg ulcers, and 2 million cases of chronic diabetic ulcers, resulting in approximately \$9.5 billion of total direct health care costs [19]. Among acute wounds, burns represent the most devastating and

debilitating injuries. It was estimated that 486,000 burn patients were treated in emergency departments, resulting in 40,000 hospitalizations in 2016 [20] and representing an annual expenditure higher than \$2 billion in direct costs. In Europe, it is estimated that 1.5–2 million people suffer from acute or chronic wounds, while between 22.7% and 50% of hospital beds are occupied by patients requiring wound management [18]. Together, these data indicate a growing trend in the global wound care market and rising demand for innovative and advanced wound management products. According to the “Wound Care Market - Global Forecast To 2022” report from Markets and Markets, the segments of advanced wound management products and chronic wounds are foreseen to account for the largest share of the global wound care market.

1.1.2. Hydrogels in wound healing

Hydrogels are water-swollen three-dimensional (3D) crosslinked networks of insoluble macromolecular polymers obtained by the formation of chemical or physical bonds between polymer chains. Depending on the polymer origin and chain crosslinking mechanism, hydrogels can be designed with a broad range of physicochemical and mechanical properties [21], making them suitable for wound healing applications. They are used to maintain a moist environment in the wound bed and promote autolytic debridement, while allowing the passage of water vapour and oxygen to the wound surface [22, 23]. Hydrogel dressings are available as either a sheet or an amorphous gel, which is covered by a secondary dressing (e.g., film, foam or hydrocolloid). Major advantages of hydrogels as dressings include the smooth nature and the ability to be applied and removed from the wound with minimal pain or trauma [24]. In order to extend their efficacy, several factors such as antimicrobial agents, growth factors and cells, can be loaded in the porous network and topically released into the wound bed to modulate the wound microenvironment through several biological pathways [25-27].

Photocrosslinkable hydrogels are promising for wound healing as they can be rapidly formed *in situ*, i.e., directly into the wound bed upon exposure to cytocompatible doses of ultraviolet (UV) or visible light. In addition, they conform to the shape of the defect and provide unique control over the spatiotemporal formation of the gel network [28, 29]. These hydrogels can be crosslinked in the presence of cells, bioactive molecules and biological tissues, allowing the design of advanced formulations capable of instructing the function of embedded cells and establishing dynamic interactions with the wound microenvironment [25, 30]. ECM components like collagen and elastin have been the first choice in the synthesis of hydrogels for wound healing due to their intrinsic biological activity [29, 31, 32]. However, the

limited control over the biochemical composition of the gel network, source variability, risk of infection and purity has driven the research for alternative sources of biomaterials.

Polysaccharides are natural polymers obtained from animals, plants or microorganisms widely used in wound healing due to their biocompatibility, availability, versatile chemical composition and bioactive properties [33, 34]. Pectin is a structural heteropolysaccharide extracted from the cell walls of plants (mostly from citrus peel and apple pomace) extensively employed in the food industry as a jellifying agent. It has also been investigated for biomedical applications owing its biocompatibility, chemical versatility, anionic nature and ionic crosslinking ability [35]. Pectin is a branched polysaccharide composed of a linear chain of α -(1,4)-linked galacturonic acid (GalA) residues, in which part of the carboxyl groups are in either methyl ester or acetyl-ester form. The content of methyl-esterified residues defines the degree of esterification (DE) and determines polymer properties such as the hydrogel formation and the strength of the crosslinked network [36]. Pectin backbone is comprised of approximately 65-70% of GalA residues that constitute the homogalacturonan domain. This domain has regions without side chains (known as “smooth regions”) and regions flanked with a variety of neutral sugars (termed as “hairy regions”) such as arabinose, galactose and rhamnose. Rhamnogalacturonan-I (RG-I) and rhamnogalacturonan-II (RG-II) are other two prominent domains in pectin that contain side chains of different sugars and are believed to be alternately linked to the homogalacturonan domain, though their exact arrangement still remains unknown [35, 37]. The complex chemical composition of pectin is responsible not only for its bioactive properties (e.g., mucoadhesiveness, wound healing, antitumor activity), but it also provides a multitude of functional groups amenable to chemical modification. These groups have been explored for the synthesis of pectin derivatives with tailored chemical, biophysical and biological properties [38-40]. Pectin and its derivatives have been converted into physical or chemical hydrogels using a variety of crosslinking mechanisms and evaluated as drug delivery carriers, cell delivery systems or matrices for tissue repair [41-46], extending their application to the fields of tissue engineering and regenerative medicine.

1.1.3. Biofabrication of hydrogels for skin reconstruction

Biofabrication is a multidisciplinary field that combines the principles of biology, engineering and material science to generate constructs with biological function. In the context of tissue engineering and regenerative medicine, biofabrication is defined as *“the automated generation of biologically functional products with structural organization from living cells, bioactive molecules, biomaterials, cell aggregates such as micro-tissues, or hybrid cell-material constructs, through bioprinting or bioassembly and subsequent tissue*

maturation processes" [47]. Bioprinting employs additive manufacturing technologies and building blocks down to molecular level (bioactive molecules, biomaterials, living single cells or cell-aggregates) to create functional constructs with prescribed organization, holding the potential to automatically generate patient-specific skin substitutes [48, 49]. Recently, a disruptive strategy involving the *in situ* bioprinting of bioinks, which consist of material formulations and biological molecules or cells directly onto the wound bed, was proposed for skin repair and reconstruction [50, 51]. Despite the developments in the bioprinting of skin constructs, major bottlenecks in the field are related to the lack of bioinks exhibiting both tuneable rheological properties for high printing resolution and cell-instructive capabilities [52, 53].

1.2. Motivation

In situ forming hydrogels have been designed to mimic specific features of the native ECM, including the fibrous nature, ability to promote cell adhesion, proteolytic degradation or growth factor delivery and sequestration [54]. These biofunctional hydrogels have become an important tool for novel wound care therapies as their biochemical and biophysical properties can be tailored to engineer physiologically relevant cellular microenvironments. While *in situ* forming hydrogels are widely used as both acellular or cellularized injectable formulations that can be crosslinked *in vitro* or *in vivo*, a limited number of hydrogels can be applied for the extrusion bioprinting of cell-laden 3D hydrogels for skin repair due to the narrow processing window.

Extrusion bioprinting dispenses continuous filaments of hydrogel materials through nozzles by the action of a piston, a screwing system or pneumatic pressure. Viscous materials with high cellular densities can be printed into 3D constructs of complex architectures, making extrusion bioprinting the most affordable technology to print biological constructs at clinically relevant dimensions [55]. However, the printing of functional skin constructs using this technology requires the design of hydrogel bioinks with specific rheological properties that simultaneously provide an instructive environment for printed cells and exhibit fast and cytocompatible crosslinking mechanisms. These strict requirements significantly limit the number of available bioinks for the bioprinting of skin tissue equivalents. The majority of hydrogel bioinks are based on protein-derived materials (e.g., collagen, gelatin and fibrinogen), eventually combined with alginate to explore its ionic crosslinking ability [56-59]. Some of the limitations of these material systems include the difficulty in decoupling the contribution of biochemical and biophysical cues to cell behaviour, limited mechanical properties, and poor control over the biochemical composition of bioinks. Thus,

there is an unmet need for alternative hydrogel materials with tuneable biochemical and biophysical properties that can be printed into complex 3D constructs holding the prescribed shape and rapidly form, both *in vitro* and *in vivo*, under cytocompatible conditions.

1.3. Objective and Specific Aims

The main aim of this doctoral thesis was to develop novel photocrosslinkable pectin hydrogels as cell-responsive bioinks for the 3D bioprinting of cell-laden constructs for skin tissue engineering. In order to successfully print functional 3D cellularized skin constructs, several challenges need to be addressed. First, the bioink must be printable under cell-compatible conditions and hold the desired shape during the deposition, allowing for high printing resolution. For this purpose, ionic gelation was explored to design a printable pectin bioink that allows for homogeneous cell suspension and maintains the shape after deposition, without the need for support structures or additional materials for viscosity modulation. Second, the bioink must be rapidly crosslinked under mild and cytocompatible conditions for preserving the viability and function of printed cells. To this end, photocrosslinkable pectin macromers were synthesized by chemical modification with methacrylate or norbornene end groups for rapid hydrogel formation through UV photopolymerization via a chain-growth or a step-growth mechanism, respectively. Third, the bioink should allow the biofunctionalization with relevant biochemical cues and exhibit tunable biophysical and rheological properties. For the functionalization of pectin macromers, two bioconjugation chemistries (thiol-Michael addition and photoinitiated thiol-ene reactions) were selected for the coupling of cell-adhesive and protease-degradable peptide sequences, by exploring the reactivity between thiols and alkene functional groups. Finally, the printed constructs should provide a cell-responsive microenvironment capable of instructing embedded cells to secrete new ECM components, ultimately supporting *in vitro* skin formation and promoting *in vivo* skin repair. The development of a single-component bioink platform fulfilling those requirements will provide new opportunities in the bioprinting of 3D skin constructs that could be explored as *in vitro* testing models and matrices for skin repair.

The specific aims of this thesis were:

- i) Design a dual-crosslinked pectin hydrogel bioink for the extrusion bioprinting of 3D cell-laden dermal constructs.
- ii) Synthesize pectin macromers by functionalization with norbornene end groups for the one-pot formation of step-growth hydrogels that support full-thickness skin formation.

- iii) Bioprinting a protease-degradable pectin bioink into 3D constructs photocrosslinked by bioorthogonal thiol-norbornene chemistry.

1.4. Thesis Outline

This thesis is divided in six chapters that provide a detailed review of literature, present the developed work, and discuss the findings and their implications for the field.

Chapter II provides a detailed overview regarding the most recent developments in the biofabrication of hydrogel constructs for skin repair and regeneration. Skin anatomy and wound healing physiology are firstly described along with the available therapeutic options. Major limitations and unmet needs are highlighted. A general overview of biofabrication processes is also provided with emphasis on bioprinting technologies that allow the deposition of cellularized bioinks and design strategies to synthesize and print photocrosslinkable hydrogels. Finally, the applications of bioprinted skin constructs are illustrated and future directions discussed in order to summarize required developments in the field.

Chapter III describes the design of a dual-crosslinkable pectin hydrogel that can be explored as a platform to study the influence of biophysical and biochemical cues on the behaviour of embedded dermal fibroblasts, or as a printable bioink to create cellularized dermal constructs. Pectin was chemically modified with methacrylate groups to allow the formation of hydrogels via UV photopolymerization, while retaining its ionic crosslinking ability. The sequential application of both crosslinking mechanisms allowed the design of a bifunctional bioink that stimulated printed cells to secrete new dermal ECM components.

Chapter IV presents a novel chemical route for the modification of pectin with norbornene end groups to create chemical hydrogels through UV photoinitiated thiol-norbornene click chemistry via a step-growth mechanism. The introduction of norbornene groups allowed the rapid formation of protease-degradable hydrogels using a matrix metalloproteinase (MMP)-sensitive peptide as a crosslinker. The photocrosslinkable hydrogel system was able to support the *in vitro* formation of bilayered full-thickness skin constructs.

Chapter V focuses on the formulation and bioprinting of a protease-degradable bioink based on the pectin macromers functionalized with norbornene end groups. Suitable printability was achieved by ionic crosslinking using two different cation sources namely calcium chloride or barium chloride. Both cations allowed the design of bioinks with tuneable rheological and viscoelastic properties that were printed into highly elastic 3D structures.

Bioprinted cell-laden constructs with tuneable properties were produced by simply changing the photocrosslinking time, leading to distinct behaviour of embedded dermal fibroblasts.

Chapter VI discusses the results and main findings of the work, establishing correlations with the knowledge in the field. This chapter also provides main conclusions of the developed work and highlights new directions for future research.

1.5. References

- [1] J. Fenner, R.A.F. Clark, Chapter 1 - Anatomy, Physiology, Histology, and Immunohistochemistry of Human Skin, in: M.Z. Albanna, J.H.H. IV (Eds.), *Skin Tissue Engineering and Regenerative Medicine*, Academic Press, Boston, 2016, pp. 1-17.
- [2] G. Solanas, S.A. Benitah, Regenerating the skin: a task for the heterogeneous stem cell pool and surrounding niche, *Nat Rev Mol Cell Biol* 14 (2013) 737-48.
- [3] A. Totaro, M. Castellan, G. Battilana, F. Zanconato, L. Azzolin, S. Giulitti, M. Cordenonsi, S. Piccolo, YAP/TAZ link cell mechanics to Notch signalling to control epidermal stem cell fate, *Nat Commun* 8 (2017) 15206.
- [4] E.A. Rayment, Z. Upton, G.K. Shooter, Increased matrix metalloproteinase-9 (MMP-9) activity observed in chronic wound fluid is related to the clinical severity of the ulcer, *Br J Dermatol* 158 (2008) 951-61.
- [5] R.D. Wolcott, J.D. Hanson, E.J. Rees, L.D. Koenig, C.D. Phillips, R.A. Wolcott, S.B. Cox, J.S. White, Analysis of the chronic wound microbiota of 2,963 patients by 16S rDNA pyrosequencing, *Wound Repair Regen* 24 (2016) 163-74.
- [6] I.B. Wall, R. Moseley, D.M. Baird, D. Kipling, P. Giles, I. Laffafian, P.E. Price, D.W. Thomas, P. Stephens, Fibroblast dysfunction is a key factor in the non-healing of chronic venous leg ulcers, *J Invest Dermatol* 128 (2008) 2526-40.
- [7] R.G. Frykberg, J. Banks, Challenges in the Treatment of Chronic Wounds, *Adv Wound Care (New Rochelle)* 4 (2015) 560-582.
- [8] R.V. Shevchenko, S.L. James, S.E. James, A review of tissue-engineered skin bioconstructs available for skin reconstruction, *J R Soc Interface* 7 (2010) 229-58.
- [9] F. Groeber, M. Holeiter, M. Hampel, S. Hinderer, K. Schenke-Layland, Skin tissue engineering--in vivo and in vitro applications, *Adv Drug Deliv Rev* 63 (2011) 352-66.
- [10] S. Pripotnev, A. Papp, Split thickness skin graft meshing ratio indications and common practices, *Burns* 43 (2017) 1775-1781.
- [11] G.C. Gurtner, M.A. Chapman, Regenerative Medicine: Charting a New Course in Wound Healing, *Adv Wound Care (New Rochelle)* 5 (2016) 314-328.

- [12] A.A. Leto Barone, M. Mastroianni, E.A. Farkash, C. Mallard, A. Albritton, R. Torabi, D.A. Leonard, J.M. Kurtz, D.H. Sachs, C.L. Cetrulo, Jr., Genetically modified porcine split-thickness skin grafts as an alternative to allograft for provision of temporary wound coverage: preliminary characterization, *Burns* 41 (2015) 565-74.
- [13] D.G. Armstrong, L.A. Lavery, C. Diabetic Foot Study, Negative pressure wound therapy after partial diabetic foot amputation: a multicentre, randomised controlled trial, *Lancet* 366 (2005) 1704-10.
- [14] A. Sood, M.S. Granick, N.L. Tomaselli, Wound Dressings and Comparative Effectiveness Data, *Adv Wound Care (New Rochelle)* 3 (2014) 511-529.
- [15] A.G. Haddad, G. Giatsidis, D.P. Orgill, E.G. Halvorson, Skin Substitutes and Bioscaffolds: Temporary and Permanent Coverage, *Clin Plast Surg* 44 (2017) 627-634.
- [16] N.S. Greaves, S.A. Iqbal, M. Baguneid, A. Bayat, The role of skin substitutes in the management of chronic cutaneous wounds, *Wound Repair Regen* 21 (2013) 194-210.
- [17] H.W. Lim, S.A.B. Collins, J.S. Resneck, Jr., J.L. Bolognia, J.A. Hodge, T.A. Rohrer, M.J. Van Beek, D.J. Margolis, A.J. Sober, M.A. Weinstock, D.R. Nerez, W. Smith Begolka, J.V. Moyano, The burden of skin disease in the United States, *J Am Acad Dermatol* 76 (2017) 958-972 e2.
- [18] C. Lindholm, R. Searle, Wound management for the 21st century: combining effectiveness and efficiency, *Int Wound J* 13 Suppl 2 (2016) 5-15.
- [19] A. Markova, E.N. Mostow, US skin disease assessment: ulcer and wound care, *Dermatol Clin* 30 (2012) 107-11, ix.
- [20] American-Burn-Association, Burn incidence and treatment in the US: 2016 fact sheet., National Burn Repository (2016).
- [21] Y.S. Zhang, A. Khademhosseini, Advances in engineering hydrogels, *Science* 356 (2017) eaaf3627.
- [22] B. Balakrishnan, M. Mohanty, P.R. Umashankar, A. Jayakrishnan, Evaluation of an in situ forming hydrogel wound dressing based on oxidized alginate and gelatin, *Biomaterials* 26 (2005) 6335-42.
- [23] G. Sun, X. Zhang, Y.I. Shen, R. Sebastian, L.E. Dickinson, K. Fox-Talbot, M. Reinblatt, C. Steenbergen, J.W. Harmon, S. Gerecht, Dextran hydrogel scaffolds enhance angiogenic responses and promote complete skin regeneration during burn wound healing, *Proc Natl Acad Sci USA* 108 (2011) 20976-81.
- [24] G. Dabiri, E. Damstetter, T. Phillips, Choosing a Wound Dressing Based on Common Wound Characteristics, *Adv Wound Care (New Rochelle)* 5 (2016) 32-41.
- [25] G. Eke, N. Mangir, N. Hasirci, S. MacNeil, V. Hasirci, Development of a UV crosslinked biodegradable hydrogel containing adipose derived stem cells to promote vascularization for skin wounds and tissue engineering, *Biomaterials* 129 (2017) 188-198.

- [26] H. Kim, W.H. Kong, K.Y. Seong, D.K. Sung, H. Jeong, J.K. Kim, S.Y. Yang, S.K. Hahn, Hyaluronate-Epidermal Growth Factor Conjugate for Skin Wound Healing and Regeneration, *Biomacromolecules* 17 (2016) 3694-3705.
- [27] Z. Fan, B. Liu, J. Wang, S. Zhang, Q. Lin, P. Gong, L. Ma, S. Yang, A Novel Wound Dressing Based on Ag/Graphene Polymer Hydrogel: Effectively Kill Bacteria and Accelerate Wound Healing, *Adv. Funct. Mater.* 24 (2014) 3933-3943.
- [28] Y. Yang, J. Zhang, Z. Liu, Q. Lin, X. Liu, C. Bao, Y. Wang, L. Zhu, Tissue-Integratable and Biocompatible Photogelation by the Imine Crosslinking Reaction, *Adv. Mater.* 28 (2016) 2724-30.
- [29] N. Annabi, D. Rana, E. Shirzaei Sani, R. Portillo-Lara, J.L. Gifford, M.M. Fares, S.M. Mithieux, A.S. Weiss, Engineering a sprayable and elastic hydrogel adhesive with antimicrobial properties for wound healing, *Biomaterials* 139 (2017) 229-243.
- [30] K. Obara, M. Ishihara, T. Ishizuka, M. Fujita, Y. Ozeki, T. Maehara, Y. Saito, H. Yura, T. Matsui, H. Hattori, M. Kikuchi, A. Kurita, Photocrosslinkable chitosan hydrogel containing fibroblast growth factor-2 stimulates wound healing in healing-impaired db/db mice, *Biomaterials* 24 (2003) 3437-44.
- [31] S.T. Boyce, D.J. Christianson, J.F. Hansbrough, Structure of a collagen-GAG dermal skin substitute optimized for cultured human epidermal keratinocytes, *J. Biomed. Mater. Res.* 22 (1988) 939-57.
- [32] K.R. Kirker, Y. Luo, J.H. Nielson, J. Shelby, G.D. Prestwich, Glycosaminoglycan hydrogel films as bio-interactive dressings for wound healing, *Biomaterials* 23 (2002) 3661-3671.
- [33] R. Pereira, A. Carvalho, D.C. Vaz, M.H. Gil, A. Mendes, P. Bartolo, Development of novel alginate based hydrogel films for wound healing applications, *Int. J. Biol. Macromol.* 52 (2013) 221-30.
- [34] K. Murakami, H. Aoki, S. Nakamura, S. Nakamura, M. Takikawa, M. Hanzawa, S. Kishimoto, H. Hattori, Y. Tanaka, T. Kiyosawa, Y. Sato, M. Ishihara, Hydrogel blends of chitin/chitosan, fucoidan and alginate as healing-impaired wound dressings, *Biomaterials* 31 (2010) 83-90.
- [35] F. Munarin, M.C. Tanzi, P. Petrini, Advances in biomedical applications of pectin gels, *Int. J. Biol. Macromol.* 51 (2012) 681-9.
- [36] I. Fraeye, I. Colle, E. Vandevenne, T. Duvetter, S. Van Buggenhout, P. Moldenaers, A. Van Loey, M. Hendrickx, Influence of pectin structure on texture of pectin-calcium gels, *Innovative Food Science & Emerging Technologies* 11 (2010) 401-409.
- [37] A. Noreen, Z.I. Nazli, J. Akram, I. Rasul, A. Mansha, N. Yaqoob, R. Iqbal, S. Tabasum, M. Zuber, K.M. Zia, Pectins functionalized biomaterials; a new viable approach for biomedical applications: A review, *Int. J. Biol. Macromol.* 101 (2017) 254-272.

- [38] E.G. Maxwell, I.J. Colquhoun, H.K. Chau, A.T. Hotchkiss, K.W. Waldron, V.J. Morris, N.J. Belshaw, Modified sugar beet pectin induces apoptosis of colon cancer cells via an interaction with the neutral sugar side-chains, *Carbohydr. Polym.* 136 (2016) 923-9.
- [39] J.C. Villanova, E. Ayres, R.L. Orefice, Design, characterization and preliminary in vitro evaluation of a mucoadhesive polymer based on modified pectin and acrylic monomers with potential use as a pharmaceutical excipient, *Carbohydr. Polym.* 121 (2015) 372-81.
- [40] R.-h. Liang, L.-h. Wang, J. Chen, W. Liu, C.-m. Liu, Alkylated pectin: Synthesis, characterization, viscosity and emulsifying properties, *Food Hydrocolloids* 50 (2015) 65-73.
- [41] M. Tummalapalli, M. Berthet, B. Verrier, B.L. Deopura, M.S. Alam, B. Gupta, Composite wound dressings of pectin and gelatin with aloe vera and curcumin as bioactive agents, *Int. J. Biol. Macromol.* 82 (2016) 104-13.
- [42] F. Munarin, S.G. Guerreiro, M.A. Grellier, M.C. Tanzi, M.A. Barbosa, P. Petrini, P.L. Granja, Pectin-based injectable biomaterials for bone tissue engineering, *Biomacromolecules* 12 (2011) 568-77.
- [43] S.C. Neves, D.B. Gomes, A. Sousa, S.J. Bidarra, P. Petrini, L. Moroni, C.C. Barrias, P.L. Granja, Biofunctionalized pectin hydrogels as 3D cellular microenvironments, *J Mater Chem B* 3 (2015) 2096-2108.
- [44] T. Marras-Marquez, J. Pena, M.D. Veiga-Ochoa, Robust and versatile pectin-based drug delivery systems, *Int. J. Pharm.* 479 (2015) 265-76.
- [45] P. Coimbra, P. Ferreira, H.C. de Sousa, P. Batista, M.A. Rodrigues, I.J. Correia, M.H. Gil, Preparation and chemical and biological characterization of a pectin/chitosan polyelectrolyte complex scaffold for possible bone tissue engineering applications, *Int. J. Biol. Macromol.* 48 (2011) 112-8.
- [46] M.R. Guilherme, T.A. Moia, A.V. Reis, A.T. Paulino, A.F. Rubira, L.H. Mattoso, E.C. Muniz, E.B. Tambourgi, Synthesis and water absorption transport mechanism of a pH-sensitive polymer network structured on vinyl-functionalized pectin, *Biomacromolecules* 10 (2009) 190-6.
- [47] G. Jürgen, B. Thomas, B. Torsten, A.B. Jason, C. Dong-Woo, D.D. Paul, D. Brian, F. Gabor, L. Qing, A.M. Vladimir, M. Lorenzo, N. Makoto, S. Wenmiao, T. Shoji, V. Giovanni, B.F.W. Tim, X. Tao, J.Y. James, M. Jos, Biofabrication: reappraising the definition of an evolving field, *Biofabrication* 8 (2016) 013001.
- [48] S. Michael, H. Sorg, C.T. Peck, L. Koch, A. Deiwick, B. Chichkov, P.M. Vogt, K. Reimers, Tissue engineered skin substitutes created by laser-assisted bioprinting form skin-like structures in the dorsal skin fold chamber in mice, *PLoS One* 8 (2013) e57741.
- [49] N. Wei Long, Q. Jovina Tan Zhi, Y. Wai Yee, N. May Win, Proof-of-concept: 3D bioprinting of pigmented human skin constructs, *Biofabrication* 10 (2018) 025005.

- [50] K.W. Binder, W. Zhao, T. Aboushwareb, D. Dice, A. Atala, J.J. Yoo, In situ bioprinting of the skin for burns, *J Am Coll Surg* 211 (2010) S76.
- [51] A. Skardal, S.V. Murphy, K. Crowell, D. Mack, A. Atala, S. Soker, A tunable hydrogel system for long-term release of cell-secreted cytokines and bioprinted in situ wound cell delivery, *J Biomed Mater Res B Appl Biomater* 105 (2017) 1986-2000.
- [52] S.V. Murphy, A. Atala, 3D bioprinting of tissues and organs, *Nat. Biotechnol.* 32 (2014) 773-85.
- [53] M. Hospodiuk, M. Dey, D. Sosnoski, I.T. Ozbolat, The bioink: A comprehensive review on bioprintable materials, *Biotechnol. Adv.* 35 (2017) 217-239.
- [54] J.-A. Yang, J. Yeom, B.W. Hwang, A.S. Hoffman, S.K. Hahn, In situ-forming injectable hydrogels for regenerative medicine, *Prog. Polym. Sci.* 39 (2014) 1973-1986.
- [55] I.T. Ozbolat, M. Hospodiuk, Current advances and future perspectives in extrusion-based bioprinting, *Biomaterials* 76 (2016) 321-43.
- [56] W. Lee, J.C. Debasitis, V.K. Lee, J.H. Lee, K. Fischer, K. Edminster, J.K. Park, S.S. Yoo, Multi-layered culture of human skin fibroblasts and keratinocytes through three-dimensional freeform fabrication, *Biomaterials* 30 (2009) 1587-95.
- [57] N. Liu, S. Huang, B. Yao, J. Xie, X. Wu, X. Fu, 3D bioprinting matrices with controlled pore structure and release function guide in vitro self-organization of sweat gland, *Sci Rep* 6 (2016) 34410.
- [58] C. Nieves, G. Marta, F.d.C. Juan, V. Diego, L.J. Jose, 3D bioprinting of functional human skin: production and in vivo analysis, *Biofabrication* 9 (2017) 015006.
- [59] L.J. Pourchet, A. Thepot, M. Albouy, E.J. Courtial, A. Boher, L.J. Blum, C.A. Marquette, Human Skin 3D Bioprinting Using Scaffold-Free Approach, *Adv Healthc Mater* 6 (2017) 1601101.

CHAPTER II

GENERAL INTRODUCTION

This chapter was based on the following publications:

- **R.F. Pereira**, A. Sousa, C.C. Barrias, A. Bayat, P.L. Granja, P.J. Bártolo, Advances in bioprinted cell-laden hydrogels for skin tissue engineering, *Bio manufacturing Reviews* 2 (2017) 1.
- **R.F. Pereira**, P.J. Bartolo, Traditional Therapies for Skin Wound Healing, *Adv Wound Care (New Rochelle)* 5 (2016) 208-229.
- **R.F. Pereira**, P.J. Bártolo, 3D bioprinting of photocrosslinkable hydrogel constructs, *J. Appl. Polym. Sci.* 132 (2015) 42458.
- **R.F. Pereira**, P.J. Bártolo, 3D Photo-Fabrication for Tissue Engineering and Drug Delivery, *Engineering* 1 (2015) 090-112.
- **R.F. Pereira**, P.J. Bártolo, Recent Advances in Additive Biomanufacturing, in: S.H.F.B.J.V.T. Yilbas (Ed.), *Comprehensive Materials Processing*, Elsevier, Oxford, 2014, pp. 265-284.
- **R.F. Pereira**, C.C. Barrias, P.L. Granja, P.J. Bartolo, Advanced biofabrication strategies for skin regeneration and repair, *Nanomedicine (Lond)* 8 (2013) 603-21.

Abstract

Skin is the largest organ of the human body, acting as a barrier with protective, immunologic and sensory functions. The reconstruction of functional skin remains a huge challenge due to its multilayer structure and the organized presence of different cell types within an intricate extracellular matrix (ECM). Bioprinting comprises one main strategy of biofabrication that allows the additive manufacturing of cellular 3D constructs for skin tissue engineering by precisely printing biocompatible materials, cells and biochemicals in predesigned spatial positions. This unique feature, combined with the computer controlled printing and medical imaging techniques, enable researchers and clinicians to generate patient-specific constructs partly replicating the compositional and architectural organization of the skin. Bioprinting has been used to automatically dispense hydrogels with skin cells located in prescribed sites to promote skin formation *in vitro* and *in vivo*. Current skin bioprinting approaches mostly rely on the sequential printing of fibroblasts and keratinocytes embedded within a homogeneous hydrogel. Recent works have also focused on the printing of additional cells, including melanocytes, amniotic fluid-derived stem cells (AFSs), endothelial progenitor cells (EPCs), and adipose-derived stem cells (ASCs). Although some of these approaches have already been translated to pre-clinical scenarios, they still present limitations in terms of fully replicating the cellular and ECM heterogeneity of native skin. The success of bioprinting for skin repair depends on the design of bioinks that exhibit suitable printability and fast crosslinking schemes, support the function of printed cells and stimulate the production of cell-secreted ECM components. Photocrosslinkable hydrogels are attractive materials for the design of bioinks as they provide fast polymerization under cytocompatible conditions and exceptional spatiotemporal control over the gelation process. To better mimic the human skin, novel developments in dedicated bioprinting technologies are necessary, namely for the design of advanced bioinks and the printing of vascularised tissue constructs.

Keywords: bioprinting; bioink; hydrogel; photopolymerization; skin tissue engineering.

2.1. Introduction

The integumentary system comprises the skin and respective appendages, being responsible for many vital functions in the body, such as the homeostasis, protection and transmission of sensorial information [1-3]. The skin is the most superficial and the largest organ of the human body, acting as an efficient barrier at the interface between the internal organs and the external environment. However, the permanent exposure to environmental stresses may result in a variety of skin injuries induced by acute trauma, thermal, chemical, mechanical, microbial or radiation effects. Additional causes of skin loss also include genetic disorders, chronic wounds and surgical interventions [2, 4]. Depending on the lesion type, extension and depth, both superficial and deep skin layers may be damaged and the innate healing ability of skin may be dramatically reduced or inhibited. In the most critical clinical scenarios (e.g., deep dermal or third degree burns and full-thickness wounds) hypodermal adipose tissue, fascia, internal tissues and organs may also be injured, leading to significant morbidity, dysfunction and potentially death [3]. Skin burns and chronic wounds represent one of the most debilitating, painful and costly health conditions, with tremendous economic and social impact. Typically, these wounds require extensive hospitalization, labour intensive clinical procedures and costly wound care products, representing a major burden over total world healthcare expenditure [5-7].

Several skin therapies and wound care products have been developed and tested through pre-clinical and randomized controlled clinical trials with the ultimate goal of promoting the repair of functional skin [8-17]. Traditional treatments are based on the use of grafts (which includes auto-, allo- and xenograft varieties), herbal and animal-derived compounds, and traditional dressings. These therapies have been used since ancient times mainly due to their acceptable clinical efficacy, simplicity and affordability, offering a broad range of therapeutic effects, such as anti-inflammatory, cell stimulatory, antimicrobial and wound debridement [18-23]. However, in certain types of wounds, such as deep burns and chronic wounds, more sophisticated and effective treatments are usually needed [15, 24-26]. Advanced therapies assume a prominent role in the management of such wounds, as they explore the basic principles and elements of tissue engineering to produce both cellular and acellular constructs for skin reconstruction [1, 2, 27]. In the most classical approach, known as scaffold-based or top-down, scaffolds are fabricated through either conventional or additive manufacturing processes, and subsequently seeded with autologous or allogeneic

cells. The cellular scaffold is then cultured *in vitro* to produce a tissue-engineered construct for subsequent implantation into the lesion site [28-31]. Although this approach allows for good control over the scaffold characteristics (when additive manufacturing processes are used) and cell-scaffold interactions, it fails to place individual cells at specific locations throughout the scaffold, thereby not mimicking the intricate cellular organization of natural tissues at micro- and nanoscale. Other important drawbacks are related with the limited cell density and insufficient vascularization, which may lead to tissue malformation and heterogeneous tissue growth [32, 33]. To address these limitations, an alternative approach, termed scaffold-free or bottom-up approach, has been used to generate 3D structures resembling the biological and functional organization of human tissues [34-38]. In this approach, one strategy of biofabrication, termed bioassembly, is applied to generate hierarchical constructs with a prescribed two-dimensional (2D) or 3D organization. Larger and complex tissue constructs are obtained through the automated assembly of pre-formed cell-containing fabrication units (e.g., cell aggregates, cell fibres, cell sheets or microtissues) produced by different techniques, such as self-assembled aggregation, microfabrication or microfluidics [34, 39, 40]. Bottom-up approach addresses some of the limitations of the top-down approach by the creation of tissue constructs with multiple cell types placed at specific 3D locations with a high cell density [32, 41, 42].

Bioprinting, another main strategy of biofabrication, is attracting significant interest from researchers working in the field of tissue engineering and regenerative medicine due to their unique ability to print single cells or cell-aggregates, bioactive molecules and biomaterials into structurally organized constructs, in a layer-by-layer fashion, with high resolution and accuracy [39, 40, 43, 44]. Bioprinting provides a powerful tool to arrange such components within a 3D environment on a length scale comparable to the complex heterogeneity found in natural tissue (10-100 μm), enabling new perspectives as well as unmatched possibilities in the design of biomimetic substitutes for tissue regeneration [39, 45, 46]. In the context of skin tissue engineering, bioprinting has been explored for the fabrication of 3D constructs containing skin cells positioned in distinct layers to resemble the anatomy of native skin [47, 48].

2.2. Skin structure and composition

The skin serves as a protective layer against the invasion of pathogens and external agents, playing a critical role in thermal regulation, homeostasis and

transmission of sensory information [3, 49, 50]. From an anatomical point, skin consists of three sequential layers of epidermis, dermis and hypodermis (**Figure 2.1**), each having distinct functions, biomechanical properties and cellular constituents (**Table 2.1**).

Epidermis is the most superficial skin layer, being composed of keratinized stratified squamous epithelium and organized into four or five main layers containing keratinocytes in different stages of proliferation, differentiation and keratinization [49, 51]. Although the epidermis is an avascular layer, it is under constant renewal due to the presence of epidermal basal cells and stem-like cells in the basal layer and hair follicles [52]. The main cellular constituents include keratinocytes, melanocytes, Merkel cells and Langerhans cells [1, 53]. The underlying dermis, separated from the epidermis by a basement membrane, is mainly composed of ECM molecules arranged in a dense matrix of connective tissue, rich in collagen and elastin fibres, that provides structural and mechanical support to the skin [54]. It is a highly dynamic, vascularized layer that supports the epidermis, provides flexibility and strength to the skin, and also contains blood vessels, sweat and sebaceous glands, hair follicles and sensory receptors [53, 55]. The predominant cells in dermis are heterogeneous subpopulations of fibroblasts, which are responsible for the production of ECM components [56]. Other cell types like mast cells and macrophages are also present, playing important roles in immune and inflammatory responses [52, 53]. Two distinct regions are present in the dermis, namely the papillary dermis and reticular dermis. The papillary region is the most superficial and is composed of higher cellular density along with less organized type I and type III collagen bundles and fine elastic fibres. The reticular dermis is a thicker and deeper region consisting of highly organized type I collagen and elastic fibres. It also contains hair follicles, sebaceous glands, sweat glands, cutaneous sensory receptors and blood vessels. The hypodermis, which acts as an energy source and heat insulator, is located just below the dermis and is mainly composed of adipose tissue and collagen, attaching the dermis to underlying tissues [53, 55]. Adnexal skin structures such as sweat, apocrine and sebaceous glands, nails and hair follicles display cosmetic, protective, and temperature regulation functions. These structures, together with the dermal vasculature, makes challenging the development of wound care products and therapies capable of fully restoring the skin anatomy and functions.

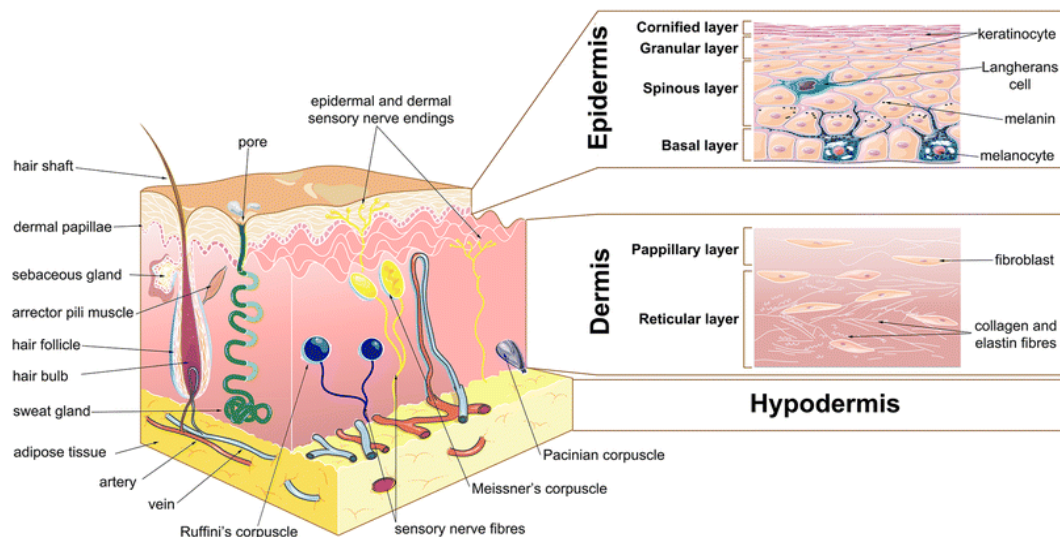


Figure 2.1. Schematic representation of the multi-layered structure of human skin. Emphasis is given to the four main layers of epidermis and its cellular constituents, including keratinocytes, Langerhans cells and melanocytes. Two distinct regions of dermis are also represented along with fibroblasts and zonal organization of both collagen and elastin fibres. Specialized elements, such as sweat glands, hair roots, sensory cells, blood, and lymph vessels are also presented. Skin structures are not to scale for simplification (image from Servier Medical Art freeware image bank).

Table 2.1. Skin cells: location and main functions.

Skin layer	Cell type	Main functions
Epidermis	Keratinocytes	Production of keratin (provides strength and protection to the skin) and lamellar granules (secret several compounds like lipids, proteins and hydrolytic enzymes, that contribute to the barrier function)
	Melanocytes	Production of melanin, a pigment that confers skin coloration and protects cell nucleus from UV radiation
	Merkel and Langerhans cells	Sensing and immunological defence
	Basal cells and stem cells	Located in the basal layer and hair follicle bulge, ensure tissue renewal
Dermis	Fibroblasts	Production of ECM components
	Mast cells and macrophages	Immune and inflammatory response
Hypodermis	Adipocytes	Energy storage and secretion of molecules that regulate processes beyond metabolism

The human skin ECM, a gel-like matrix secreted by fibroblasts and epidermal cells as an intricate structural scaffold, contains several macromolecules (**Table 2.2**). It surrounds the cells and is composed of a variety of polysaccharides, collagen proteins, and water. ECM molecules can be divided into (1) fibrous structural proteins, which provide strength, and (2) proteoglycans that confer hydration and controlled permeability. Ideally, the composition of wound care products should contain ECM molecules present in the native skin. However, despite the efforts in the extraction, isolation and purification of these ECM molecules, the extraction yield is often low and the associated costs still remain too high.

Table 2.2. Examples of extracellular matrix molecules present in the human skin [51].

ECM molecule	Location and functions
Collagen I, III and IV	Structural components of the ECM, responsible for the dermis integrity Collagen III is prominent in the early proliferation phase of the healing process, being replaced by collagen I in the remodelling phase Type IV associates with specialized molecules like laminin and proteoglycans to form the basement membrane
Elastin and fibrillin	Main components of the elastic fibres located in deeper dermis Provide skin resilience, allowing flexibility and recoil after stretching
Fibronectin	Found in dermis and basement membrane Plays an important role in cell adhesion and communication
Laminin	Cell adhesion molecules found in the basal lamina Multiple roles throughout the healing process, including angiogenesis
Hyaluronic acid	Distributed throughout the epidermis and dermis Provides hydration to the dermis
Dermatopontin	Distributed throughout the ECM Involved in cell attachment and collagen fibril formation
Periostin	Present around hair follicles Stimulates keratinocyte proliferation

2.3. Wound healing process

Wounds can be defined as an injury or disruption to the anatomical structure that compromises tissue function. Depending on the underlying cause, wounds can be classified into acute or chronic. Major causes of acute wounds include mechanical and chemical injuries, burns and surgical incisions. Chronic wounds exhibit a slow healing

rate and often involve significant tissue loss, ultimately affecting internal tissues and organs. They are mostly caused by vascular insufficiency, diabetes mellitus, local-pressure effects and arterial occlusion.

From the onset of injury, the human body initiates a series of complex and coordinated signalling pathways, involving the interaction between several ECM components, cells, cytokines and growth factors, aimed at tissue repair and reconstruction of lost cutaneous tissue [51, 57]. The healing of an acute wound proceeds in a sequence of overlapping and well-orchestrated events throughout different phases of haemostasis, inflammation, migration, proliferation and maturation (**Figure 2.2**). The transition between these phases is tightly regulated by wound healing mediators such as cytokines, chemokines and growth factors, which are produced by several cell types. Acute wounds proceed orderly and timely throughout these phases until repair, while in chronic wounds underlying pathophysiology or microbial invasion arrests the wound healing process, usually in the inflammatory phase, resulting in the failure of granulation tissue formation and subsequent reepithelialisation for a period longer than three months [58].

2.3.1. Acute wound healing

2.3.1.1. Haemostasis

The first response of the human body to an injury is haemostasis, which is mediated by platelets, and involves the formation of a fibrin clot that circumvents the bleeding, acts as a provisional ECM for cell migration, and loosely joins the wound edges [59, 60]. In an early stage, platelets release several factors (e.g., platelet factor 4, angiostatin) that sequester various growth factors and promote initial inhibition of angiogenesis [61]. In a later stage, platelets trapped within the clot suffer degranulation and release a plethora of cytokines and growth factors (e.g. transforming growth factor- β (TGF- β), fibroblast growth factor (FGF), transforming growth factor- α (TGF- α), vascular endothelial growth factor (VEGF), platelet-derived growth factor (PDGF), and epidermal growth factor (EGF)) that are responsible for attracting fibroblasts, inflammatory and vascular cells to the wound site [57, 59, 62].

2.3.1.2. Inflammation

Inflammation is essential in wound healing, allowing not only tissue breakdown and removal of non-functional cells and pathogens, but also stimulating keratinocytes, fibroblasts and endothelial cells [57, 59, 62]. Early inflammatory response mobilizes several cells to the wound site for wound cleaning and removal of contaminants. Neutrophils are the first cells to arrive in the wound site, playing a key role in host defence and debridement of damaged tissues, by generating free radicals and releasing proteolytic enzymes (e.g., serine proteases). Neutrophils also release inflammatory mediators like tumour necrosis factor alpha (TNF- α) and interleukin-1 (IL-1), which recruit and activate fibroblasts and epithelial cells. After neutrophils are depleted in the wound, circulating monocytes are attracted to the wound site by soluble mediators and degraded ECM components (e.g., collagen and fibronectin fragments), bind to the ECM via integrin receptors, and differentiate into tissue macrophages. These macrophages display a phagocytic function and produce collagenases and elastase to facilitate the breaking down of devitalised tissues. They also produce inhibitors for these enzymes, which is essential for the regulation of their proteolytic activity. In addition, macrophages regulate the transition between the inflammatory and proliferative phases of the wound healing through the release of a variety of growth factors and cytokines, including the PDGF, FGF, VEGF, IL-1, interleukin-6 (IL-6), insulin-like growth factor-one (IGF-1), TGF- α and TGF- β [63]. These soluble mediators are responsible for stimulating angiogenesis and the recruitment and activation of fibroblasts.

2.3.1.3. Proliferation

In the proliferative phase, the wound healing proceeds with the formation of a scab and the migration, proliferation and differentiation of epithelial cells, dermal fibroblasts, and vascular endothelial cells from the adjacent healthy tissue. Keratinocytes, located at the wound periphery, are stimulated to migrate and proliferate into the lesion site to promote re-epithelialization by the synthesis of new epidermis [57]. Fibroblasts and endothelial cells are also recruited to initiate the synthesis of ECM components, the formation of granulation tissue, and the growth of new blood vessels from existing ones [51, 59, 64]. The movement of fibroblasts through the ECM and the provisional matrix depends on the concentration gradient of chemotactic factors and the alignment of fibrils. Fibroblasts initially bind to the ECM components (e.g., collagen, fibronectin, vitronectin and fibrin) via cell-surface integrin receptors and then extend a cytoplasmic projection to find another binding site. At this moment, MMPs, mostly

MMP-1, MMP-2, MMP-3, and MMP-9 are secreted by the cells to breakdown the attachment to the original ECM site, allowing the migration. MMPs degrade denatured collagen and other ECM components, which is essential for cells to interact with functional ECM. However, their activity must be tightly regulated by tissue inhibitors of metalloproteinases (TIMPs) to prevent degradation of functional matrix. Fibroblasts that migrate into the provisional matrix proliferate and produce granulation tissue, rich in collagen, elastin and proteoglycans. Some of fibroblasts are converted into myofibroblasts, which are involved in wound contraction and re-epithelialization [57, 62, 64].

2.3.1.4. Remodelling

At the final stage, the wound healing involves a long maturation phase, in which the wound edges move towards the centre (wound contraction), and the new tissue is continuously remodelled in order to approximate its properties to those of the native skin. This phase can take several weeks to months, and is marked by changes in the ECM composition, with re-organization of collagen fibres and collagen crosslinking [57, 65]. Despite the continuous remodelling process, adult wound healing predictably results in a scar tissue with a tensile strength that only achieves 80% of its native properties, and also impairs the flexibility, mobility and esthetical outcomes [51].

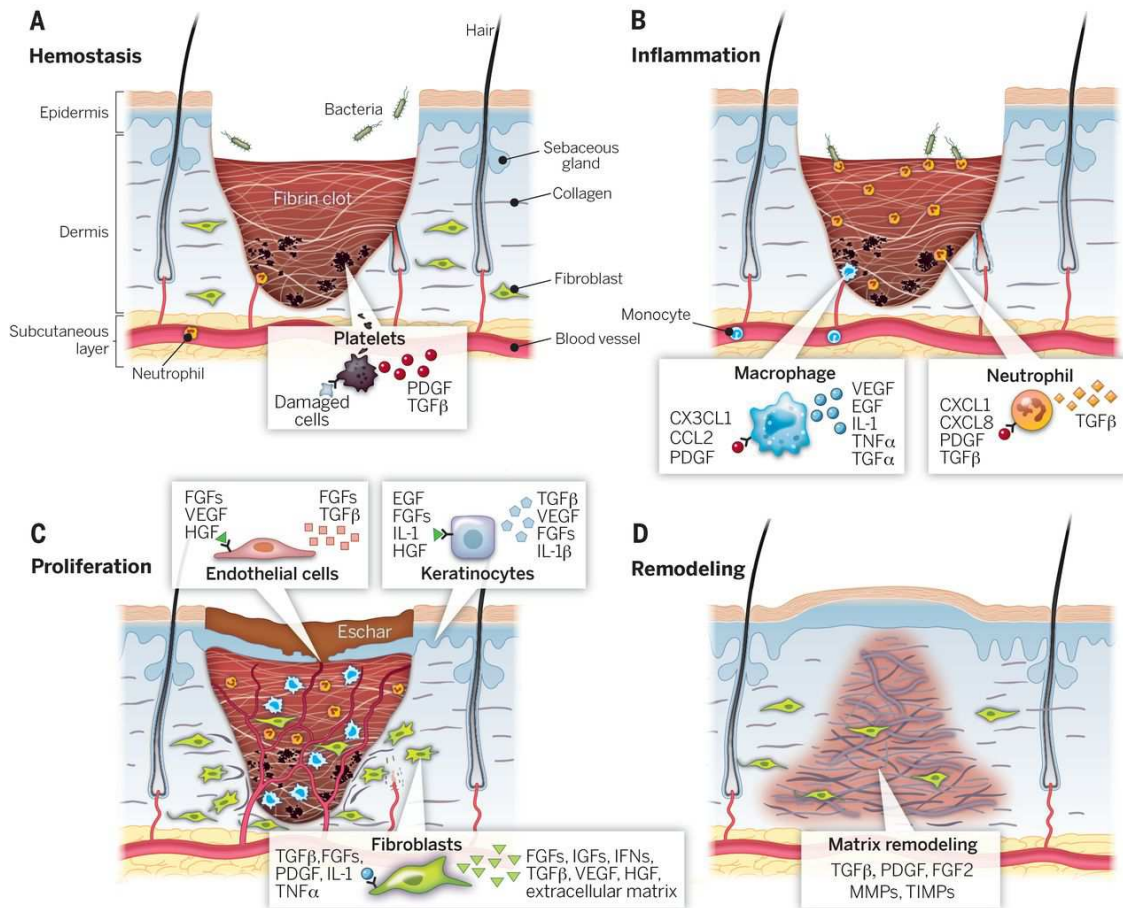


Figure 2.2. Acute wound healing process. Classical stages of wound healing are divided into four phases of **(A)** haemostasis, **(B)** inflammation, **(C)** proliferation, and **(D)** remodelling [63]. Abbreviations: PDGF – platelet-derived growth factor; TGF – transforming growth factor; FGFs – fibroblast growth factors; IL-1 – interleukin-1; TNF – tumour necrosis factor; KGF – keratinocyte growth factor; IGF – insulin-like growth factor; IFN – interferon; VEGF – vascular endothelial growth factor; HGF – hepatocyte growth factor; MMP – matrix metalloproteinase; TIMP – tissue inhibitor of metalloproteinase.

2.3.2. Chronic wound healing

Chronic wounds are often associated with microbial contamination, persistent infection, excessive production of exudate and repeated tissue trauma, failing to achieve tissue repair. Although the molecular mechanisms that lead to impaired wound healing are not fully understood, the healing failure in chronic wounds is attributed, in part, to both prolonged inflammation and deregulation of proteases and their inhibitors, which leads to an imbalance between ECM deposition and degradation [66].

Chronic wounds are characterized by increased levels of proinflammatory cellular infiltrates (e.g., polymorphonuclear leukocytes, neutrophils, macrophages,

foreign body giant cells) and deregulation of proinflammatory cytokines [67, 68]. Increased infiltration of poly and mononuclear cells results in excessive production of proteases (e.g., elastase, MMP-8, MMP-9) and ROS, which cause extensive tissue damage and contribute to prolong the inflammatory phase [69, 70]. Elevated levels of certain MMPs (e.g., MMP-9) can also ablate important growth factors and other pro-healing molecules, arresting the healing process and stimulating inflammation. Another important feature of chronic wound healing is the premature cell senescence due to the excessive production of ROS that can cause direct damage to cell membranes [71]. Depending on the level and length of ROS exposure, as well as on the physiologic state of the cell, oxidative stress can induce either senescence or apoptosis, leading to alterations on the cell phenotype and functions or dead, respectively [72]. These alterations were observed in senescent fibroblasts derived from chronic wounds, which showed compromised migratory capacity [71]. Although the mechanisms underlying cell senescence in chronic wounds are poorly understood, premature aging can affect not only the deposition of ECM molecules and granulation formation, but also impair the ability of cells to secret and release factors for cell recruitment [73].

Another important feature of chronic wounds is the common presence of high levels of bacteria in the wound bed, which results in direct tissue damage and stimulates the continual recruitment of inflammatory cells (e.g., neutrophils and macrophages) with consequent release of cytokines and ROS that contribute to trigger and maintain inflammatory cascades [74]. Pathogens in the wound bed contribute not only to altered ECM homeostasis and increased protease levels, but can also secrete proteolytic enzymes that can activate host MMPs [66]. Bacteria that colonise chronic wounds often form polymicrobial biofilms composed of an ECM containing several types of extracellular polymeric substances that provides an optimal microenvironment in which embedded bacteria develop higher resistance to both the host immune response and the action of antibiotics [75]. The main distinctive features between acute and chronic wounds are summarized in **Table 2.3**.

Table 2.3. Main events of the wound healing process and distinctive characteristics between acute and chronic wounds [76, 77].

Healing phase	Target	Acute wound	Chronic wound
Haemostasis and inflammation	Haemostasis		Deposition of fibrin matrix
	Bacteria load Activation of keratinocytes and inflammatory cells	Deposition of fibrin matrix Neutrophil invasion	Hyperinflammation with increased proteolytic activity
Proliferation	Proliferation and migration of keratinocytes	Provisional matrix composed of collagen, proteoglycans, and elastin	Constant matrix degradation by proteolytic activity
	Proliferation of fibroblasts ECM deposition	Migration of fibroblasts and endothelial cells into the wound	Non-migratory epidermis Reduced fibroblast migration and blood vessel formation
	Angiogenesis	Inflammation resolved	Persistent inflammation
Remodelling	ECM remodelling	Reorganization of collagen fibres	Failure to progress to the remodelling phase Persistent inflammation
	Restoration of the barrier properties	Minimal scarring	Deficient vascularization Formation of immature matrix

2.4. Therapeutic options for skin reconstruction

The most suitable therapeutic treatment for skin wounds depends on numerous factors including the wound type, number of affected skin layers, level of exudate, extension of injury, and the overall health status of the patient [59]. Wound healing therapies can be broadly classified into conventional and advanced therapies, which have distinct levels of efficacy, clinical acceptance, and side effects.

2.4.1. Conventional therapies

Conventional wound care therapies comprise autografts and allografts, traditional dressings, solutions, creams, ointments and therapies based on traditional medicine.

Practices and compounds arising from traditional and complementary medicine (T&CM) have been used to create alternative therapies for wound healing due to their therapeutic activities, availability, affordability and relative low cost [78]. According to the World Health Organization (WHO), traditional medicine (TM), also referred as "alternative" or "complementary" medicine, underlies the use of traditional therapies towards the maintenance of health and the prevention, diagnosis, improvement or treatment of physical and mental illness [78]. More recently, the WHO proposed new definitions for the terms TM,¹ complementary medicine (CM),² and T&CM³ based on their history and integration into the dominant health-care system [79]. These therapies comprise practices, products, and knowledge from different countries, involving the use of living organisms and natural compounds obtained from a wide range of sources (e.g. animals, plants, fungi, minerals). Recent developments on extraction procedures, purification methods, processing methodologies, and clinical treatments allowed a significant increase in the quality, efficacy and safety of traditional therapies. However, the use of some therapies is largely supported by wisdom and experience acquired over years, rather than by strong scientific evidence. In the last few years, several laboratories focused on the mechanisms behind the therapeutic efficacy of traditional healing compounds, increasing the knowledge about their action mechanisms and biological activities.

2.4.1.1. Autografts and allografts

In the case of patients with skin lesions extended to the dermis or hypodermis, a complex treatment procedure is required. In these cases, the clinical 'gold standard' procedure relies on the use of split-thickness skin autografts or allografts, which contain all of the epidermis and marginal parts of the dermis [1, 2, 4]. For severe burns like deep partial- and full-thickness injuries, the early excision of the necrotic tissue followed by autologous skin grafting constitute the most effective treatment. Although the meshing technique maximizes the wound area covered by the grafts, autografts are naturally limited in their extent, induce scarring at donor sites and patient morbidity, and are associated to lengthy hospital stays, while allografts present ethical and safety issues related with disease transmission and may lead to immune rejection [80].

¹ "Traditional medicine has a long history. It is the sum total of the knowledge, skill, and practices based on the theories, beliefs, and experiences indigenous to different cultures, whether explicable or not, used in the maintenance of health as well as in the prevention, diagnosis, improvement or treatment of physical and mental illness."

² "The terms "complementary medicine" or "alternative medicine" refer to a broad set of health care practices that are not part of that country's own tradition or conventional medicine and are not fully integrated into the dominant health-care system. They are used interchangeably with traditional medicine in some countries."

³ "T&CM merges the terms TM and CM, encompassing products, practices and practitioners."

2.4.1.2. Herbal-derived compounds

Herbal-derived compounds are the most commonly used traditional therapies for the treatment of skin lesions. They include the application of herbs, herbal preparations and finished herbal products, containing biologically active compounds that stimulate the healing process. A variety of plants, native from different regions of the world, have been investigated and applied for the treatment of skin lesions [81, 82]. Examples include *Aloe vera*, *Calendula officinalis*, *Angelica sinensis*, and *Rosmarinus officinalis* L [83-85]. Herbal-based products are applied as extracts, emulsions, creams and ointments, being administered through topical, systemic and oral routes. Alternatively, some of these products have also been incorporated within dressings or nanoparticles in order to improve their stability and achieve a more controlled release [86, 87]. *Aloe vera*, also known as *Aloe barbadensis* Miller, is the most popular herb in wound healing. The gel extracted from the plant leaves is the most valuable product for the treatment of skin lesions, containing several biologically active compounds with anti-inflammatory, anti-septic and antimicrobial properties [83, 88]. Although the use of both topical and oral *Aloe vera* preparations is considered safe without serious side effects [89], some adverse reactions have been experienced by the patients. Topical preparations are commonly associated to skin itching, irritation, contact dermatitis, erythema and photodermatitis, while oral administration can lead to diarrhea and vomiting [83, 90].

2.4.1.3. Animal-derived products

Animal origin products, like honey and propolis, have been used in wound care since ancient times due to their therapeutic properties. Honey is a highly viscous and super concentrated acidic sugar solution (pH ~4.0) derived from nectar and modified by the honeybee, *Apis mellifera*. Its chemical composition includes carbohydrates (e.g., fructose, glucose, and sucrose), water, amino-acids, antioxidants, vitamins, minerals, and enzymes [81, 91]. Several therapeutic activities have been assigned to honey, including antibacterial, anti-inflammatory, antifungal, and the ability to stimulate angiogenesis, granulation, wound contraction and epithelialization. It also provides debriding effect, reduces edema and deodorizes the wound [92]. The administration of honey as a natural healing agent is considered safe, rarely resulting in allergic reactions or adverse effects. However, there are clinical trials reporting that the use of honey may result in itching, while the contact between honey and the wound site can be painful for the patient due to its acidic nature [93]. Propolis, also known as bee glue, is a resinous-like substance collected by honeybees from several tree species. It has a

complex composition, containing resin and balsam, wax, essential and aromatic oils, pollen and other substances [94, 95]. Among these constituents, the most representative are polyphenols like flavonoids (e.g. quercetin, galangin, chrysin), phenolic acids (e.g. *p*-Coumaric acid, caffeic acid, ferulic acid), and aromatic compounds, which play an important role in the pharmacological activities of propolis [95]. Propolis has been used in traditional medicine due to the wide range of biological properties (e.g., anti-oxidant, anti-inflammatory and antibacterial activity) and low toxicity [94]. Although the adverse reactions related to the use of propolis in wounds are poorly documented in the literature, contact dermatitis is referred as the most common side effect [96].

2.4.1.4. Living organisms

Living organisms like maggots and leeches are used in wound care to provide wound debridement and treat venously congested wounds, respectively. Maggot debridement therapy, also termed larval therapy or biosurgery, is rapidly growing due to its therapeutic effects such as wound debridement, capacity to inhibit or even eradicate the biofilm formation, and antimicrobial activity [97, 98]. Medicinal maggots are used for the debridement of diverse types of wounds (e.g., chronic, non-healing traumatic wounds) through the digestion and removal of devitalized or necrotic tissue, due to the secreted powerful proteolytic enzymes (e.g. collagenase, trypsin-like and chymotrypsin-like enzymes) [99]. Sterile maggots are introduced into the wound with the support of traditional bandages (e.g. gauzes) or modern dressings (e.g. Le Flap™), providing either free or constrained access to the lesion site [100]. The clinical use of maggot therapy is considered safe without significant side effects or allergic reactions for the patients. The most common adverse reactions include pain and discomfort associated to escaping maggots [101]. Leech therapy or hirudotherapy, is an alternative therapeutic treatment for diverse skin disorders that involves the administration of medicinal leeches (*Hirudo medicinalis*) into the injured site. Hirudotherapy has been used in plastic and reconstructive surgery since the ancient times to promote the healing of a wide range of lesions, including venously congested tissues, free flaps, pedicled flaps, replanted tissues and glaucoma [102]. The action mechanism underlying the medicinal leeches relies on the secretion of a complex mixture of compounds (e.g. vasodilators, anti-coagulants, anaesthetics, analgesics) with relevant biological and pharmacological properties from the salivary glands into the lesion site, locally stimulating the healing process. The main constituent of leech saliva is hirudin, which is a potent natural anticoagulant that inhibits the blood

coagulation through the binding to thrombin, allowing the ingestion of blood by the leeches. Hirudin also acts as a bacteriostatic and bactericidal agent [102, 103]. Possible side effects include bacterial infections, bleeding, local itching, allergies and anaemia [102-104].

2.4.1.5. Solutions, creams and ointments

Liquid and semi-solid preparations, such as creams (e.g. silver sulphadiazine) and solutions (e.g. povidone-iodine, sodium hypochlorite), have also been used as supportive anti-infective wound care products in daily clinical practice. They are commonly used as cleaning and antimicrobial agents, allowing wound bed preparation and decontamination [105, 106]. To extend their efficacy and facilitate their handling, most of these therapeutic compounds have been embedded within gauzes or incorporated within dressing materials [107, 108].

2.4.1.6. Traditional dressings

Traditional dressings like gauzes, cotton wool and natural or synthetic bandages are commonly used in wound care [109]. When applied to the wound, these products absorb high volumes of exudate, which may lead to the drying of the wound bed, and ultimately result in cell death and inhibition of the healing process. Additionally, traditional dressings are not able to provide a moist wound environment and may also adhere to the wound bed, which can cause trauma and removal of new epidermis [110]. As a result of these limitations, traditional dressings are commonly applied as secondary dressings or combined with other products such as hydrocolloid and alginate dressings, protecting the wound from the entrance of pathogens and absorbing exudates.

2.4.2. Advanced therapies

Advanced wound care therapies comprise modern wound dressings, bioengineered skin substitutes, and therapy devices. These therapies involve the use of biomaterials to design interactive dressings for wound management, biofabrication technologies to produce matrices for skin reconstruction, or devices to assist in the wound bed preparation and wound healing. Advanced therapies are usually applied in difficult-to-heal wounds (e.g., infected wounds), chronic wounds and extensive burns. Although these therapies are more effective, the costs associated to their manufacturing and treatments are generally higher when compared to conventional therapies.

2.4.2.1. Modern wound dressings

Lesions involving the loss of high amounts of skin require the immediate use of a dressing to protect the wound. Wound dressings are widely used due to their relatively low cost, ease of use, and effectiveness to clean, cover and protect the wound from the external environment. An ideal wound dressing should provide a moist environment to the wound bed, remove the excess of exudate, avoid maceration, minimize scar formation, protect the wound from infection and maintain an adequate exchange of gases. They must be flexible, permeable to water vapour, fit the lesion region, exhibit good adhesion to the wound bed and adequate mechanical properties [111, 112]. Some dressings also act as drug delivery systems, incorporating and releasing therapeutic agents into the wound bed [113, 114].

Modern dressings represent a viable alternative to traditional dressings and are often applied in the management of burns and chronic wounds. They are designed to provide wound coverage, prevent infection and skin desiccation, and create favourable conditions for the healing. A fundamental requirement of modern wound dressings is the ability to maintain a moist environment in the wound bed to promote cellular proliferation and migration, while absorbing the excess of exudate to avoid periwound damage [110]. Modern dressings can be obtained from natural and synthetic polymers or a combination of both [115, 116]. There are hundreds of wound dressings in the market available in different physical forms and material formulations. Depending on the application, dressings can perform additional functions such as wound hydration, release of bioactive agents and autolytic debridement [117]. As the wound healing is a dynamic process that leads to alterations in the wound bed and exudate levels in a time-dependent manner, changing the dressing type is often required along the healing process. Major categories of wound dressings commercially available are summarized in **Table 2.4**.

Table 2.4. Selected examples of commercially available wound dressings, main properties, and indications for use.

Dressing	Key characteristics	Indications	Products
Alginate	Soft, conformable, haemostatic	Irregular-shaped wounds, pressure ulcers, infected wounds, and venous insufficiency ulcers	CarboFLEX [®] (ConvaTEC) Suprasorb [®] (L&R USA, Inc)
Antimicrobial	Modify the wound bed bioburden	Wounds with risk of infection or infected*	AQUACEL [®] Ag Foam (ConvaTEC)
Collagen	Component of the skin; can form a gel on contact with the wound exudate	Partial- and full-thickness chronic wounds, surgical wounds, second-degree burns, abrasions and traumatic wounds	ColActive [®] Plus (Covalon Technologies)
Foam dressings	Absorption of high exudate volumes, provide a barrier to bacterial contamination	Partial- and full-thickness wounds	ALLEVYN* LIFE (Smith & Nephew, Inc)
Hydrocolloids	Absorb exudate, autolytic debridement, lower wound pH	Partial- and full-thickness wounds with or without necrotic tissue	DuoDERM [®] (ConvaTEC)
Hydrogels	Donate moisture to the wound bed; autolytic debridement	Sloughy or necrotic wounds; partial- and full-thickness wounds, necrotic wounds and minor burns	DermaSyn [™] (DermaRite Industries, LLC)
Medical Grade Honey	Manuka honey reduces edema, lowers wound pH, and debriding slough and eschar	Partial- and full-thickness wounds, pressure ulcers, leg ulcers, burns, donor sites, and surgical wounds	MANUKAhd lite [®] (ManukaMed USA, LLC)
Silicone Gel Sheets	Prevent or improve hypertrophic and keloid scars	Scar wounds	CICA-CARE [®] (Smith & Nephew, Inc)
Transparent Films	Wound inspection, impermeable to liquids, permeable to oxygen and moisture vapour	Partial-thickness wounds with little or no exudate	Suprasorb [®] F (L&R USA, Inc)

*Exudate absorption depends on each specific product.

2.4.2.2. Bioengineered skin substitutes

Bioengineered skin substitutes are manufactured wound care products based on cells, ECM-like biomaterials or their combination, being the most sophisticated products available for skin wounds. Skin substitutes are available as either cellular or acellular products, allowing the reconstruction of both epidermal and dermal skin layers (**Table 2.5**). They consist of a temporary or permanent scaffold material that serves as a template for cell adhesion, proliferation and differentiation, guiding the new tissue formation [118]. Skin substitutes are used in the treatment of difficult-to-heal wounds, chronic wounds and extensive burns, where the available donor skin is extremely limited (e.g., patients with >50% total body surface area). These products perform several key functions such as protecting the wound, reducing inflammatory responses, providing the dermal component to the wound bed, and reducing scarring [80, 118]. They can be classified as biological substitutes, synthetic substitutes or a combination of both. Biological substitutes can be further categorized into (1) natural scaffolds (e.g., decellularized matrix), (2) constructed scaffolds (e.g., crosslinked collagen matrix) or (3) cultured scaffolds (e.g., cultured epithelial graft) [80]. Skin substitutes are also classified based on the number of skin layers and the degree of functional similarity to the native skin, into epidermal, dermal and dermo-epidermal (composite) products. Commercially available skin substitutes are mainly composed of natural materials (e.g., collagen, chondroitin-6-sulfate, elastin, hyaluronic acid, and fibrin), with only few of them using synthetic materials (e.g., silicon, poly(ethylene oxide)–poly(butylene terephthalate (PEO/PBT), polyglycolic acid/poly(lactic acid) (PGA/PLA)). Most of the skin substitutes are made of decellularized allogeneic tissue derived from cadaver skin or xenogeneic tissue mainly of porcine and bovine origin. Allogenic biological products are associated to the risk of disease transmission and reduced skin graft take or rejection. Synthetic materials are free from the risk of disease transmission and contamination with biological molecules [80]. Major limitations are the permanent wound closure, poor vascularization, high manufacturing costs and lack of skin appendages [1, 24].

Epidermal skin substitutes

Epidermal substitutes are used in the treatment of epidermal lesions, and generally comprise a sheet of autologous keratinocytes isolated from the patient through a small biopsy (2–5 cm²). The fabrication of stratified cultured epithelial autografts (CEAs) is time-consuming and costly, resulting in a fragile sheet (difficult to handle and apply) with a shelf life of less than 24 hours [4]. CEAs have been

associated to variable clinical outcomes, which could be related to the confluency of cell layers. Subconfluent keratinocytes have also been investigated and can be applied to the wound bed through an aerosol of the cell suspension (e.g., CellSpray), in either culture medium or fibrin glue, showing better outcomes. Alternatively, subconfluent keratinocytes can also be cultured on delivery membranes (e.g., MySkin), precluding enzymatic detachment.

Dermal skin substitutes

Dermal substitutes are used to replace lost dermis, playing a major role in the treatment of chronic wounds and full-thickness burns. Dermal replacements consist of a 3D matrix, from natural or synthetic origin, that must be covered by a permanent epidermal substitute, usually an autologous split-thickness skin graft [118]. The majority of these substitutes are based on decellularized human cadaveric skin that closely mimics the composition and organization of native tissue, providing a natural ECM and a basement membrane. Amniotic membrane has also been explored for the development of human-derived products (FlōGraft[®] Amniotic Fluid-Derived Allograft), allowing temporary wound coverage. Animal-derived products have also been used, including collagen from cadaveric skin of foetal bovine, porcine small intestinal submucosa, porcine urinary bladder (e.g., Keramatrix[®], Integra[®] PriMatrix[®], Matristem[®]) and skin fish (e.g., Kerecis[™] Omega3 Wound). Dermal substitutes are available as acellular or cellularized products. The presence of viable cells in the dermal matrix provides the wound bed with several growth factors that stimulate the host cells, promoting faster cellular infiltration, angiogenesis and reepithelialisation [119]. Despite these outcomes, there is a general consensus about the need for clinical evidence regarding the efficacy of cellular substitutes compared to acellular matrices.

Dermo-epidermal skin substitutes

Dermo-epidermal substitutes comprise both epidermal and dermal layers in order to better mimic the anatomical structure of the skin. They are the most sophisticated and expensive tissue-engineered products for skin reconstruction. Most of these products contain allogeneic skin cells incorporated into a dermal matrix, acting as a temporary scaffold that provides growth factors, cytokines and ECM components to stimulate host cells in the wound bed. Dermo-epidermal substitutes are often associated to host rejection as allogeneic keratinocytes do not survive for long periods of time in the wound [4].

Table 2.5. Selected examples of commercially available bioengineered skin substitutes.

Skin substitute	Matrix	Cells	
Epidermal	CellSpray [®] (Clinical Cell Culture)	None	Autologous cultured keratinocytes (subconfluent cell suspension)
	Epicel [®] (Genzyme Biosurgery)	None	Autologous cultured keratinocytes (confluent cell sheet)
	MySkin [®] (CellTran Ltd)	Silicone support layer	Autologous cultured keratinocytes (subconfluent cell sheet)
Dermal (single layer)	Alloderm [®] (LifeCell Corporation)	Human acellular lyophilized dermis	None
	Dermagraft [®] (Advanced BioHealing)	PGA/PLA, ECM	Allogeneic neonatal foreskin fibroblasts
	Hyalograft 3D [®] (Fidia Advanced Biopolymers)	Hyaluronic acid membrane	Cultured fibroblasts
	Permacol [®] (Tissue Science Laboratories)	Porcine acellular diisocyanite crosslinked dermis	None
Dermal (double layer)	Integra [®] (Integra LifeSciences Corp)	Polysiloxane, bovine cross-linked tendon collagen, GAG	None
	Hyalomatrix [™] (Fidia Advanced Biopolymers)	Silicone membrane, hyaluronic aci	None
	TransCyte [®] (Advanced BioHealing)	Silicon film, porcine dermal collagen-coated nylon mesh	Allogeneic neonatal foreskin fibroblasts
Dermo-epidermal	Apligraf [®] (Organogenesis Inc)	Bovine collagen	Cultured allogeneic keratinocytes and fibroblasts
	OrCel [®] (Ortec International)	Bovine collagen sponge	Xenogeneic cultured keratinocytes and fibroblasts
	PolyActive [®] (Symatase)	Synthetic PEO/PBT matrix	Autologous cultured keratinocytes and fibroblasts

2.4.2.3. Growth factor therapy

Growth factors are endogenous signalling molecules that regulate several cellular processes required for wound healing such as migration, proliferation and differentiation. The topical delivery of growth factors into the wound bed is promising to improve the treatment of chronic wounds, which have shown deregulation on the levels of several growth factors, including PDGF and VEGF [120].

Platelet-derived growth factors play numerous roles in wound healing such as mediating cell infiltration during the inflammatory phase and stimulating fibroblasts to secrete ECM components. Becaplermin, a recombinant human PDGF, was approved in 1997 by the Food and Drug Administration (FDA) for the treatment of diabetic foot ulcers and commercialized as Regranex[®] becaplermin Gel 0.01% (Smith & Nephew, Inc). It has shown to accelerate the wound closure of diabetic foot ulcers in randomized clinical trials [121, 122] and the healing of pressure ulcers [123]. However, in 2008, FDA warned that patients who have received three or more tubes of Regranex[®] have an increased risk of cancer. Alternative approaches involve gene therapy to target PDGF expression to venous leg ulcers [124]. Granulocyte macrophage-colony stimulating factor (GM-CSF) is a cytokine that stimulates neutrophils during the inflammatory phase and upregulates the proliferation and migration of several cells (e.g., keratinocytes, fibroblasts, and endothelial cells). Sargramostim (tradename Leukine), an injectable recombinant human-GM-CSF (rh-GM-CSF), was approved in 1991 by the FDA as an immune-stimulator following chemotherapy and bone marrow transplantation. Sargramostim and its analogue molgramostim (tradename Leucomax) are commercially available as injectable formulations. The topical application of rh-GM-CSF and GM-CSF showed positive effects on the healing of venous leg and diabetic foot ulcers of a small number of patients in randomized, controlled studies [125]. Clinical studies in deep, partial-thickness burn wounds also showed improved wound healing with topical application of rh-GM-CSF [15]. Vascular endothelial growth factor A (VEGF-A) has been investigated as a potential target for wound healing due to its ability to promote angiogenesis. Topical application of a recombinant human-VEGF (rh-VEGF), Telbermin, was tested in a Phase I clinical trial in patients with neuropathic diabetic foot ulcers, showing positive indications in the wound healing [126]. Growth factors have been tested in animal models to promote healing, with satisfactory outcomes. However, the overall efficacy of topical growth factors in humans has been limited, probably due to the highly proteolytic environment in chronic wounds.

2.4.2.4. Biophysical agents

Biophysical technologies are usually used in the treatment of difficult-to-heal, chronic and infected wounds, including the following therapies: electrical stimulation, electromagnetic, oxygen (hyperbaric and transcutaneous), phototherapy, shockwave, ultrasound and negative pressure wound therapy (NPWT) [127, 128]. Electrical stimulation devices deliver an exogenous electrical current to facilitate wound healing, while in electromagnetic therapy an electromagnet is used to generate electric current to improve the wound healing. Oxygen therapy devices provide oxygen to the wound bed via transdermal, systemic, or topical routes. Phototherapy provides wound treatment by using energy from the electromagnetic light spectrum. Depending on the selected light wavelength, phototherapy can be used to control wound bioburden (UVC 200–280 nm) or to stimulate the wound healing. Shockwave therapy is indicated for diabetic foot ulcers and utilizes non-invasive high-energy shock waves to trigger cellular response and improve micro-circulation. Ultrasound therapy employs high- or low-frequency ultrasound to enhance wound healing outcomes. NPWT is employed to convert an open wound into a temporarily closed environment to promote faster healing and reduce complications (e.g., infection, dehydration), removing fluids like wound exudate, irrigation fluids, or infectious materials.

2.5. Biofabrication technologies

Biofabrication is a multidisciplinary field that combines the principles of engineering, biology and materials science for the automated fabrication of biologically and structurally functional products using living cells, bioactive molecules, biomaterials, cell aggregates like micro-tissues, or hybrid cell-material constructs. Bioprinting or bioassembly approaches are used to generate functional constructs for subsequent tissue maturation processes [40, 129]. Bioprinting produces bioengineered structures through computer-aided transfer processes that allow the patterning and assembly of living and non-living materials. It also encompasses the additive manufacturing of cell-instructive 3D scaffolds capable of directing cells to develop into a tissue mimetic or tissue analogue structure. Bioassembly involves the fabrication of hierarchical constructs with prescribed 2D or 3D organization by the automated assembly of preformed cell-containing units. These fabrication units are often created using microfabricated moulds or microfluidics [129].

Biofabrication technologies can be broadly classified according to the printing principle into: (i) light-based technologies, (ii) fused deposition modelling, (iii) 3D™

printing, (iv) wet-spun automated extrusion systems, (v) electrospinning, (vi) inkjet bioprinting, and (vii) extrusion bioprinting. Among these technologies, light-based processes like vat photopolymerization (single- and two-photon stereolithography) and laser-assisted bioprinting, inkjet bioprinting and extrusion bioprinting allow the direct processing of living and non-living materials into 3D constructs, being described in the next sections.

2.5.1. Light-based technologies

Light-based technologies comprise additive manufacturing processes that use light energy to trigger the photocrosslinking of a photosensitive solution or the ejection of a bioink from a print ribbon. Bioinks consist of hydrogel precursor solutions or decellularized ECM, loadable with cells and/or bioactive factors, playing a pivotal role on the reproducibility of the printing process and quality of the constructs [130-133].

2.5.1.1. Vat photopolymerization

Vat photopolymerization or stereolithographic processes produce 3D solid objects in a layer-by-layer procedure through the selective photoinitiated curing reaction of a liquid photosensitive material. The curing reaction is triggered by the incidence of light with an appropriate wavelength (UV, visible, or near-infrared (near-IR) light), intensity and duration. The curing reaction can be induced by either single-photon polymerization or two-photon polymerization (2PP). Although the chemical principle of these processes is similar, single-photon polymerization involves the absorption of a sole photon, while in 2PP the molecule simultaneously absorbs two photons with relatively low intensity, and is excited to a higher singlet state. As the probability of the electronic excitation of a molecule by simultaneous absorption of two photons depends quadratically on the incident light intensity, 2PP allows a submicron 3D resolution (~200 nm) with greater depth and ultrafast fabrication [134, 135].

Stereolithographic processes produce 3D constructs in a layer-by-layer fashion using two fundamental irradiation approaches: (i) direct or laser writing and (ii) mask-based writing (**Figure 2.3A**). The first employs a focused laser beam to selectively induce the polymerization of a liquid photopolymer, while the second transfers an entire image to a liquid prepolymer by irradiating through a patterned mask that contains transparent zones corresponding to the sections of the model to be built. The major advantage of the mask-based approach is the fast processing and the low-density flux of light over the prepolymer, which avoid undesirable polymerizations [135, 136].

Although conventional stereolithography has superior resolution than other technologies, advances in photonics have led to the development of alternative processes with higher resolution, such as the microstereolithography and 2PP stereolithography. In microstereolithography the laser beam is more precisely focused, which reduces the spot size to a few micrometers in diameter and improves the resolution of the process. For example, in digital micromirror devices (DMDs) based microstereolithography, the achievable lateral and vertical resolutions are $\sim 2 \mu\text{m}$ and $\sim 1 \mu\text{m}$, respectively [137]. 2PP stereolithography is the most advanced technique, allowing ultra-fast fabrication of constructs with 3D submicron resolution ($> 65 \text{ nm}$), by using a focused femtosecond near-IR ($\sim 800 \text{ nm}$ wavelength) to induce polymerization [138]. Polymerization can occur under the material surface, but is limited to the focal point of the femtosecond laser, due to the strong decrease in the number of excited molecules as the distance from this region increases. As a result, 2PP stereolithography allows for a fine control over polymerization in a 3D environment [138]. However, 2PP systems are very expensive and operate with a single material, which precludes the fabrication of multi-material constructs [134, 139]. To circumvent these limitations, Bártolo and coworkers developed a mask-based multi-photon and multi-material stereolithographic system, designated as micro stereo-thermal-lithography (μSTLG) [140]. This system can operate in three distinct modes by using UV and near-IR radiation effects, alone or simultaneously, to generate free radicals for polymerization (**Figure 2.3B**). Rather than processing one material at a time, the μSTLG apparatus includes a multi-vat system that enables the fabrication of multi-material constructs [139, 141, 142]. Projection-based stereolithography represents another useful variant of traditional stereolithography, in which 2D patterns generated by DMDs are projected over the liquid resin through a transparent, non-adhering plate. In this setup, the support platform dips into the resin, and the structure is not exposed to oxygen during light irradiation, significantly reducing the oxygen inhibition [135, 143].

Vat photopolymerization technologies have been explored to create 3D scaffolds with intricate microarchitectures for direct implant into the lesion or for cell seeding and subsequent implantation. The range of processable materials is very broad, including biodegradable thermoplastic polymers, such as propylene fumarate (PPF) [144], poly(ϵ -caprolactone) (PCL) [145], poly(D,L-lactide) (PDLLA) [146], and poly(trimethylene carbonate) (PTMC) [147]. The ability of vat photopolymerization to allow the incorporation of cells into the biofabrication process provides the possibility of engineering complex 3D microenvironments *in vitro* that resemble the structural and compositional characteristics of the natural ECM. Such environments are fabricated by

the selective photopolymerization of cell-laden hydrogel precursors, and provide a useful tool the study of cell response to biochemical cues and the elucidation of mechanisms underlying cell-cell and cell-material interactions [148, 149].

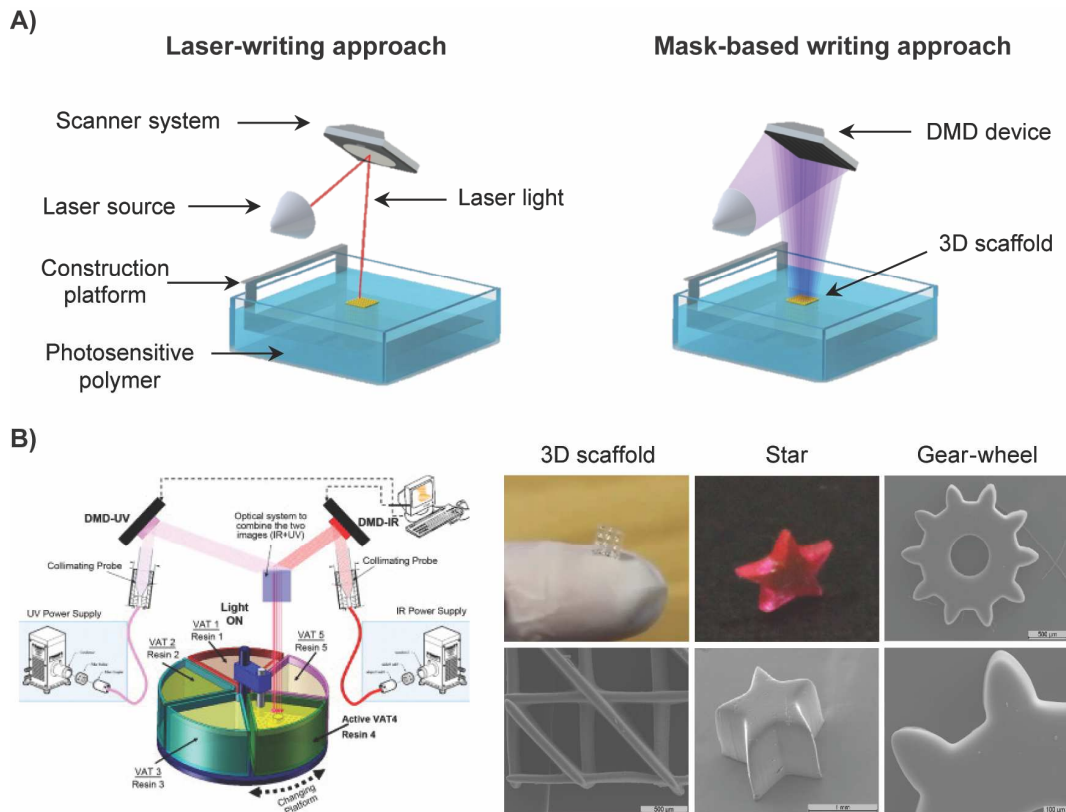


Figure 2.3. Stereolithographic processes for tissue engineering. (A) Illustration of light irradiation approaches in stereolithography. **(B)** Micro stereo-thermal-lithography system and examples of produced 3D structures.

2.5.1.2. Laser-assisted bioprinting

Laser-assisted bioprinting (LAB) evolved from the conventional laser-induced forward transfer process, originally developed to the direct writing of metals [150]. Its operation principle involves the application of a high-energetic pulsed laser (often a near-IR laser) onto a donor ribbon coated with the bioink to be printed in order to generate the local ejection of small droplets (**Figure 2.4A**). The incident laser light is primarily focused on a laser-transparent substrate (e.g. glass or quartz substrate), which is coated with a thin metal (e.g. gold, titanium) layer that absorbs the light energy and promotes its transfer to the bioink. At this moment, a high-pressure bubble is generated, and a small droplet is propelled towards a receiving platform [45, 151, 152]. The mechanisms of droplet formation and the effects of biofabrication parameters on

the printing resolution and cell functions are well documented in the literature [152-156]. Deleterious effects to the cells mainly result from the thermal heating, interaction with laser light and impact with the receiving substrate [151, 153]. However, several works showed that these effects can be significantly reduced, or even eliminated, by controlling the laser pulse characteristics, the bioink viscosity, the thickness of absorbing layer and the substrate properties [153, 157, 158]. LAB is one of the most promising technologies for cell printing applications (**Figure 2.4B**) due to its unique resolution (10-100 μm), high-throughput, reproducibility, and possibility of printing multiple biomaterials and cell types by incorporating those compounds in the same ribbon or having multiple parallel ribbons [43]. Its nozzle-free nature precludes clogging issues and affords the deposition of bioinks with a large range of viscosities (1-300 mPa/s) and cell concentration (10^8 cells/ml) [45]. For printing 3D constructs maintaining the prescribed resolution in the positioning of cells and biomaterials, LAB requires the development of biomaterials exhibiting fast crosslinking mechanisms compatible with the light-wavelengths emitted by the laser sources. LAB was also employed for the *in situ* bioprinting of mesenchymal stromal cells, associated with collagen and nano-hydroxyapatite, into a calvaria defect model in mice [159]. The biofabrication of clinically relevant constructs through LAB takes long periods of time and eventually the preparation of multiple ribbons containing different materials and cell types.

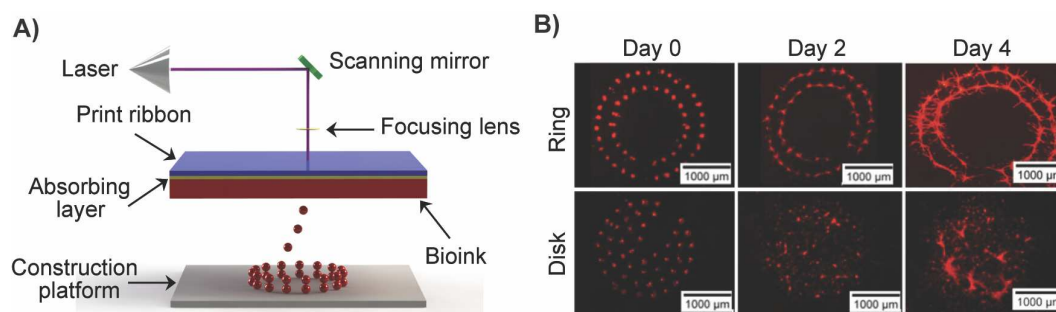


Figure 2.4. Laser-assisted bioprinting for tissue engineering. (A) Illustration of the LAB technology and main components. **(B)** Fluorescence images of ring and disk printed tomato-positive multipotent mouse bone marrow stromal precursor cells using LAB technology [159].

2.5.2. Inkjet bioprinting

Inkjet is a high-throughput printing technology based on the dispensing of small drops (typically 1-100 picolitres) of a liquid bioink onto a collector substrate (**Figure 2.5A**) [160]. Drops can be generated by either continuous inkjet or drop-on-demand

(DOD) inkjet printing [161]. DOD printing is the most popular method affording a rapid and fully controlled generation of droplets (20-50 μm) through the application of a pressure pulse to the bioink loaded into a reservoir placed just behind the printing nozzle [161-163].

DOD printing can be further categorized according to the mechanism used for the droplet formation and ejection as thermal inkjet (vapour bubble formation) or piezoelectric inkjet (mechanical actuation). Thermal inkjet printers use a heating element to vaporize a small volume of fluid, generating a bubble that expands and ejects a controlled volume of fluid as a single droplet. The main concern associated to thermal inkjet relies on the high temperatures generated close to the heating element during the printing process, which may affect the biomolecules and cells to be printed [160, 162, 164]. However, it has been demonstrated that, due to the short duration of the heating pulses ($\sim 2 \mu\text{s}$), the increase in temperature of the bioink is only a few degrees, allowing the printing of viable cells with a low percentage of cell dead [165]. In piezoelectric inkjet, the droplet generation and ejection is achieved through the mechanical deformation of a piezoelectric transducer controlled by the application of external voltage, which precludes the temperature increase to suprphysiological levels [161, 162, 166]. In order to prevent clogging issues, bioinks for inkjet bioprinting must exhibit low viscosity (1-10 mPa/s) and limited cell densities (typically $<10^6$ cells/ml), which causes additional constrains in the printing process, such as cell settling and sedimentation, droplet spreading, loss of resolution, and limited fabrication of 3D constructs with controlled architectures [43, 45, 163, 167]. Despite these challenges, inkjet bioprinting has been explored for several tissue engineering applications, including the generation of hollow structures for vascularization (**Figure 2.5B**).

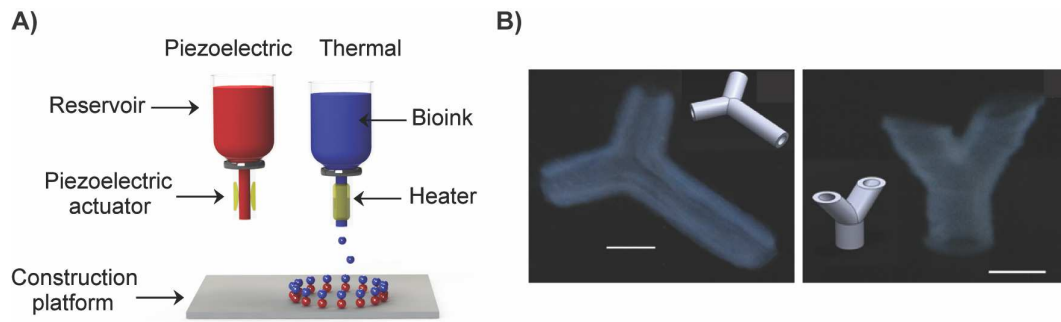


Figure 2.5. Illustration of inkjet bioprinting technology. (A) Piezoelectric and thermal inkjet bioprinting. **(B)** Acellular alginate bifurcated structures generated by inkjet bioprinting (scale bars: 3mm) [168].

2.5.3. Extrusion bioprinting

Extrusion bioprinting is the most popular method to fabricate 3D cell-laden constructs for tissue regeneration. In a typical setup, cells suspended in polymer solutions are loaded within disposable medical grade syringes or reservoirs, and subsequently printed onto a platform driven by pressurized air or mechanical forces generated by either a piston or a rotating screw (**Figure 2.6A**) [43, 45]. Temperature controlled modules are often employed to adjust the temperature of both the bioink and the construction platform during fabrication, which is particularly relevant to control the bioink viscosity and to induce the *in situ* gelation of temperature-sensitive polymers [169]. Light sources and spraying nozzles can also be coupled to the bioprinting system to provide additional crosslinking schemes, improving the printing fidelity and the structural stability of tissue constructs [170-172]. Compression forces and shear stresses generated during printing are the major sources of cell damage, requiring a careful optimization of the processing parameters (e.g. cellular density, bioink viscosity, temperature and air pressure) to prevent cell damage. Although there are several works indicating how these effects can be controlled to increase the printing accuracy and cell viability [173-176], there is a need for systematic studies accessing the post-printing functionality of the cells.

A major advantage of extrusion bioprinting is the ability to print highly viscous polymer solutions containing a wide range of cell densities ($\sim 10^7$ cells/mL) [177, 178]. It also enables the biofabrication of clinically relevant 3D constructs by the deposition of continuous and larger hydrogel strands through a nozzle with variable diameters, usually in a range of 150-300 μm [43, 45, 177]. Limitations are related to the reduced resolution (approximately 200 μm), nozzle clogging, and difficulties in fabricating 3D

constructs maintaining the predesigned shape and providing a suitable environment for the cells [43, 45]. The printing of 3D constructs with complex and intricate microarchitectures still remains a huge challenge in bioprinting. Until now, the most common approach to address this issue involves the use of highly concentrated polymer solutions, which imposes severe restrictions to cell mobility within the polymer network and might ultimately lead to cell death [178]. More recently, alternative approaches based on the combination of multiple crosslinking pathways (e.g. photocrosslinking and thermal gelation) [169, 179], integration of bioprinting with melt extrusion [132, 180-182], and the use of partial crosslinked hydrogels [172, 178] have been explored with promising outcomes (**Figure 2.6B-D**).

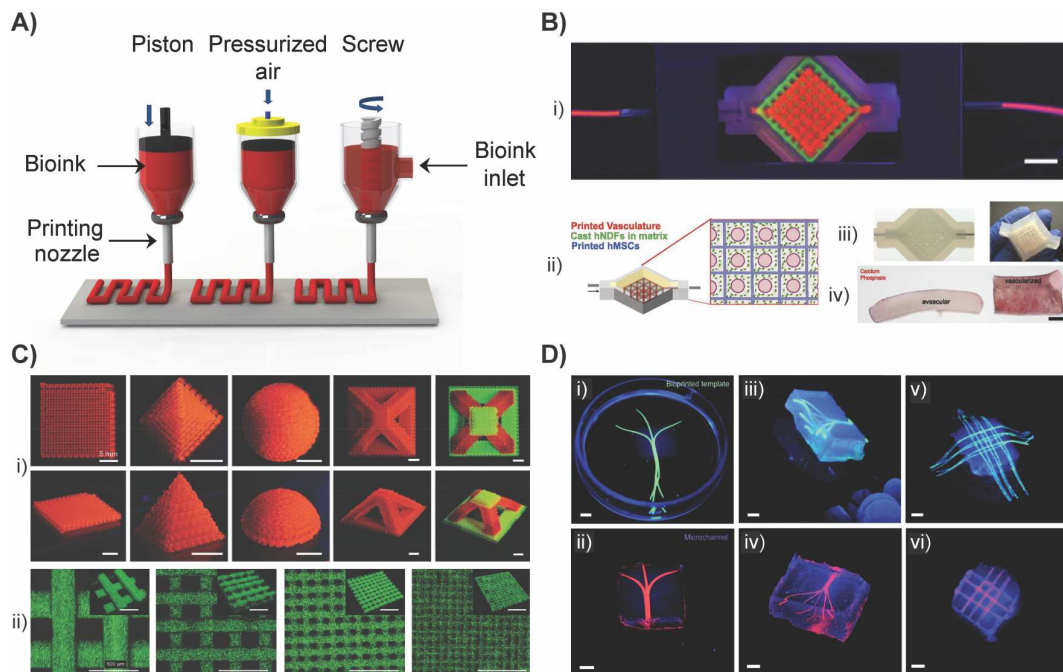


Figure 2.6. Extrusion bioprinting and examples of tissue engineering applications. (A) Extrusion bioprinting modalities and main components. **(B)** Bioprinted 3D vascularized tissue through the deposition of fugitive (vascular) bioink and cell-laden bioinks within a 3D perfusion chip; (i) photograph of printed construct housed within a perfusion chamber (scale bar: 5mm); (ii): schematic of printed heterogeneous tissue within a perfusion chip; (iii) photographs of printed construct within and removed from the customized perfusion chip; (iv) cross-sections of avascular (left) and vascularized tissue (right) after 30 days of osteogenic media perfusion with alizarin red stain showing the location of calcium phosphate (scale bar: 5 mm) [177]. **(C)** Extrusion bioprinting of programmed bacterial cells: (i) Optical images of 3D bioprinted constructs of Pluronic F127 diacrylate labelled with rhodamine B (red) or fluorescein (green) (scale bars: 5mm); (ii) confocal images of green fluorescence protein positive bacterial cell-laden hydrogel scaffolds printed with varying degrees of resolution (from left to right: 200 μm , 100 μm , 50 μm ,

and 30 μm ; scale bars: 500 μm) [183]. **(D)** Extrusion bioprinting of functional and perfusable microchannels. (i) photographs of planar bifurcated agarose fibres (green) within the methacrylated gelatin construct and (ii) respective network after perfusion; (iii) 3D branched agarose templates embedded in the gelMA hydrogel and (iv) resulting 3D branched network after perfusion; (v) 3D lattice template within the methacrylated gelatin network before and (vi) after perfusion (scale bars: 3 mm) [41].

2.6. Bioprinting of photocrosslinkable hydrogel bioinks

The development of advanced bioinks exhibiting appropriate printability and tuneable biomechanical properties, while simultaneously providing a suitable microenvironment where entrapped cells can migrate, proliferate and synthesize new ECM remains a key challenge in bioprinting. A major bottleneck in the field consists on the formulation of bioinks that allow the printing of complex 3D constructs with high levels of shape fidelity, without compromising cell functions, which is essential to ensure proper resolution in the placement of cells, biological molecules and biomaterials. One approach to improve the printing fidelity of bioinks relies on the design of material formulations with tuneable rheological properties that can be rapidly crosslinked during or post-printing. Photocrosslinking has evolved as an attractive solution to achieve rapid crosslinking of photosensitive bioinks, allowing the bioprinting of both viscous [184] and non-viscous [185] hydrogel bioinks into complex 3D constructs. The application of photopolymerization reactions in bioprinting has been receiving a great deal of interest due to its unique spatiotemporal control over the hydrogel formation and fast polymerization under cytocompatible conditions. Photopolymerization can be employed during the bioprinting [185], or just after the deposition [174], in order to induce the rapid establishment of crosslinks between polymer chains, contributing to address current challenges in the field, including the fabrication of structurally stable 3D constructs with intricate architectures, enhanced spatial resolution and printing fidelity.

2.6.1. Hydrogels as ECM mimics

At a basic structural level, biological tissues are composed of cell populations surrounded by a fibrous ECM that displays several functions, namely by serving as a physical support for the cells, providing cues to regulate cellular activities and interactions, promoting the maintenance of differentiated tissues, and ensuring tissue repair upon injury [186]. From a structural point of view, the ECM is a hydrated gel

network composed of an intricate meshwork of structural protein fibres (e.g., collagen, elastin, fibrin) embedded within a ground substance made of GAGs (e.g., hyaluronic acid, chondroitin-sulfate), proteoglycans (e.g., aggrecan, decorin) and adhesive glycoproteins (e.g., fibronectin, laminin, tenascin) (**Figure 2.7**). It also comprises a myriad of soluble (e.g., growth factors, cytokines) and matrix-linked (e.g., fibronectin, laminin) signals, which together with the dynamic reciprocity of cell-cell and cell-ECM interactions are responsible for the regulation and coordination of cell fate [186, 187]. Rather than a static structure, ECM is a highly dynamic environment which properties such as composition, architecture and crosslinking degree are under constant remodelling (i.e., assembly and degradation), varying according to the anatomical site and tissue physiology [188]. Due to its instructive nature, ECM also serves as a storage depot for growth factors, cytokines and chemokines, regulating their spatiotemporal and tissue-specific presentation to cells [189]. This well-orchestrated activity dictates how the mechanical forces are transmitted to the cells and determines several cell functions such as adhesion, proliferation, migration, differentiation and remodelling [187]. In a reciprocal way, cells are able to sense and interact with the ECM via binding between adhesion motifs in ECM and transmembrane cell surface receptors (e.g., integrins, immunoglobulins and selectins) that result in intracellular signalling. Matrix anchorage is essential for cells to sense the matrix elasticity and to exert traction forces on the substrate towards migration [190]. As a consequence of this dynamic, bidirectional cell-ECM crosstalk, macromolecular components of ECM are locally degraded by cell-secreted and cell-activated proteases (MMPs, serine proteases, and cysteine proteases). This allows cells to specifically degrade components of the matrix (e.g., proteins, proteoglycans), which is often required for 3D cell migration, proliferation and invasion throughout the surrounding environment, as further elucidated using synthetic extracellular matrices [187, 191].

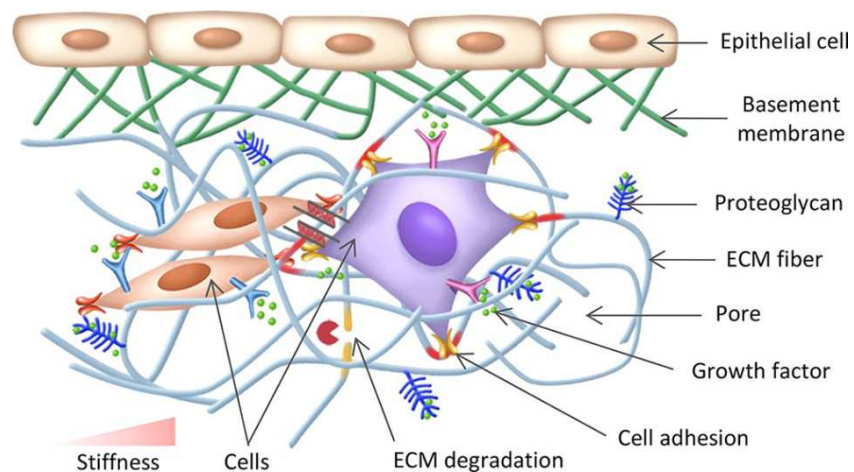


Figure 2.7. Schematic representation of the ECM composition and cell-ECM interactions. Cells are surrounded by a dynamic ECM that provides several biochemical and biophysical cues to regulate the cell fate [188].

Recapitulating the complexity and instructive nature of the ECM milieu is fundamental for the bioprinting of functional tissue constructs. However, it still remains a major challenge given the multiscale architecture of the ECM and the spatiotemporal specificity of its interaction with the surrounding cells. Due to their unique properties of high water content and tissue-like elasticity, hydrogels are widely used to develop 3D ECM analogues that closely resemble the natural microenvironment of most soft tissues [192]. However, the design of functional hydrogels that mimic the ECM is challenging, as it needs to consider a multitude of biochemical (e.g., cell adhesion ligands, bioactive factor immobilization and chemical functional groups) and biophysical (e.g., structural properties, mechanical properties, degradability and electrical conductivity) cues that determine cell functions (**Figure 2.8**).

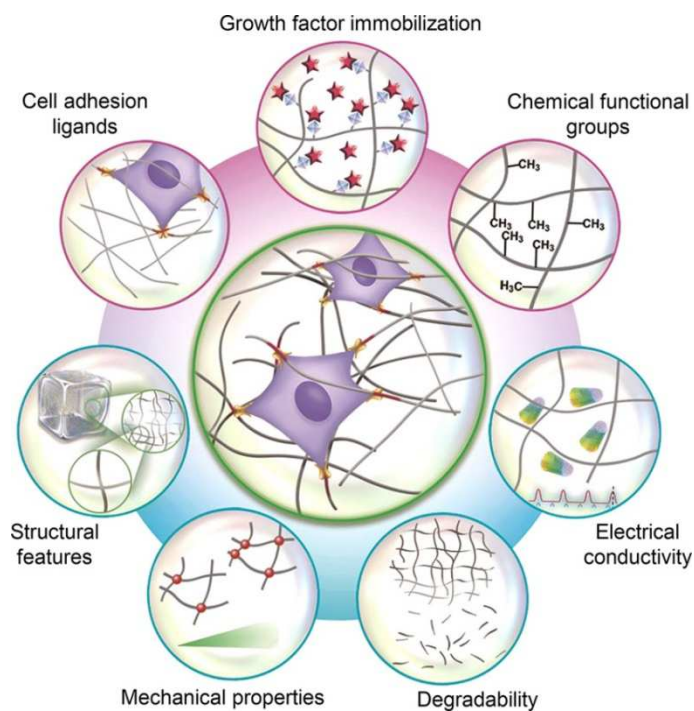


Figure 2.8. Considerations on the design of hydrogels to recapitulate the 3D cell microenvironment. The development of such hydrogel networks requires the consideration of biophysical, biochemical and biological properties [188].

Hydrogels are water-insoluble, hydrophilic 3D networks made of chemically or physically crosslinked polymer chains that exhibit high porosity and permeability to oxygen and nutrients, allowing effective exchange of soluble factors within the gel. Chemical hydrogels involve the formation of covalent bonds, while physical hydrogels are obtained when physical interactions are established between polymeric chains (molecular entanglement, ionic interaction and hydrogen bonding) [193-195]. A myriad of physical (e.g., thermal and ionic gelation) and chemical (e.g., radical polymerization, aldehyde complementation) gelation methods can be adopted to generate hydrogels (**Figure 2.9**). The thermodynamic compatibility of hydrogels with water confers them a soft and elastic nature that allows for a good biocompatibility and minimal inflammatory reactions. Hydrogels are the most commonly explored materials for the fabrication of cell-laden constructs through bioprinting, as they provide a soft and porous matrix for entrapped cells and their properties can be easily tuned [43, 196-198]. One attractive characteristic of hydrogels is their ability to undergo sol-gel transition *in situ*, under cytocompatible conditions, using a variety of chemistries. This feature, together with the tuneable rheological properties of hydrogel precursor solutions has been attracting increased interest to translate these materials for bioprinting. Although the intrinsic

properties of hydrogels resemble many features of ECM, their biochemical and biophysical functionality often needs to be adjusted to a particular cell and tissue environment. Since hydrogels are very versatile materials, their properties are easily modified via numerous approaches. Significantly, by combining the versatility of natural and synthetic polymers with the advances in chemistry and materials science, biofunctional hydrogels can be engineered to meet specific requisites, including cell-adhesiveness, growth factor tethering and delivery, or ability to undergo degradation through hydrolysis and/or proteolytic cleavage. For instance, the biological and degradation properties of hydrogels can be tailored by the incorporation of cell-adhesion motifs (e.g. Arginyl-glycyl-aspartic acid, RGD) [199, 200] and cell-proteolytic domains into the polymer backbone [201, 202], whereas the biomechanical characteristics can be adjusted by varying the polymer molecular weight or the crosslinking density [203, 204]. The wide spectrum of crosslinking schemes and the large range of network properties also give hydrogels high versatility for application in different tissues, including cartilage, bone, cardiovascular and skin [194, 205].

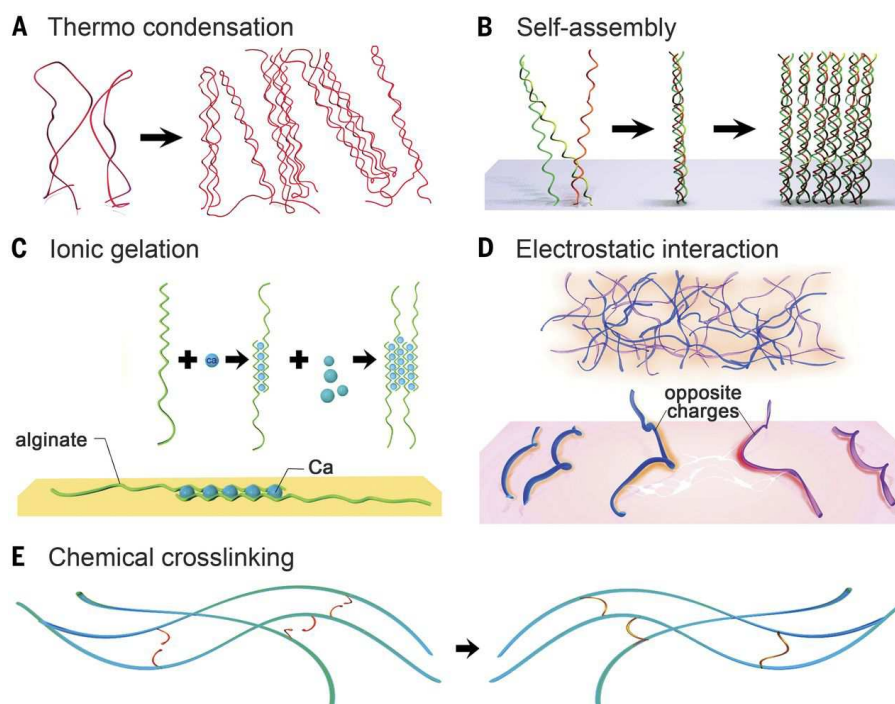


Figure 2.9. Examples of physical and chemical gelation methods for hydrogel crosslinking. (A) Thermally induced entanglement of polymer chains. **(B)** Molecular self-assembly. **(C)** Ionic gelation. **(D)** Electrostatic interaction. **(E)** Chemical cross-linking [195].

2.6.2. Photopolymerization Reactions

Photopolymerization reactions for hydrogel formation can be classified into free-radical-initiated chain polymerization and bio-orthogonal click reactions [206].

Free-radical photopolymerization is the most popular reaction to create chemically crosslinked cell-laden hydrogels through a multistep process of initiation, propagation and termination reactions. In the first step, a photosensitive system containing unsaturated prepolymers, cells and photoinitiators is irradiated with a sufficient dosage of light energy to excite the photoinitiators and trigger the formation of free radicals. Then, these reactive species propagate across vinyl moieties on prepolymers in solution, resulting in both generation of new free radicals and the establishment of crosslinks between the polymer chains. As the reaction proceeds, the number of crosslinks in the system increases and a highly crosslinked network structure is obtained via a chain-growth mechanism [193, 207]. Free-radical photopolymerization, based on (meth)acrylate functionalized prepolymers and occurring through a chain-growth mechanism, is the most popular method to crosslink hydrogel bioinks. It is widely accepted that acrylates possess the highest reactivity, followed by vinyl ester, vinyl carbonate, vinyl carbamate, methacrylate, and fumarate derivatives [208, 209]. Although the reactivity of acrylates enables high reaction kinetics and double-bond conversion, the cytotoxicity and skin irritancy of acrylates still remain as major pitfalls for biomedical applications [209]. On the other hand, the main limitation of methacrylates is the limited reactivity due to the sterical hindrance and inductive stabilization of radicals from the methyl group [210]. Major drawbacks of free radical photopolymerization include the oxygen inhibition, lack of control over the crosslinking kinetics, and the generation of network heterogeneities [206, 207]. These heterogeneities in the network resulting from the random chain polymerization have a significant impact in the mechanical integrity of the constructs [211].

Recently, photopolymerization reactions based on bio-orthogonal click reactions are emerging in bioprinting as promising alternatives to the free radical photopolymerization counterpart [212, 213]. These reactions are characterized by orthogonal reactivity and the step-growth mechanism of the polymerization reaction [206, 211, 212, 214]. In addition, click chemistry is insensitive to both water and oxygen, can proceed under mild reaction conditions with higher efficiency, selectivity, and faster kinetics when compared to free-radical polymerization [213-215]. Among the myriad of existing bio-orthogonal click schemes, the thiol-norbornene photoclick reaction has emerged as a powerful method for engineering biocompatible hydrogels,

mostly due to the faster rate of thiol-ene conjugation of norbornene end groups compared to other alkenes (norbornene > vinyl ether > alkene > vinyl ester > allyl ether > acrylate > N-substituted maleimide > methacrylate > conjugated dienes) [216]. This reaction is triggered by an external light source, proceeding in a step-growth mechanism with the formation of structurally uniform hydrogels with minimal network defects, which provides better control over the gel crosslinking density and hydrogel properties [206, 207]. It involves the light-mediated orthogonal reactions between multifunctionalized macromers that are end-capped with norbornene functionalities and sulfhydryl-containing linkers, in the presence of low amounts of photoinitiator [206, 213, 214, 216]. Under UV or visible light irradiation, the thiol-ene reaction promotes the rapid radical-mediated addition of thiols (e.g., bis-cysteine peptides and dithiothreitol, DTT) to carbon-carbon double bonds within functionalized prepolymers (e.g., norbornene-functionalized 4-arm polyethylene glycol), yielding thioether bonds without inducing cytotoxic effects on embedded cells (**Figure 2.10**) [215, 217, 218]. The reaction is photochemically controlled and affords the localized covalent tethering of pendant bioactive moieties, e.g. MMP-degradable and/or adhesive peptide sequences, resulting in enhanced control over hydrogel degradation, cell-matrix interactions and cell fate [215]. Thiol-norbornene photopolymerization has numerous advantages, as it is not inhibited by oxygen, proceeds in a faster magnitude than chain-growth photopolymerization, and can be performed in the presence of cells [207, 214]. It has successfully been applied for the fabrication of cell-laden hydrogels using natural and synthetic polymers functionalized with norbornene moieties [218-220]. Photocrosslinkable hydrogels can also be obtained from mixed-mode polymerizations (e.g. thiol-acrylate) resulting in the formation of hydrogel networks by a combination of chain- and step-growth polymerization, due to the competing reactions between acrylate groups and thiol-ene coupling [207, 221].

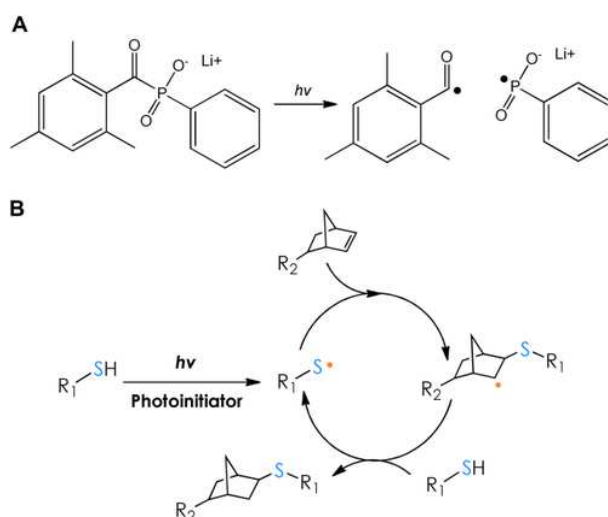


Figure 2.10. Radical-mediated step-growth thiol–norbornene reaction. (A) Incident light decomposes cleave-type photoinitiators (e.g., type I photoinitiator lithium arylphosphinite) into radicals. **(B)** Free radicals abstract protons from the sulfhydryl groups to form thiyl radicals that react with strained vinyl bonds in the norbornene moiety on functionalized polymer, yielding a thiol–ether bond and a carbon-centered radical capable of generating another thiyl radical [206].

Major concerns with photopolymerization reactions in the presence of cells and biological tissues arise from three major issues: (i) potential deleterious effects of UV light irradiation, (ii) cytotoxicity of radicals generated by the dissociation of photoinitiators, and (iii) local inflammation due to unreacted double bonds. For cell entrapment applications, light sources emitting either in the UV-A range (320–400 nm) or visible light are usually employed to reduce deleterious effects [127]. Despite several studies have shown that cell damage caused by UV irradiation can be significantly reduced or even eliminated by choosing appropriate light wavelengths, intensity and irradiation time, great efforts are currently being done towards the development of photosensitive systems (hydrogel precursors and photoinitiators) capable of undergoing photocrosslinking upon exposure to safe visible light wavelengths [221, 222]. In parallel to the light source, photoinitiators are a key element for photopolymerization, as they generate free radicals that promote the formation of crosslinks between the polymer chains. However, these radicals can react with cellular components during photopolymerization, either via direct contact or the formation of reactive oxygen species, which may compromise cell viability and ultimately induce deoxyribonucleic acid (DNA) damage [223, 224]. To prevent cell damage and ensure cell functionality for new tissue formation, the wavelength of emitted light must overlap the absorption spectra of photoinitiator, and its concentration must be carefully

optimized, taking into account the compromise between the crosslinking time and cell viability. The selection of the most appropriated photoinitiator can be partially determined by the number and reactivity of functional groups in the polymer backbone. The functionalization of natural and synthetic polymers with reactive side groups such as acrylates, methacrylates, fumarates and vinyl esters, is an indispensable requisite for the photopolymerization. These reactive groups are introduced in the polymer chain through chemical reactions with functional groups already present in the native polymer structure. The type and number of reactive groups introduced in the polymer backbone is often determined by the cytotoxicity and reactivity of the functional group, being very important to ensure a maximal consumption of reactive groups during the photopolymerization in order to prevent local inflammation and non-specific side reactions with surrounding proteins upon implantation [207].

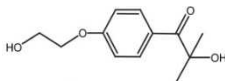
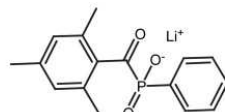
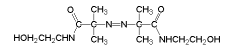
2.6.3. Cytocompatible photoinitiators

The selection of suitable photoinitiators is a prime requisite to ensure an adequate polymerization rate and avoid cytotoxic effects for both embedded cells and surrounding tissues. When selecting a photoinitiator, key characteristics should be considered, including water solubility, stability, absorption spectrum, molar absorptivity, and efficiency in generating free radicals [218, 225]. Currently available photoinitiators can be divided into two main categories: radical or cationic [134]. Radical photoinitiators are the most used due to their superior biocompatibility, while cationic photoinitiators result in the formation of protonic acids, making them less useful for biomedical applications [225]. According to the mechanism involved in the generation of free radicals, radical photoinitiators can be further categorized as photo-cleavable photoinitiators (type I) or bimolecular photoinitiators (type II). Upon light exposure, type I photoinitiators (e.g., benzoin derivatives, benzyl ketal, acetophenone derivatives, hydroxyalkylphenones and acylphosphine oxides) absorb incident photons and decompose into two primary radicals that initiate the crosslinking, whereas type II photoinitiators (e.g., benzophenone, camphorquinone, and thioxanthone) abstract the hydrogen from a co-initiator to generate secondary radicals for crosslinking [134, 218]. Although type I initiators are usually the first choice because of their superior initiation efficiency [214], there has been an increasing interest in type II initiators for visible light-mediated polymerization (**Table 2.6**).

The main concern associated with the use of photoinitiators relies on the potential cytotoxicity of the generated free radicals. Cytotoxic effects of several photoinitiators on primary cells and cell-lines are well-documented and strongly depend

on the photoinitiator type and concentration, exposure time and light intensity [223, 224, 226-228]. The photoinitiator 1-[4-(2-hydroxyethoxy)-phenyl]-2-hydroxy-2-methyl-1-propane-1-one (I2959) is the most commonly used photoinitiator due to its moderate water solubility and low cytotoxicity. However, its low molar extinction coefficient in the UV-A spectral range and its low initiation efficiency boosted the research on alternative photoinitiators exhibiting enhanced biocompatibility and/or efficiency, such as 2,2'-azobis[2-methyl-N-(2-hydroxyethyl)propionamide] (VA-086) and lithium phenyl-2,4,6-trimethylbenzoylphosphinate (LAP) [174, 226, 229, 230]. In parallel, researchers also concentrated efforts on the formulation of photopolymerizable systems containing visible-light sensitive photoinitiators (e.g., camphorquinone, riboflavin, Eosin-Y, tris(2,2'-bipyridyl)dichloro-ruthenium(II) hexahydrate with sodium persulfate), in order to mitigate potential deleterious effects of UV light on entrapped cells [218, 222, 231].

Table 2.6. Examples of the most common photoinitiators in photopolymerization reactions and examples of polymerization systems used for the fabrication of cell-laden hydrogels.

Photoinitiator			Photopolymerizable system					Reference
Name	Type	Chemical structure	Photocrosslinking reaction	Irradiation conditions	Hydrogel precursor	Encapsulated cells	Cell viability	
I2959	I		Free-radical polymerization	UV light (360-480 nm), 6.9mW/cm ² , 15s	Gelatin methacrylate, 0.5% (w/v) I2959	NIH 3T3 fibroblasts (5 x 10 ⁶ cells/ml)	75-92%, 8h post-encapsulation	[232]
			Thiol-ene click chemistry	UV light, 10mW/cm ² , 30s	HA-norbornene, DTT, 0.05 wt% IR2959	hMSCs (1 x 10 ⁷ cells/ml)	96% (1d) and 88% (3d) post-encapsulation	[219]
LAP	I		Free-radical polymerization	Visible light (405nm)/UV light (365nm) 10 mW/cm ² , 5 min	PEGDA, 2.2/0.22mM LAP	Human neonatal fibroblast (1 x 10 ⁶ cells/ml)	>95%, 24h post-encapsulation	[229]
			Thiol-ene click chemistry	UV light (365 nm), 5mW/cm ² , 2min	PEG-norbornene, 0.05 wt% LAP	hMSCs (5 x 10 ⁶ cells/ml)	Cells survive, 14d post-encapsulation*	[233]
VA-086	I		Free-radical polymerization	UV light (365nm), 2mW/cm ² , 5 min	Alginate Methacrylate, VA-086	Bovine articular chondrocytes (50 x 10 ⁶ cells/mL)	>90%, 48h post-encapsulation	[226]

		Free-radical polymerization	UV light (365nm), 4mW/cm ² , 1800mJ /cm ²	Gelatin methacrylamide, 20 mol%VA-086	HepG2 cells (1.5 x 10 ⁶ cells/ml)	>95%, 24h post-encapsulation	[174]
Eosin-Y	II	Mixed mode (chain and step-growth reactions) [§]	Visible light (525 nm), 5 mW/cm ² (7 min) /100 mW/cm ² (1.5 min)	PEGDA, Thiolated heparin, TEOA, 0.01% Eosin-Y	NIH 3T3 fibroblasts (2 x 10 ⁶ cells/ml)	>96%	[234]
		Thiol-ene click chemistry	Visible light (515 nm), 10 mW/cm ² , 4 min	PEG4NB, TEOA, NVP, 0.1 x 10 ⁻³ M Eosin-Y	Human mesenchymal stem cells (5 x 10 ⁶ cells/ml)	~95%, 14h post-encapsulation	[218]
Riboflavin	II**	Free-radical polymerization	Visible light: (780 nm femtosecond laser, followed by 1min at 570nm light)	PEGDA, TEOA, 200 μM riboflavin	Bovine aortic endothelial cells (1 x 10 ⁶ cells/ml)	>90%, after 24h ^{\$\$}	[235]
		Free-radical polymerization	Visible light 400-500 nm), 300 mW/cm ² , 120-600s	Methacrylated glycol chitosan/HA, 6 μM Riboflavin	Auricular chondrocytes (2 x 10 ⁶ cells/ml)	60-90%, 24h post-encapsulation [#]	[236]

Abbreviations: Irgacure 651 (2,2-dimethoxy-2-phenylacetophenone); PEG4NB (Poly(ethylene glycol)-tetra-norbornene); PEG (Poly(ethylene glycol)); PEGDA (Poly(ethylene glycol) Diacrylate); HA (Hyaluronic acid); TEOA (Triethanolamine); NVP (1-vinyl-2 pyrrolidinone); hMSCs (Human mesenchymal stem cells); DTT (Dithiothreitol); HepG2 (hepatocarcinoma cell line). *Quantitative data about cell viability is not available, but authors reported that cells survived and retain differentiation ability. [§]Authors state a predominance of thiol-ene reaction and negligible acrylate polymerization rates. **Riboflavin can form either singlet or triplet-excited states upon light absorption. ^{\$\$}Cell viability was assessed by culturing cells in the presence of photopolymer extract solutions, instead of cell encapsulation [#]Depending on the irradiation time and presence of HA.

2.6.4. Photocrosslinkable bioinks

In addition to the classical properties that biomaterials should present for tissue engineering [39, 237], bioinks must fulfil additional requirements, such as enable printing under cell-compatible conditions, exhibit fast gelation, allow the material to maintain structural integrity after deposition, and provide an interactive microenvironment for entrapped cells [43, 45, 178]. In contrast to traditional hydrogel materials, which often display low viscosity, bioinks must possess enough viscosity (paste-like consistency) to allow the deposition of stable filaments, and exhibit shear-thinning behaviour and fast recovery after extrusion to avoid deformation of the 3D bioprinted construct (**Figure 2.11A**). Rather than simply providing a suitable environment for supporting cells viability and function, advanced bioinks must be capable of providing specific spatiotemporal cues to embedded cells towards directing cellular activities such as adhesion, proliferation, differentiation and morphogenesis (**Figure 2.11B**). Approaches already applied in modern biomaterials, such as incorporation of cell-adhesion sites for cell anchorage, and proteolytically sensitive domains for cell-mediated matrix remodelling [197, 198, 238], can now be applied in the design of advanced bioinks.

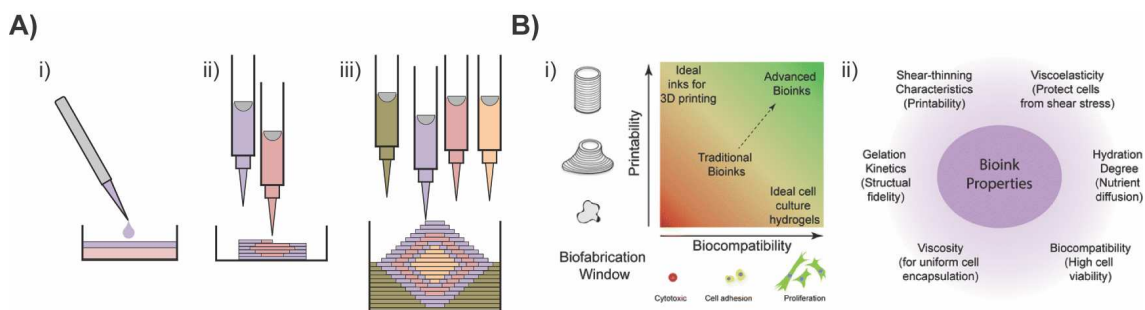


Figure 2.11. Main requisites of advanced bioinks for 3D bioprinting. (A) Differences of traditional hydrogel precursors *versus* bioinks; (i) hydrogels are usually generated from low viscosity polymer solutions within constrained spaces such as well plates or moulds, as these solutions cannot hold their shape after deposition; (ii) bioinks often possess moderate-to-high viscosities allowing the extrusion of filaments that maintain the shape after deposition without need for moulds; (iii) depending on the purpose, bioinks can be design to act as a temporary support material (gold) during the printing, structural material (purple) to provide rigidity, functional material (red) that support and direct cell functions, and sacrificial material (orange), which is soluble or rapidly degradable and may be incorporated within the construct to permit the inclusion of porous regions [239]. **(B)** Complexity on the design of cell-laden bioinks: (i) biofabrication window for the design of bioinks considering the compromise between printability requirements and biocompatibility of printed constructs; (ii) General requirements of advanced bioinks [240].

A multitude of natural and synthetic polymers have been modified for application as photocrosslinkable bioinks (**Table 2.7**). Although polymeric materials inherently contain several functional groups (e.g., carboxyl, amine, hydroxyl) in their native chemical structure, most do not contain photoreactive moieties, which precludes the occurrence of light-mediated reactions [241]. Thus, the design of hydrogel precursors for light-mediated chemistries primarily involves the chemical modification of polymers with reactive pendant groups (e.g., acrylates, methacrylates, or norbornene), which must be selected according to the photopolymerization scheme to be used, and their inherent cytotoxicity, reactivity and biodegradability. The type and number of reactive groups to be introduced into the polymer backbone should also be carefully optimized to prevent dramatic changes in the physicochemical properties of the polymer (e.g., hydrophilicity, charge, water solubility, elasticity, mesh size and diffusivity), which may ultimately impair the hydrogel cytocompatibility, biodegradability and bioactivity.

Most photocrosslinkable bioinks are crosslinked via free-radical polymerization through the homopolymerization of acrylate or methacrylate functional groups. One of the most widespread chemical modifications consists of the (meth)acrylation of polymers, through a reaction with glycidyl methacrylate, methacrylic anhydride or acryloyl chloride. Depending on the polymer chemistry and reactive agent, the esterification reaction proceeds predominantly through the primary hydroxyl groups [242], carboxylic groups [243] and amine side groups [232] of the polymer. Although non-organic solvents are usually the first choice for the modification of natural polymers due to their hydrophilic nature [174, 226], reactive agents easily hydrolyse under these conditions. Alternatively, natural polymers can be converted to a tetrabutylammonium (TBA) salt in order to allow dissolution in organic solvents [244], or reacted under heterogeneous conditions by using a co-solvent mixture that reduces the hydrolysis of functionalizing agents and enhances the degree of modification [245].

To explore the selective reactivity and fast gelation of bio-orthogonal reactions, bioinks crosslinked by photoinitiated thiol-ene click chemistry were recently developed for bioprinting. The natural polymers hyaluronic acid and gelatin were modified with 5-norbornene-2-carboxylic acid and allyl glycidyl ether, respectively, yielding norbornene-modified hyaluronic acid and allylated gelatin macromers [185, 246]. The synthetic polymer poly(glycidol), a structural analogue of PEG, was also modified through the introduction of either thiol or allyl functional groups for thiol-ene reaction [247]. These macromers allow the formulation of bioinks that undergo thiol-ene reaction in the presence of a photoinitiator and a dithiol (e.g., DTT, MMP-degradable peptide crosslinkers) via UV or visible light photopolymerization.

Table 2.7. Selected examples of photocrosslinkable bioinks for 3D bioprinting.

Bioink composition	Photocrosslinking (Photoinitiator)	Bioprinted cells	Application	Reference
Decellularized heart tissue ECM	UV free-radical polymerization (Riboflavin)	Cardiac progenitor cells	Not specified	[248]
Heprasil, Gelin-S, Extralink, multi-arm PEG crosslinkers, decellularized ECM solution	UV Thiol-ene click chemistry (I2959)	Liver spheroids	Liver tissue	[130]
Gelatin methacryloyl, alginate, gold nanorods	UV free-radical polymerization (I2959)	Cardiomyocytes and cardiac fibroblasts	Cardiac tissue	[249]
Gelatin methacryloyl, alginate, PEGTA	UV free-radical polymerization (I2959)	HUVECs, MSCs	Vascularized tissues	[250]
Allyl-functionalized gelatin	UV/Visible light Thiol-ene click chemistry (I2959, Ru/SPS)	Chondrocytes	Not specified	[251]
Heprasil or glycosil, gelin-S, Extralink	UV Thiol-ene click chemistry (I2959)	Amniotic fluid-derived stem cells	Skin tissue	[252]
pNIPAAm- or methacrylate-modified hyaluronic acid	UV free-radical polymerization (LAP)	Chondrocytes	Cartilage tissue	[253]
PEGDA, Iaponite XLG nanoclay, hyaluronic acid*	UV free-radical polymerization (IR 1173)	Osteoblasts	Bone tissue	[254]
Allyl- or thiol-modified poly(glycidol), hyaluronic acid	UV Thiol-ene click chemistry (I2959)	Human bone marrow-derived stromal cells	Not specified	[247]

Abbreviations: Heprasil – thiolated hyaluronic acid with conjugated heparin groups; Gelin-S – thiolated gelatin; Extralink – poly(ethylene glycol) diacrylate (PEGDA) cross-linker; PEGTA – 4-arm poly(ethylene glycol)-tetraacrylate; HUVECs – Human umbilical vein endothelial cells; MSCs – Human mesenchymal stem cells; Ru/SPS – tris(2,2'-bipyridyl)dichloro-ruthenium(II) hexahydrate with sodium persulfate; Glycosil – thiolated hyaluronic acid; pNIPAAm – poly(N-isopropylacrylamide); *PEG-clay nanocomposite bioink was used as a support material, while the hyaluronic acid bioink was loaded with cells.

2.7. Bioprinting hydrogels for skin tissue engineering

The interest in bioprinting technologies to produce cell-laden constructs for skin tissue engineering has been significantly increasing due to their ability to pattern heterogeneous cell populations, soluble factors and biomaterials in predesigned 3D locations with high degree of automation and reproducibility. These features provide new possibilities in the development of biomimetic constructs resembling the anatomical and cellular organization of the skin, with potential to address the limitations of current therapeutic options for skin reconstruction [1, 2]. Bioprinting processes also enable the integration with medical imaging techniques (e.g., micro-computed tomography, magnetic resonance imaging) and path-planning devices, allowing the design of patient-specific implants for direct printing either *in vitro* or *in situ* [47, 255]. Despite these attributes, the bioprinting of skin constructs is a complex and multidisciplinary task involving knowledge and professionals from different areas (**Figure 2.12**).

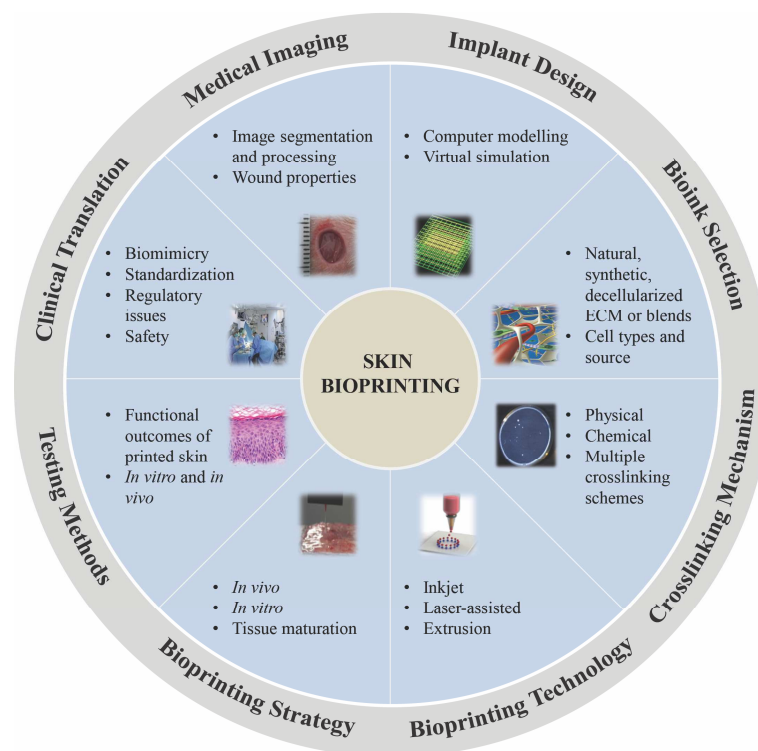


Figure 2.12. Illustration of the tasks involved in the design of 3D constructs for skin repair and regeneration using bioprinting technologies. The development of skin substitutes through bioprinting is a multidisciplinary process that involves the interplay between several disciplines.

2.7.1. Requirements of printed skin

Printed skin constructs are currently explored for several purposes including wound healing and *in vitro* models for pharmaceutical testing and disease studies (e.g., inflammatory skin disease). Advances in microfluidic and bioprinting technologies have also allowed the miniaturization of skin models through the development of skin-on-a-chip devices, which offer a valuable surrogate to animal experimentation [256]. In order to closely reproduce the main properties of native skin and provide reliable models for clinical translation, printed skin must replicate key compositional and functional characteristics of native skin.

2.7.1.1. Cellular composition

As already discussed, native skin is composed of multiple layers containing distinct cellular populations. The epidermal layer contains keratinocytes, melanocytes, Merkel and Langerhans cells. In the dermis, fibroblasts are the predominant cells, while the hypodermis is composed of adipocytes. To closely replicate the heterogeneous cellular composition of native skin, each cell type should be precisely dispensed at specific 3D locations in the respective layer. The density and ratio between cell populations within the construct must be controlled, in order to promote cell-cell interactions that regulate autocrine and paracrine signalling.

2.7.1.2. Biochemical composition

In the dermal region, cells are embedded within a rich ECM that provides cell-adhesion and cell-remodelling sites, allowing cells to remodel and interact with the surrounding matrix. The basement membrane physically separates skin layers, providing motifs for cell anchorage, which is essential for stabilization and diffusion of molecules. In printed skin, the biochemical cues, their function, location and density must be precisely controlled. The presence of cell-adhesion sites and cell-proteolytic domains is fundamental to replicate the dynamic and interactive nature of ECM. Also the ability to sequester and release bioactive molecules, for instance via growth factor-binding domains, is of paramount importance for the sustained release of cytokines and growth factors during wound healing.

2.7.1.3. Zonal organization and material composition

Native skin is a highly complex tissue with cells surrounded by an intricate ECM, which composition and ratio between ECM components vary according to the region. The dermal layer is rich in collagens (I, III, IV, VII), fibronectin and glycosaminoglycans. Dermis is also organized into an upper 'papillary' (high ratio of collagen type III to type I) and a lower

'reticular' (low ratio of collagen type III to type I) region [257]. At the epidermal–dermal junction, a basement membrane mostly composed of laminin and collagen IV provides a physical barrier between two layers [54]. Materials for skin printing should consider the fibrillar and hydrated nature of ECM. Although it is difficult to develop a formulation containing all the skin components, it is fundamental to engineer advanced materials with tuneable stiffness and composition, which could be readily altered according to the location throughout the construct.

2.7.1.4. Tissue architecture and shape

Skin thickness is in the range of 1.0 to 2.5 mm, depending on the location in the body, with the epidermis measuring approximately 0.2 mm [258]. The thin papillary region contains higher cellular density along randomly orientated collagen fibre bundles, while the thicker reticular dermis consists of highly orientated fibre bundles. The heterogeneity of skin throughout the body calls for the precise control over the layer thickness in bioprinted constructs, in order to matching the wound depth. In addition, the thickness and fibre orientation in both papillary and reticular dermis should be considered to improve biomimicry. The shape of the printed construct should also be defined according to the specific application.

2.7.1.5. Barrier function

Epidermis contains keratinocytes at different stages of differentiation with fully stratified keratinocyte layers providing an efficient barrier to the penetration of external agents across the skin. Lamellar granules, produced by keratinocytes, secrete several key compounds (lipids, proteins, hydrolytic enzymes) for skin barrier properties [53]. To recreate the barrier properties of skin, printed constructs must contain an epidermal region consisting of densely packed keratinocytes. Constructs need to be cultured at air–liquid interface (ALI) to promote stratification and the barrier properties must be carefully evaluated. Late or incomplete stratification and keratinization of printed constructs must be evaluated, particularly when immortalized keratinocytes are used.

2.7.1.6. Appendages and pigmentation

Skin contains adnexal structures such as nails, hair follicles, sweat, apocrine and sebaceous glands. Melanocytes produce melanin, a pigment that confers coloration to the skin and protects from UV light. Merkel and Langerhans cells participate in sensing and immunological defence, respectively. The development of skin appendages in printed skin is a major challenge in the field. Skin pigmentation can be addressed by printing melanocytes

in the epidermis, while sweat glands can be engineered by printing epidermal-derived stem/progenitor cells [259, 260].

2.7.1.7. Vascularization

Dermis contains numerous blood vessels that provide nutritional support to the skin. Vasculature includes larger blood vessels at the interface between the reticular dermis and hypodermis, which branch into small vessels to supply superficial plexus at the junction between the papillary and reticular dermis, as well as the epidermis by diffusion. The ability to engineer functional vasculature in 3D is critical for nutrient supply throughout thick skin constructs. Printing branched, perfusable channels could be a viable solution to promote efficient mass transfer of the skin. Complementary strategies could also involve the co-printing of stromal and endothelial cells [177].

2.7.2. Hydrogel bioinks for skin bioprinting

Hydrogels are attractive materials for skin reconstruction as they provide a hydrated and highly permeable microenvironment in which, depending on the composition (e.g., cell-adhesion and proteolytically sensitive motifs) and properties (e.g., stiffness), entrapped cells might migrate and proliferate in a similar way to what happens in the native ECM [43]. Hydrogels have been widely used to assist the regenerative and reparative processes of many tissues [205, 261, 262] and several studies were performed assessing their potential for wound healing [109, 263-265]. Hydrogels display many of the desired characteristics of an ideal skin substitute, as they promote wound debridement, while providing a suitable moist environment to stimulate the healing process. In addition, they can absorb wound exudates, allow gaseous exchanges and prevent bacterial invasion. Hydrogels also provide thermal isolation and display low adherence to the wound bed, which facilitates dressing change without trauma to the patient. Furthermore, the fine-tuning of hydrogel properties is easy to achieve, allowing control over stiffness, biodegradability rates and permeability to either cells or soluble factors. Transparent hydrogels also allow to follow-up the wound healing process without removal.

A major challenge in skin bioprinting is the design of suitable bioinks to produce 3D cellular constructs with intricate geometries, shape fidelity, and high resolution in the placement of cells. Traditional approaches to generate such constructs often involve (i) the sequential printing of cell-laden hydrogels or melt extruded thermoplastic fibres, (ii) the formulation of viscous bioinks by adding high molecular weight polymers (e.g., hyaluronic acid), or (iii) the use of increased polymer concentrations and crosslinking densities [182,

266-268]. The combination of hydrogel bioprinting with melt extrusion has been successfully explored to design well-defined 3D constructs with improved mechanical properties, which is of special interest for load-bearing tissues [46], but of limited application in soft tissues. The printing process of viscous bioinks might affect the distribution of cells throughout the construct, ultimately leading to tissue heterogeneity, while highly crosslinked hydrogels may lead to excessively stiff matrices that impose severe restrictions to cell spreading, migration and proliferation [232, 269, 270]. Thus, it is crucial to ensure that the bioink has the appropriate rheological properties to be printed and, at the same time, is able to maintain the shape upon deposition. Alternative strategies have been tested to improve the printing fidelity without compromising the bioink cytocompatibility, including the printing of partially crosslinked hydrogels, the crosslinking of hydrogel solutions during bioprinting, and the deposition of biocompatible sacrificial materials that provide initial support for the printed hydrogel pattern [185, 271].

The development of hydrogel bioinks is a complex and multidisciplinary process that involves knowledge about the principles of printing mechanisms and the fluid properties required for a given liquid to be printable. The interactions between the bioink and the receiving substrate, as well as its rheological properties, are important parameters determining the resolution and accuracy of printed constructs [43, 151, 161, 272, 273]. By placing suitable cell types in appropriate positions, the tissue construct may then mature into a tissue/organ and later achieve functionality either inside a bioreactor or *in vivo* [274]. The ideal properties of hydrogels for bioprinting include stability, sterilization, biodegradability, adequate mechanical properties and swelling characteristics, but it is also required that both hydrogel chemistry and crosslinking mechanisms promote cell function [275]. For extrusion bioprinting, in which the bioink flows through a nozzle towards the substrate, rheological properties are particularly relevant. The rheological behaviour of bioink determines how the viscosity is affected during the printing as a response to the shear stress. Printing cells embedded in a hydrogel precursor solution also requires careful selection of the viscosity in order to ensure homogenous distribution of cells and prevent nozzle clogging. Moreover, the bioink should also undergo a fast and cytocompatible gelation after deposition in order to maintain the prescribed shape and spatial location of cells at high resolution.

Despite recent advances in the design of printable bioinks for various applications the number of bioinks for bioprinting cellular skin substitutes is still limited to a restricted number of natural hydrogels including alginate, collagen, gelatin, fibrin and hyaluronic acid (**Table 2.8**). The interest in these materials mainly relies on the fact that their composition and structure resembles the ECM properties of native tissues [276]. These polymers can also be easily converted into either physical or chemical hydrogels under cell-compatible conditions

through a myriad of crosslinking pathways [194]. In addition, certain natural polymers (e.g., collagen) also present cell-proteolytic domains and/or adhesion motifs, providing recognition sites for embedded cells and allowing the cell-mediated degradation of the hydrogel network in a similar way to the remodelling of native ECM. Natural hydrogels, in particular protein-derived hydrogels, usually present concerns regarding their weak mechanical properties, high immunogenicity and virus/disease transmission, though they retain their biological activity being the most widely used ECM-mimicking materials [136, 197]. Synthetic hydrogels constitute an interesting alternative due to their controlled chemical composition and tuneable mechanical properties. The drawback of synthetic materials is the lack of cell-adhesion moieties, which can be solved by the incorporation of cell instructive cues into the polymer backbone, as already discussed [186].

Table 2.8. Bioinks for 3D bioprinting of skin constructs.

Bioink composition	Crosslinking	Bioprinted cells	Bioprinting strategy	Bioprinting technology	Reference
Decellularized skin-derived ECM	Thermal gelation	Keratinocytes, fibroblasts, EPCs, ASCs	<i>In vitro</i> bioprinting	Extrusion	[277]
Gelatin methacrylamide and collagen doped with tyrosinase	Enzymatic and UV free-radical polymerization	Keratinocytes, melanocytes, fibroblasts	<i>In vitro</i> bioprinting, followed by 3 days of culture and <i>in vivo</i> implantation	Extrusion	[278]
Heprasil or glycosil, gelin-S, Extralink	UV Thiol-ene click chemistry	Amniotic fluid-derived stem cells	<i>In situ</i> bioprinting	Inkjet bioprinting	[252]
Gelatin, alginate, fibrinogen	Ionic gelation and polycondensation	Fibroblasts and seeded keratinocytes	<i>In vitro</i> bioprinting	Extrusion	[279]
Collagen	Sodium bicarbonate neutralization	Keratinocytes, melanocytes, fibroblasts	<i>In vitro</i> bioprinting	Inkjet bioprinting	[280]
Gelatin, alginate, mouse plantar dermis components, EGF	Ionic gelation	Epidermal progenitor cells	<i>In vitro</i> bioprinting, followed by <i>in vivo</i> implantation	Extrusion	[260]
Collagen	Sodium bicarbonate neutralization	Keratinocytes, fibroblasts	<i>In vitro</i> bioprinting	LAB	[281]
Collagen, fibrinogen	Polycondensation	Amniotic fluid-derived stem cells, bone marrow-derived MSCs	<i>In situ</i> bioprinting	Inkjet bioprinting	[47]

2.7.3. Bioprinted constructs for skin repair

One application of printed skin constructs is to promote wound repair and regeneration. Functional skin is an important need in the medical field to treat patients with a variety of injuries, including (i) burn wounds that lack the skin barrier and are more susceptible to infection, (ii) chronic wounds that are difficult to heal and are associated to high healthcare costs, and (iii) scars that cause severe aesthetic limitations and movement disabilities. To address these needs, bioprinting has been explored to create sophisticated bi-layered skin substitutes containing dermal and epidermal components.

In a pioneer work, LAB was used to produce multi-layered cellular skin constructs for *in vivo* regeneration of full-thickness skin wounds in nude mice [48] (**Figure 2.13A**). Skin substitutes were created by printing 20 layers of NIH3T3 fibroblasts followed by 20 layers of HaCaT keratinocytes suspended in collagen onto a sheet of Matriderm[®], and subsequently incubated under submerged conditions overnight. After 11 days of *in vivo* implantation, skin substitutes showed a good integration into the native tissue with small blood vessels being detected in the printed skin substitutes. Immunohistochemistry assays confirmed the presence of E-cadherin between the keratinocytes, indicating the establishment of cell-cell contacts. This work demonstrated the capability of LAB to produce 3D skin substitutes capable of developing functional tissues *in vitro* and promote skin regeneration *in vivo*, which represents an exciting advance in the field of 3D skin bioprinting.

In a recent work, a skin-derived ECM bioink was used to print *in vitro* 3D full-thickness skin models and 3D pre-vascularized skin patches for *in vivo* skin reconstruction (**Figure 2.13B**) [277]. Skin models were generated by the bioprinting of dermal fibroblasts in the dermal region, followed by the printing of human neonatal epidermal keratinocytes to recreate the epidermal region. Bioprinted skin models showed little contraction during culture, supporting the deposition of collagen type I in the dermal layer and showing expression of differentiation makers (keratin 10 and involucrin) on the epidermal layer. Pre-vascularized skin patches were created through the bioprinting of a bioink loaded with EPCs and ASCs, cultured *in vitro* for 3 days, and subsequently implanted in full-thickness excisional wounds created on BALB/cA-nu/nu mice. Results showed that bioprinted skin patches resulted in superior wound closure and re-epithelialization compared to the control groups. Laser Doppler perfusion imaging also indicated that skin patches improved the blood flow in the early phase of wound healing, enhancing neovascularization.

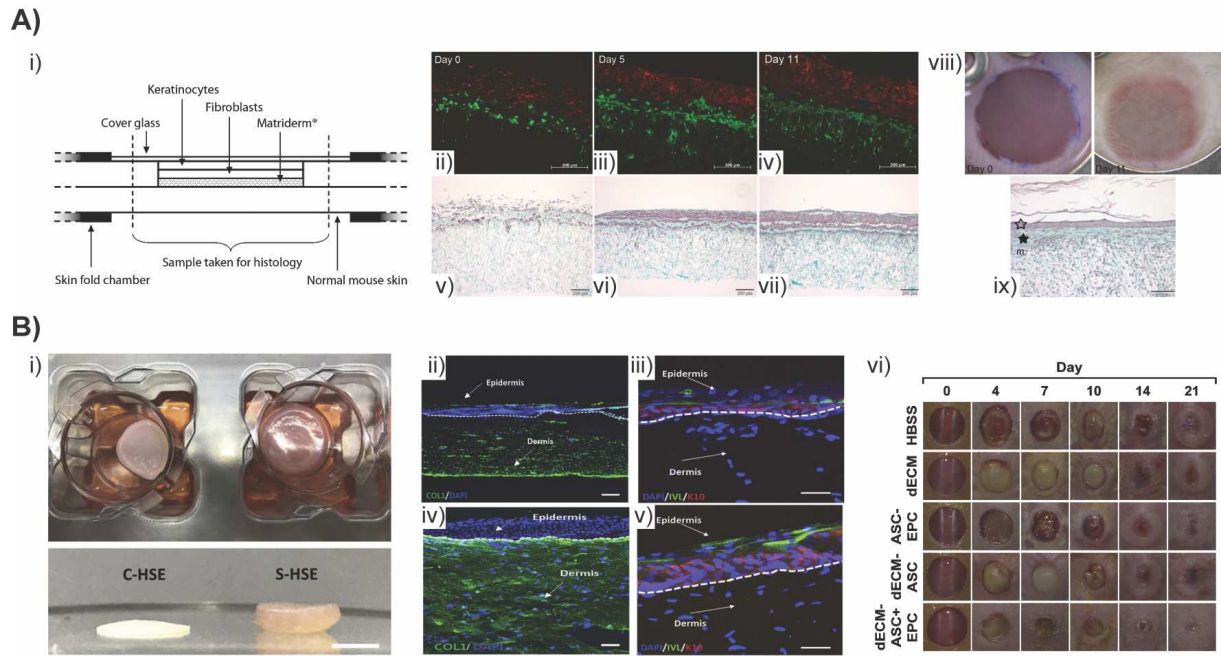


Figure 2.13. Bioprinted 3D constructs for *in vivo* skin repair. (A) Bilayered skin substitute produced by LAB through the printing of fibroblasts and keratinocytes: (i) schematics of used dorsal skin fold chambers in mice; (ii-iv) fluorescent microscopy images showing the presence of keratinocytes (red) and fibroblasts (green) after 11 days of *in vitro* ALI culture; (v-vii) masson's trichrome staining of sections containing collagen (green) and cells (reddish), indicating the formation of a dense epidermis on day 5; (viii) construct in the dorsal skin fold chamber in nude mice immediately upon implantation (left) and after 11 days (right); (ix) histological section of the tissue construct stained with Masson's trichrome showing a dense epidermis (empty asterisks) and a corneal layer [48]. (B) Extrusion bioprinting of human skin equivalents and 3D pre-vascularized patches for *in vivo* skin reconstruction: (i) photographs of printed skin equivalents using type I collagen (C-HSE) and skin-derived bioink (S-HSE) (scale bar: 2 mm); expression of proteins in C-HSE (ii, iii) and S-HSE (iv, v) on day 10 after ALI culture (Involucrin (IVL): early epidermal differentiation marker, keratin 10 (K10): late epidermal differentiation marker) (scale bars: 50 μ m); (vi) photographs of skin wounds throughout 21 days of treatment with 1) Hank's Balanced Salt Solution (HBSS), 2) cell-free skin patch using dECM (dECM), 3) ASCs + EPCs injection (ASC + EPC), 4) ASC-printed skin patch using dECM (dECM-ASC), 5) ASCs + EPCs-printed skin patch using dECM (dECM-ASC + EPC) [277].

2.7.4. Bioprinted constructs as *in vitro* skin models

The interest in bioprinting human skin models as platforms for toxicity and efficacy testing of topical medications and cosmetics has been significantly increasing due to the need for cost-effective alternatives to animal experimentation. Although there are several works demonstrating the printing and characterization of bilayered skin constructs [279, 282], there is a lack of studies exploring their applicability for pharmaceutical or cosmetic testing. The majority of these studies employ skin equivalents exclusively created by manual

methods [283, 284] or fabricated using components obtained by 3D printing technologies combined with manual deposition of cell-laden solutions [256].

Lee et al [285] used a robotic cell dispensing technology to fabricate 3D cell-laden constructs mimicking the native skin anatomy. Their approach involved the printing of collagen hydrogel precursor solutions and keratinocytes or fibroblasts in suspension, followed by the crosslinking of each printed layer using a nebulized sodium bicarbonate solution as a gelation agent (**Figure 2.14A**). No significant differences on the viability of printed cells were found between printed and manually plated cells, while confocal microscope images of printed 3D constructs showed distinct layers of fibroblasts and keratinocytes after 4 days of *in vitro* culture. This strategy was further explored and optimized by the same group, where particular attention was given to the optimization of printing parameters, cell densities and histological characterization of skin constructs [286]. Printed multi-layered constructs were cultured under submerged conditions followed by exposure to the air-liquid interface to stimulate proliferation of keratinocytes. At day 14, printed constructs exhibited a dense epidermal layer and a sparsely populated dermal layer without cell invasion and migration across the two regions. Histological analysis revealed epidermis compaction along the period of ALI culture, accompanied by the formation of terminally differentiated stratum corneum and thigh junctions between keratinocytes. Printed constructs maintained the shape and dimensions without shrinkage during the culture period, while conventional constructs obtained by manual deposition presented continuous shrinkage and shape modification (**Figure 2.14B**). Further improvements on the density of fibroblasts in the dermis, as well as on the stratification and keratinization, are required to better mimic the native skin.

LAB was also explored to produce 3D skin grafts consisting of a collagen matrix containing fibroblasts and keratinocytes in two main regions, aiming at mimicking the anatomic organization of native skin [155]. The bilayered 3D skin substitute was created by printing 20 layers of fibroblasts followed by 20 layers of keratinocytes. Both cell types were embedded in a collagen matrix and transferred onto a receiving slide coated with MatrigelTM. After 10 days of *in vitro* culture, cells remained viable and located at the printed positions, without mixing between fibroblasts and keratinocytes. Immunohistochemical analyses revealed the formation of a laminin layer between the fibroblasts and keratinocytes layers. In another study, Cubo et al [287] used an extrusion-based bioprinter to create a human plasma-derived bilayered skin using fibroblasts and keratinocytes. The dermal component was created by printing fibroblasts embedded within a plasma-derived fibrin hydrogel, which was allowed to polymerize for 30 minutes before the seeding of keratinocytes to generate the epidermal component. For *in vitro* testing, skin constructs were

printed on Transwell inserts, allowed to differentiate at the air–liquid interface for 17 days, and evaluated for their resemblance to the native tissue. Histological analysis showed the formation of skin equivalents with structural resemblance to the human skin. To evaluate the *in vivo* differentiation capability of printed constructs, the substitutes were printed, incubated overnight, and immediately grafted on full-thickness wounds created on the backs of immunodeficient athymic mice. Immunofluorescence results indicated the presence of stratum basal, stratum spinosum, stratum granulosum and stratum corneum on the epidermal component, as well as the formation of the dermo-epidermal junction at the interface with the dermal component. Recently, Kim et al [288] developed a hybrid bioprinting approach to fabricate a human skin model with a functional Transwell system in a single-step process. In their strategy, an extrusion module capable of printing hydrogel bioinks and thermoplastics was used to print the dermal compartment and a PCL mesh to reduce collagen shrinkage during the construct maturation, respectively. The fibroblast-loaded collagen bioink was printed onto the PCL mesh to create the dermal region, while an inkjet module was subsequently applied to print the epidermal region through the deposition of keratinocytes on top of the dermis-like layer. The dermal region exhibited smaller shrinkage compared to the control group (fibroblasts in collagen gel), while keratinocytes displayed a more uniform distribution and higher proliferation rate when compared to manually deposited cells.

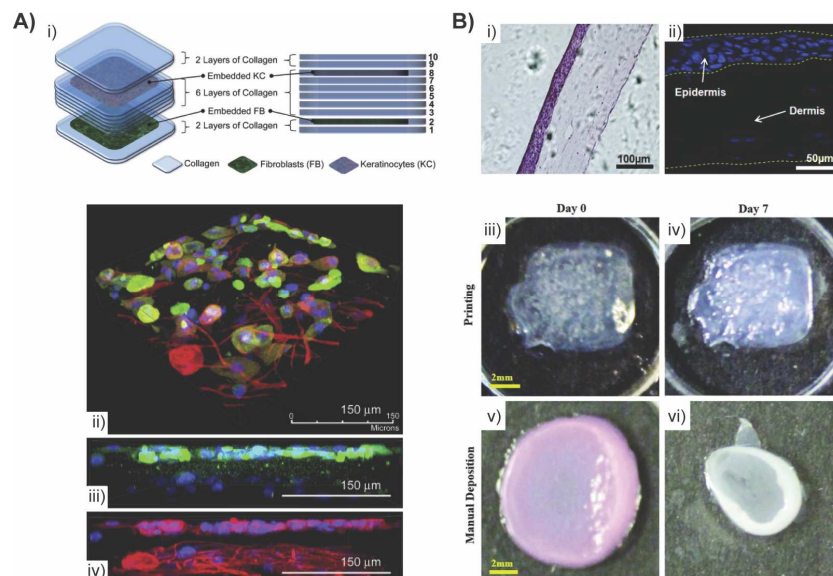


Figure 2.14. Bioprinting of 3D human skin constructs as *in vitro* models. (A) Extrusion bioprinting of 3D skin models: (i) schematic illustration of bioprinting strategy and composition of skin constructs; (ii) immunofluorescent images of multi-layered skin constructs and its projection of (iii) keratin-containing keratinocytes layer and (iv) β -tubulin-containing keratinocytes and fibroblasts [285]. **(B)** *In*

in vitro skin models generated by bioprinting: (i) histological images of printed skin construct using haematoxylin and eosin and (ii) nuclear staining at day 14 of ALL culture; (iii-vi) macroscopic images of constructs produced by bioprinting and manual deposition at day 0 or day 7 of submerged culture [286].

2.7.5. Bioprinted constructs with skin appendages and pigmentation

To create biomimetic skin constructs, the complexity of the tissue must be addressed behind generating the two major macro-structures of the skin, i.e., dermal and epidermal layers. Thus, a great deal of interest has recently been focused on the integration of appendage structures into skin constructs, including sweat glands and pigmentation.

The regeneration of sweat glands using 3D printed ECM-mimic environments was addressed by Huang et al [260] using a gelatin-based bioink. The bioink composed of gelatin, alginate, mouse plantar dermis components (collection of protein molecules with bone morphogenetic protein (BMP-4)), and EGF was designed to provide a 3D niche to promote differentiation of epidermal progenitors into sweat gland cells. Several bioink compositions (with or without EGF and with plantar or dorsal dermis components) were printed using an extrusion system, crosslinked with calcium chloride, and their properties evaluated regarding cell viability and differentiation. *In vitro* tests showed that cells embedded within the hydrogel containing EGF and plantar dermis components differentiated into sweat gland cells, as observed by expression of luminal epithelial markers. After *in vitro* characterization, 3D constructs were implanted into mice burned paws to assess their performance. Printed hydrogels containing both EGF and plantar dermis components restored the sweat gland function upon 14 days, performing better than the other tested groups (**Figure 2.15A**). Histological analysis also revealed the formation of sweat glands in regenerated skin and degradation of the hydrogel network. Although this study did not reveal the mechanisms of sweat gland restoration, this bioprinting strategy could be a useful tool for further research on the restoration of skin appendages. In a later study, the same research group demonstrated that the 3D architecture of printed constructs determines the sweat gland morphogenesis [289]. 3D porous constructs ($20 \times 20 \times 5 \text{ mm}^3$) were printed using different bioinks (with and without plantar dermis components) and printing nozzles (300 and 400 μm) (**Figure 2.15A**) and their effect on sweat gland cell differentiation and morphogenesis was evaluated. After 14 days of culture, epithelial progenitors in constructs produced with the 300 μm nozzle showed higher expression of luminal epithelial markers, which is characteristic of differentiation into sweat gland cells. At later culture period (28 days), specific morphology of sweat gland tissue was only present in constructs printed with the 300 μm nozzle and the plantar dermis-containing bioink. The authors suggest that the larger pore size of constructs

produced with the 300 μm nozzle together with the release of plantar dermis components (inductive factors) from the constructs might influence and guide the differentiation of printed cells. However, the mechanisms and cues that regulate cell response to the 3D architecture and drive cell differentiation and sweat gland formation still remain unknown.

Skin pigmentation is associated to the production of melanin from melanocytes and its transfer to the surrounding keratinocytes, being an important requirement of skin constructs. Min et al [280] used a micro-valve based bioprinter that deposits small liquid droplets to create full-thickness skin constructs containing pigmentation. The dermal component was created by printing five layers of collagen precursor solution, which was crosslinked through neutralization with sodium bicarbonate. During the fabrication, a suspension of fibroblasts was printed and embedded in the layers 2-4. After 1 day of culture, a suspension of melanocytes was printed on top of the dermal layer in two different configurations (**Figure 2.15B**). After 4 days of culture, a suspension of primary keratinocytes was then printed on top of the constructs, followed by submerged culture (1 day) and ALI culture for 4 days. Histological characterization showed the formation of distinct dermal and epidermal layers with terminal differentiation of keratinocytes, as shown by loricrin staining. Printed melanocytes in the epidermal layer formed multiple clusters of dark pigmentation, as observed by visual inspection and bright-field microscopic images. However, constructs exhibited non-uniform pigmentation, being necessary further optimization to improve the homogeneity in skin pigmentation.

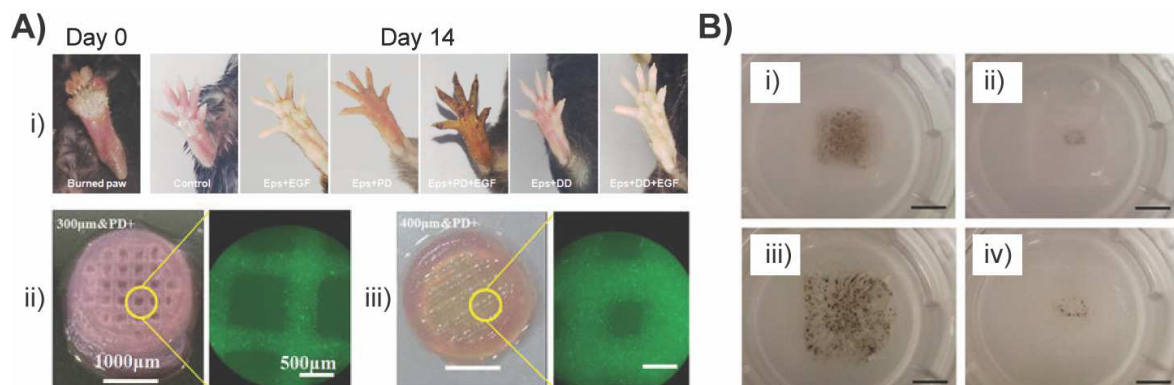


Figure 2.15. Bioprinted skin constructs with appendages. (A) Regeneration of sweat glands on burned paws of mice with bioprinted skin constructs: (i) iodine/starch-based sweat test on paws of mice 14 days after implantation of the constructs (dark spots, indicative of sweat secretion, were only detected in the foot paw pads of Eps + PD + EGF group) [260]; (ii) photographs and cell distribution within bioprinted 3D porous constructs with different architectures (300 μm or 400 μm nozzle diameters) after 24 hours of culture [289]. **(B)** Bioprinted skin constructs containing melanocytes: (i-iv) macroscopic images of constructs with melanocytes printed in the area model or spot model before

(i,ii) and after ALI culture (iii,iv) (scale bars: 5 mm) [280]. Abbreviations: PD – mouse plantar dermis; EGF – epidermal growth factor; Eps – epithelial progenitors; DD – mouse dorsal dermis.

2.7.6. Bioprinted vascularized skin constructs

The formation of biologically relevant constructs containing a functional, perfusable vascular network is a major hurdle towards the full implementation and clinical translation of skin bioprinting. Vascularization of bioprinted skin constructs is essential to recapitulate the vasculature of dermis and to provide nutrients and oxygen to the embedded cells. It also plays a key role in the integration of implanted constructs with the host tissue, which remains a limitation of current skin substitutes. In the absence of a functional vascular network, nutrients, oxygen and soluble factors are supplied to the cells by diffusion, which is a slow and inefficient process that may lead to suboptimal cell nutrition, cell necrosis or delayed new tissue formation [290]. *In vivo*, vascularized tissues contain an organized system of larger blood vessels that branch into smaller vessels, which ultimately branch into capillaries distributed throughout the tissue. Capillaries are in the close proximity (maximum ~200µm) to the cells allowing nutrition, oxygenation and removal of waste products [291]. The natural formation of a vascular network *in vivo* is regulated by two underlying processes of vasculogenesis and angiogenesis. The first predominates during early embryonic development to form a primitive capillary network, while the second takes place in adults aiming at the revascularization of damaged or diseased tissues from existing blood vessels [291, 292]. Recapitulating these biological processes in printed tissues is challenging and requires a proper spatiotemporal interplay between vascular cells, resident cells and surrounding ECM. Although several strategies have been explored to promote vascularization in skin constructs [11, 293], engineering branched vascularization in 3D hierarchical architectures remains a great challenge. Bioprinting technologies are attractive to engineer a vascular tree within thick constructs by the precise layer by layer deposition of multiple cell types and ECM-like bioinks into prescribed spatial locations at high resolution [294]. Promising approaches to generate vascular networks have been reported using inkjet [295, 296], LAB [297], and extrusion bioprinting [41, 177, 298]. In general, these approaches are based on four main strategies: (i) direct patterning of vascular cells onto a receiving substrate [297], (ii) continuous printing of polymeric bioink loaded with endothelial cells followed by polymer removal [299], (iii) printing of perfusable channels in a 3D construct for subsequent injection of a cell suspension into the empty channel [177], and (iv) printing of multicellular spheroids [298].

To address the need for vascularization in skin substitutes, Yanez et al [296] used the inkjet technology to fabricate capillary-like endothelial networks into a dermo-epidermal skin

graft consisting of neonatal human dermal fibroblasts and neonatal human epidermal keratinocytes embedded in a fibrin-collagen matrix. Human dermal microvascular endothelial cells (HMVECs) were mixed with thrombin and inkjet printed on top of a manually plated layer of collagen-neonatal human dermal fibroblasts cells containing fibrinogen. After formation of the fibrin hydrogel, a layer of collagen containing neonatal human epidermal keratinocytes cells was pipetted on top of it to produce bilayered structures. These structures were then implanted into skin full-thickness wounds on the back of athymic nude mice to investigate healing properties and integration with the native tissue. Wounds treated with printed substitutes required 14-16 days to heal, contrasting with 21 days in the control group (no skin graft) and 28 days in the group implanted with Apligraf[®]. Histological characterization of the wounds treated with the printed substitutes on post-operative day 14 showed the formation of dermal and epidermal skin layers similar to the native skin, accompanied by the presence of new micro-vessels in the mouse tissue. It was suggested that new blood vessel formation was stimulated by the presence of endothelial cells, indicating partial integration of the skin graft into the host tissue, which was further confirmed by the presence of human cells in the mouse tissue. More recently, Abaci et al [300] developed an integrated strategy to generate perfusable vascular networks in human skin equivalents using primary and induced pluripotent stem cell (iPSC)-derived endothelial cells (iECs). 3D printing technology was explored to create moulds with the desired vasculature pattern and functional components for the fabrication of embedded vasculature. Sacrificial channels composed of crosslinked alginate were printed and embedded with dermal fibroblasts embedded with a collagen matrix. After 7 days of culture, keratinocytes were seeded on the top of the dermal compartment, cultured under submerged conditions for 7 days and subsequently maintained at ALI interface for additional 7 days. After this period of time, perfusable channels were created by removing the alginate using a sodium citrate solution, followed by the injection of either human umbilical vein endothelial cells (HUVECs) or iECs, which established proper endothelial barrier function. Vascularized skin constructs grafted on the back of immunodeficient mice for 14 days were perfused with blood, while both non-vascularized constructs and constructs with acellular channels remained non-perfused, which suggest that engineered vasculature promotes and guides neovascularization of skin constructs. Although the skin construct was created by manual deposition of cell-laden solutions rather than using bioprinting technologies, this study reports an integrated approach to generate vascularized skin equivalents for tissue engineering applications. A similar approach to fabricate perfusable vascular channels within skin equivalents was recently reported by Mori et al [256], who demonstrated the applicability of vascularized skin equivalents for dermatological studies and drug testing.

2.7.7. *In situ* bioprinting of skin substitutes

In addition to the bioprinting of 3D skin constructs *in vitro* for subsequent implantation, key advances have also been achieved on the development of integrated bioprinting strategies for the *in situ* printing of cellular skin substitutes. *In situ* skin bioprinting is challenging as it requires the development of dedicated bioprinting devices, the integration with imaging systems to obtain data from the wound site, and the design of bioinks capable of instructing printed cells to perform their native functions. In a pioneer work, Binder et al [47, 301] developed a device for *in situ* skin printing composed of a cartridge delivery system containing a series of inkjet nozzles and a laser scanning system, both mounted on a portable XYZ plotting system. The data obtained from the laser was used to reconstruct a 3D model of the wound, which was subsequently employed to determine the skin area that was missing from the wound. Afterwards, the printheads filled the wound site with a bioink containing skin cells. The potential of the system to promote skin reconstruction was firstly evaluated through the printing of human keratinocytes and fibroblasts suspended in a fibrinogen-collagen precursor solution into full thickness skin lesions ($3.0 \times 2.5 \text{ cm}^2$) created on nu/nu mice [301]. After printing each layer, a thrombin solution was sprayed on top of the deposited layer to induce hydrogel formation. Results showed the complete closure of the wound in 3 weeks and the formation of new skin with similar properties to the native tissue. Histological analyses also revealed that the newly formed skin contained organized dermal collagen and a fully developed epidermis. The same research group used a similar procedure and bioprinting technique to print AFSs and bone marrow-derived mesenchymal stem cells (MSCs) suspended in a fibrinogen-collagen gel into full-thickness skin wounds in mice [47]. The bioink was dispensed to the skin wounds ($2.0 \times 2.0 \text{ cm}^2$) with uniform cell distribution. The closure and re-epithelialization of wounds treated with printed AFSs and MSC were superior to those of wounds treated only with the fibrin-collagen hydrogel. Histological sections of skin samples harvested 2 weeks after printing showed well-defined and organized epidermal layers of the regenerated skin in MSC and AFSs-treated wounds, which was accompanied by increased neovascularization and blood vessel maturation, particularly in the case of AFSs-treated wounds. However, findings also demonstrated that cells only remained transiently at the lesion site and did not permanently integrate with the host tissue. Another limitation of this bioprinting approach relies on the slow crosslinking time of the bioink system, which increased the overall length of the procedure.

Besides suitable mechanical, swelling and biodegradation characteristics, bioinks for *in situ* skin bioprinting should exhibit fast crosslinking to reduce the printing time, support cell activity, and eventually act as a delivery vehicle of biological factors. In order to meet such requirements, Skardal et al [252] recently developed a photocrosslinkable heparin-

conjugated hyaluronic acid (HA-HP) hydrogel capable of sequestering and releasing cell-secreted growth factors. The bioink system, composed of thiolated hyaluronic acid with conjugated heparin, thiolated gelatin, PEGDA crosslinker and I2959 as photoinitiator, was loaded with AFSs and printed directly onto full thickness skin wounds ($2.0 \times 2.0 \text{ cm}^2$) in a nu/nu murine model (**Figure 2.16**). After printing, the bioink was crosslinked *in situ* via thiol-ene photopolymerization upon exposure to UV light. *In vitro* tests indicated the effectiveness of heparin-mediated growth factor binding in modulating the release of proangiogenic AFS-secreted FGF and VEGF from HA-HP hydrogels. Wounds treated with cell-laden HA-HP hydrogels showed slightly higher closure rate and re-epithelialization compared to both hyaluronic acid-treated and non-treated wounds, though the differences between groups were not statistically significant after 14 days post-printing. Histological characterization of the harvested skin tissue indicated that HA-HP hydrogels promoted higher microvessel density, which may be due to the sequestration of and release of AFS cell-secreted growth factors as well as increased deposition of elastin. Although this work demonstrates the potential of photopolymerizable heparin-containing hyaluronic acid based bioinks combined with AFSs for *in situ* skin printing, further characterization regarding the effectiveness of this strategy on the wound healing and quality of new skin is necessary.

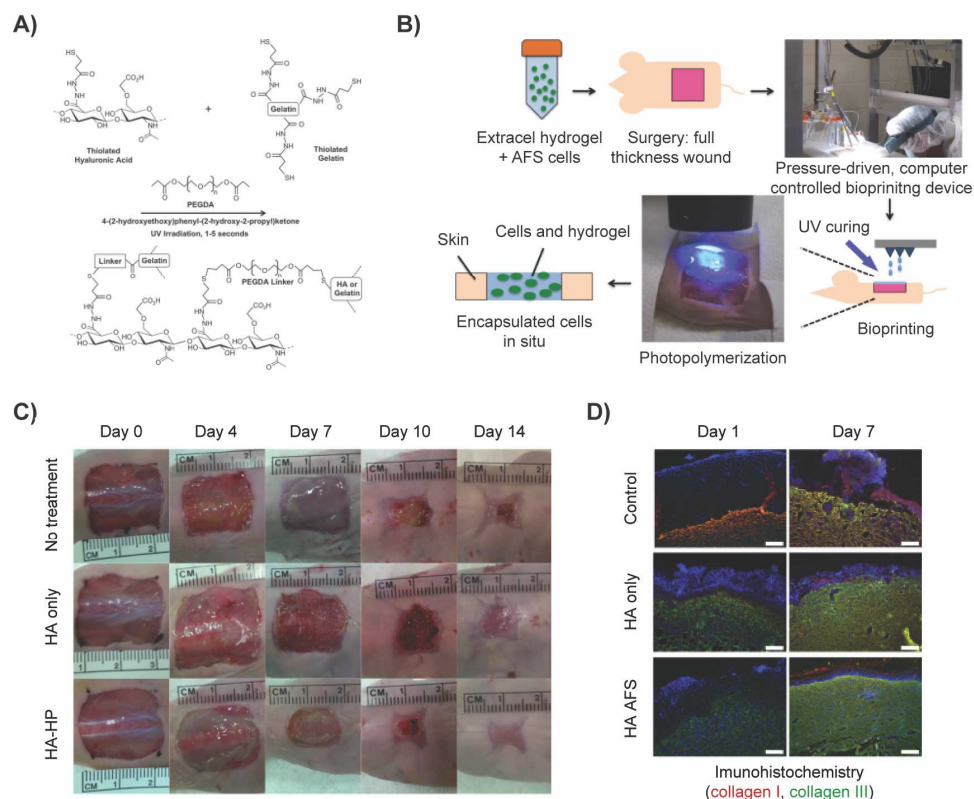


Figure 2.16. *In situ* bioprinting of a photocrosslinkable heparin-conjugated hyaluronic acid hydrogel system loaded with AFSs into full-thickness skin wounds in a nu/nu murine model.

(A) Schematic representation of UV light photoinitiated thiol-ene polymerization of the hydrogel system. (B) Illustration of the *in situ* bioprinting strategy. (C) Macroscopic images of the wounds over the study, showing enhanced closure of wounds treated with the hydrogel system compared to the control groups (HA: hyaluronic acid). (D) Immunohistochemistry analysis of tissue sections stained for collagen type I (red), collagen type III (green), and DAPI (blue) [252].

2.8. Conclusions

The field of skin bioprinting has experienced exciting advances in the direct printing of cellularized hydrogel constructs as effective alternatives to current therapies for skin repair and regeneration. Bioprinting technologies have been applied to create 3D constructs that recapitulate, to some extent, the architecture and cellular composition of native skin. Although those processes allow the precise patterning of skin cells and ECM components in the form of 3D constructs capable of promoting *in vitro* and *in vivo* skin formation, the field of skin bioprinting is still in an early stage, facing numerous challenges in diverse areas.

A critical issue is the availability of bioprinters capable of producing constructs that replicate the intricate ECM composition of skin. Since most of the bioprinters currently used in laboratories result from technical modifications of available technologies and/or equipment, they usually have limited resolution and accuracy, which imposes serious restrictions to the processing conditions, range of printable biomaterials and characteristics of the printed construct. Despite the existence of dedicated bioprinting technologies capable of processing biologically relevant biomaterials and living cells already available in the market (e.g., 3D Bioplotter[®], 3DDiscovery[®]), the printing speed and resolution should be increased in order to better reproduce the heterogeneity found in natural tissues and produce constructs with clinically-relevant dimensions in acceptable periods of time. Another important aspect relies on the inclusion of physical and chemical crosslinking methods in the bioprinting process to induce rapid gelation during biofabrication, in order to maintain shape fidelity and prevent loss of resolution. The development of hybrid bioprinting approaches for skin tissue engineering, through the combination of bioprinting and other biofabrication techniques with different scales of resolution, is also an important challenge that could enhance the functional outcomes of constructs and overcome technical limitations.

Another important limiting factor in skin bioprinting is the lack of printable bioinks exhibiting appropriate rheological, mechanical and biological properties. As a result of the distinctive requisites of each bioprinting strategy, most of the natural and synthetic hydrogels that have been applied for skin wound healing need to be re-engineered to allow adequate processing through bioprinting. Besides printability, such materials must exhibit a plethora of

characteristics, including biocompatibility, biodegradability, ability to preserve cell viability and function during/upon printing, appropriate immunological properties and the ability to promote integration with host tissue. Bioinks should also allow the introduction of cell adhesion sites and cleavable moieties to control cell behaviour and biomaterial degradation rate, respectively. Current bioinks for skin bioprinting are essentially limited to the use of alginate, collagen, hyaluronic acid and fibrin, which restricts the range of mechanical and biological properties of the fabricated constructs. Although the ability of bioprinting approaches to generate 3D constructs with complex architectures, while allowing control over the spatial location of biomaterials, cells and biologically active compounds, has already been demonstrated, replicating the complexity of native skin has not yet been successfully achieved.

To improve the level of biomimicry, efforts should be made to consider additional aspects regarding the skin appendages, gradients of ECM components, and functional vascular networks. Skin appendages are responsible for several important functions, including protection, sensing and temperature regulation, while the gradients of ECM components play a primordial role in both cell behaviour and biomechanical properties of the skin. Novel bioinks allowing the reproduction of ECM gradients present in different skin layers should be designed and their effects on cell viability and function well characterized and documented towards regulatory approval. Although vascularization is essential for the long-term viability of the construct, it remains a huge challenge in almost all tissue engineering strategies. Recent developments in bioprinting of functional vascular networks can be explored to design 3D hierarchical skin constructs with embedded vascular cells, which will represent an important advance in the field.

Finally, efforts should be concentrated in the translation of bioprinting therapies into clinical practice. This is a long and difficult issue that depends on several factors, including the scale-up of the process, and many regulatory and commercialization aspects. Since novel bioprinting approaches for skin repair and regeneration are complex and multidisciplinary, aspects related to the bioprinting technology, bioinks, cell sources, integration with existing medical devices (e.g., robotic surgical arms, medical imaging systems, real-time imaging technology), automation, reproducibility and affordability must be considered right from an early stage to reduce the time to reach the market. Collaborative work should also be focused on the establishment of good manufacturing practices, standardization of assays to control the properties of manufactured constructs, and methods for the monitoring and inspection of the printing process.

2.9. References

- [1] R.F. Pereira, C.C. Barrias, P.L. Granja, P.J. Bartolo, Advanced biofabrication strategies for skin regeneration and repair, *Nanomedicine (Lond)* 8 (2013) 603-21.
- [2] F. Groeber, M. Holeiter, M. Hampel, S. Hinderer, K. Schenke-Layland, Skin tissue engineering--in vivo and in vitro applications, *Adv Drug Deliv Rev* 63 (2011) 352-66.
- [3] S.W. Volk, S.A. Iqbal, A. Bayat, Interactions of the Extracellular Matrix and Progenitor Cells in Cutaneous Wound Healing, *Adv Wound Care (New Rochelle)* 2 (2013) 261-272.
- [4] R.V. Shevchenko, S.L. James, S.E. James, A review of tissue-engineered skin bioconstructs available for skin reconstruction, *J R Soc Interface* 7 (2010) 229-58.
- [5] C.K. Sen, G.M. Gordillo, S. Roy, R. Kirsner, L. Lambert, T.K. Hunt, F. Gottrup, G.C. Gurtner, M.T. Longaker, Human skin wounds: a major and snowballing threat to public health and the economy, *Wound Repair Regen* 17 (2009) 763-71.
- [6] M. Augustin, L.K. Brocatti, S.J. Rustenbach, I. Schafer, K. Herberger, Cost-of-illness of leg ulcers in the community, *Int Wound J* 11 (2014) 283-92.
- [7] C.J. Phillips, I. Humphreys, J. Fletcher, K. Harding, G. Chamberlain, S. Macey, Estimating the costs associated with the management of patients with chronic wounds using linked routine data, *Int Wound J* 13 (2016) 1193-1197.
- [8] S. Gibbs, H.M. van den Hoogenband, G. Kirtschig, C.D. Richters, S.W. Spiekstra, M. Breetveld, R.J. Scheper, E.M. de Boer, Autologous full-thickness skin substitute for healing chronic wounds, *Br J Dermatol* 155 (2006) 267-74.
- [9] K. Murakami, H. Aoki, S. Nakamura, S. Nakamura, M. Takikawa, M. Hanzawa, S. Kishimoto, H. Hattori, Y. Tanaka, T. Kiyosawa, Y. Sato, M. Ishihara, Hydrogel blends of chitin/chitosan, fucoidan and alginate as healing-impaired wound dressings, *Biomaterials* 31 (2010) 83-90.
- [10] G. Sun, X. Zhang, Y.I. Shen, R. Sebastian, L.E. Dickinson, K. Fox-Talbot, M. Reinblatt, C. Steenbergen, J.W. Harmon, S. Gerecht, Dextran hydrogel scaffolds enhance angiogenic responses and promote complete skin regeneration during burn wound healing, *Proc Natl Acad Sci USA* 108 (2011) 20976-81.
- [11] A.S. Klar, S. Guven, T. Biedermann, J. Luginbuhl, S. Bottcher-Haberzeth, C. Meuli-Simmen, M. Meuli, I. Martin, A. Scherberich, E. Reichmann, Tissue-engineered dermo-epidermal skin grafts prevascularized with adipose-derived cells, *Biomaterials* 35 (2014) 5065-78.
- [12] S.J. Liu, Y.C. Kau, C.Y. Chou, J.K. Chen, R.C. Wu, W.L. Yeh, Electrospun PLGA/collagen nanofibrous membrane as early-stage wound dressing, *J Membr Sci* 355 (2010) 53-59.

- [13] G. Khorasani, S.J. Hosseinimehr, M. Azadbakht, A. Zamani, M.R. Mahdavi, Aloe versus silver sulfadiazine creams for second-degree burns: a randomized controlled study, *Surg Today* 39 (2009) 587-91.
- [14] J.C. Dumville, G. Worthy, J.M. Bland, N. Cullum, C. Dowson, C. Iglesias, J.L. Mitchell, E.A. Nelson, M.O. Soares, D.J. Torgerson, V.I. Team, Larval therapy for leg ulcers (VenUS II): randomised controlled trial, *British Medical Journal* 338 (2009).
- [15] L. Zhang, J. Chen, C. Han, A multicenter clinical trial of recombinant human GM-CSF hydrogel for the treatment of deep second-degree burns, *Wound Repair Regen* 17 (2009) 685-9.
- [16] C. Tong, H. Hao, L. Xia, J. Liu, D. Ti, L. Dong, Q. Hou, H. Song, H. Liu, Y. Zhao, X. Fu, W. Han, Hypoxia pretreatment of bone marrow-derived mesenchymal stem cells seeded in a collagen-chitosan sponge scaffold promotes skin wound healing in diabetic rats with hindlimb ischemia, *Wound Repair Regen* 24 (2016) 45-56.
- [17] H. Kim, W.H. Kong, K.Y. Seong, D.K. Sung, H. Jeong, J.K. Kim, S.Y. Yang, S.K. Hahn, Hyaluronate-Epidermal Growth Factor Conjugate for Skin Wound Healing and Regeneration, *Biomacromolecules* 17 (2016) 3694-3705.
- [18] R.F. Pereira, P.J. Bartolo, Traditional Therapies for Skin Wound Healing, *Adv Wound Care (New Rochelle)* 5 (2016) 208-229.
- [19] R.K. Sivamani, B.R. Ma, L.N. Wehrli, E. Maverakis, Phytochemicals and Naturally Derived Substances for Wound Healing, *Adv Wound Care (New Rochelle)* 1 (2012) 213-217.
- [20] M.K. Rashidi, N. Mirazi, A. Hosseini, Effect of topical mixture of honey, royal jelly and olive oil-propolis extract on skin wound healing in diabetic rats, *Wound Medicine* 12 (2016) 6-9.
- [21] P.N. Li, H. Li, L.X. Zhong, Y. Sun, L.J. Yu, M.L. Wu, L.L. Zhang, Q.Y. Kong, S.Y. Wang, D.C. Lv, Molecular events underlying maggot extract promoted rat in vivo and human in vitro skin wound healing, *Wound Repair Regen* 23 (2015) 65-73.
- [22] A.A. Leto Barone, M. Mastroianni, E.A. Farkash, C. Mallard, A. Albritton, R. Torabi, D.A. Leonard, J.M. Kurtz, D.H. Sachs, C.L. Cetrulo, Jr., Genetically modified porcine split-thickness skin grafts as an alternative to allograft for provision of temporary wound coverage: preliminary characterization, *Burns* 41 (2015) 565-74.
- [23] G.P. Sidgwick, D. McGeorge, A. Bayat, A comprehensive evidence-based review on the role of topicals and dressings in the management of skin scarring, *Arch Dermatol Res* 307 (2015) 461-77.
- [24] N.S. Greaves, S.A. Iqbal, M. Baguneid, A. Bayat, The role of skin substitutes in the management of chronic cutaneous wounds, *Wound Repair Regen* 21 (2013) 194-210.
- [25] R.S. Kirsner, W.A. Marston, R.J. Snyder, T.D. Lee, D.I. Cargill, H.B. Slade, Spray-applied cell therapy with human allogeneic fibroblasts and keratinocytes for the treatment of

chronic venous leg ulcers: a phase 2, multicentre, double-blind, randomised, placebo-controlled trial, *Lancet* 380 (2012) 977-85.

[26] C.S. Blok, L. Vink, E.M. de Boer, C. van Montfrans, H.M. van den Hoogenband, M.C. Mooij, S.A. Gauw, J.A. Vloemans, I. Bruynzeel, A. van Kraan, J. Kuik, T. Waaijman, R.J. Scheper, S. Gibbs, Autologous skin substitute for hard-to-heal ulcers: retrospective analysis on safety, applicability, and efficacy in an outpatient and hospitalized setting, *Wound Repair Regen* 21 (2013) 667-76.

[27] S. MacNeil, Progress and opportunities for tissue-engineered skin, *Nature* 445 (2007) 874-80.

[28] F.P.W. Melchels, M.A.N. Domingos, T.J. Klein, J. Malda, P.J. Bartolo, D.W. Hutmacher, Additive manufacturing of tissues and organs, *Prog. Polym. Sci.* 37 (2012) 1079-1104.

[29] R.F. Pereira, P.J. Bártolo, 10.10 - Recent Advances in Additive Biomanufacturing, in: S.H.F.B.J.V.T. Yilbas (Ed.), *Comprehensive Materials Processing*, Elsevier, Oxford, 2014, pp. 265-284.

[30] T. Hodgkinson, A. Bayat, Dermal substitute-assisted healing: enhancing stem cell therapy with novel biomaterial design, *Arch Dermatol Res* 303 (2011) 301-15.

[31] R.V. Shevchenko, M. Eeman, B. Rowshanravan, I.U. Allan, I.N. Savina, M. Illsley, M. Salmon, S.L. James, S.V. Mikhalovsky, S.E. James, The in vitro characterization of a gelatin scaffold, prepared by cryogelation and assessed in vivo as a dermal replacement in wound repair, *Acta Biomater* 10 (2014) 3156-66.

[32] V. Mironov, R.P. Visconti, V. Kasyanov, G. Forgacs, C.J. Drake, R.R. Markwald, Organ printing: tissue spheroids as building blocks, *Biomaterials* 30 (2009) 2164-74.

[33] R.F. Pereira, P.J. Bártolo, 3D Photo-Fabrication for Tissue Engineering and Drug Delivery, *Engineering* 1 (2015) 90-112.

[34] J.W. Nichol, A. Khademhosseini, Modular Tissue Engineering: Engineering Biological Tissues from the Bottom Up, *Soft Matter* 5 (2009) 1312-1319.

[35] B.S. Schon, G.J. Hooper, T.B. Woodfield, Modular Tissue Assembly Strategies for Biofabrication of Engineered Cartilage, *Ann Biomed Eng* 45 (2017) 100-114.

[36] J.S. Liu, Z.J. Gartner, Directing the assembly of spatially organized multicomponent tissues from the bottom up, *Trends Cell Biol* 22 (2012) 683-91.

[37] C. Palmiero, G. Imparato, F. Urciuolo, P. Netti, Engineered dermal equivalent tissue in vitro by assembly of microtissue precursors, *Acta Biomater* 6 (2010) 2548-53.

[38] G. Imparato, F. Urciuolo, C. Casale, P.A. Netti, The role of microscaffold properties in controlling the collagen assembly in 3D dermis equivalent using modular tissue engineering, *Biomaterials* 34 (2013) 7851-61.

- [39] P. Bajaj, R.M. Schweller, A. Khademhosseini, J.L. West, R. Bashir, 3D biofabrication strategies for tissue engineering and regenerative medicine, *Annu Rev Biomed Eng* 16 (2014) 247-76.
- [40] G. Jürgen, B. Thomas, B. Torsten, A.B. Jason, C. Dong-Woo, D.D. Paul, D. Brian, F. Gabor, L. Qing, A.M. Vladimir, M. Lorenzo, N. Makoto, S. Wenmiao, T. Shoji, V. Giovanni, B.F.W. Tim, X. Tao, J.Y. James, M. Jos, Biofabrication: reappraising the definition of an evolving field, *Biofabrication* 8 (2016) 013001.
- [41] L.E. Bertassoni, M. Cecconi, V. Manoharan, M. Nikkhah, J. Hjortnaes, A.L. Cristino, G. Barabaschi, D. Demarchi, M.R. Dokmeci, Y. Yang, A. Khademhosseini, Hydrogel bioprinted microchannel networks for vascularization of tissue engineering constructs, *Lab Chip* 14 (2014) 2202-11.
- [42] A.Y. Rioja, R. Tiruvannamalai Annamalai, S. Paris, A.J. Putnam, J.P. Stegemann, Endothelial sprouting and network formation in collagen- and fibrin-based modular microbeads, *Acta Biomater* 29 (2016) 33-41.
- [43] J. Malda, J. Visser, F.P. Melchels, T. Jungst, W.E. Hennink, W.J. Dhert, J. Groll, D.W. Hutmacher, 25th anniversary article: Engineering hydrogels for biofabrication, *Adv. Mater.* 25 (2013) 5011-28.
- [44] I.T. Ozbolat, Bioprinting scale-up tissue and organ constructs for transplantation, *Trends Biotechnol.* 33 (2015) 395-400.
- [45] S.V. Murphy, A. Atala, 3D bioprinting of tissues and organs, *Nat. Biotechnol.* 32 (2014) 773-85.
- [46] H.W. Kang, S.J. Lee, I.K. Ko, C. Kengla, J.J. Yoo, A. Atala, A 3D bioprinting system to produce human-scale tissue constructs with structural integrity, *Nat. Biotechnol.* 34 (2016) 312-9.
- [47] A. Skardal, D. Mack, E. Kapetanovic, A. Atala, J.D. Jackson, J. Yoo, S. Soker, Bioprinted amniotic fluid-derived stem cells accelerate healing of large skin wounds, *Stem Cells Transl Med* 1 (2012) 792-802.
- [48] S. Michael, H. Sorg, C.T. Peck, L. Koch, A. Deiwick, B. Chichkov, P.M. Vogt, K. Reimers, Tissue engineered skin substitutes created by laser-assisted bioprinting form skin-like structures in the dorsal skin fold chamber in mice, *PLoS One* 8 (2013) e57741.
- [49] E. Proksch, J.M. Brandner, J.M. Jensen, The skin: an indispensable barrier, *Exp Dermatol* 17 (2008) 1063-72.
- [50] M. Pasparakis, I. Haase, F.O. Nestle, Mechanisms regulating skin immunity and inflammation, *Nat Rev Immunol* 14 (2014) 289-301.
- [51] G.P. Sidgwick, A. Bayat, Extracellular matrix molecules implicated in hypertrophic and keloid scarring, *J Eur Acad Dermatol Venereol* 26 (2012) 141-52.

- [52] R.A. Kamel, J.F. Ong, E. Eriksson, J.P. Junker, E.J. Caterson, Tissue engineering of skin, *J Am Coll Surg* 217 (2013) 533-55.
- [53] A. Baroni, E. Buommino, V. De Gregorio, E. Ruocco, V. Ruocco, R. Wolf, Structure and function of the epidermis related to barrier properties, *Clin Dermatol* 30 (2012) 257-62.
- [54] D.T. Behrens, D. Villone, M. Koch, G. Brunner, L. Sorokin, H. Robenek, L. Bruckner-Tuderman, P. Bruckner, U. Hansen, The epidermal basement membrane is a composite of separate laminin- or collagen IV-containing networks connected by aggregated perlecan, but not by nidogens, *J. Biol. Chem.* 287 (2012) 18700-9.
- [55] N. Mayet, Y.E. Choonara, P. Kumar, L.K. Tomar, C. Tyagi, L.C. Du Toit, V. Pillay, A comprehensive review of advanced biopolymeric wound healing systems, *J. Pharm. Sci.* 103 (2014) 2211-30.
- [56] R.R. Driskell, F.M. Watt, Understanding fibroblast heterogeneity in the skin, *Trends Cell Biol* 25 (2015) 92-9.
- [57] B. Mahdavian Delavary, W.M. van der Veer, M. van Egmond, F.B. Niessen, R.H. Beelen, Macrophages in skin injury and repair, *Immunobiology* 216 (2011) 753-62.
- [58] R.G. Frykberg, J. Banks, Challenges in the Treatment of Chronic Wounds, *Adv Wound Care (New Rochelle)* 4 (2015) 560-582.
- [59] S. Guo, L.A. Dipietro, Factors affecting wound healing, *J Dent Res* 89 (2010) 219-29.
- [60] F. Strodbeck, Physiology of wound healing, *Newborn and Infant Nursing Reviews* 1 (2001) 43-52.
- [61] R.J. Bodnar, Chemokine Regulation of Angiogenesis During Wound Healing, *Adv Wound Care (New Rochelle)* 4 (2015) 641-650.
- [62] P. Martin, S.J. Leibovich, Inflammatory cells during wound repair: the good, the bad and the ugly, *Trends Cell Biol* 15 (2005) 599-607.
- [63] B.K. Sun, Z. Siprashvili, P.A. Khavari, Advances in skin grafting and treatment of cutaneous wounds, *Science* 346 (2014) 941-5.
- [64] N.S. Greaves, K.J. Ashcroft, M. Baguneid, A. Bayat, Current understanding of molecular and cellular mechanisms in fibroplasia and angiogenesis during acute wound healing, *J Dermatol Sci* 72 (2013) 206-17.
- [65] G.P. Sidgwick, D. McGeorge, A. Bayat, A comprehensive evidence-based review on the role of topicals and dressings in the management of skin scarring, *Arch Dermatol Res* (2015) 1-17.
- [66] V.R. Krishnaswamy, D. Mintz, I. Sagi, Matrix metalloproteinases: The sculptors of chronic cutaneous wounds, *Biochim Biophys Acta Mol Cell Res* 1864 (2017) 2220-2227.
- [67] J.L. Lazaro, V. Izzo, S. Meaume, A.H. Davies, R. Lobmann, L. Uccioli, Elevated levels of matrix metalloproteinases and chronic wound healing: an updated review of clinical evidence, *J Wound Care* 25 (2016) 277-87.

- [68] E.A. Rayment, Z. Upton, G.K. Shooter, Increased matrix metalloproteinase-9 (MMP-9) activity observed in chronic wound fluid is related to the clinical severity of the ulcer, *Br J Dermatol* 158 (2008) 951-61.
- [69] A.N. Moor, D.J. Vachon, L.J. Gould, Proteolytic activity in wound fluids and tissues derived from chronic venous leg ulcers, *Wound Repair Regen* 17 (2009) 832-9.
- [70] S. Schreml, R.M. Szeimies, L. Prantl, S. Karrer, M. Landthaler, P. Babilas, Oxygen in acute and chronic wound healing, *Br J Dermatol* 163 (2010) 257-68.
- [71] I.B. Wall, R. Moseley, D.M. Baird, D. Kipling, P. Giles, I. Laffafian, P.E. Price, D.W. Thomas, P. Stephens, Fibroblast dysfunction is a key factor in the non-healing of chronic venous leg ulcers, *J Invest Dermatol* 128 (2008) 2526-40.
- [72] R.A. Clark, Oxidative stress and "senescent" fibroblasts in non-healing wounds as potential therapeutic targets, *J Invest Dermatol* 128 (2008) 2361-4.
- [73] L. Gould, P. Abadir, H. Brem, M. Carter, T. Conner-Kerr, J. Davidson, L. DiPietro, V. Falanga, C. Fife, S. Gardner, E. Grice, J. Harmon, W.R. Hazzard, K.P. High, P. Houghton, N. Jacobson, R.S. Kirsner, E.J. Kovacs, D. Margolis, F. McFarland Horne, M.J. Reed, D.H. Sullivan, S. Thom, M. Tomic-Canic, J. Walston, J. Whitney, J. Williams, S. Ziemann, K. Schmader, Chronic wound repair and healing in older adults: current status and future research, *Wound Repair Regen* 23 (2015) 1-13.
- [74] R.L. McInnes, B.M. Cullen, K.E. Hill, P.E. Price, K.G. Harding, D.W. Thomas, P. Stephens, R. Moseley, Contrasting host immuno-inflammatory responses to bacterial challenge within venous and diabetic ulcers, *Wound Repair Regen* 22 (2014) 58-69.
- [75] T. Bjarnsholt, The role of bacterial biofilms in chronic infections, *APMIS Suppl* 121 (2013) 1-51.
- [76] A. Wells, A. Nuschke, C.C. Yates, Skin tissue repair: Matrix microenvironmental influences, *Matrix Biol.* 49 (2016) 25-36.
- [77] S.A. Eming, P. Martin, M. Tomic-Canic, Wound repair and regeneration: mechanisms, signaling, and translation, *Sci Transl Med* 6 (2014) 265sr6.
- [78] W.H. Organization, WHO Traditional Medicine Strategy: 2002-2005 (2002).
- [79] W.H. Organization, WHO Traditional Medicine Strategy: 2014-2023 (2013).
- [80] Y. Wang, J. Beekman, J. Hew, S. Jackson, A.C. Issler-Fisher, R. Parungao, S.S. Lajevardi, Z. Li, P.K.M. Maitz, Burn injury: Challenges and advances in burn wound healing, infection, pain and scarring, *Adv Drug Deliv Rev* 123 (2018) 3-17.
- [81] S. Vujanovic, J. Vujanovic, Bioresources in the pharmacotherapy and healing of burns: A mini-review, *Burns* 39 (2013) 1031-8.
- [82] T. Maver, U. Maver, K. Stana Kleinschek, D.M. Smrke, S. Kreft, A review of herbal medicines in wound healing, *Int J Dermatol* 54 (2015) 740-51.

- [83] A.D. Dat, F. Poon, K.B. Pham, J. Doust, Aloe vera for treating acute and chronic wounds, *Cochrane Database Syst Rev* (2012) CD008762.
- [84] C.Y. Hsiao, C.Y. Hung, T.H. Tsai, K.F. Chak, A Study of the Wound Healing Mechanism of a Traditional Chinese Medicine, *Angelica sinensis*, Using a Proteomic Approach, *Evid Based Complement Alternat Med* 2012 (2012) 467531.
- [85] M.A. Abu-Al-Basal, Healing potential of *Rosmarinus officinalis* L. on full-thickness excision cutaneous wounds in alloxan-induced-diabetic BALB/c mice, *J. Ethnopharmacol.* 131 (2010) 443-50.
- [86] R. Pereira, A. Carvalho, D.C. Vaz, M.H. Gil, A. Mendes, P. Bartolo, Development of novel alginate based hydrogel films for wound healing applications, *Int. J. Biol. Macromol.* 52 (2013) 221-30.
- [87] A. Baghizadeh, S. Ranjbar, V.K. Gupta, M. Asif, S. Pourseyedi, M.J. Karimi, R. Mohammadinejad, Green synthesis of silver nanoparticles using seed extract of *Calendula officinalis* in liquid phase, *J. Mol. Liq.* 207 (2015) 159-163.
- [88] A. Oryan, A. Mohammadalipour, A. Moshiri, M.R. Tabandeh, Topical Application of Aloe vera Accelerated Wound Healing, Modeling, and Remodeling: An Experimental Study, *Ann Plast Surg* 77 (2016) 37-46.
- [89] L. Langmead, R.M. Feakins, S. Goldthorpe, H. Holt, E. Tsironi, A. De Silva, D.P. Jewell, D.S. Rampton, Randomized, double-blind, placebo-controlled trial of oral aloe vera gel for active ulcerative colitis, *Aliment Pharmacol Ther* 19 (2004) 739-47.
- [90] M.D. Boudreau, F.A. Beland, An evaluation of the biological and toxicological properties of *Aloe barbadensis* (miller), *Aloe vera*, *J Environ Sci Health C Environ Carcinog Ecotoxicol Rev* 24 (2006) 103-54.
- [91] T. Sato, G. Miyata, The nutraceutical benefit, part iii: honey, *Nutrition* 16 (2000) 468-9.
- [92] A. Oryan, E. Alemzadeh, A. Moshiri, Biological properties and therapeutic activities of honey in wound healing: A narrative review and meta-analysis, *J Tissue Viability* 25 (2016) 98-118.
- [93] A. Jull, N. Walker, V. Parag, P. Molan, A. Rodgers, c. Honey as Adjuvant Leg Ulcer Therapy trial, Randomized clinical trial of honey-impregnated dressings for venous leg ulcers, *Br J Surg* 95 (2008) 175-82.
- [94] A. Oryan, E. Alemzadeh, A. Moshiri, Potential role of propolis in wound healing: Biological properties and therapeutic activities, *Biomed Pharmacother* 98 (2018) 469-483.
- [95] F. Pellati, F.P. Prencipe, D. Bertelli, S. Benvenuti, An efficient chemical analysis of phenolic acids and flavonoids in raw propolis by microwave-assisted extraction combined with high-performance liquid chromatography using the fused-core technology, *J. Pharm. Biomed. Anal.* 81-82 (2013) 126-32.

- [96] S.E. Walgrave, E.M. Warshaw, L.A. Glesne, Allergic contact dermatitis from propolis, *Dermatitis* 16 (2005) 209-15.
- [97] J.C. Dumville, G. Worthy, J.M. Bland, N. Cullum, C. Dowson, C. Iglesias, J.L. Mitchell, E.A. Nelson, M.O. Soares, D.J. Torgerson, U.S.I.I.t. Ven, Larval therapy for leg ulcers (VenUS II): randomised controlled trial, *BMJ* 338 (2009) b773.
- [98] G. Cazander, K.E. van Veen, L.H. Bouwman, A.T. Bernards, G.N. Jukema, The influence of maggot excretions on PAO1 biofilm formation on different biomaterials, *Clin Orthop Relat Res* 467 (2009) 536-45.
- [99] A.J. Horobin, K.M. Shakesheff, D.I. Pritchard, Maggots and wound healing: an investigation of the effects of secretions from *Lucilia sericata* larvae upon the migration of human dermal fibroblasts over a fibronectin-coated surface, *Wound Repair Regen* 13 (2005) 422-33.
- [100] A.G. Smith, R.A. Powis, D.I. Pritchard, S.T. Britland, Greenbottle (*Lucilia sericata*) larval secretions delivered from a prototype hydrogel wound dressing accelerate the closure of model wounds, *Biotechnol Prog* 22 (2006) 1690-6.
- [101] L. Gilead, K.Y. Mumcuoglu, A. Ingber, The use of maggot debridement therapy in the treatment of chronic wounds in hospitalised and ambulatory patients, *J Wound Care* 21 (2012) 78, 80, 82-85.
- [102] A.P. Singh, Medicinal leech therapy (hirudotherapy): a brief overview, *Complement Ther Clin Pract* 16 (2010) 213-5.
- [103] A.R. Elyassi, J. Terres, H.H. Rowshan, Medicinal leech therapy on head and neck patients: a review of literature and proposed protocol, *Oral Surg Oral Med Oral Pathol Oral Radiol* 116 (2013) e167-72.
- [104] A. Michalsen, S. Klotz, R. Ludtke, S. Moebus, G. Spahn, G.J. Dobos, Effectiveness of leech therapy in osteoarthritis of the knee: a randomized, controlled trial, *Ann Intern Med* 139 (2003) 724-30.
- [105] B.S. Atiyeh, S.A. Dibo, S.N. Hayek, Wound cleansing, topical antiseptics and wound healing, *Int Wound J* 6 (2009) 420-30.
- [106] M.J. Hoekstra, S.J. Westgate, S. Mueller, Povidone-iodine ointment demonstrates in vitro efficacy against biofilm formation, *Int Wound J* 14 (2017) 172-179.
- [107] F. Abedini, A. Ahmadi, A. Yavari, V. Hosseini, S. Mousavi, Comparison of silver nylon wound dressing and silver sulfadiazine in partial burn wound therapy, *Int Wound J* 10 (2013) 573-8.
- [108] F. Jurczak, T. Dugre, A. Johnstone, T. Offori, Z. Vujovic, D. Hollander, A.A.S.T.W.S. Group, Randomised clinical trial of Hydrofiber dressing with silver versus povidone-iodine gauze in the management of open surgical and traumatic wounds, *Int Wound J* 4 (2007) 66-76.

- [109] J.S. Boateng, K.H. Matthews, H.N. Stevens, G.M. Eccleston, Wound healing dressings and drug delivery systems: a review, *J. Pharm. Sci.* 97 (2008) 2892-923.
- [110] V. Jones, J.E. Grey, K.G. Harding, Wound dressings, *BMJ* 332 (2006) 777-780.
- [111] J. Boateng, O. Catanzano, Advanced Therapeutic Dressings for Effective Wound Healing - A Review, *J. Pharm. Sci.* 104 (2015) 3653-80.
- [112] G. Dabiri, E. Damstetter, T. Phillips, Choosing a Wound Dressing Based on Common Wound Characteristics, *Adv Wound Care (New Rochelle)* 5 (2016) 32-41.
- [113] I. Garcia-Orue, G. Gainza, F.B. Gutierrez, J.J. Aguirre, C. Evora, J.L. Pedraz, R.M. Hernandez, A. Delgado, M. Igartua, Novel nanofibrous dressings containing rhEGF and Aloe vera for wound healing applications, *Int. J. Pharm.* 523 (2017) 556-566.
- [114] J. Devalliere, K. Dooley, Y. Hu, S.S. Kelangi, B.E. Uygun, M.L. Yarmush, Co-delivery of a growth factor and a tissue-protective molecule using elastin biopolymers accelerates wound healing in diabetic mice, *Biomaterials* 141 (2017) 149-160.
- [115] R.F. Pereira, A. Carvalho, M.H. Gil, A. Mendes, P.J. Bartolo, Influence of Aloe vera on water absorption and enzymatic in vitro degradation of alginate hydrogel films, *Carbohydr. Polym.* 98 (2013) 311-20.
- [116] M. Mir, M.N. Ali, A. Barakullah, A. Gulzar, M. Arshad, S. Fatima, M. Asad, Synthetic polymeric biomaterials for wound healing: a review, *Prog Biomater* 7 (2018) 1-21.
- [117] A. Sood, M.S. Granick, N.L. Tomaselli, Wound Dressings and Comparative Effectiveness Data, *Adv Wound Care (New Rochelle)* 3 (2014) 511-529.
- [118] A.G. Haddad, G. Giatsidis, D.P. Orgill, E.G. Halvorson, Skin Substitutes and Bioscaffolds: Temporary and Permanent Coverage, *Clin Plast Surg* 44 (2017) 627-634.
- [119] S.T. Boyce, A.L. Lalley, Tissue engineering of skin and regenerative medicine for wound care, *Burns Trauma* 6 (2018) 4.
- [120] S. Barrientos, H. Brem, O. Stojadinovic, M. Tomic-Canic, Clinical application of growth factors and cytokines in wound healing, *Wound Repair Regen* 22 (2014) 569-78.
- [121] J.M. Smiell, T.J. Wieman, D.L. Steed, B.H. Perry, A.R. Sampson, B.H. Schwab, Efficacy and safety of becaplermin (recombinant human platelet-derived growth factor-BB) in patients with nonhealing, lower extremity diabetic ulcers: a combined analysis of four randomized studies, *Wound Repair Regen* 7 (1999) 335-46.
- [122] T.J. Wieman, J.M. Smiell, Y. Su, Efficacy and Safety of a Topical Gel Formulation of Recombinant Human Platelet-Derived Growth Factor-BB (Becaplermin) in Patients With Chronic Neuropathic Diabetic Ulcers: A phase III randomized placebo-controlled double-blind study, *Diabetes Care* 21 (1998) 822-827.
- [123] M.C. Robson, L.G. Phillips, A. Thomason, B.W. Altrock, P.C. Pence, J.P. Heggors, A.F. Johnston, T.P. McHugh, M.S. Anthony, L.E. Robson, et al., Recombinant human platelet-

derived growth factor-BB for the treatment of chronic pressure ulcers, *Ann Plast Surg* 29 (1992) 193-201.

[124] D.J. Margolis, L.M. Morris, M. Papadopoulos, L. Weinberg, J.C. Filip, S.A. Lang, S.S. Vaikunth, T.M. Crombleholme, Phase I study of H5.020CMV.PDGF-beta to treat venous leg ulcer disease, *Mol Ther* 17 (2009) 1822-9.

[125] F. Cianfarani, R. Tommasi, C.M. Failla, M.T. Viviano, G. Annessi, M. Papi, G. Zambruno, T. Odorisio, Granulocyte/macrophage colony-stimulating factor treatment of human chronic ulcers promotes angiogenesis associated with de novo vascular endothelial growth factor transcription in the ulcer bed, *Br J Dermatol* 154 (2006) 34-41.

[126] J.R. Hanft, R.A. Pollak, A. Barbul, C. van Gils, P.S. Kwon, S.M. Gray, C.J. Lynch, C.P. Semba, T.J. Breen, Phase I trial on the safety of topical rhVEGF on chronic neuropathic diabetic foot ulcers, *J Wound Care* 17 (2008) 30-2, 34-7.

[127] A. Gupta, P. Avci, T. Dai, Y.Y. Huang, M.R. Hamblin, Ultraviolet Radiation in Wound Care: Sterilization and Stimulation, *Adv Wound Care (New Rochelle)* 2 (2013) 422-437.

[128] H. Korzendorfer, H. Hettrick, Biophysical Technologies for Management of Wound Bioburden, *Adv Wound Care (New Rochelle)* 3 (2014) 733-741.

[129] L. Moroni, T. Boland, J.A. Burdick, C. De Maria, B. Derby, G. Forgacs, J. Groll, Q. Li, J. Malda, V.A. Mironov, C. Mota, M. Nakamura, W. Shu, S. Takeuchi, T.B.F. Woodfield, T. Xu, J.J. Yoo, G. Vozzi, *Biofabrication: A Guide to Technology and Terminology*, *Trends Biotechnol.* 36 (2018) 384-402.

[130] A. Skardal, M. Devarasetty, H.W. Kang, I. Mead, C. Bishop, T. Shupe, S.J. Lee, J. Jackson, J. Yoo, S. Soker, A. Atala, A hydrogel bioink toolkit for mimicking native tissue biochemical and mechanical properties in bioprinted tissue constructs, *Acta Biomater* 25 (2015) 24-34.

[131] A.L. Rutz, K.E. Hyland, A.E. Jakus, W.R. Burghardt, R.N. Shah, A multimaterial bioink method for 3D printing tunable, cell-compatible hydrogels, *Adv. Mater.* 27 (2015) 1607-14.

[132] F. Pati, J. Jang, D.H. Ha, S. Won Kim, J.W. Rhie, J.H. Shim, D.H. Kim, D.W. Cho, Printing three-dimensional tissue analogues with decellularized extracellular matrix bioink, *Nat Commun* 5 (2014) 3935.

[133] C. Li, A. Faulkner-Jones, A.R. Dun, J. Jin, P. Chen, Y. Xing, Z. Yang, Z. Li, W. Shu, D. Liu, R.R. Duncan, Rapid formation of a supramolecular polypeptide-DNA hydrogel for in situ three-dimensional multilayer bioprinting, *Angew. Chem. Int. Ed. Engl.* 54 (2015) 3957-61.

[134] P. Bártolo, *Stereolithographic Processes*, in: P.J. Bártolo (Ed.), *Stereolithography*, Springer US (2011), pp. 1-36.

[135] F.P. Melchels, J. Feijen, D.W. Grijpma, A review on stereolithography and its applications in biomedical engineering, *Biomaterials* 31 (2010) 6121-30.

- [136] R. Pereira, P. Bártolo, Photocrosslinkable Materials for the Fabrication of Tissue-Engineered Constructs by Stereolithography, in: P.R. Fernandes, P.J. Bartolo (Eds.), *Tissue Eng.*, Springer Netherlands 2014, pp. 149-178.
- [137] J.-W. Choi, R. Wicker, S.-H. Lee, K.-H. Choi, C.-S. Ha, I. Chung, Fabrication of 3D biocompatible/biodegradable micro-scaffolds using dynamic mask projection microstereolithography, *J. Mater. Process. Technol.* 209 (2009) 5494-5503.
- [138] J. Torgersen, X.-H. Qin, Z. Li, A. Ovsianikov, R. Liska, J. Stampfl, Hydrogels for Two-Photon Polymerization: A Toolbox for Mimicking the Extracellular Matrix, *Adv. Funct. Mater.* 23 (2013) 4542-4554.
- [139] R. Pereira, H. Almeida, P. Bártolo, Biofabrication of Hydrogel Constructs, in: J. Coelho (Ed.), *Drug Delivery Systems: Advanced Technologies Potentially Applicable in Personalised Treatment*, Springer Netherlands (2013), pp. 225-254.
- [140] P.J. Bartolo, G. Mitchell, Stereo-thermal-lithography: a new principle for rapid prototyping, *Rapid Prototyping Journal* 9 (2003) 150-156.
- [141] T. Patrício, R. Pereira, L. Oliveira, P. Bártolo, Polyethylene Glycol and Polyethylene Glycol/Hydroxyapatite Constructs Produced through Stereo-Thermal Lithography, *Advanced Materials Research* 749 (2013) 87-92.
- [142] P. Bartolo, J.-P. Kruth, J. Silva, G. Levy, A. Malshe, K. Rajurkar, M. Mitsuishi, J. Ciurana, M. Leu, Biomedical production of implants by additive electro-chemical and physical processes, *CIRP Annals - Manufacturing Technology* 61 (2012) 635-655.
- [143] Y.J. Seol, D.Y. Park, J.Y. Park, S.W. Kim, S.J. Park, D.W. Cho, A new method of fabricating robust freeform 3D ceramic scaffolds for bone tissue regeneration, *Biotechnol. Bioeng.* 110 (2013) 1444-55.
- [144] K.W. Lee, S. Wang, B.C. Fox, E.L. Ritman, M.J. Yaszemski, L. Lu, Poly(propylene fumarate) bone tissue engineering scaffold fabrication using stereolithography: effects of resin formulations and laser parameters, *Biomacromolecules* 8 (2007) 1077-84.
- [145] L. Elomaa, S. Teixeira, R. Hakala, H. Korhonen, D.W. Grijpma, J.V. Seppala, Preparation of poly(epsilon-caprolactone)-based tissue engineering scaffolds by stereolithography, *Acta Biomater* 7 (2011) 3850-6.
- [146] F.P. Melchels, J. Feijen, D.W. Grijpma, A poly(D,L-lactide) resin for the preparation of tissue engineering scaffolds by stereolithography, *Biomaterials* 30 (2009) 3801-9.
- [147] S. Schuller-Ravoo, S.M. Teixeira, J. Feijen, D.W. Grijpma, A.A. Poot, Flexible and elastic scaffolds for cartilage tissue engineering prepared by stereolithography using poly(trimethylene carbonate)-based resins, *Macromol Biosci* 13 (2013) 1711-9.
- [148] Y. Lu, G. Mapili, G. Suhali, S. Chen, K. Roy, A digital micro-mirror device-based system for the microfabrication of complex, spatially patterned tissue engineering scaffolds, *J Biomed Mater Res A* 77 (2006) 396-405.

- [149] P. Zorlutuna, J.H. Jeong, H. Kong, R. Bashir, Stereolithography-Based Hydrogel Microenvironments to Examine Cellular Interactions, *Adv. Funct. Mater.* 21 (2011) 3642-3651.
- [150] C.B. Arnold, P. Serra, A. Piqué, Laser Direct-Write Techniques for Printing of Complex Materials, *MRS Bull.* 32 (2007) 23-31.
- [151] F. Guillemot, A. Souquet, S. Catros, B. Guillotin, Laser-assisted cell printing: principle, physical parameters versus cell fate and perspectives in tissue engineering, *Nanomedicine (Lond)* 5 (2010) 507-15.
- [152] F. Guillemot, A. Souquet, S. Catros, B. Guillotin, J. Lopez, M. Faucon, B. Pippenger, R. Bareille, M. Remy, S. Bellance, P. Chabassier, J.C. Fricain, J. Amedee, High-throughput laser printing of cells and biomaterials for tissue engineering, *Acta Biomater* 6 (2010) 2494-500.
- [153] S. Catros, B. Guillotin, M. Bacakova, J.C. Fricain, F. Guillemot, Effect of laser energy, substrate film thickness and bioink viscosity on viability of endothelial cells printed by Laser-Assisted Bioprinting, *Appl. Surf. Sci.* 257 (2011) 5142-5147.
- [154] C. Sylvain, F. Jean-Christophe, G. Bertrand, P. Benjamin, B. Reine, R. Murielle, L. Eric, D. Bernard, A. Joëlle, G. Fabien, Laser-assisted bioprinting for creating on-demand patterns of human osteoprogenitor cells and nano-hydroxyapatite, *Biofabrication* 3 (2011) 025001.
- [155] L. Koch, A. Deiwick, S. Schlie, S. Michael, M. Gruene, V. Coger, D. Zychlinski, A. Schambach, K. Reimers, P.M. Vogt, B. Chichkov, Skin tissue generation by laser cell printing, *Biotechnol. Bioeng.* 109 (2012) 1855-63.
- [156] A. Ovsianikov, M. Gruene, M. Pflaum, L. Koch, F. Maiorana, M. Wilhelmi, A. Haverich, B. Chichkov, Laser printing of cells into 3D scaffolds, *Biofabrication* 2 (2010) 014104.
- [157] M. Gruene, A. Deiwick, L. Koch, S. Schlie, C. Unger, N. Hofmann, I. Bernemann, B. Glasmacher, B. Chichkov, Laser printing of stem cells for biofabrication of scaffold-free autologous grafts, *Tissue Eng Part C Methods* 17 (2011) 79-87.
- [158] Y. Lin, D. Bourell, G. Huang, Y. Huang, T.R. Jeremy Tzeng, D. Chrisey, Effect of laser fluence in laser-assisted direct writing of human colon cancer cell, *Rapid Prototyping Journal* 16 (2010) 202-208.
- [159] V. Keriquel, H. Oliveira, M. Remy, S. Ziane, S. Delmond, B. Rousseau, S. Rey, S. Catros, J. Amedee, F. Guillemot, J.C. Fricain, In situ printing of mesenchymal stromal cells, by laser-assisted bioprinting, for in vivo bone regeneration applications, *Sci Rep* 7 (2017) 1778.
- [160] R.E. Saunders, B. Derby, Inkjet printing biomaterials for tissue engineering: bioprinting, *Int. Mater. Rev.* 59 (2014) 430-448.

- [161] B. Derby, Inkjet Printing of Functional and Structural Materials: Fluid Property Requirements, Feature Stability, and Resolution, *Annual Review of Materials Research*, Vol 40 40 (2010) 395-414.
- [162] R.E. Saunders, J.E. Gough, B. Derby, Delivery of human fibroblast cells by piezoelectric drop-on-demand inkjet printing, *Biomaterials* 29 (2008) 193-203.
- [163] D. Chahal, A. Ahmadi, K.C. Cheung, Improving piezoelectric cell printing accuracy and reliability through neutral buoyancy of suspensions, *Biotechnol. Bioeng.* 109 (2012) 2932-40.
- [164] Q. Zheng, J. Lu, H. Chen, L. Huang, J. Cai, Z. Xu, Application of inkjet printing technique for biological material delivery and antimicrobial assays, *Anal. Biochem.* 410 (2011) 171-6.
- [165] X. Cui, D. Dean, Z.M. Ruggeri, T. Boland, Cell damage evaluation of thermal inkjet printed Chinese hamster ovary cells, *Biotechnol. Bioeng.* 106 (2010) 963-9.
- [166] L. Barbara, H. Wen-Kai, M.H. Ian, R.M. Keith, Adult rat retinal ganglion cells and glia can be printed by piezoelectric inkjet printing, *Biofabrication* 6 (2014) 015001.
- [167] E. Hoch, T. Hirth, G.E.M. Tovar, K. Borchers, Chemical tailoring of gelatin to adjust its chemical and physical properties for functional bioprinting, *J. Mater. Chem. B* 1 (2013) 5675-5685.
- [168] K. Christensen, C. Xu, W. Chai, Z. Zhang, J. Fu, Y. Huang, Freeform inkjet printing of cellular structures with bifurcations, *Biotechnol. Bioeng.* 112 (2015) 1047-55.
- [169] S. Wust, M.E. Godla, R. Muller, S. Hofmann, Tunable hydrogel composite with two-step processing in combination with innovative hardware upgrade for cell-based three-dimensional bioprinting, *Acta Biomater* 10 (2014) 630-40.
- [170] S. Ahn, H. Lee, J. Puetzer, L.J. Bonassar, G. Kim, Fabrication of cell-laden three-dimensional alginate-scaffolds with an aerosol cross-linking process, *J. Mater. Chem.* 22 (2012) 18735-18740.
- [171] L.A. Hockaday, K.H. Kang, N.W. Colangelo, P.Y. Cheung, B. Duan, E. Malone, J. Wu, L.N. Girardi, L.J. Bonassar, H. Lipson, C.C. Chu, J.T. Butcher, Rapid 3D printing of anatomically accurate and mechanically heterogeneous aortic valve hydrogel scaffolds, *Biofabrication* 4 (2012) 035005.
- [172] E.B. Luiz, C.C. Juliana, M. Vijayan, L.C. Ana, S.B. Nupura, A.A. Wesleyan, Z. Pinar, E.V. Nihal, M.G. Amir, R.D. Mehmet, K. Ali, Direct-write bioprinting of cell-laden methacrylated gelatin hydrogels, *Biofabrication* 6 (2014) 024105.
- [173] N.E. Fedorovich, W. Schuurman, H.M. Wijnberg, H.J. Prins, P.R. van Weeren, J. Malda, J. Alblas, W.J. Dhert, Biofabrication of osteochondral tissue equivalents by printing topologically defined, cell-laden hydrogel scaffolds, *Tissue Eng Part C Methods* 18 (2012) 33-44.

- [174] T. Billiet, E. Gevaert, T. De Schryver, M. Cornelissen, P. Dubruel, The 3D printing of gelatin methacrylamide cell-laden tissue-engineered constructs with high cell viability, *Biomaterials* 35 (2014) 49-62.
- [175] R. Chang, J. Nam, W. Sun, Effects of dispensing pressure and nozzle diameter on cell survival from solid freeform fabrication-based direct cell writing, *Tissue Eng Part A* 14 (2008) 41-8.
- [176] K. Nair, M. Gandhi, S. Khalil, K.C. Yan, M. Marcolongo, K. Barbee, W. Sun, Characterization of cell viability during bioprinting processes, *Biotechnol J* 4 (2009) 1168-77.
- [177] D.B. Kolesky, K.A. Homan, M.A. Skylar-Scott, J.A. Lewis, Three-dimensional bioprinting of thick vascularized tissues, *Proc Natl Acad Sci USA* 113 (2016) 3179-84.
- [178] A. Skardal, J. Zhang, L. McCoard, X. Xu, S. Oottamasathien, G.D. Prestwich, Photocrosslinkable hyaluronan-gelatin hydrogels for two-step bioprinting, *Tissue Eng Part A* 16 (2010) 2675-85.
- [179] M. Kesti, M. Müller, J. Becher, M. Schnabelrauch, M. D'Este, D. Eglin, M. Zenobi-Wong, A versatile bioink for three-dimensional printing of cellular scaffolds based on thermally and photo-triggered tandem gelation, *Acta Biomater* 11 (2015) 162-172.
- [180] H. Lee, S. Ahn, L.J. Bonassar, G. Kim, Cell(MC3T3-E1)-printed poly(ϵ -caprolactone)/alginate hybrid scaffolds for tissue regeneration, *Macromol. Rapid Commun.* 34 (2013) 142-9.
- [181] N.R. Schiele, D.B. Chrisey, D.T. Corr, Gelatin-based laser direct-write technique for the precise spatial patterning of cells, *Tissue Eng Part C Methods* 17 (2011) 289-98.
- [182] W. Schuurman, V. Khristov, M.W. Pot, P.R. van Weeren, W.J. Dhert, J. Malda, Bioprinting of hybrid tissue constructs with tailorable mechanical properties, *Biofabrication* 3 (2011) 021001.
- [183] X. Liu, H. Yuk, S. Lin, G.A. Parada, T.C. Tang, E. Tham, C. de la Fuente-Nunez, T.K. Lu, X. Zhao, 3D Printing of Living Responsive Materials and Devices, *Adv. Mater.* 30 (2018) 1704821.
- [184] W. Liu, M.A. Heinrich, Y. Zhou, A. Akpek, N. Hu, X. Liu, X. Guan, Z. Zhong, X. Jin, A. Khademhosseini, Y.S. Zhang, Extrusion Bioprinting of Shear-Thinning Gelatin Methacryloyl Bioinks, *Adv Healthc Mater* 6 (2017) 1601451.
- [185] L. Ouyang, C.B. Highley, W. Sun, J.A. Burdick, A Generalizable Strategy for the 3D Bioprinting of Hydrogels from Nonviscous Photo-crosslinkable Inks, *Adv. Mater.* 29 (2017) 1604983.
- [186] M.P. Lutolf, J.A. Hubbell, Synthetic biomaterials as instructive extracellular microenvironments for morphogenesis in tissue engineering, *Nat. Biotechnol.* 23 (2005) 47-55.

- [187] W.P. Daley, S.B. Peters, M. Larsen, Extracellular matrix dynamics in development and regenerative medicine, *J. Cell Sci.* 121 (2008) 255-64.
- [188] G. Huang, F. Li, X. Zhao, Y. Ma, Y. Li, M. Lin, G. Jin, T.J. Lu, G.M. Genin, F. Xu, Functional and Biomimetic Materials for Engineering of the Three-Dimensional Cell Microenvironment, *Chem. Rev.* 117 (2017) 12764-12850.
- [189] H.K. Kleinman, D. Philp, M.P. Hoffman, Role of the extracellular matrix in morphogenesis, *Curr. Opin. Biotechnol.* 14 (2003) 526-32.
- [190] A.J. Engler, S. Sen, H.L. Sweeney, D.E. Discher, Matrix elasticity directs stem cell lineage specification, *Cell* 126 (2006) 677-89.
- [191] G.P. Raeber, M.P. Lutolf, J.A. Hubbell, Molecularly engineered PEG hydrogels: a novel model system for proteolytically mediated cell migration, *Biophys. J.* 89 (2005) 1374-88.
- [192] M. Guvendiren, J.A. Burdick, Engineering synthetic hydrogel microenvironments to instruct stem cells, *Curr. Opin. Biotechnol.* 24 (2013) 841-6.
- [193] F.P. Rúben, J.B. Paulo, Photopolymerizable hydrogels in regenerative medicine and drug delivery, *Hot Topics in Biomaterials*, Future Science Ltd (2014), pp. 6-28.
- [194] J.-A. Yang, J. Yeom, B.W. Hwang, A.S. Hoffman, S.K. Hahn, In situ-forming injectable hydrogels for regenerative medicine, *Prog. Polym. Sci.* 39 (2014) 1973-1986.
- [195] Y.S. Zhang, A. Khademhosseini, Advances in engineering hydrogels, *Science* 356 (2017) eaaf3627.
- [196] A. Skardal, A. Atala, Biomaterials for integration with 3-D bioprinting, *Ann Biomed Eng* 43 (2015) 730-46.
- [197] K.B. Fonseca, P.L. Granja, C.C. Barrias, Engineering proteolytically-degradable artificial extracellular matrices, *Prog. Polym. Sci.* 39 (2014) 2010-2029.
- [198] J.J. Rice, M.M. Martino, L. De Laporte, F. Tortelli, P.S. Briquez, J.A. Hubbell, Engineering the regenerative microenvironment with biomaterials, *Adv Healthc Mater* 2 (2013) 57-71.
- [199] S.C. Neves, D.B. Gomes, A. Sousa, S.J. Bidarra, P. Petrini, L. Moroni, C.C. Barrias, P.L. Granja, Biofunctionalized pectin hydrogels as 3D cellular microenvironments, *J. Mater. Chem. B* 3 (2015) 2096-2108.
- [200] E.A. Phelps, N.O. Enemchukwu, V.F. Fiore, J.C. Sy, N. Murthy, T.A. Sulchek, T.H. Barker, A.J. Garcia, Maleimide cross-linked bioactive PEG hydrogel exhibits improved reaction kinetics and cross-linking for cell encapsulation and in situ delivery, *Adv. Mater.* 24 (2012) 64-70, 2.
- [201] J. Patterson, J.A. Hubbell, Enhanced proteolytic degradation of molecularly engineered PEG hydrogels in response to MMP-1 and MMP-2, *Biomaterials* 31 (2010) 7836-45.

- [202] K.B. Fonseca, D.B. Gomes, K. Lee, S.G. Santos, A. Sousa, E.A. Silva, D.J. Mooney, P.L. Granja, C.C. Barrias, Injectable MMP-sensitive alginate hydrogels as hMSC delivery systems, *Biomacromolecules* 15 (2014) 380-90.
- [203] E.Y. Tokuda, J.L. Leight, K.S. Anseth, Modulation of matrix elasticity with PEG hydrogels to study melanoma drug responsiveness, *Biomaterials* 35 (2014) 4310-8.
- [204] G. Zhang, C.T. Drinnan, L.R. Geuss, L.J. Suggs, Vascular differentiation of bone marrow stem cells is directed by a tunable three-dimensional matrix, *Acta Biomater* 6 (2010) 3395-403.
- [205] S. Van Vlierberghe, P. Dubruel, E. Schacht, Biopolymer-based hydrogels as scaffolds for tissue engineering applications: a review, *Biomacromolecules* 12 (2011) 1387-408.
- [206] C.C. Lin, C.S. Ki, H. Shih, Thiol-norbornene photo-click hydrogels for tissue engineering applications, *J. Appl. Polym. Sci.* 132 (2015) 41563.
- [207] C.C. Lin, K.S. Anseth, PEG hydrogels for the controlled release of biomolecules in regenerative medicine, *Pharm. Res.* 26 (2009) 631-43.
- [208] C. Heller, M. Schwentenwein, G. Russmüller, T. Koch, D. Moser, C. Schopper, F. Varga, J. Stampfl, R. Liska, Vinylcarbonates and vinylcarbamates: Biocompatible monomers for radical photopolymerization, *J. Polym. Sci., Part A: Polym. Chem.* 49 (2011) 650-661.
- [209] B. Husar, R. Liska, Vinyl carbonates, vinyl carbamates, and related monomers: synthesis, polymerization, and application, *Chem. Soc. Rev.* 41 (2012) 2395-405.
- [210] C. Heller, M. Schwentenwein, G. Russmueller, F. Varga, J. Stampfl, R. Liska, Vinyl esters: Low cytotoxicity monomers for the fabrication of biocompatible 3D scaffolds by lithography based additive manufacturing, *J. Polym. Sci., Part A: Polym. Chem.* 47 (2009) 6941-6954.
- [211] M.W. Tibbitt, A.M. Kloxin, L. Sawicki, K.S. Anseth, Mechanical Properties and Degradation of Chain and Step Polymerized Photodegradable Hydrogels, *Macromolecules* 46 (2013) 2785-2792.
- [212] M.A. Azagarsamy, K.S. Anseth, Bioorthogonal Click Chemistry: An Indispensable Tool to Create Multifaceted Cell Culture Scaffolds, *ACS Macro Lett* 2 (2013) 5-9.
- [213] Y. Jiang, J. Chen, C. Deng, E.J. Suuronen, Z. Zhong, Click hydrogels, microgels and nanogels: emerging platforms for drug delivery and tissue engineering, *Biomaterials* 35 (2014) 4969-85.
- [214] C.E. Hoyle, C.N. Bowman, Thiol-ene click chemistry, *Angew. Chem. Int. Ed. Engl.* 49 (2010) 1540-73.
- [215] C.A. DeForest, B.D. Polizzotti, K.S. Anseth, Sequential click reactions for synthesizing and patterning three-dimensional cell microenvironments, *Nat Mater* 8 (2009) 659-64.
- [216] M.A. Tasdelen, Y. Yagci, Light-induced click reactions, *Angew. Chem. Int. Ed. Engl.* 52 (2013) 5930-8.

- [217] K.A. Kyburz, K.S. Anseth, Three-dimensional hMSC motility within peptide-functionalized PEG-based hydrogels of varying adhesivity and crosslinking density, *Acta Biomater* 9 (2013) 6381-92.
- [218] H. Shih, C.C. Lin, Visible-light-mediated thiol-ene hydrogelation using eosin-Y as the only photoinitiator, *Macromol. Rapid Commun.* 34 (2013) 269-73.
- [219] W.M. Gramlich, I.L. Kim, J.A. Burdick, Synthesis and orthogonal photopatterning of hyaluronic acid hydrogels with thiol-norbornene chemistry, *Biomaterials* 34 (2013) 9803-11.
- [220] Z. Muñoz, H. Shih, C.-C. Lin, Gelatin hydrogels formed by orthogonal thiol–norbornene photochemistry for cell encapsulation, *Biomater. Sci.* 2 (2014) 1063-1072.
- [221] Y. Hao, H. Shih, Z. Munoz, A. Kemp, C.C. Lin, Visible light cured thiol-vinyl hydrogels with tunable degradation for 3D cell culture, *Acta Biomater* 10 (2014) 104-14.
- [222] J. Hu, Y. Hou, H. Park, B. Choi, S. Hou, A. Chung, M. Lee, Visible light crosslinkable chitosan hydrogels for tissue engineering, *Acta Biomater* 8 (2012) 1730-8.
- [223] I. Mironi-Harpaz, D.Y. Wang, S. Venkatraman, D. Seliktar, Photopolymerization of cell-encapsulating hydrogels: crosslinking efficiency versus cytotoxicity, *Acta Biomater* 8 (2012) 1838-48.
- [224] N.E. Fedorovich, M.H. Oudshoorn, D. van Geemen, W.E. Hennink, J. Alblas, W.J. Dhert, The effect of photopolymerization on stem cells embedded in hydrogels, *Biomaterials* 30 (2009) 344-53.
- [225] K.T. Nguyen, J.L. West, Photopolymerizable hydrogels for tissue engineering applications, *Biomaterials* 23 (2002) 4307-14.
- [226] A.D. Rouillard, C.M. Berglund, J.Y. Lee, W.J. Polacheck, Y. Tsui, L.J. Bonassar, B.J. Kirby, Methods for photocrosslinking alginate hydrogel scaffolds with high cell viability, *Tissue Eng Part C Methods* 17 (2011) 173-9.
- [227] S.J. Bryant, C.R. Nuttelman, K.S. Anseth, Cytocompatibility of UV and visible light photoinitiating systems on cultured NIH/3T3 fibroblasts in vitro, *J Biomater Sci Polym Ed* 11 (2000) 439-57.
- [228] C.G. Williams, A.N. Malik, T.K. Kim, P.N. Manson, J.H. Elisseeff, Variable cytocompatibility of six cell lines with photoinitiators used for polymerizing hydrogels and cell encapsulation, *Biomaterials* 26 (2005) 1211-8.
- [229] B.D. Fairbanks, M.P. Schwartz, C.N. Bowman, K.S. Anseth, Photoinitiated polymerization of PEG-diacrylate with lithium phenyl-2,4,6-trimethylbenzoylphosphine: polymerization rate and cytocompatibility, *Biomaterials* 30 (2009) 6702-7.
- [230] Z. Li, J. Torgersen, A. Ajami, S. Muhleder, X. Qin, W. Husinsky, W. Holthoner, A. Ovsianikov, J. Stampfl, R. Liska, Initiation efficiency and cytotoxicity of novel water-soluble two-photon photoinitiators for direct 3D microfabrication of hydrogels, *RSC Advances* 3 (2013) 15939-15946.

- [231] K.S. Lim, B.S. Schon, N.V. Mekhileri, G.C.J. Brown, C.M. Chia, S. Prabakar, G.J. Hooper, T.B.F. Woodfield, New Visible-Light Photoinitiating System for Improved Print Fidelity in Gelatin-Based Bioinks, *ACS Biomater Sci Eng* 2 (2016) 1752-1762.
- [232] J.W. Nichol, S.T. Koshy, H. Bae, C.M. Hwang, S. Yamanlar, A. Khademhosseini, Cell-laden microengineered gelatin methacrylate hydrogels, *Biomaterials* 31 (2010) 5536-44.
- [233] S.B. Anderson, C.C. Lin, D.V. Kuntzler, K.S. Anseth, The performance of human mesenchymal stem cells encapsulated in cell-degradable polymer-peptide hydrogels, *Biomaterials* 32 (2011) 3564-74.
- [234] A. Fu, K. Gwon, M. Kim, G. Tae, J.A. Kornfield, Visible-light-initiated thiol-acrylate photopolymerization of heparin-based hydrogels, *Biomacromolecules* 16 (2015) 497-506.
- [235] A.K. Nguyen, S.D. Gittard, A. Koroleva, S. Schlie, A. Gaidukeviciute, B.N. Chichkov, R.J. Narayan, Two-photon polymerization of polyethylene glycol diacrylate scaffolds with riboflavin and triethanolamine used as a water-soluble photoinitiator, *Regen Med* 8 (2013) 725-38.
- [236] H. Park, B. Choi, J. Hu, M. Lee, Injectable chitosan hyaluronic acid hydrogels for cartilage tissue engineering, *Acta Biomater* 9 (2013) 4779-86.
- [237] P.M. Kharkar, K.L. Kiick, A.M. Kloxin, Designing degradable hydrogels for orthogonal control of cell microenvironments, *Chem. Soc. Rev.* 42 (2013) 7335-72.
- [238] F.R. Maia, K.B. Fonseca, G. Rodrigues, P.L. Granja, C.C. Barrias, Matrix-driven formation of mesenchymal stem cell-extracellular matrix microtissues on soft alginate hydrogels, *Acta Biomater* 10 (2014) 3197-208.
- [239] D. Williams, P. Thayer, H. Martinez, E. Gatenholm, A. Khademhosseini, A perspective on the physical, mechanical and biological specifications of bioinks and the development of functional tissues in 3D bioprinting, *Bioprinting* 9 (2018) 19-36.
- [240] D. Chimene, K.K. Lennox, R.R. Kaunas, A.K. Gaharwar, Advanced Bioinks for 3D Printing: A Materials Science Perspective, *Ann Biomed Eng* 44 (2016) 2090-102.
- [241] L. Fertier, H. Koleilat, M. Stemmelen, O. Giani, C. Joly-Duhamel, V. Lapinte, J.-J. Robin, The use of renewable feedstock in UV-curable materials – A new age for polymers and green chemistry, *Prog. Polym. Sci.* 38 (2013) 932-962.
- [242] J.F. Almeida, P. Ferreira, A. Lopes, M.H. Gil, Photocrosslinkable biodegradable responsive hydrogels as drug delivery systems, *Int. J. Biol. Macromol.* 49 (2011) 948-54.
- [243] O. Jeon, C. Powell, L.D. Solorio, M.D. Krebs, E. Alsberg, Affinity-based growth factor delivery using biodegradable, photocrosslinked heparin-alginate hydrogels, *J Control Release* 154 (2011) 258-66.
- [244] S. Sahoo, C. Chung, S. Khetan, J.A. Burdick, Hydrolytically degradable hyaluronic acid hydrogels with controlled temporal structures, *Biomacromolecules* 9 (2008) 1088-92.

- [245] S.A. Bencherif, A. Srinivasan, F. Horkay, J.O. Hollinger, K. Matyjaszewski, N.R. Washburn, Influence of the degree of methacrylation on hyaluronic acid hydrogels properties, *Biomaterials* 29 (2008) 1739-49.
- [246] S. Bertlein, G. Brown, K.S. Lim, T. Jungst, T. Boeck, T. Blunk, J. Tessmar, G.J. Hooper, T.B.F. Woodfield, J. Groll, Thiol-Ene Clickable Gelatin: A Platform Bioink for Multiple 3D Biofabrication Technologies, *Adv. Mater.* 29 (2017) 1703404-n/a.
- [247] S. Stichler, T. Jungst, M. Schamel, I. Zilkowski, M. Kuhlmann, T. Bock, T. Blunk, J. Tessmar, J. Groll, Thiol-ene Clickable Poly(glycidol) Hydrogels for Biofabrication, *Ann Biomed Eng* 45 (2017) 273-285.
- [248] J. Jang, T.G. Kim, B.S. Kim, S.W. Kim, S.M. Kwon, D.W. Cho, Tailoring mechanical properties of decellularized extracellular matrix bioink by vitamin B2-induced photo-crosslinking, *Acta Biomater* 33 (2016) 88-95.
- [249] K. Zhu, S.R. Shin, T. van Kempen, Y.C. Li, V. Ponraj, A. Nasajpour, S. Mandla, N. Hu, X. Liu, J. Leijten, Y.D. Lin, M.A. Hussain, Y.S. Zhang, A. Tamayol, A. Khademhosseini, Gold Nanocomposite Bioink for Printing 3D Cardiac Constructs, *Adv. Funct. Mater.* 27 (2017) n/a-n/a.
- [250] W. Jia, P.S. Gungor-Ozkerim, Y.S. Zhang, K. Yue, K. Zhu, W. Liu, Q. Pi, B. Byambaa, M.R. Dokmeci, S.R. Shin, A. Khademhosseini, Direct 3D bioprinting of perfusable vascular constructs using a blend bioink, *Biomaterials* 106 (2016) 58-68.
- [251] S. Stichler, S. Bertlein, J. Tessmar, T. Jüngst, J. Groll, Thiol-ene Cross-Linkable Hydrogels as Bioinks for Biofabrication, *Macromolecular Symposia* 372 (2017) 102-107.
- [252] A. Skardal, S.V. Murphy, K. Crowell, D. Mack, A. Atala, S. Soker, A tunable hydrogel system for long-term release of cell-secreted cytokines and bioprinted in situ wound cell delivery, *J Biomed Mater Res B Appl Biomater* 105 (2017) 1986-2000.
- [253] M. Kesti, M. Muller, J. Becher, M. Schnabelrauch, M. D'Este, D. Eglin, M. Zenobi-Wong, A versatile bioink for three-dimensional printing of cellular scaffolds based on thermally and photo-triggered tandem gelation, *Acta Biomater* 11 (2015) 162-72.
- [254] X. Zhai, C. Ruan, Y. Ma, D. Cheng, M. Wu, W. Liu, X. Zhao, H. Pan, W.W. Lu, 3D-Bioprinted Osteoblast-Laden Nanocomposite Hydrogel Constructs with Induced Microenvironments Promote Cell Viability, Differentiation, and Osteogenesis both In Vitro and In Vivo, *Adv Sci (Weinh)* 5 (2018) 1700550.
- [255] K. Virginie, G. Fabien, A. Isabelle, G. Bertrand, M. Sylvain, A. Joëlle, F. Jean-Christophe, C. Sylvain, In vivo bioprinting for computer- and robotic-assisted medical intervention: preliminary study in mice, *Biofabrication* 2 (2010) 014101.
- [256] N. Mori, Y. Morimoto, S. Takeuchi, Skin integrated with perfusable vascular channels on a chip, *Biomaterials* 116 (2017) 48-56.

- [257] G. Sriram, P.L. Bigliardi, M. Bigliardi-Qi, Fibroblast heterogeneity and its implications for engineering organotypic skin models in vitro, *Eur J Cell Biol* 94 (2015) 483-512.
- [258] K. Tsukahara, Y. Takema, S. Moriwaki, T. Fujimura, G. Imokawa, Dermal fluid translocation is an important determinant of the diurnal variation in human skin thickness, *British Journal of Dermatology* 145 (2001) 590-596.
- [259] N. Wei Long, Q. Jovina Tan Zhi, Y. Wai Yee, N. May Win, Proof-of-concept: 3D bioprinting of pigmented human skin constructs, *Biofabrication* 10 (2018) 025005.
- [260] S. Huang, B. Yao, J. Xie, X. Fu, 3D bioprinted extracellular matrix mimics facilitate directed differentiation of epithelial progenitors for sweat gland regeneration, *Acta Biomater* 32 (2016) 170-177.
- [261] J.L. Drury, D.J. Mooney, Hydrogels for tissue engineering: scaffold design variables and applications, *Biomaterials* 24 (2003) 4337-4351.
- [262] S.R. Van Tomme, G. Storm, W.E. Hennink, In situ gelling hydrogels for pharmaceutical and biomedical applications, *Int. J. Pharm.* 355 (2008) 1-18.
- [263] R.J. Hinchliffe, G.D. Valk, J. Apelqvist, D.G. Armstrong, K. Bakker, F.L. Game, A. Hartemann-Heurtier, M. Londahl, P.E. Price, W.H. van Houtum, W.J. Jeffcoate, A systematic review of the effectiveness of interventions to enhance the healing of chronic ulcers of the foot in diabetes, *Diabetes Metab Res Rev* 24 Suppl 1 (2008) S119-44.
- [264] K.S. Masters, S.J. Leibovich, P. Belem, J.L. West, L.A. Poole-Warren, Effects of nitric oxide releasing poly(vinyl alcohol) hydrogel dressings on dermal wound healing in diabetic mice, *Wound Repair Regen* 10 (2002) 286-94.
- [265] Y.X. Dong, A. Sigen, M. Rodrigues, X.L. Li, S.H. Kwon, N. Kosaric, S. Khong, Y.S. Gao, W.X. Wang, G.C. Gurtner, Injectable and Tunable Gelatin Hydrogels Enhance Stem Cell Retention and Improve Cutaneous Wound Healing, *Adv. Funct. Mater.* 27 (2017) n/a-n/a.
- [266] L. Pescosolido, W. Schuurman, J. Malda, P. Matricardi, F. Alhaique, T. Coviello, P.R. van Weeren, W.J. Dhert, W.E. Hennink, T. Vermonden, Hyaluronic acid and dextran-based semi-IPN hydrogels as biomaterials for bioprinting, *Biomacromolecules* 12 (2011) 1831-8.
- [267] A. Tirella, A. Orsini, G. Vozzi, A. Ahluwalia, A phase diagram for microfabrication of geometrically controlled hydrogel scaffolds, *Biofabrication* 1 (2009) 045002.
- [268] W. Schuurman, P.A. Levett, M.W. Pot, P.R. van Weeren, W.J. Dhert, D.W. Hutmacher, F.P. Melchels, T.J. Klein, J. Malda, Gelatin-methacrylamide hydrogels as potential biomaterials for fabrication of tissue-engineered cartilage constructs, *Macromol Biosci* 13 (2013) 551-61.
- [269] A. Banerjee, M. Arha, S. Choudhary, R.S. Ashton, S.R. Bhatia, D.V. Schaffer, R.S. Kane, The influence of hydrogel modulus on the proliferation and differentiation of encapsulated neural stem cells, *Biomaterials* 30 (2009) 4695-9.

- [270] C. Branco da Cunha, D.D. Klumpers, W.A. Li, S.T. Koshy, J.C. Weaver, O. Chaudhuri, P.L. Granja, D.J. Mooney, Influence of the stiffness of three-dimensional alginate/collagen-I interpenetrating networks on fibroblast biology, *Biomaterials* 35 (2014) 8927-36.
- [271] K. Dubbin, Y. Hori, K.K. Lewis, S.C. Heilshorn, Dual-Stage Crosslinking of a Gel-Phase Bioink Improves Cell Viability and Homogeneity for 3D Bioprinting, *Adv Healthc Mater* 5 (2016) 2488-2492.
- [272] T. Jungst, W. Smolan, K. Schacht, T. Scheibel, J. Groll, Strategies and Molecular Design Criteria for 3D Printable Hydrogels, *Chem. Rev.* 116 (2016) 1496-539.
- [273] A. Muhammad, P. Emeline, D. Alexandre, F. Aurelien, G. Fabien, Controlling laser-induced jet formation for bioprinting mesenchymal stem cells with high viability and high resolution, *Biofabrication* 6 (2014) 045001.
- [274] T. Boland, V. Mironov, A. Gutowska, E.A. Roth, R.R. Markwald, Cell and organ printing 2: fusion of cell aggregates in three-dimensional gels, *Anat Rec A Discov Mol Cell Evol Biol* 272 (2003) 497-502.
- [275] S.V. Murphy, A. Skardal, A. Atala, Evaluation of hydrogels for bio-printing applications, *J Biomed Mater Res A* 101 (2013) 272-84.
- [276] S.R. Caliari, J.A. Burdick, A practical guide to hydrogels for cell culture, *Nat Methods* 13 (2016) 405-14.
- [277] B.S. Kim, Y.W. Kwon, J.S. Kong, G.T. Park, G. Gao, W. Han, M.B. Kim, H. Lee, J.H. Kim, D.W. Cho, 3D cell printing of in vitro stabilized skin model and in vivo pre-vascularized skin patch using tissue-specific extracellular matrix bioink: A step towards advanced skin tissue engineering, *Biomaterials* 168 (2018) 38-53.
- [278] Z. Hong Bo, Y. Shi, T. Xing, R. Yin, S. Yang, W. Jie, Z. Wenjun, *Biomedical Materials* (2018).
- [279] L.J. Pourchet, A. Thepot, M. Albouy, E.J. Courtial, A. Boher, L.J. Blum, C.A. Marquette, Human Skin 3D Bioprinting Using Scaffold-Free Approach, *Adv Healthc Mater* 6 (2017) 1601101.
- [280] D. Min, W. Lee, I.H. Bae, T.R. Lee, P. Croce, S.S. Yoo, Bioprinting of biomimetic skin containing melanocytes, *Exp Dermatol* 27 (2018) 453-459.
- [281] L. Koch, S. Kuhn, H. Sorg, M. Gruene, S. Schlie, R. Gaebel, B. Polchow, K. Reimers, S. Stoelting, N. Ma, P.M. Vogt, G. Steinhoff, B. Chichkov, Laser printing of skin cells and human stem cells, *Tissue Eng Part C Methods* 16 (2010) 847-54.
- [282] M. Rimann, E. Bono, H. Annaheim, M. Bleisch, U. Graf-Hausner, Standardized 3D Bioprinting of Soft Tissue Models with Human Primary Cells, *J Lab Autom* 21 (2016) 496-509.

- [283] C.M. Reijnders, A. van Lier, S. Roffel, D. Kramer, R.J. Scheper, S. Gibbs, Development of a Full-Thickness Human Skin Equivalent In Vitro Model Derived from TERT-Immortalized Keratinocytes and Fibroblasts, *Tissue Eng Part A* 21 (2015) 2448-59.
- [284] Y. Xie, S.C. Rizzi, R. Dawson, E. Lynam, S. Richards, D.I. Leavesley, Z. Upton, Development of a three-dimensional human skin equivalent wound model for investigating novel wound healing therapies, *Tissue Eng Part C Methods* 16 (2010) 1111-23.
- [285] W. Lee, J.C. Debasitis, V.K. Lee, J.H. Lee, K. Fischer, K. Edminster, J.K. Park, S.S. Yoo, Multi-layered culture of human skin fibroblasts and keratinocytes through three-dimensional freeform fabrication, *Biomaterials* 30 (2009) 1587-95.
- [286] V. Lee, G. Singh, J.P. Trasatti, C. Bjornsson, X. Xu, T.N. Tran, S.S. Yoo, G. Dai, P. Karande, Design and fabrication of human skin by three-dimensional bioprinting, *Tissue Eng Part C Methods* 20 (2014) 473-84.
- [287] C. Nieves, G. Marta, F.d.C. Juan, V. Diego, L.J. Jose, 3D bioprinting of functional human skin: production and in vivo analysis, *Biofabrication* 9 (2017) 015006.
- [288] K. Byoung Soo, L. Jung-Seob, G. Ge, C. Dong-Woo, Direct 3D cell-printing of human skin with functional transwell system, *Biofabrication* 9 (2017) 025034.
- [289] N. Liu, S. Huang, B. Yao, J. Xie, X. Wu, X. Fu, 3D bioprinting matrices with controlled pore structure and release function guide in vitro self-organization of sweat gland, *Sci Rep* 6 (2016) 34410.
- [290] M. Radisic, L. Yang, J. Boublik, R.J. Cohen, R. Langer, L.E. Freed, G. Vunjak-Novakovic, Medium perfusion enables engineering of compact and contractile cardiac tissue, *Am J Physiol Heart Circ Physiol* 286 (2004) H507-16.
- [291] J. Rouwkema, A. Khademhosseini, Vascularization and Angiogenesis in Tissue Engineering: Beyond Creating Static Networks, *Trends Biotechnol.* 34 (2016) 733-745.
- [292] E.C. Novosel, C. Kleinhaus, P.J. Kluger, Vascularization is the key challenge in tissue engineering, *Adv Drug Deliv Rev* 63 (2011) 300-11.
- [293] B. Hendrickx, J.J. Vranckx, A. Luttun, Cell-based vascularization strategies for skin tissue engineering, *Tissue Eng Part B Rev* 17 (2011) 13-24.
- [294] C. Vyas, R. Pereira, B. Huang, F. Liu, W. Wang, P. Bartolo, Engineering the vasculature with additive manufacturing, *Current Opinion in Biomedical Engineering* 2 (2017) 1-13.
- [295] X. Cui, T. Boland, Human microvasculature fabrication using thermal inkjet printing technology, *Biomaterials* 30 (2009) 6221-7.
- [296] M. Yanez, J. Rincon, A. Dones, C. De Maria, R. Gonzales, T. Boland, In vivo assessment of printed microvasculature in a bilayer skin graft to treat full-thickness wounds, *Tissue Eng Part A* 21 (2015) 224-33.

- [297] P.K. Wu, B.R. Ringeisen, Development of human umbilical vein endothelial cell (HUVEC) and human umbilical vein smooth muscle cell (HUVSMC) branch/stem structures on hydrogel layers via biological laser printing (BioLP), *Biofabrication* 2 (2010) 014111.
- [298] C. Norotte, F.S. Marga, L.E. Niklason, G. Forgacs, Scaffold-free vascular tissue engineering using bioprinting, *Biomaterials* 30 (2009) 5910-7.
- [299] V.K. Lee, D.Y. Kim, H. Ngo, Y. Lee, L. Seo, S.S. Yoo, P.A. Vincent, G. Dai, Creating perfused functional vascular channels using 3D bio-printing technology, *Biomaterials* 35 (2014) 8092-102.
- [300] H.E. Abaci, Z. Guo, A. Coffman, B. Gillette, W.H. Lee, S.K. Sia, A.M. Christiano, Human Skin Constructs with Spatially Controlled Vasculature Using Primary and iPSC-Derived Endothelial Cells, *Adv Healthc Mater* 5 (2016) 1800-7.
- [301] K.W. Binder, W. Zhao, T. Aboushwareb, D. Dice, A. Atala, J.J. Yoo, In situ bioprinting of the skin for burns, *J Am Coll Surg* 211 (2010) S76.

CHAPTER III

A SINGLE-COMPONENT HYDROGEL BIOINK FOR BIOPRINTING OF BIOENGINEERED 3D CONSTRUCTS FOR DERMAL TISSUE ENGINEERING

This chapter was based on the following publication:

R.F. Pereira, A. Sousa, C.C. Barrias, P.J. Bártolo, P.L. Granja, A single-component hydrogel bioink for bioprinting of bioengineered 3D constructs for dermal tissue engineering, *Materials Horizons* 5 (2018) 1100-1111.

Abstract

Bioprinting is attractive to create cellularized constructs for skin repair. However, the vast majority of bioinks present limitations in the printing of chemically defined 3D constructs with controllable biophysical and biochemical properties. To address this challenge, a single-component hydrogel bioink with controlled density of cell-adhesive ligands, tuneable mechanical properties and adjustable rheological behaviour is developed for extrusion bioprinting and applied for the fabrication of 3D dermal constructs. A methacrylate modified pectin bioink is designed to allow the tethering of integrin-binding motifs and the formation of hydrogels by UV photopolymerization and ionic gelation. The rheological behaviour of a low polymer concentration (1.5 wt%) solution is adjusted by ionic crosslinking, yielding a printable bioink that holds the pre-designed shape upon deposition for postprinting photocrosslinking. Printed constructs provide a suitable microenvironment that supports the deposition of endogenous extracellular matrix, rich in collagen and fibronectin, by entrapped dermal fibroblasts. This approach enables the design of chemically defined and cell-responsive bioinks for tissue engineering applications and particularly for the generation of biomimetic skin constructs.

Keywords: 3D bioprinting; dermal tissue engineering; cell-responsive bioink; dermal fibroblasts; pectin.

3.1. Introduction

Skin is the outermost organ of the human body, providing protection, thermal regulation and transmission of sensory information [1]. It is composed of an epidermal layer located on top of a vascularized dermal layer. The dermis is a highly dynamic layer consisting of an intricate extracellular matrix (ECM) mainly composed of fibroblasts, which produce connective tissue components and several cytokines that regulate homeostasis [2]. As the dermis has limited self-reparative ability upon injury, bioprinted 3D cellularized constructs capable of instructing entrapped cells to secrete new ECM components are attractive for dermal repair [3].

Bioprinting has emerged as a promising technology to create hierarchical tissue constructs through the layer-by-layer deposition of cellularized formulations in pre-designed spatial locations [4-7]. Extrusion bioprinting is the most popular technology due to its low cost, ease of operation and ability to print several material formulations loadable with living cells and biological molecules, termed as bioinks, into millimetre size constructs [8-10]. Although extrusion bioprinting has been used to produce skin constructs, existing bioinks are mostly limited to collagen, gelatin and fibrin [11-13]. Protein-based bioinks are attractive owing their phase transition temperature and the presence of biochemical cues in native composition. However, to overcome shrinkage issues and limited mechanical properties of these materials, additional polymers like alginate are often included in the printable formulation [13], resulting in multimaterial bioinks of increased complexity and reduced control over the cellular responses. These bioinks inherently contain cell-adhesion and cell-proteolytic cues in the native composition, which difficult to decouple macromer concentration and matrix mechanical properties from ligand density. Moreover, changes in macromer concentration inevitably alter key matrix characteristics that affect cellular responses, such as the density of adhesive ligands, fibre density structure and mechanical properties [14].

Natural polymers lacking of bioactive cues in the native composition represent an attractive alternative to design chemically defined bioinks, which biochemical, mechanical and rheological properties can be independently tailored to induce specific cellular responses. Pectin, an anionic heteropolysaccharide extracted from the cell walls of plants, has gained attention in the biomedical field due to its biocompatibility, abundance of modifiable functional groups and ability to form physical hydrogels through interaction between calcium ions and blocks of galacturonic acid residues [15]. It is composed of a backbone of (1,4)-linked α -D-galacturonic acid residues, which can be partially acetylated and methyl esterified, and a variety of neutral sugars side chains such as rhamnose,

galactose and arabinose [16]. Although pectin shares key properties with alginate, its branched nature and complex chemical composition provide a range of bioactive properties (e.g., bioadhesivity, anti-cancerous effect and immunomodulatory activity) [17-19] and could potentially enhance the in vivo degradation/dissolution, which is useful for tissue engineering applications. Importantly, pectin lacks of cell-adhesive and protease-cleavable sites in native composition [15], acting as a “blank slate” and providing the possibility to engineer biofunctionalized macromers for the formation of chemically defined hydrogels. Biofunctionalized pectin hydrogels have been explored as vehicles for entrapment, supporting the viability and/or differentiation of several cell types such as MC3T3-E1 pre-osteoblast cells, mesenchymal stromal cells and dermal fibroblasts [20-22].

In this work, we report on the design of a novel single-component pectin bioink with tuneable mechanical and rheological properties that can be biofunctionalized with relevant peptide ligands for bioprinting of cellularized 3D dermal constructs. Contrary to other strategies based on the use of multiple polymers or sacrificial materials to achieve suitable printability [13, 23], the properties of the developed pectin bioink are exclusively tailored via macromer chemistry without the need for additional polymers to achieve both proper rheological profiles and biological responses. Conceptually, we hypothesized that the incorporation of methacrylate groups into the pectin backbone allows the design of a macromer that would undergo chemical crosslinking through UV photopolymerization, while retaining inherent ionic gelation ability via interaction with calcium ions. By independently applying these two crosslinking chemistries to the designed pectin macromer is possible to engineer hydrogel networks with defined biochemical composition and tuneable properties that can be explored as both hydrogel systems for cell entrapment and bioinks for extrusion bioprinting. First, to demonstrate the versatility of this hydrogel platform for tissue engineering applications, a low polymer concentration solution was used to generate chemical hydrogels that may subsequently undergo ionic gelation to further tailor the hydrogel elastic modulus (G') and cell response. Second, by inverting the crosslinking sequence, a tuneable and printable bioink exhibiting suitable rheological behaviour was obtained by the reaction of the macromer solution with calcium ions. After printing, the ionically crosslinked hydrogel bioink undergoes chemical crosslinking by UV photopolymerization for shape fixation, yielding cellularized tissue constructs with high shape fidelity. Cell response within printed 3D constructs was characterized regarding viability, spreading and deposition of key ECM components.

3.2. Materials and Methods

3.2.1. Synthesis of methacrylate-functionalized pectin

Low methoxyl citrus pectin (Classic CU701) with galacturonic acid unit content of 86% and degree of methylation of 37%, was kindly provided by Herbstreith & Fox (Neuenbürg, Germany). Prior to chemical modification, raw pectin was purified using a published protocol [22]. Pectin methacrylate (PECMA) was synthesized by reacting purified pectin with methacrylic anhydride (MA, Sigma-Aldrich). Pectin was dissolved in phosphate buffered saline (PBS, pH 7.4) at 1.25 wt% and stirred at room temperature until complete dissolution. To this solution, MA was added dropwise (0.5 mL/min) and left to react protected from light under vigorous stirring. The pH was periodically adjusted to 8.0 by the addition of 5.0 M NaOH. After 24 h, pectin was collected by twice precipitation with a ten-fold excess of cold acetone (4°C), followed by drying at 40°C in a vacuum oven. For further purification, the polymer was dissolved in ultrapure water (Millipore) and dialyzed (MWCO 3500, Spectra/Por®, SpectrumLabs) for 5 days. The final product was sterile filtered using 0.22 μm filter membranes (Steriflip® filter unit, Millipore), frozen, lyophilized, and stored at -20 °C until further use. The extent of methacrylate substitution was determined by ^1H NMR recorded with a 400 MHz spectrometer AVANCE III (Bruker). Polymers were dissolved (8.5 mg/mL) in deuterated water (D_2O , Euriso-top) and transferred to NMR tubes containing a glass capillary loaded with 3-(trimethylsilyl)propionic-2,2,3,3- d_4 acid sodium salt (TSP- d_4 , Euriso-top) as internal standard ($\delta = 0$ ppm).

3.2.2. Conjugation of cell-adhesive peptide

The custom synthesized integrin-binding peptide CGGGGRGDSP (Genscript, cell-adhesive domain underlined) was conjugated to PECMA macromers through a base-catalysed thiol-Michael addition click reaction. For coupling the integrin-binding peptide, a solution of PECMA (1.0 wt%) was dissolved in triethanolamine (0.25 M, TEOA, Acros Organics) buffer at pH 8.5. After the addition of cell-adhesive peptide (64 mg/g polymer), the solution was protected from light and allowed to react under agitation and inert atmosphere. After 48 h, the solution was diluted with ultrapure water, purified by dialysis, and lyophilized. The coupling efficiency was quantified through the colorimetric DC Protein Assay (Bio-Rad) according to the manufacturer's instructions, with some modifications. Briefly, the macromer was dissolved in ultrapure water (1.0 wt%) and the solution (20 μL) transferred to a 96-well plate. To this solution, alkaline copper tartrate solution (25 μL) and dilute Folin reagent (200 μL) were then added, followed by mixing using a multi-channel micropipette. The solutions

were allowed to react at RT for 30 min, and the protein content determined with a micro-plate reader (Synergy MX, BioTek) at 750 nm. Absorbance values were converted to peptide concentrations using a standard curve of free peptide in PECMA, and normalized against control polymer solutions that were subjected to the conjugation process but in the absence of peptide.

3.2.3. Preparation of pectin hydrogels

To produce photocrosslinked hydrogels, PECMA macromer was dissolved in 0.9 wt% NaCl containing 0.05 wt% of 2-hydroxy-4-(2-hydroxyethoxy)-2-methylpropiophenone (I2959, Sigma) as radical photoinitiator. The solution was pipetted into a teflon plate with 750 μm spacers, covered with a SigmaCote treated glass slide, and exposed to UV light (7 mW/cm^2 , 365 nm) using a BlueWave[®] 200 curing spot lamp (Dymax) for different durations (40–300 s). For the preparation of dual-crosslinked hydrogels two strategies were adopted: (1) photocrosslinked hydrogel samples were incubated in Dulbecco's Modified Eagle's Medium (DMEM, Gibco) with different concentrations of calcium chloride dihydrate (0–1.8 $\times 10$ mM), at 37 °C in a humidified atmosphere of 5% CO_2 ; (2) PECMA macromer solutions (1.5 wt%) dissolved in 0.9 wt% NaCl containing I2959 were mixed with calcium chloride (CaCl_2) dihydrate at different concentrations (0–7 mM), yielding weakly crosslinked physical gels, followed by UV photopolymerization for 160 s.

3.2.4. Characterization of gel fraction, swelling ratio, microstructure and *in vitro* degradation

To determine the gel fraction, hydrogel samples (30 μL , $n = 5$) were lyophilized and weighted to determine the initial dry weight (W_{ID}). Dry samples were incubated in ultrapure water (1 mL) at 37 °C for 24 h and then were carefully removed from the solution, gently dabbed with a tissue paper to remove superficial water, and lyophilized to determine the final dry weight (W_{FD}). Gel fraction was determined based on the dry mass of hydrogels before (W_{ID}) and after (W_{FD}) incubation, according to Equation (1):

$$\text{Gel fraction (\%)} = \frac{W_{FD}}{W_{ID}} \times 100 \quad (1)$$

The swelling ratio was determined by soaking freeze-dried hydrogels in ultrapure water (1 mL) at 37 °C for 24 h. Samples were collected, the hydrogel's superficial excess water was gently removed with a tissue paper, and the swollen weight (W_S) determined. Swelling ratio (q) was calculated by dividing the weight of hydrated hydrogel (W_S) by its initial

dry weight (W_{ID}). The microstructure of hydrogels was observed by cryogenic scanning electron microscopy (cryoSEM). Immediately after preparation, hydrogel samples were frozen in slush nitrogen (N_2) and mechanically fractured to reveal the internal structure. After sublimation, samples were coated with gold/palladium and transferred to the cryoSEM microscope chamber (JEOL JSM 6301F/Oxford INCA Energy 350/Gatan Alto 2500). The degradation rate of hydrogels was enzymatically studied *in vitro* through the incubation of freeze-dried samples ($n = 9$) in ultrapure water (1 mL) supplemented with pectinase (0.05 mg/mL) from *Aspergillus niger* (Sigma-Aldrich) at 37 °C. At pre-determined time points, samples were gently washed with ultrapure water, freeze-dried and weighted (W_D). The percentage mass loss of hydrogels was calculated using Equation (2):

$$Mass\ Loss\ (\%) = \frac{W_{ID} - W_D}{W_{ID}} \times 100 \quad (2)$$

3.2.5. Characterization of hydrogel stiffness

The mechanical properties of hydrogels were analysed using a strain-controlled Kinexus Pro rheometer (Malvern). All tests were conducted with 4 mm diameter hydrogel samples ($n = 5$) in a humidified environment at physiological temperature (37 °C) to minimize hydrogel dehydration during analysis. To ensure an appropriate contact between the parallel plates, samples were compressed at 10% of their initial height. Strain amplitude sweeps were conducted from 0.1 to 10 % at 1 Hz, while frequency sweeps were carried out from 0.01 to 10 Hz at 0.5% strain, after determining the linear viscoelastic region.

3.2.6. Assessment of hydrogel's biological behaviour

Human neonatal dermal fibroblasts (hNDFs) isolated from human neonatal foreskin samples (Coriell Institute for Medical Research, USA) were cultured in DMEM supplemented with 10% fetal bovine serum (FBS, Gibco), antibiotics (100 U/mL penicillin and 100 µg/mL streptomycin, Sigma) and amphotericin B (2.5 mg/L, Sigma). Cells were cultured in 5 % CO_2 at 37 °C in tissue culture polystyrene flasks. To assess the behavior of hNDFs within PECMA hydrogels, cells (passage 3 to 8) were trypsinized using a 0.05 wt% trypsin/ethylenediamine tetraacetic acid (EDTA) solution (Sigma) before reaching confluence (70–80%) and centrifuged at 1200 rpm for 5 min. The cell pellet was suspended and mixed within the PECMA solutions (1.5 wt%) containing 0.05 wt% of I2959 at a final density of 1×10^7 cells/mL. Cell-laden polymer solutions (20 µL) were pipetted onto a teflon plate with 500 µm spacers, covered with a SigmaCote treated glass slide and exposed to UV light (7 mW cm^{-2}) for 160 s. Cell-laden hydrogels were soaked in 0.9 wt% NaCl (0.5 mL) for 30 min, followed by the

addition of culture media. At predetermined time periods, cellular hydrogels were collected and characterized for their metabolic activity, cell viability and cell morphology.

3.2.7. Bioink preparation, assessment of rheological properties and bioprinting

PECMA low macromer biofunctionalized with the RGD-peptide was dissolved in 0.9 wt% NaCl containing I2959 as radical initiator. After solubilization, CaCl₂ (5 mM) was added dropwise under vigorous agitation as the ionic crosslinking agent, and the solution incubated at 25 °C and 1400 rpm (> 1 h) until *G'* stabilization. Then, hNDFs were detached from the tissue culture plate, centrifuged at 1200 rpm for 5 min, suspended in 0.9 wt% NaCl, and mixed within the bioink at a concentration of 1×10⁷ cells/mL. Final concentrations of PECMA, I2959 and CaCl₂ were 1.5 wt%, 0.05 wt% and 5 mM, respectively.

To determine the rheological properties of the cell-laden bioink and to assess the effect of CaCl₂ concentration on its viscosity, bioink formulations with CaCl₂ at 0, 1, 3, 5 or 7 mM were tested using a Kinexus Pro rheometer (Malvern). Tests were performed at 25 °C in a humidified environment to prevent evaporation, using a shear ramp test (1 to 1000 s⁻¹ shear rate) over the course of 2 min. Two loading cycles with 1 min intervals were performed before the rheological data acquisition. To determine the yield stress, bioinks were subjected to a shear stress ramp, ranging from 1 to 100 Pa (2 min) with plate–plate geometry (0.5 mm distance).

For bioprinting, the cell-laden bioink was loaded in a sterile syringe with a 23 G cylindrical nozzle (7018314, Nordson EFD) and printed using a commercial bioprinter Regemat 3D V1 (Regemat 3D, Spain). Proprietary software was used to automatically generate G-code to control the bioprinter to fabricate desired constructs. Immediately after bioprinting, constructs were exposed to UV light (7 mW/cm², 365 nm) using a BlueWave® 200 curing spot lamp (Dymax Corporation) for covalent crosslinking. Printed constructs were incubated in culture media and characterized for cell viability, metabolic activity, morphology and ECM deposition.

3.2.8. Determination of metabolic activity and cell viability

The metabolic activity of cells within PECMA hydrogels was assessed by the resazurin assay. Resazurin (resazurin sodium salt at 0.1 mg/mL, Sigma-Aldrich) was diluted (20 v/v%) in DMEM and incubated with the hydrogels for 2 h at 37 °C. Samples were measured using a microplate reader (Synergy MX; Biotek) at 530 nm (excitation) and 590 nm (emission). Cell viability was determined with the live/dead assay. CyTRAK Orange™ (10

μM) and DRAQ7TM (3 μM) (Biostatus) were diluted in DMEM and used as dyes for live cell and dead cells, respectively. Both dyes were incubated for 10 min at RT before the visualization of hydrogels using a laser scanning microscope (CLSM, Leica TCS-SP5 AOBS, Leica Microsystems).

3.2.9. Bioprinted cell morphology and ECM synthesis

For observation of cell morphology/cytoskeletal structure and ECM deposition, immunofluorescence staining of F-actin, fibronectin, collagen type-I, laminin and nuclei was performed for the cell-laden hydrogels after predetermined time points of culture. Samples were fixed in 4 v/v% paraformaldehyde (PFA, Sigma) in PBS for 30 min, followed by extensive washing with PBS. Samples were permeabilized for 10 min with 0.2 v/v% Triton X-100 (Sigma) in PBS. Samples were incubated in blocking solution (1 w/v% bovine serum albumin in PBS) for 1 h at RT, and left overnight at 4 °C with appropriate primary antibodies. Then, samples were rinsed three times with PBS and incubated for 45 min with appropriate secondary antibodies and the conjugated probe phalloidin/Alexa Fluor® 488 (1:40, Molecular Probes-Invitrogen) for F-actin staining. For nuclei, hydrogel samples were counterstained with Vectashield with DAPI (Vector Labs) immediately before confocal visualization (CLSM, Leica SP5AOBS, Leica Microsystems). For laminin staining, samples were incubated in blocking solution (1 w/v% bovine serum albumin and 4 v/v% FBS in PBS) for 1 h and incubated with the primary antibody according the steps described above. Primary and secondary antibodies are listed in the Table S1, Supporting Information.

3.2.10. Statistical Analysis

Statistical analyses were performed in the GraphPad Prism 7.0 software. The results were reported as the mean \pm standard deviation (SD). The non-parametric Mann–Whitney test was applied with 95% confidence interval and statistically significant differences marked with $P < 0.05$ (*), $P < 0.01$ (**), $P < 0.001$ (***) and $P < 0.0001$ (****).

3.3. Results and Discussion

3.3.1. Synthesis of pectin methacrylate and hydrogel design

Pectin methacrylate (PECMA) was synthesized by partial substitution of secondary hydroxyl groups in polymer backbone by pendant methacrylate moieties via reaction with methacrylic anhydride (MA) (**Figure 3.1A**). The presence of new characteristic peaks of MA,

originally absent in the pure polymer (**Supplementary Figure S3.1**), including two peaks at 5.72 and 6.16 ppm assigned to the methylene group in the vinyl bonds and a sharp peak at 1.89 ppm corresponding to the methyl group, was confirmed by ^1H NMR analysis (**Figure 3.1B**). The extent of chemical functionalization, i.e., the degree of methacrylation (DM), was modulated between 21.7% and 56.6% by varying the molar ratio of MA to hydroxyl groups (MA/OH) of pectin in a range of 2.5–25 and determined by ^1H NMR (**Supplementary Figure S3.2**). Reaction conditions were optimized to balance the water-solubility of synthesized macromers and sufficient DM to form hydrogels at low polymer concentration. The DM increased with the addition of higher MA volumes, reaching a maximum conjugation of 56.6% at a molar ratio of 25. Increasing the molar ratio resulted in the introduction of excessive hydrophobic methacrylate moieties, yielding pectin derivatives with reduced water-solubility (**Supplementary Figure S3.3**). As the DM dictates the number of methacrylate functions available for photocrosslinking, consequently determining the biophysical properties of hydrogels [24], pectin macromers were synthesized with low (21.7%, PECMA low), medium (42.6%, PECMA medium) and high (50.2%, PECMA high) DM. To evaluate the cytotoxicity, macromers were dissolved in culture medium and incubated in the presence of human neonatal dermal fibroblasts (hNDFs) for 24 h. No cytotoxic effects to the cells were verified at any tested concentration (**Supplementary Figure S3.4**). All macromers allowed the fabrication of structurally robust hydrogels at low polymer concentration (1.5 wt%) upon exposure to UV light (160 s, 7 mW/cm²). Macromers retained the ability to form physical hydrogels by ionic interaction with calcium ions, allowing the design of dual-crosslinked hydrogels, which properties could be modulated by varying the calcium content (**Figure 3.1C**).

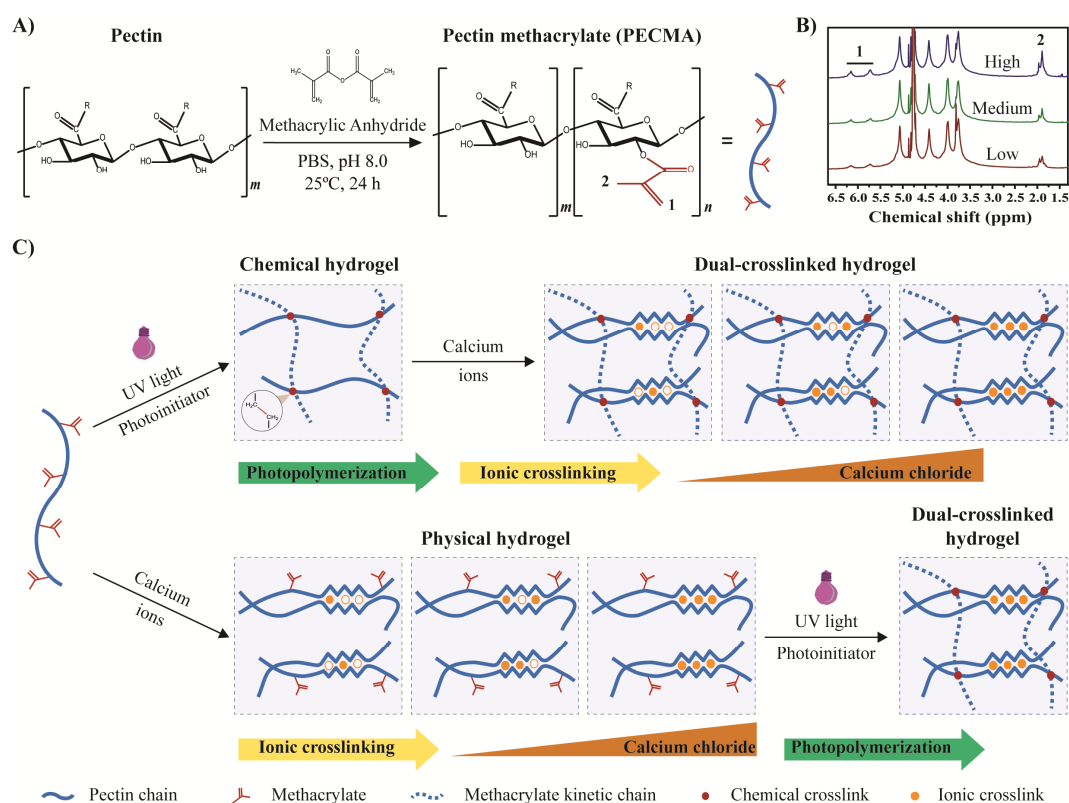


Figure 3.1. Pectin chemical modification and strategies for the preparation of dual-crosslinked hydrogels. (A) Chemical modification of pectin with methacrylate groups by reaction with MA, yielding pectin methacrylate (PECMA) derivatives. (B) ^1H NMR spectra of PECMA synthesized with different degrees of methacrylation. (C) Schematic illustration depicting the versatility of PECMA macromers for the preparation of hydrogels through independent crosslinking chemistries. Pectin macromers, dissolved in the photoinitiator (I2959) solution, can be applied for the formation of chemical hydrogels via UV photopolymerization, and subsequently incubated with calcium ions to tune their mechanical properties via ionic gelation between adjacent carboxylic groups (optional). PECMA can also be firstly reacted with calcium ions to trigger the ionic gelation for bioink design, followed by UV photopolymerization.

3.3.2. Photopolymerization of pectin hydrogels with tuneable properties

To demonstrate the versatility of PECMA macromers and their application as cell carriers, acellular hydrogels were prepared and critical properties susceptible to determine the fate of embedded cells characterized. Hydrogels were formed as cylindrical discs using a low polymer fraction (1.0–2.5 wt%) by the exposure to cytocompatible doses of UV light irradiation using Irgacure 2959 (I2959, 0.05 wt%) as radical initiator. To investigate the effects of DM, crosslinking time and polymer concentration in the hydrogel formation, the sol-gel fraction was determined as a qualitative indicator of the methacrylate conversion and crosslinking efficiency. Gel fraction curves showed that the sol-gel conversion depends on

both DM and UV exposure time (**Figure 3.2A, B**). The gel content increased as the DM increases due to the formation of a highly crosslinked gel network, which correlates with both lower swelling ratio (**Supplementary Figure S3.5**) and enhanced resistance to enzymatic degradation (**Figure 3.2C**). Similarly, the minimum UV exposure time required to produce stable gel networks also decreased with higher DM. For hydrogels prepared from PECMA low, measurable gel fractions (24.3%) were only obtained for crosslinking times higher than 120 s. However, by simply increasing the DM, the minimum crosslinking time required to form stable hydrogels was reduced for 60 s (PECMA medium, 30.0% gel fraction) and 40 s (PECMA high, 44.9% gel fraction). For the highest DM, a plateau value for the gel fractions determined at 1.5 wt% macromer concentration was obtained after 160 s of irradiation, which was set as the photopolymerization time. Although methacrylates are less reactive than other alkenes (e.g., acrylates, norbornenes) [25], structurally robust hydrogels were obtained at low macromer concentrations under a low-dose of UV irradiation, which is relevant for the entrapment of cells and bioactive molecules [26]. An important consideration in the design of hydrogels to be used as provisional cellularized matrices for tissue engineering is the ability to tailor the viscoelastic properties in order to match the biomechanical requirements of the target tissue. To study the effect of macromer concentration on the viscoelastic properties, PECMA solutions at different concentrations were photopolymerized (160 s) and the hydrogel properties determined. The G' of hydrogels was tailored in a broad range (79.6 ± 7.7 Pa – 2.6 ± 0.3 kPa) by changing the initial polymer concentration from 1.5 to 2.5 wt% (**Figure 3.2D**). Different combinations of polymer concentration and DM were also tested to demonstrate that the hydrogel stiffness could be adjusted using macromers with different DM. Swollen hydrogels (1.5 wt%) showed a significant reduction on the G' due to the relaxation of the gel network (**Figure 3.2E**).

Photopolymerization reactions are widely used to crosslink hydrogel bioinks as they provide unique control over the gelation process both in space and time [6, 27]. To illustrate the ability to tailor the viscoelastic properties of hydrogels by varying the UV light exposure time, precursor solutions (1.5 wt%) were photopolymerized for different times and the viscoelastic properties determined. Increasing the irradiation time resulted in stiffer hydrogels due to the formation of more crosslinks between the polymer chains. The G' of hydrogels was modulated from values lower than 100 Pa to approximately 1000 Pa, while keeping the polymer concentration, photoinitiator content, and UV light intensity constant (**Figure 3.2F**). For PECMA low hydrogels, the stiffness increased from 79.6 ± 7.7 Pa to 254.2 ± 9.9 Pa (3.2-fold increase) by increasing the crosslinking time from 160 s to 300 s. In the opposite way, the stiffness of PECMA medium and PECMA high hydrogels was reduced to 86.2 ± 9.9 Pa and 98.8 ± 8.7 Pa by decreasing the UV exposure time to 80 s and 40 s, respectively. In

addition to the changes in gel fraction and mechanical properties, alterations in the DM also affected the microstructure of hydrogels and the pore distribution as observed by CryoSEM analysis (**Figure 3.2G**). The influence of crosslinking time and polymer concentration in the microstructure of hydrogels was also assessed using the macromer with medium DM (PECMA medium). Increasing the crosslinking time from 80 to 160 s enhanced the average number of pores, while increasing the polymer concentration from 1.5 to 2.5 wt% resulted in the formation of a highly crosslinked hydrogel network with a more compact pore structure (**Supplementary Figure S3.6**).

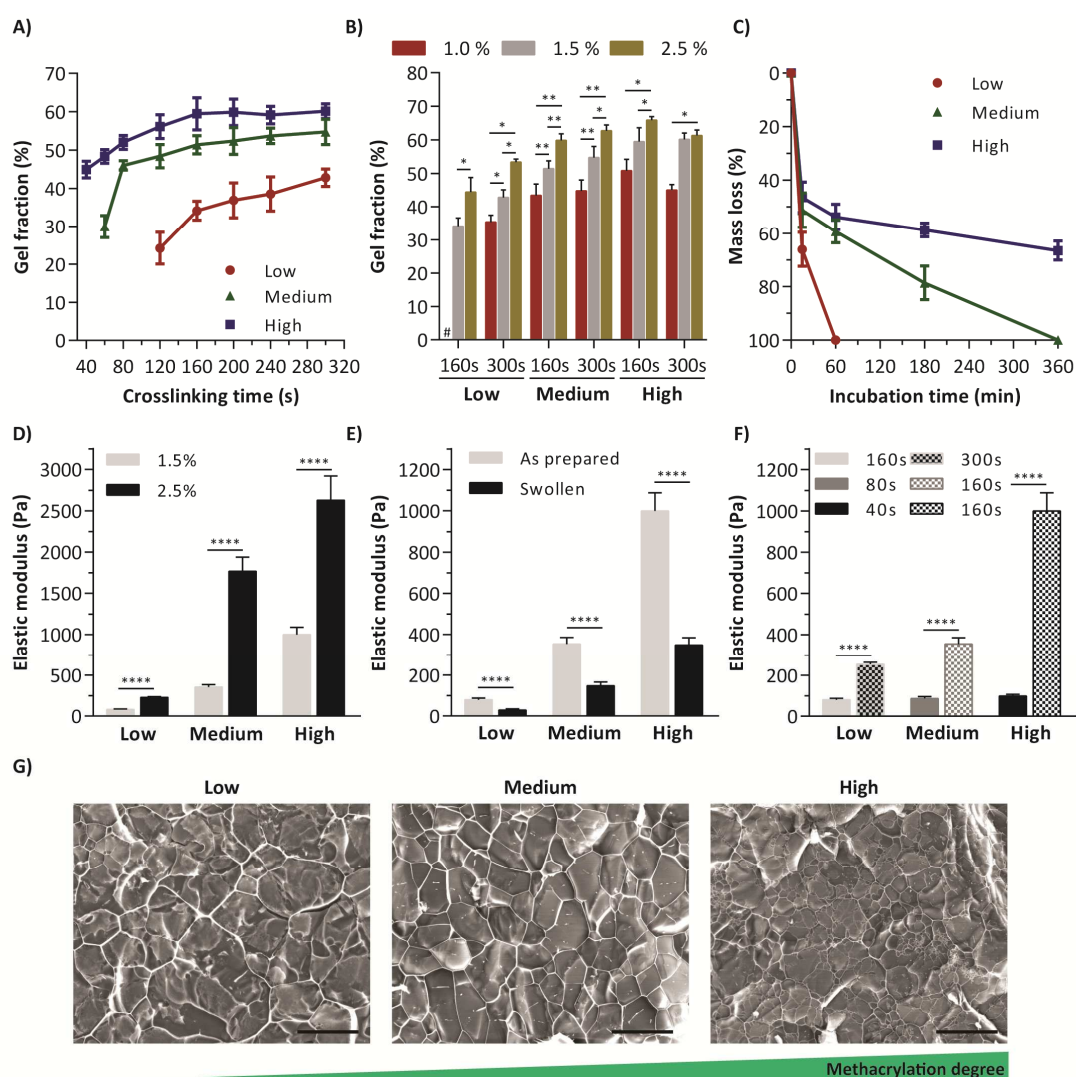


Figure 3.2. Modulating the physical and mechanical properties of photocrosslinked PECMA hydrogels with different DM. (A) Influence of UV exposure time on the gel fraction of hydrogels (1.5 wt%). **(B)** Effect of polymer concentration and UV exposure time on gel fraction of hydrogels. **(C)** *In vitro* enzymatic degradation profiles of PECMA hydrogels (1.5 wt%, 160 s UV) in the presence of pectinase (0.05 mg/mL). **(D)** Elastic moduli of hydrogels with different polymer concentrations (160 s

UV). **(E)** Elastic moduli of swollen hydrogels (1.5 wt%, 160 s UV) after incubation in PBS at 37 °C. **(F)** Influence of UV exposure time on the elastic moduli of hydrogels (1.5 wt%) tested immediately after preparation. **(G)** Microstructure of hydrogels (1.5 wt%) prepared with different DM observed by CryoSEM (scale bars: 50 μ m). * $P < 0.05$; ** $P < 0.01$; **** $P < 0.0001$.

3.3.3. Biofunctionalized hydrogels support the viability and spreading of embedded dermal fibroblasts

The clinical success of cell-laden hydrogels depends on the ability to tune their physicochemical, mechanical, and biological properties in order to create a cell-instructive microenvironment that guides morphogenesis [28, 29]. After demonstrating how to tailor the physicochemical and mechanical properties of photocrosslinked hydrogels, PECMA macromers were biofunctionalized with a cell-adhesive peptide containing the amino acid sequence RGD to promote integrin-mediated cell adhesion and cell-matrix interactions within the otherwise inert hydrogel network [30]. Since pectin lacks specific integrin-binding sites in the native composition [20], the base-catalysed thiol-Michael addition click reaction was used to conjugate the cell-adhesive peptide to the polymer backbone. The conjugation reaction was performed by exploring the reactivity between activated carbon double bonds (C=C) of methacrylates and a thiolate anion of cysteine amino acid in the peptide sequence (**Figure 3.3A**) [31]. This chemistry was chosen because it allows the incorporation of RGD motifs via the formation of water-stable thioether bonds, preventing non-specific hydrolysis of the peptide-polymer bond [32]. Reaction conditions were optimized to allow a constant density of cell-adhesive peptide within the hydrogel (200 μ M) in the same range of that found in ECM-derived biological matrices [33], independently of the final polymer concentration. The ability to precisely control the density of cell-adhesive peptide in the hydrogel network constitutes a major advantage of pectin compared to other natural polymers (e.g., gelatin, fibrin), allowing the design of chemically defined hydrogels. RGD-functionalized macromers could be converted into cell-laden chemical hydrogels by photopolymerization, and eventually undergo a secondary physical crosslinking reaction through subsequent incubation in culture medium containing calcium chloride (CaCl_2) (**Figure 3.3A**). To preserve the intrinsic ionic interaction ability of pectin, a methacrylate functionalization strategy targeting the hydroxyl groups instead of carboxyl functionalities was selected. This chemical modification procedure left the carboxylic acid groups available for ionic crosslinking without altering the anionic character of the polymer (**Figure 3.3B**), which is essential to modulate the viscoelastic and rheological properties of PECMA via calcium-mediated ionic crosslinking. To characterize the influence of ionic crosslinking on the mechanical properties, photocrosslinked hydrogels (1.5 wt%, 160 s UV) were incubated in Dulbecco's Minimum Essential Medium (DMEM) containing CaCl_2

(1.8 mM) and the G' recorded by rheological analysis. The G' of dual-crosslinked hydrogels (“Dual”) was significantly higher than that of photocrosslinked hydrogels (“Photo”) (**Figure 3.3C**). As an example, the G' of PECMA medium hydrogels at 1.5 wt% concentration increased from 259.1 ± 11.0 Pa to 3552.0 ± 123.9 Pa, which represents a 13.7-fold increase. The G' of these hydrogels was further enhanced to 6667.9 ± 149.7 Pa by increasing the initial polymer concentration to 2.5 wt% (**Figure 3.3D**). To test the effect of calcium concentration on the stiffness, chemical PECMA medium hydrogels (1.5 wt%, 160 s UV) were incubated in DMEM containing different concentrations of CaCl_2 (0, 0.45, 0.90, 1.8 mM) and the G' of hydrogels recorded. As shown in **Figure 3.3E**, the G' was modulated between 259.1 ± 11 and 3552.0 ± 123.9 Pa, highlighting the versatility of this hydrogel platform in tailoring the viscoelastic properties in a relevant physiological range for soft tissue applications. As the main aim of this study was to design a single-component bioink for extrusion bioprinting of 3D constructs for dermal repair, hNDFs were selected as they play a pivotal role in cutaneous wound healing by the deposition of several ECM components [2]. To assess the cytocompatibility of the hydrogel platform and to decouple the influence of cell-adhesion ligand and matrix stiffness, hNDFs were embedded within hydrogels containing RGD at 0 or 200 μM concentration. Cell-laden PECMA solutions (1.5 wt%) with different DM were photocrosslinked for 160 s and incubated in culture medium containing CaCl_2 (1.8 mM) to obtain a dual-crosslinked gel network. Live/dead staining showed that cells present excellent viability after 24 h of entrapment, independently of both DM and RGD concentration (**Supplementary Figure S3.7**). Cells embedded within dual-crosslinked RGD-hydrogels photocrosslinked for 160 s exhibited high levels of cell viability and metabolic activity throughout 14 days of culture within gels with the lowest DM, while cells within PECMA medium and PECMA high hydrogels displayed a strong reduction on the metabolic activity and viability at day 3 (**Supplementary Figure S3.8**). To demonstrate that by reducing the initial hydrogel stiffness embedded cells remain metabolically active independently of the DM, hNDFs were embedded within RGD-PECMA medium and RGD-PECMA high hydrogels photocrosslinked for 80 s and 40 s, respectively. Results showed that by decreasing the UV exposure time, and consequently the hydrogel stiffness (PECMA medium: 86.2 ± 9.9 Pa, PECMA high: 98.8 ± 8.7 Pa), cells maintained high levels of metabolic activity after 7 days of culture (**Supplementary Figure S3.9**).

By exploiting the ability to independently tune the cell-adhesive ligand density, mechanical properties, and polymer fraction of hydrogels, we next showed how to tailor the cell response within the hydrogels. Cells cultured within dual-crosslinked PECMA low hydrogels without incorporated cell-binding sites adopted a typical rounded morphology, while cells within RGD-PECMA hydrogels showed limited cell spreading with typical F-actin

structure and fibronectin detected in the vicinity of the cells (**Supplementary Figure S3.10**), which is attributed to the matrix stiffness and resistance of the hydrogel network to deformation. As previously reported, the behaviour of fibroblasts within 3D hydrogels depends on the hydrogel stiffness and composition [34, 35]. To demonstrate that this hydrogel platform supports cell spreading at low levels of matrix stiffness, cells were embedded within RGD-PECMA high hydrogels photopolymerized for 40 s (designated “Photo”). Fibroblasts remained metabolically active (**Supplementary Figure S3.11**) and adopted a typical spindle-shaped morphology after 7 days of culture, which was accompanied by the deposition of fibronectin (**Figure 3.3F**). In contrast, when these hydrogels underwent secondary ionic crosslinking (designated “Dual”), cell spreading was significantly inhibited. These outcomes highlight the versatility offered by this hydrogel platform in designing cell-responsive hydrogels capable of inducing distinct cell behaviours.

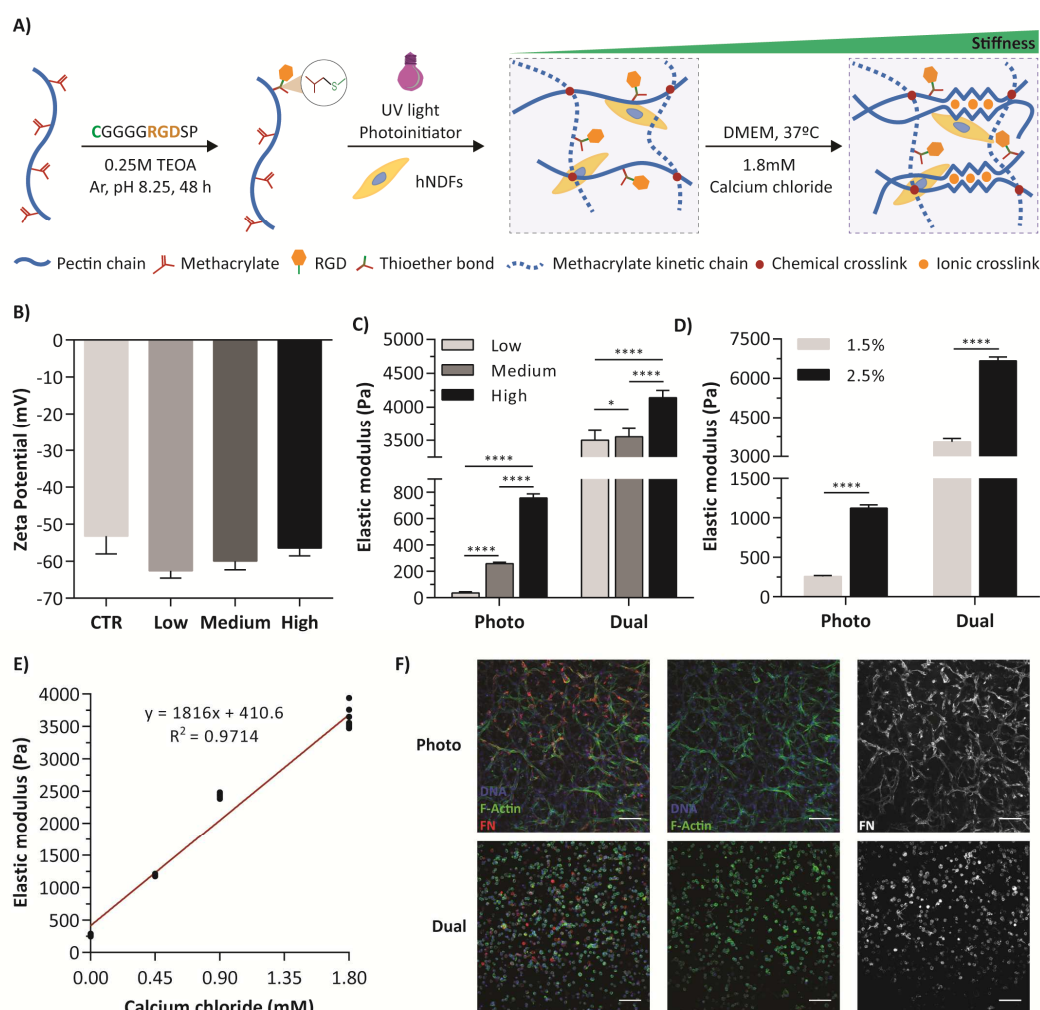


Figure 3.3. Biofunctionalization of PECMA with cell-adhesive peptide and its effect on the behaviour of embedded dermal fibroblasts. (A) Illustration of the functionalization scheme for the

conjugation of cell-adhesion moieties to methacrylate groups via thiol-Michael addition click chemistry. Unreacted methacrylates were subsequently used for the formation of hydrogels by photopolymerization, allowing the incorporation of hNDFs within the hydrogel network. Cell-laden hydrogels can eventually undergo ionic crosslinking with calcium ions. **(B)** Zeta potential of pure pectin and PECMA with different DM. **(C)** Effect of ionic gelation (1.8 mM CaCl₂) in the stiffness of photocrosslinked hydrogels prepared with varying DM (1.5 wt%, 160 s UV). **(D)** Effect of dual-crosslinking (1.8 mM CaCl₂) on the stiffness of PECMA hydrogels with medium DM prepared with different macromer concentrations. **(E)** Elastic moduli of PECMA medium hydrogels (1.5 wt%, 160 s UV) recorded as a function of the CaCl₂ concentration. **(F)** Confocal microscopy images depicting the morphology of hNDFs embedded within RGD-PECMA high hydrogels (1.5 wt%, 40 s UV), stained for nuclei (blue), F-actin (green) and fibronectin (red, FN) (scale bars: 50 μm). **P* < 0.05; *****P* < 0.0001.

3.3.4. Bioprinting cell-laden 3D constructs using a dual-crosslinked, single-component hydrogel bioink

Several hydrogels have been proposed to develop bioinks for extrusion bioprinting [36]. Despite the progress on novel materials, printing strategies and crosslinking chemistries, the bioprinting of a single-component bioink at low polymer concentration is challenging due to the difficulty in controlling multiple properties using a single polymer, including the rheological behaviour (e.g., viscosity, yield stress, printability), biochemical cues (e.g., cell-adhesive moieties), mechanical properties (e.g., elastic modulus) and cell response (e.g., ECM deposition). Thus, most of the bioinks employ relatively high macromer concentrations (2–10 wt%) to achieve enough viscosity for bioprinting [9, 37–39], often resulting in highly crosslinked hydrogel constructs in which cell spreading and migration are usually restricted. In this study, we took advantage of the complementary ionic and photocrosslinking ability of PECMA to design a cell-responsive, single-component hydrogel bioink with optimal rheological properties for extrusion bioprinting (**Figure 3.4A**). A major advantage of the developed bioink is the ability to print 3D constructs at low polymer concentration (1.5 wt%) maintaining the shape after deposition without requiring additional materials for viscosity modulation and precluding washing steps to leach out sacrificial materials. This distinctive feature allows the fabrication of soft and highly porous microenvironments, which is relevant for soft tissue engineering applications. In addition, the printing process is performed directly onto a receiving substrate without the need for heating modules, coaxial nozzles, printing baths or in situ photopolymerization to ensure shape fidelity of the printed constructs. The bioprinting strategy of the developed single-component pectin bioink is based on a modular approach that combines the calcium-mediated ionic gelation to adjust the rheological behaviour prior deposition and the post-printing UV photopolymerization to provide shape fixation and tailor the viscoelastic properties of 3D

constructs. In the first step, the viscosity of a PECMA low solution (1.5 wt%) dissolved in I2959 was precisely tailored by adding different concentrations of CaCl_2 (0–5 mM). After CaCl_2 addition, the bioink was vigorously mixed and reacted under agitation during 1 h for G' stabilization (**Supplementary Figure S3.12**). After this period of time, hNDFs were homogeneously suspended within the weakly crosslinked bioink for bioprinting. Rheological studies (**Figure 3.4B, C**) showed that the bioink viscosity increased with the addition of higher CaCl_2 concentrations due to the formation of a more crosslinked gel phase (**Figure 3.4D**). All solutions exhibited a shear-thinning behaviour, characterized by a decrease in the viscosity as the shear rate increases, which is fundamental for extrusion bioprinting [40, 41]. Ionic crosslinking also resulted in a significant increase of the yield stress, i.e., the minimum stress to induce flow in the polymer solution (3mM: 1.18Pa to 5mM: 9.16 Pa). The yield stress is a key parameter that governs the printability of bioinks and determines the ability to homogeneously mix the cell pellet [42, 43]. Notably, we observed that the addition of CaCl_2 within the tested range of concentrations did not result in the formation of highly crosslinked bioinks, which could prevent the flow, injectability and the mixing with a cell pellet flow. To qualitatively evaluate the printability, bioinks with varying CaCl_2 concentrations were manually injected through a metal cylindrical nozzle (23 Gauge) and tested for their ability to form a continuous filament. Formulations were considered printable when a continuous filament, instead of droplets, is formed at the nozzle. Bioinks containing CaCl_2 at 0 and 1 mM did not display a clear yield stress, formed droplets at the nozzle (**Figure 3.4E**) and spread onto the receiving substrate, which is not suitable for bioprinting. The bioink with 3 mM CaCl_2 formed an irregular filament at very low mass flow rate with printed filaments becoming flattened and unable to support the subsequent layers without fusion and collapse of the entire construct (**Supplementary Figure S3.13**). The bioink with 5 mM CaCl_2 formed a continuous filament at the nozzle, allowing the bioprinting of stable filaments that support the subsequent layers without collapsing (**Supplementary Figure S3.13**). An additional concentration of 7 mM CaCl_2 that allows the formation of a printable bioink was also tested to determine its influence on the G' of 3D hydrogels. Increasing the CaCl_2 content from 5 mM to 7 mM enhanced the yield stress point of the bioink and the mechanical properties of hydrogels (**Supplementary Figure S3.14**), which indicates the effect of ionic crosslinking not only in the rheological properties, but also in the G' of constructs. In the second step, the bioink (PECMA 1.5 wt%, 5 mM CaCl_2) was used for the bioprinting of both acellular solid and porous 3D constructs with high structural fidelity that maintain the predesigned shape immediately after printing without additional gelation mechanisms (**Figure 3.4F**). The constructs exhibited enough integrity to support printed layers and maintain the shape after deposition, allowing for post-printing photopolymerization. Solid square-shaped constructs were printed with 15 layers without collapsing, clearly demonstrating the ability of the

developed bioink for the printing of thick constructs. Porous constructs were also created to demonstrate the printing of more complex structures. To evaluate the ability of the bioink to support viable cells, hNDFs were suspended within the ionically crosslinked bioink and printed into porous constructs. In the third step, printed cellularized 3D constructs were exposed to UV light (160 s) to trigger the formation of chemical bonds between adjacent methacrylate groups, providing shape consolidation and long-term stabilization. Cell viability was qualitatively evaluated by live/dead assay 24h post-printing, showing that the bioink successfully supported the printing of viable cells within the deposited filaments (**Figure 3.4G**). These data demonstrated the versatility of using physical and chemical crosslinking chemistries to tailor the properties of the hydrogel bioink for extrusion bioprinting, while holding the polymer fraction and cell-adhesive ligand density constant. This strategy also allows to decouple the contribution of each individual parameter on the bioink performance, which is particularly challenging when using a single-component bioink based on natural polymers.

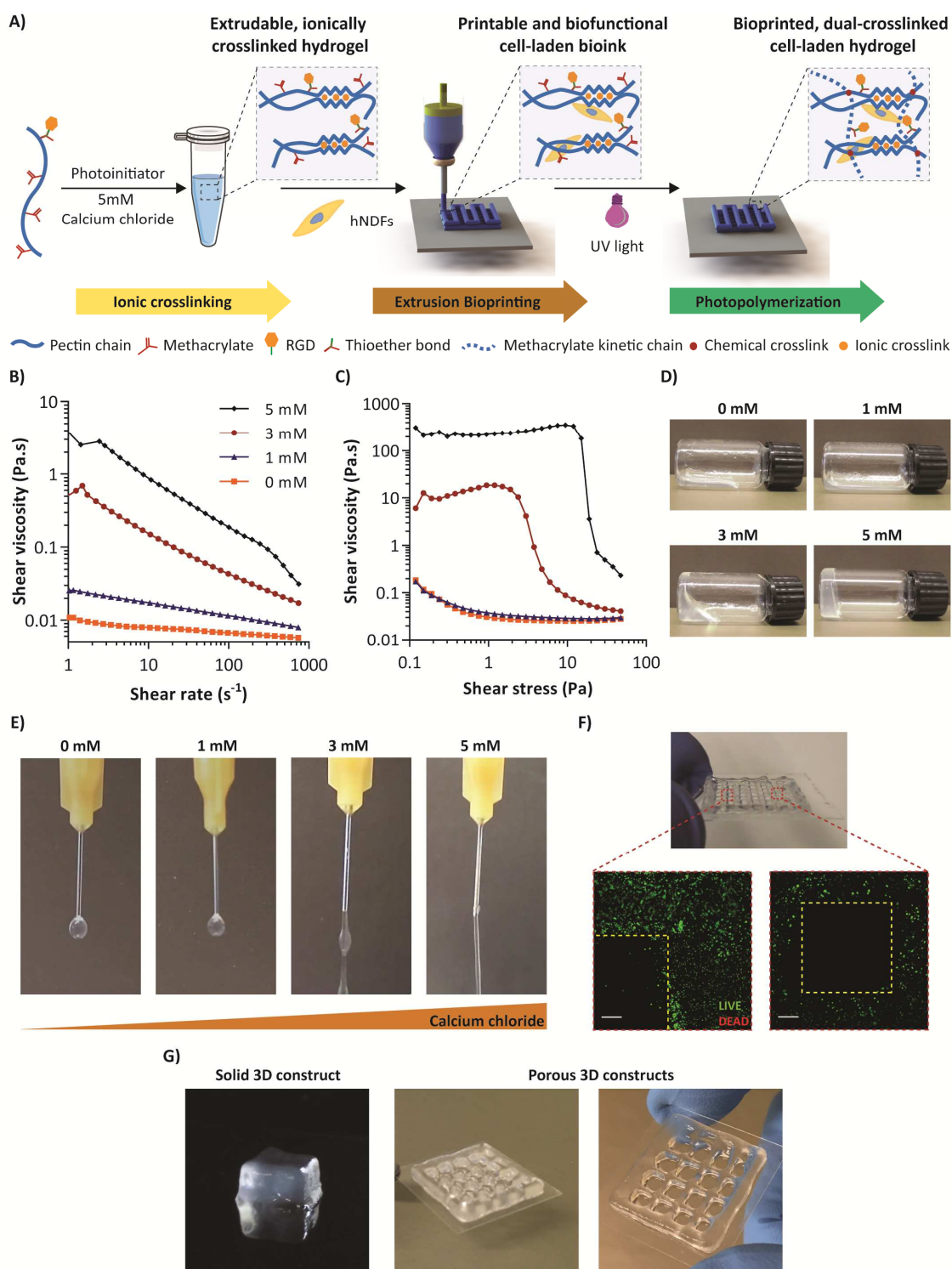


Figure 3.4. Design, formulation and bioprinting of a single-component PECMA bioink into 3D constructs. (A) Schematic illustration of the design and preparation of the biofunctional bioink for extrusion bioprinting. In a first stage, CaCl₂ was added to the polymer solution to adjust the rheological properties and allow the printing of 3D constructs. Then, dermal fibroblasts were suspended within the pre-crosslinked bioink and printed into 3D constructs. After printing, the constructs were exposed to UV light for consolidation and shape maintenance. (B) Viscosity of bioinks (RGD-PECMA low 1.5 wt%) prepared using different CaCl₂ concentrations. (C) Yield behaviour of bioinks as a function of CaCl₂

concentration. **(D)** Influence of CaCl_2 concentration on the flow behaviour of the bioink at room temperature. **(E)** Effect of CaCl_2 on the filament formation of bioink. **(F)** Images of bioprinted acellular, multilayered 3D constructs: solid construct ($8 \text{ (L)} \times 8 \text{ (W)} \times 4.5 \text{ (H)} \text{ mm}^3$) printed with 15 layers and porous constructs ($17 \text{ (L)} \times 17 \text{ (W)} \times 2.4 \text{ (H)} \text{ mm}^3$). **(G)** Representative confocal microscopy images of live/dead staining of fibroblasts embedded within the cell-laden 3D porous constructs ($14 \text{ (L)} \times 14 \text{ (W)} \times 0.6 \text{ (H)} \text{ mm}^3$) 24 h postprinting (scale bars: $200 \mu\text{m}$). Dash lines and square represent the pore/filament interface.

3.3.5. Bioprinted 3D constructs provide a cell-instructive microenvironment for the deposition of endogenous dermal ECM components

Advanced bioinks must allow not only the printing of viable cells, but also guide cell functions towards the formation of functional tissues. Despite the fact that several works have reported on bioinks capable of supporting live cells, only a limited number of studies have evaluated whether printed cells remain functional after deposition [5, 10, 44]. In this regard, the control over key properties of bioprinted constructs is essential to direct cell functions and new tissue formation. In order to demonstrate the ability to tailor the properties of bioprinted 3D constructs, RGD-PECMA low bioinks prepared using different macromer concentrations (1.5 or 2.5 wt%, 5 mM CaCl_2) were printed and photocrosslinked for 80 s, 160 s or 300 s. As observed, the gel fraction of hydrogels increased as a function of both higher macromer concentration and photocrosslinking time, varying in a range of $23.5 \pm 3.0 \%$ to $30.5 \pm 1.5 \%$ (1.5 wt%) and $21.2 \pm 2.1 \%$ to $40.9 \pm 0.8 \%$ (2.5 wt%) (**Figure 3.5A**). However, an opposite behaviour was observed for the swelling ratio (**Figure 3.5B**), indicating the formation of a denser gel network. Acellular hydrogels prepared from 1.5 wt% bioink and photocrosslinked for 80 s resulted in a loosely crosslinking gel network that exhibited low structural integrity upon incubation in ultrapure water, precluding the determination of gel fraction and swelling ratio. However, when these hydrogels were incubated in culture medium (1.8mM CaCl_2) the 3D structure was maintained. The mechanical properties of 3D bioprinted constructs determined after incubation in culture medium indicated that the G' can be modulated between $154.7 \pm 18.7 \text{ Pa}$ and $1210.0 \pm 148.5 \text{ Pa}$ by changing the macromer concentration and the photocrosslinking time (**Figure 3.5C**). The G' of dual-crosslinked hydrogels prepared from the 1.5 wt% bioink was tailored in a narrow range ($154.7 \pm 18.7 \text{ Pa}$ to $297.0 \pm 10.2 \text{ Pa}$) by increasing the photocrosslinking time when compared to the 2.5 wt% bioink ($465.9 \pm 43.4 \text{ Pa}$ to $1210.0 \pm 148.5 \text{ Pa}$). The G' of dual-crosslinked hydrogels obtained by ionic crosslinking followed by UV photopolymerization displayed a soft gel network compared to hydrogels prepared by UV photopolymerization followed by ionic crosslinking (**Figure 3.3C, D**). These data suggest that upon ionic gelation for viscosity modulation, the dual-crosslinked gel

network is less susceptible to later stiffening probably due to the spatial constraints in the polymer backbone induced by the crosslinking reactions. To determine the influence of matrix stiffness on cell response, hNDFs were loaded within bioinks (1.5 or 2.5 wt%), printed into 3D constructs (8 mm × 8 mm, three-layer), and photocrosslinked for different times. At day 7, cells displayed spread morphology in both periphery and centre of the 1.5 wt% constructs, though cell spreading seems to be favoured in constructs photocrosslinked for 160 s (229.8 ± 44.0 Pa) and 300 s (297.0 ± 10.2 Pa). In the 2.5 wt% constructs, cells were able to spread in hydrogels photocrosslinked for 80 s (465.9 ± 43.4 Pa), while limited cell elongation was observed in stiffer gels (160 s: 842.0 ± 97.8 Pa; 300 s: 1210.0 ± 148.5 Pa) (**Supplementary Figure S3.15**). At day 14, extensive cell spreading was detected throughout the 1.5 wt% constructs regardless the matrix stiffness, while in the 2.5 wt% constructs photocrosslinked for 80 s cell elongation was slightly limited, especially in the centre of the hydrogels. Physical constraints imposed by stiffer 2.5 wt% constructs (160 s and 300 s) significantly limited cell spreading and cell-cell interactions with the majority of entrapped cells displaying a round morphology (**Figure 3.5D**). Accordingly, these results indicate that the matrix stiffness plays a major role on the cell behaviour with stiffer networks severely restricting normal cell functions such as spreading and the establishment of cell-cell interactions.

Based on these data, both the 1.5 wt% bioink formulation and photocrosslinking time of 160 s, which support normal cell behaviour, were selected to deeply evaluate the cell response and deposition of new ECM components within the 3D constructs. After 14 days of culture, printed constructs exhibited good structural integrity, while embedded cells remained viable and metabolically active as qualitatively observed by live/dead assay (**Figure 3.5Ei**) and quantitatively determined by the resazurin-based assay (**Supplementary Figure S3.16**). To confirm that cell behaviour was unaffected by the bioprinting process, the cell-laden bioink was casted, showing similar cell-spreading compared to printed constructs (**Supplementary Figure S3.17**). Contrary to other gel-phase bioink formulations, in which cells are incubated within the bioink for long periods of time (2 h) until achieving a printable consistency [45], in our approach cells are directly mixed within the printable bioink immediately before bioprinting. This prevents cell settling issues and significantly reduces the time frame between cell suspension and bioprinting, potentially increasing the cell viability. More than satisfying printability and cytocompatibility requirements, novel bioink formulations should be capable of instructing the embedded cells to perform their functions within the construct, which is essential for clinical translation of bioprinted tissue constructs. In this context, we investigated the ability of the PECMA bioink to induce cell spreading and instruct embedded cells to produce new ECM. Printed cells, initially homogeneously dispersed within the 3D

construct, assumed a spread, spindle-shaped morphology throughout the hydrogel (**Figure 3.5Eii**) and formed interconnected multicellular networks embedded by a fibronectin-rich network (**Figure 3.5Eiii**). Fibronectin is an ubiquitous fibrous ECM protein in skin, playing a key role in several essential processes such as wound healing, embryogenesis, cell adhesion and migration. Moreover, it has been shown that fibronectin may be required for subsequent deposition and maintenance of other ECM proteins, including collagen type-I [46, 47]. Detailed analysis concerning the spatial distribution of both embedded cells and fibronectin network confirmed that extensive cell spreading and fibronectin deposition were not limited to the periphery of printed constructs and could be detected within the bulk hydrogel. The magnified high-resolution confocal reconstruction images of the 3D construct clearly revealed the ability of the bioink to induce characteristic cytoskeleton organization and to support the deposition of a dense, fibrillar ECM fibronectin matrix surrounding the embedded cells, forming an extensive mesh of elongated branching fibrils (**Figure 3.5Eiv**). As dermal fibroblasts are intimately associated to the ECM synthesis and remodelling [2], the ability of printed cells to secrete and deposit other prominent ECM proteins was further evaluated by the immunodetection of collagen type-I and laminin. Collagen is the most abundant fibrous protein in the skin, performing multiple functions such as providing tensile strength and regulating cell-adhesion, while laminin influences many aspects of cell behaviour, including adhesion, differentiation, migration and resistance to apoptosis.[48, 49] After 14 days of culture, printed constructs showed the presence of cell-secreted collagen type-I located in both intracellular and extracellular spaces (**Figure 3.5Ev**). At this time point, an extracellular network of laminin was also detected (**Figure 3.5Evi**), revealing the ability of dermal fibroblasts to secrete a variety of endogenous ECM proteins within the printed constructs. In addition to the deposition of pivotal fibrous ECM proteins present in the dermis, proliferative cells were also detected at day 14 of culture through immunodetection of Ki67 proliferation marker (**Supplementary Figure S3.18**). These data showed that printed constructs provide an adequate microenvironment capable of guiding hNDFs to secrete new ECM, which indicates the potential of the developed bioink for bioprinting of bioengineered dermal substitutes and full-thickness skin.

Advanced bioinks and bioprinting technologies allow the generation of biomimetic 3D skin constructs with controlled positioning of multiple cells, mimicking multiple layers found in native tissue, which is extremely difficult to obtain by using conventional fabrication methods and traditional hydrogels. A major challenge to create functional skin and dermal constructs containing a vascular network, nerves and appendages relies on the control over the positioning of multiple cells in 3D [3]. This is essential to promote specific cell-cell and cell-ECM interactions that could potentially lead to the development of those specialized

structures. As both cell-cell and cell-ECM interactions depend not only on the cell location and construct dimensionality, but also on the biophysical and biochemical properties of the surrounding microenvironment [50, 51], bioinks with controllable and tuneable properties are essential to tackle these challenges and generate biomimetic skin constructs. As the developed pectin bioink allows the bioprinting of 3D constructs with user-defined biochemical and mechanical properties supporting de novo deposition of ECM components, it constitutes an alternative bioink to existing protein-based bioinks with distinctive features. Bioprinting, using suitable bioinks provides unique advantages compared to non-additive fabrication and traditional hydrogels [7], including the generation of large volumes of patient-specific 3D constructs with high reproducibility and the automatic dispensing of bioinks in prescribed sites to promote skin formation *in vitro* and *in vivo*. Bioprinting also allows the fabrication of dermal constructs with heterogeneous cellular composition and properties throughout the construct, which is essential for the generation of cell-laden substitutes for skin repair and *in vitro* skin models with improved biomimicry [52].

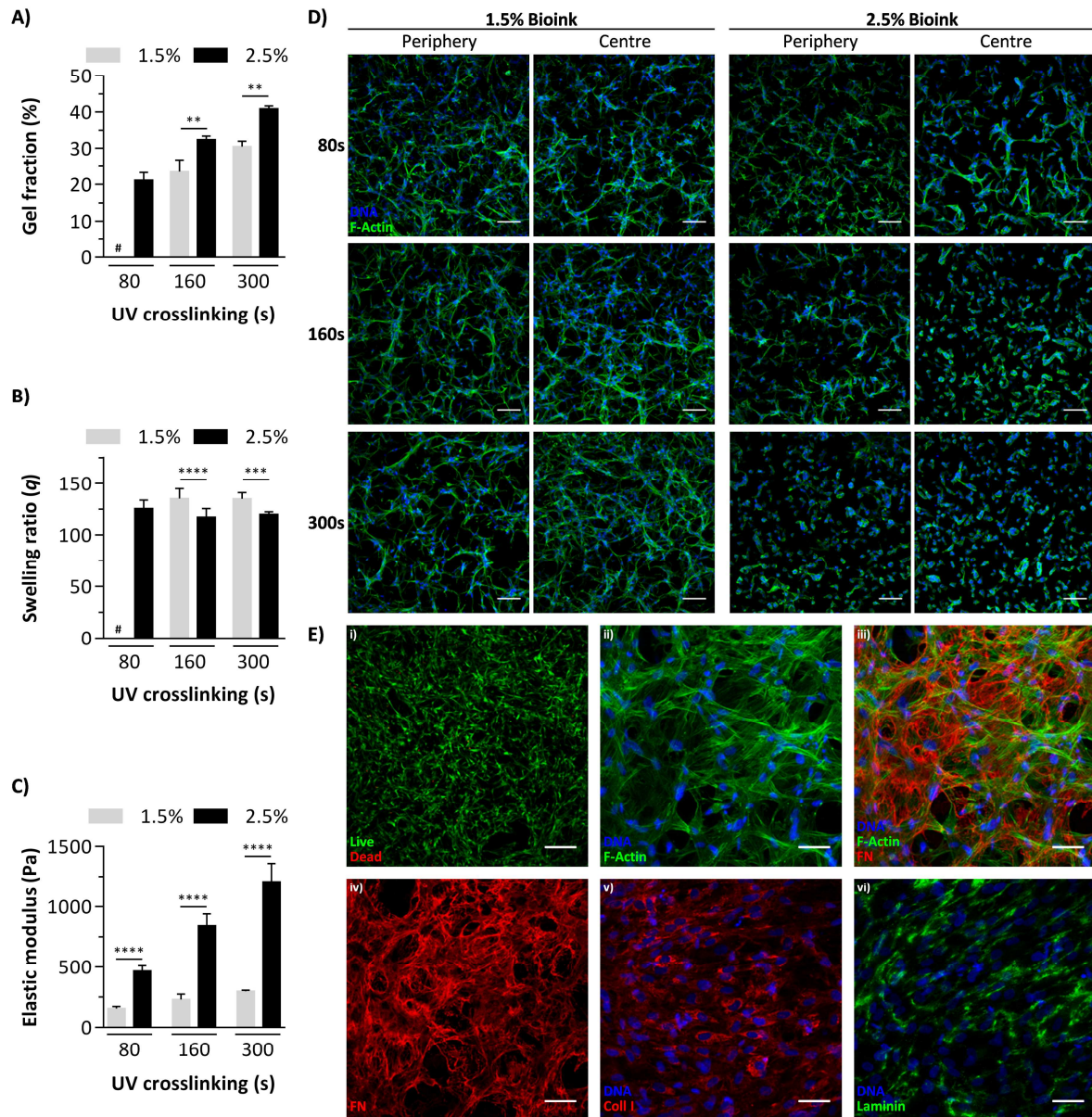


Figure 3.5. Tailoring the physical, mechanical and biological properties of bioprinted 3D constructs. (A-C) Influence of polymer fraction and UV photopolymerization time in the gel fraction, swelling ratio and elastic modulus of hydrogels (# indicates poor structural integrity of the hydrogel). **(D)** Effect of matrix stiffness on the morphology and spreading of dermal fibroblasts within bioprinted 3D constructs after 14 days of culture (scale bar: 100 μm). **(E)** Representative confocal microscopy images showing the performance of bioprinted 3D dermal constructs at day 14 of culture: (i) live/dead staining of dermal fibroblasts within the construct; (ii) F-actin (green) and DAPI (blue) staining showing the spread morphology of fibroblasts; (iii) morphology and spatial distribution of fibroblasts surrounded by a fibronectin (red, FN) network; (iv-vi) expression of fibronectin (red, FN), collagen type-I (Coll I, red) and laminin (green) throughout the bioprinted constructs (scale bars: (i) 200 μm ; (ii-vi) 50 μm).

3.4. Conclusions

In summary, a biofunctional, single-component pectin bioink exhibiting cell-responsive properties and capable of instructing printed dermal fibroblasts to secrete new ECM was developed for the extrusion bioprinting of dermal 3D constructs. The hydrogel bioink is highly versatile, allowing a fine tuning of the rheological and viscoelastic properties independently of the cell-adhesive ligand density. Remarkably, the rheological properties of the bioink at a low polymer concentration were tailored by exploring the ionic crosslinking without compromising both homogeneous cell dispersion and cell viability post-printing. The bioink also allowed for UV photopolymerization after printing, providing construct consolidation and long-term stabilization. A distinctive characteristic of the bioink relies on its ability to instruct printed cells to secrete an endogenous ECM distributed throughout the construct in response to the microenvironment provided by the gel network. Printed cells were able to transform a provisional matrix lacking of ECM proteins into a collagen- and fibronectin-rich network, resembling the native dermal tissue. In future studies we envisage that the bioink could be used in combination with other skin cells and eventually biofunctionalized with additional relevant ligands. In addition, as fibroblasts are the major cells responsible for the production of ECM components, the bioink is not limited to skin bioprinting and can be explored to generate other tissues. Besides the development of 3D constructs for tissue repair, this tuneable bioink can be explored for several applications, ranging from the printing of complex 3D models for pharmaceutical testing in diagnostic studies, such as in organs-on-chip, or for studying tissue morphogenesis in fundamental biological studies.

3.5. Acknowledgements

P.B. and P.G. contributed equally to this work. This work was supported by the project Norte-01-0145-FEDER-000012 - Structured program on bioengineered therapies for infectious diseases and tissue regeneration, supported by Norte Portugal Regional Operational Programme (NORTE 2020), under the PORTUGAL 2020 Partnership Agreement, through the European Regional Development Fund (ERDF), and by the Portuguese Foundation for Science and Technology (FCT) through the project PTDC/BBB-ECT/2145/2014. R.P., A.S. and C.B. thank FCT for the doctoral grant SFRH/BD/91151/2012, post-doctoral grant SFRH/BPD/90047/2012 and the FCT Investigator research position IF/00296/2015 (FCT and POPH/ESF), respectively. The authors acknowledge D.S. and M.A. from CEMUP (Centro de Materiais da Universidade do Porto) for the cryoSEM and ¹H NMR analyses, respectively.

3.6. References

- [1] R.F. Pereira, C.C. Barrias, P.L. Granja, P.J. Bartolo, Advanced biofabrication strategies for skin regeneration and repair, *Nanomedicine (Lond)* 8 (2013) 603-21.
- [2] L.E. Tracy, R.A. Minasian, E.J. Caterson, Extracellular Matrix and Dermal Fibroblast Function in the Healing Wound, *Adv Wound Care (New Rochelle)* 5 (2016) 119-136.
- [3] R.F. Pereira, A. Sousa, C.C. Barrias, A. Bayat, P.L. Granja, P.J. Bartolo, Advances in bioprinted cell-laden hydrogels for skin tissue engineering, *Biofabrication Reviews* 2 (2017) 1.
- [4] H.W. Kang, S.J. Lee, I.K. Ko, C. Kengla, J.J. Yoo, A. Atala, A 3D bioprinting system to produce human-scale tissue constructs with structural integrity, *Nat. Biotechnol.* 34 (2016) 312-9.
- [5] D.B. Kolesky, K.A. Homan, M.A. Skylar-Scott, J.A. Lewis, Three-dimensional bioprinting of thick vascularized tissues, *Proc Natl Acad Sci USA* 113 (2016) 3179-84.
- [6] R.F. Pereira, P.J. Bartolo, 3D bioprinting of photocrosslinkable hydrogel constructs, *J. Appl. Polym. Sci.* 132 (2015) 42458.
- [7] F.P.W. Melchels, M.A.N. Domingos, T.J. Klein, J. Malda, P.J. Bartolo, D.W. Huttmacher, Additive manufacturing of tissues and organs, *Prog. Polym. Sci.* 37 (2012) 1079-1104.
- [8] J. Jang, H.J. Park, S.W. Kim, H. Kim, J.Y. Park, S.J. Na, H.J. Kim, M.N. Park, S.H. Choi, S.H. Park, S.W. Kim, S.M. Kwon, P.J. Kim, D.W. Cho, 3D printed complex tissue construct using stem cell-laden decellularized extracellular matrix bioinks for cardiac repair, *Biomaterials* 112 (2017) 264-274.
- [9] T. Billiet, E. Gevaert, T. De Schryver, M. Cornelissen, P. Dubruel, The 3D printing of gelatin methacrylamide cell-laden tissue-engineered constructs with high cell viability, *Biomaterials* 35 (2014) 49-62.
- [10] K. Zhu, S.R. Shin, T. van Kempen, Y.C. Li, V. Ponraj, A. Nasajpour, S. Mandla, N. Hu, X. Liu, J. Leijten, Y.D. Lin, M.A. Hussain, Y.S. Zhang, A. Tamayol, A. Khademhosseini, Gold Nanocomposite Bioink for Printing 3D Cardiac Constructs, *Adv. Funct. Mater.* 27 (2017) 1605352.
- [11] V. Lee, G. Singh, J.P. Trasatti, C. Bjornsson, X. Xu, T.N. Tran, S.S. Yoo, G. Dai, P. Karande, Design and fabrication of human skin by three-dimensional bioprinting, *Tissue Eng Part C Methods* 20 (2014) 473-84.
- [12] C. Nieves, G. Marta, F.d.C. Juan, V. Diego, L.J. Jose, 3D bioprinting of functional human skin: production and in vivo analysis, *Biofabrication* 9 (2017) 015006.
- [13] L.J. Pourchet, A. Thepot, M. Albouy, E.J. Courtial, A. Boher, L.J. Blum, C.A. Marquette, Human Skin 3D Bioprinting Using Scaffold-Free Approach, *Adv Healthc Mater* 6 (2017) 1601101.

- [14] J.W. Nichol, S.T. Koshy, H. Bae, C.M. Hwang, S. Yamanlar, A. Khademhosseini, Cell-laden microengineered gelatin methacrylate hydrogels, *Biomaterials* 31 (2010) 5536-44.
- [15] F. Munarin, M.C. Tanzi, P. Petrini, Advances in biomedical applications of pectin gels, *Int. J. Biol. Macromol.* 51 (2012) 681-9.
- [16] A. Noreen, Z.I. Nazli, J. Akram, I. Rasul, A. Mansha, N. Yaqoob, R. Iqbal, S. Tabasum, M. Zuber, K.M. Zia, Pectins functionalized biomaterials; a new viable approach for biomedical applications: A review, *Int. J. Biol. Macromol.* 101 (2017) 254-272.
- [17] A.B. Servais, A. Kienzle, C.D. Valenzuela, A.B. Ysasi, W.L. Wagner, A. Tsuda, M. Ackermann, S.J. Mentzer, Structural Heteropolysaccharide Adhesion to the Glycocalyx of Visceral Mesothelium, *Tissue Eng Part A* 24 (2018) 199-206.
- [18] V.J. Morris, N.J. Belshaw, K.W. Waldron, E.G. Maxwell, The bioactivity of modified pectin fragments, *Bioactive Carbohydrates and Dietary Fibre* 1 (2013) 21-37.
- [19] H. Salman, M. Bergman, M. Djaldetti, J. Orlin, H. Bessler, Citrus pectin affects cytokine production by human peripheral blood mononuclear cells, *Biomed Pharmacother* 62 (2008) 579-82.
- [20] F. Munarin, S.G. Guerreiro, M.A. Grellier, M.C. Tanzi, M.A. Barbosa, P. Petrini, P.L. Granja, Pectin-based injectable biomaterials for bone tissue engineering, *Biomacromolecules* 12 (2011) 568-77.
- [21] A.R. Silini, V. Spoldi, S. De Munari, E. Vertua, F. Munarin, P. Petrini, S. Fare, O. Parolini, Immunological and Differentiation Properties of Amniotic Cells Are Retained After Immobilization in Pectin Gel, *Cell Transplant* 27 (2018) 70-76.
- [22] R.F. Pereira, C.C. Barrias, P.J. Bartolo, P.L. Granja, Cell-instructive pectin hydrogels crosslinked via thiol-norbornene photo-click chemistry for skin tissue engineering, *Acta Biomater* 66 (2018) 282-293.
- [23] W. Jia, P.S. Gungor-Ozkerim, Y.S. Zhang, K. Yue, K. Zhu, W. Liu, Q. Pi, B. Byambaa, M.R. Dokmeci, S.R. Shin, A. Khademhosseini, Direct 3D bioprinting of perfusable vascular constructs using a blend bioink, *Biomaterials* 106 (2016) 58-68.
- [24] N. Annabi, S.M. Mithieux, P. Zorlutuna, G. Camci-Unal, A.S. Weiss, A. Khademhosseini, Engineered cell-laden human protein-based elastomer, *Biomaterials* 34 (2013) 5496-505.
- [25] T. Billiet, B. Van Gasse, E. Gevaert, M. Cornelissen, J.C. Martins, P. Dubruel, Quantitative contrasts in the photopolymerization of acrylamide and methacrylamide-functionalized gelatin hydrogel building blocks, *Macromol Biosci* 13 (2013) 1531-45.
- [26] I. Mironi-Harpaz, D.Y. Wang, S. Venkatraman, D. Seliktar, Photopolymerization of cell-encapsulating hydrogels: crosslinking efficiency versus cytotoxicity, *Acta Biomater* 8 (2012) 1838-48.
- [27] R.F. Pereira, P.J. Bártolo, 3D Photo-Fabrication for Tissue Engineering and Drug Delivery, *Engineering* 1 (2015) 90-112.

- [28] H.W. Ooi, S. Hafeez, C.A. van Blitterswijk, L. Moroni, M.B. Baker, Hydrogels that listen to cells: a review of cell-responsive strategies in biomaterial design for tissue regeneration, *Mater Horiz* 4 (2017) 1020-1040.
- [29] A.L. Torres, S.J. Bidarra, M.T. Pinto, P.C. Aguiar, E.A. Silva, C.C. Barrias, Guiding morphogenesis in cell-instructive microgels for therapeutic angiogenesis, *Biomaterials* 154 (2018) 34-47.
- [30] S.J. Bidarra, C.C. Barrias, K.B. Fonseca, M.A. Barbosa, R.A. Soares, P.L. Granja, Injectable in situ crosslinkable RGD-modified alginate matrix for endothelial cells delivery, *Biomaterials* 32 (2011) 7897-904.
- [31] C. Resetco, B. Hendriks, N. Badi, F. Du Prez, Thiol-ene chemistry for polymer coatings and surface modification - building in sustainability and performance, *Mater Horiz* 4 (2017) 1041-1053.
- [32] D.P. Nair, M. Podgorski, S. Chatani, T. Gong, W.X. Xi, C.R. Fenoli, C.N. Bowman, The Thiol-Michael Addition Click Reaction: A Powerful and Widely Used Tool in Materials Chemistry, *Chem. Mater.* 26 (2014) 724-744.
- [33] N. Huebsch, P.R. Arany, A.S. Mao, D. Shvartsman, O.A. Ali, S.A. Bencherif, J. Rivera-Feliciano, D.J. Mooney, Harnessing traction-mediated manipulation of the cell/matrix interface to control stem-cell fate, *Nat Mater* 9 (2010) 518-26.
- [34] K. Bott, Z. Upton, K. Schrobback, M. Ehrbar, J.A. Hubbell, M.P. Lutolf, S.C. Rizzi, The effect of matrix characteristics on fibroblast proliferation in 3D gels, *Biomaterials* 31 (2010) 8454-64.
- [35] C. Branco da Cunha, D.D. Klumpers, W.A. Li, S.T. Koshy, J.C. Weaver, O. Chaudhuri, P.L. Granja, D.J. Mooney, Influence of the stiffness of three-dimensional alginate/collagen-I interpenetrating networks on fibroblast biology, *Biomaterials* 35 (2014) 8927-36.
- [36] M. Hospodiuk, M. Dey, D. Sosnoski, I.T. Ozbolat, The bioink: A comprehensive review on bioprintable materials, *Biotechnol. Adv.* 35 (2017) 217-239.
- [37] W. Liu, M.A. Heinrich, Y. Zhou, A. Akpek, N. Hu, X. Liu, X. Guan, Z. Zhong, X. Jin, A. Khademhosseini, Y.S. Zhang, Extrusion Bioprinting of Shear-Thinning Gelatin Methacryloyl Bioinks, *Adv Healthc Mater* 6 (2017) 1601451.
- [38] L.L. Ouyang, C.B. Highley, C.B. Rodell, W. Sun, J.A. Burdick, 3D Printing of Shear-Thinning Hyaluronic Acid Hydrogels with Secondary Cross-Linking, *ACS Biomater Sci Eng* 2 (2016) 1743-1751.
- [39] L. Ouyang, C.B. Highley, W. Sun, J.A. Burdick, A Generalizable Strategy for the 3D Bioprinting of Hydrogels from Nonviscous Photo-crosslinkable Inks, *Adv. Mater.* 29 (2017) 1604983.
- [40] T. Jungst, W. Smolan, K. Schacht, T. Scheibel, J. Groll, Strategies and Molecular Design Criteria for 3D Printable Hydrogels, *Chem. Rev.* 116 (2016) 1496-539.

- [41] M. Kesti, C. Eberhardt, G. Pagliccia, D. Kenkel, D. Grande, A. Boss, M. Zenobi-Wong, Bioprinting Complex Cartilaginous Structures with Clinically Compliant Biomaterials, *Adv. Funct. Mater.* 25 (2015) 7406-7417.
- [42] H.M.M. Vivian, P.W.M. Ferry, V. Jetze, J.A.D. Wouter, G. Debby, M. Jos, Yield stress determines bioprintability of hydrogels based on gelatin-methacryloyl and gellan gum for cartilage bioprinting, *Biofabrication* 8 (2016) 035003.
- [43] P. Naomi Claire, S. Willi, B. Thomas, P.W.M. Ferry, G. Juergen, J. Tomasz, *Biofabrication* 9 (2017) 044107.
- [44] H. Martínez Ávila, S. Schwarz, N. Rotter, P. Gatenholm, 3D bioprinting of human chondrocyte-laden nanocellulose hydrogels for patient-specific auricular cartilage regeneration, *Bioprinting* 1-2 (2016) 22-35.
- [45] A.L. Rutz, K.E. Hyland, A.E. Jakus, W.R. Burghardt, R.N. Shah, A multimaterial bioink method for 3D printing tunable, cell-compatible hydrogels, *Adv. Mater.* 27 (2015) 1607-14.
- [46] J. Sottile, F. Shi, I. Rublyevska, H.Y. Chiang, J. Lust, J. Chandler, Fibronectin-dependent collagen I deposition modulates the cell response to fibronectin, *Am J Physiol Cell Physiol* 293 (2007) C1934-46.
- [47] A.J. Zollinger, M.L. Smith, Fibronectin, the extracellular glue, *Matrix Biol.* 60-61 (2017) 27-37.
- [48] C. Frantz, K.M. Stewart, V.M. Weaver, The extracellular matrix at a glance, *J. Cell Sci.* 123 (2010) 4195-200.
- [49] A. Domogatskaya, S. Rodin, K. Tryggvason, Functional diversity of laminins, *Annu. Rev. Cell Dev. Biol.* 28 (2012) 523-53.
- [50] Y.C. Hsu, L. Li, E. Fuchs, Emerging interactions between skin stem cells and their niches, *Nat Med* 20 (2014) 847-56.
- [51] C.A. Higgins, J.C. Chen, J.E. Cerise, C.A. Jahoda, A.M. Christiano, Microenvironmental reprogramming by three-dimensional culture enables dermal papilla cells to induce de novo human hair-follicle growth, *Proc Natl Acad Sci USA* 110 (2013) 19679-88.
- [52] B.S. Kim, Y.W. Kwon, J.S. Kong, G.T. Park, G. Gao, W. Han, M.B. Kim, H. Lee, J.H. Kim, D.W. Cho, 3D cell printing of in vitro stabilized skin model and in vivo pre-vascularized skin patch using tissue-specific extracellular matrix bioink: A step towards advanced skin tissue engineering, *Biomaterials* 168 (2018) 38-53.

3.7. Supplementary Information

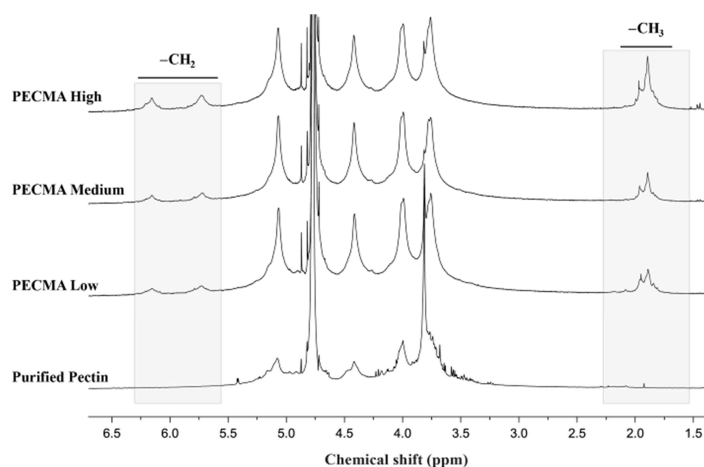


Figure S3.1. ^1H NMR spectra of purified pectin and pectin methacrylate (PECMA) with different degrees of methacrylation. New peaks corresponding to methyl ($-\text{CH}_3$) and methylene ($-\text{CH}_2$) groups are absent in the spectra of pure pectin, but present in the backbone of macromers modified with methacrylic anhydride.

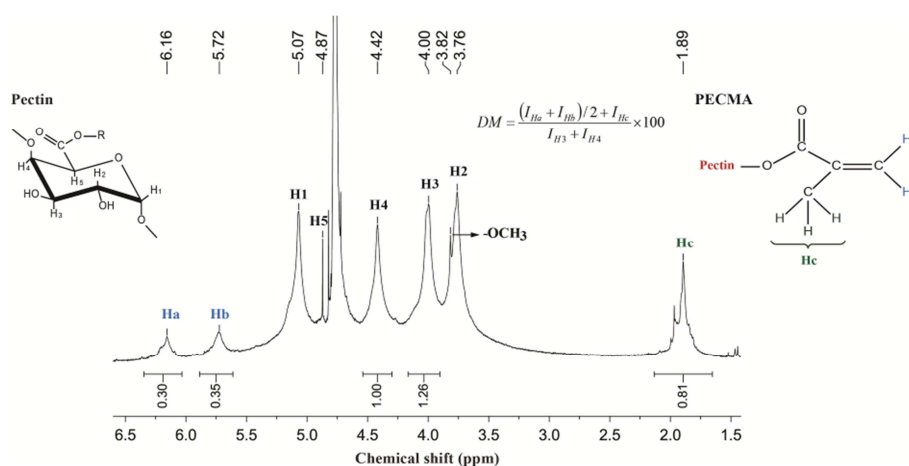


Figure S3.2. Representative ^1H NMR spectrum of PECMA, detailing the peaks corresponding to native protons of pectin and new methacrylate function. The identification of native peaks in pectin structure was performed based on published data [1]. The degree of methacrylation (DM) was defined as the ratio of methyl ($-\text{CH}_3$) and methylene ($-\text{CH}_2$) groups of methacrylate function introduced in the polymer backbone to the pectin protons located in position 3 (H3) and 4 (H4). This value was calculated by the integration of peaks at 1.89 ppm (CH_3), 6.16 ppm (CH_2), 5.72 ppm (CH_2), 4.00 ppm (H3), and 4.42 ppm (H4).

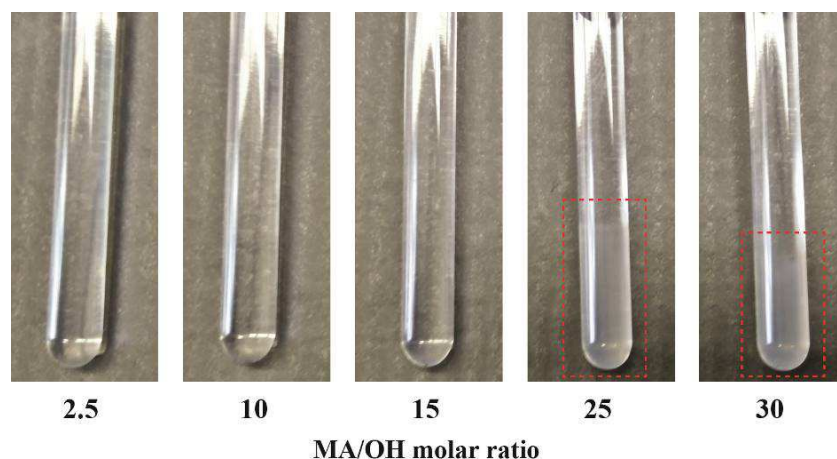


Figure S3.3. Macroscopic images of PECMA solutions in D_2O after chemical modification with different MA/OH molar ratios. For the ratios 2.5, 10 and 15, the solutions prepared showed complete dissolution, while using higher ratios it was possible to observe poor solubilization and polymer precipitation.

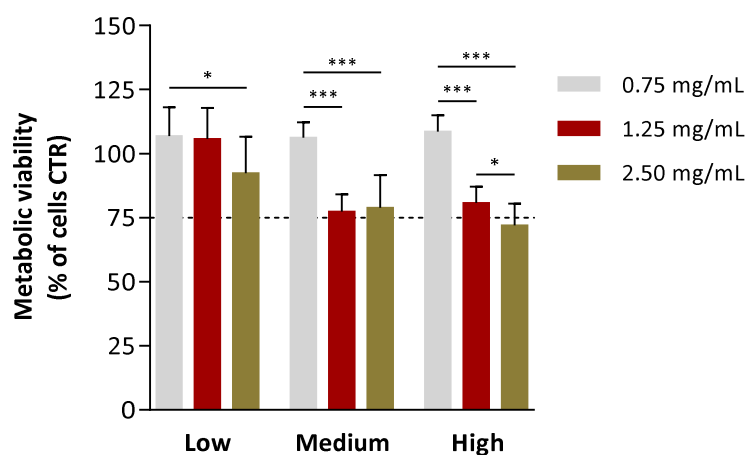


Figure S3.4. Effect of soluble PECMA macromer solutions prepared with varying degrees of methacrylation and polymer concentration on the metabolic activity of fibroblasts. Macromer solutions were dissolved in culture media at different concentrations and incubated with adherent fibroblasts cultured in monolayer for 24 h (* $P < 0.05$; *** $P < 0.001$).

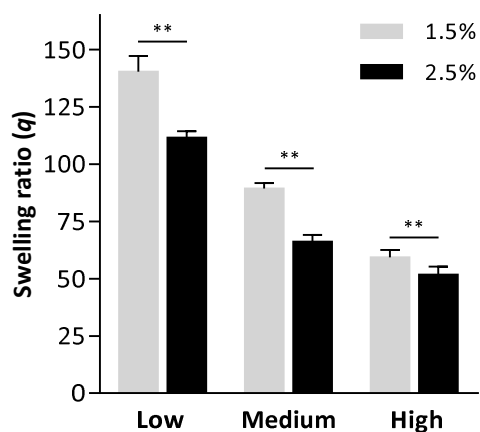


Figure S3.5. Swelling ratio of PECMA hydrogels with varying degrees of methacrylation tested at 1.5 and 2.5 wt% concentrations. Hydrogels were photocrosslinked by exposure to UV light for 160 s and then incubated in ultrapure water at 37 °C for 24 h (** $P < 0.01$).

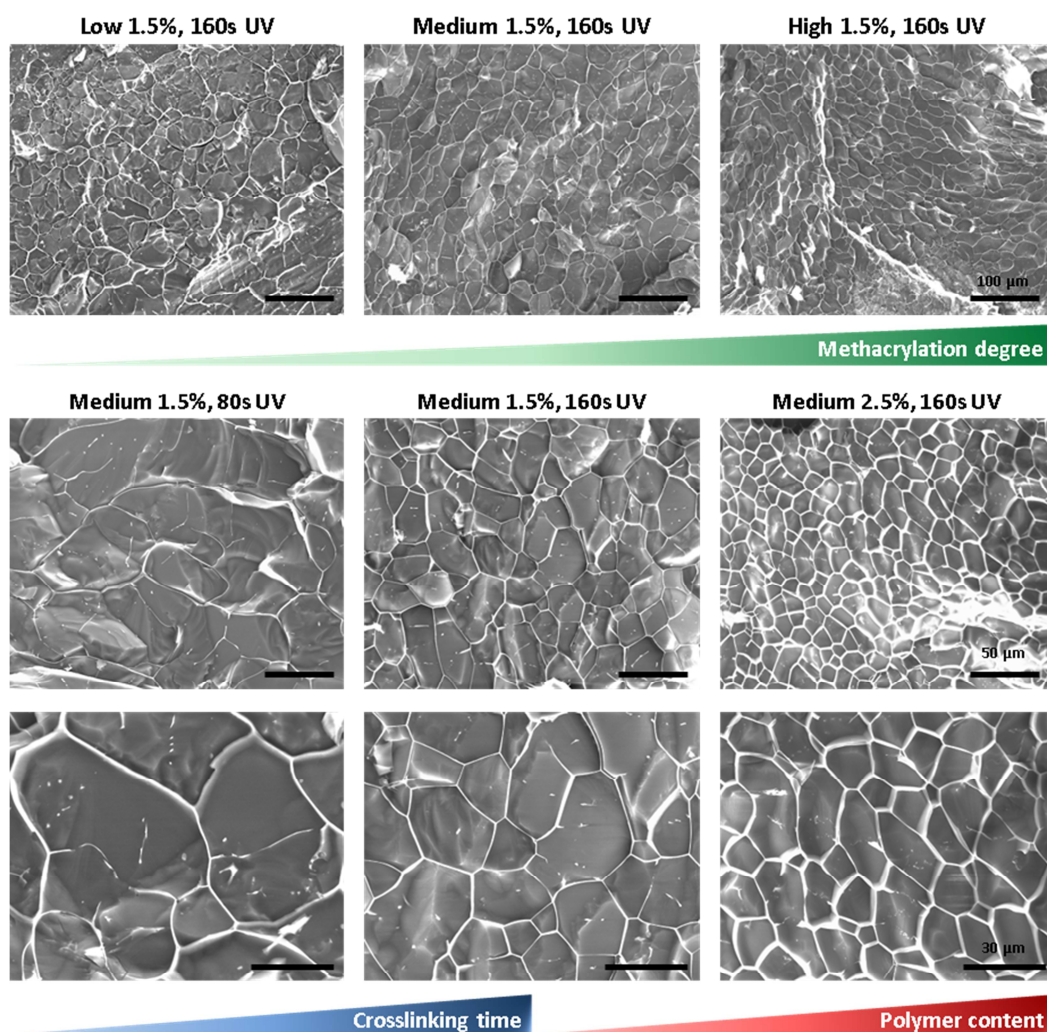


Figure S3.6. Influence of crosslinking time and macromer concentration on the microstructure of PECMA medium hydrogels visualized by CryoSEM analysis.

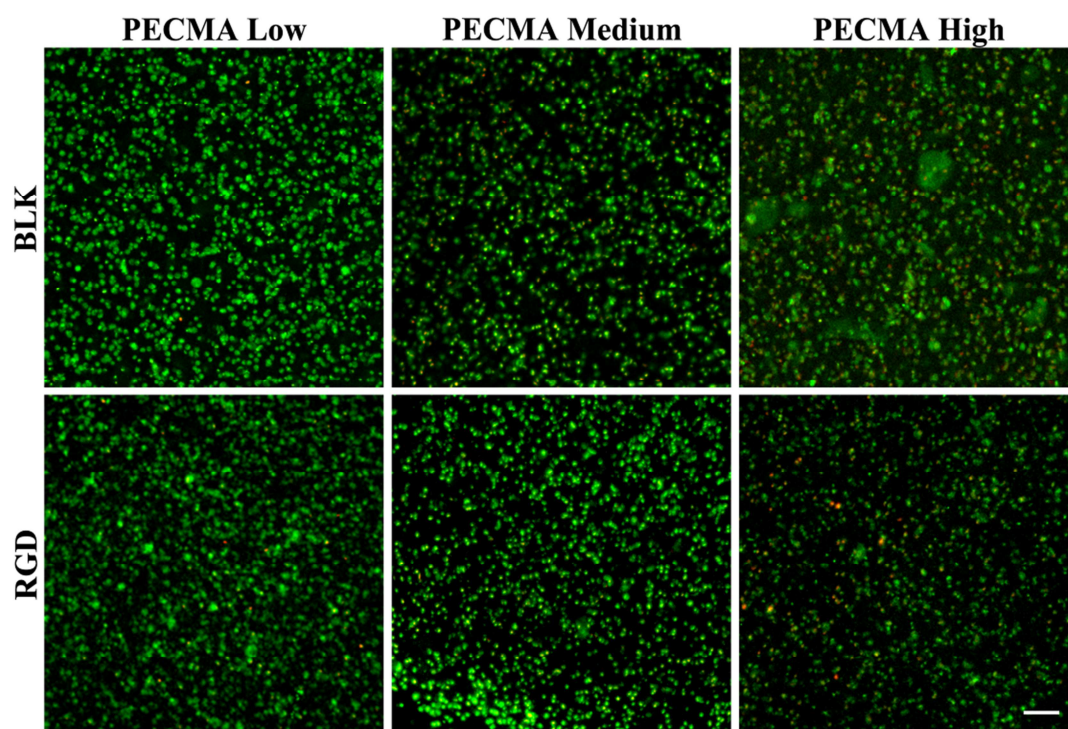


Figure S3.7. Effect of tethered RGD-peptide on the viability of fibroblasts entrapped within dual-crosslinked PECMA hydrogels (1.5 wt%, 160 s UV) after 24 h. CyTRAK Orange™ is colored in green (live cells) and DRAQ7™ is colored in red (dead cells). Scale bar is 100 μm .

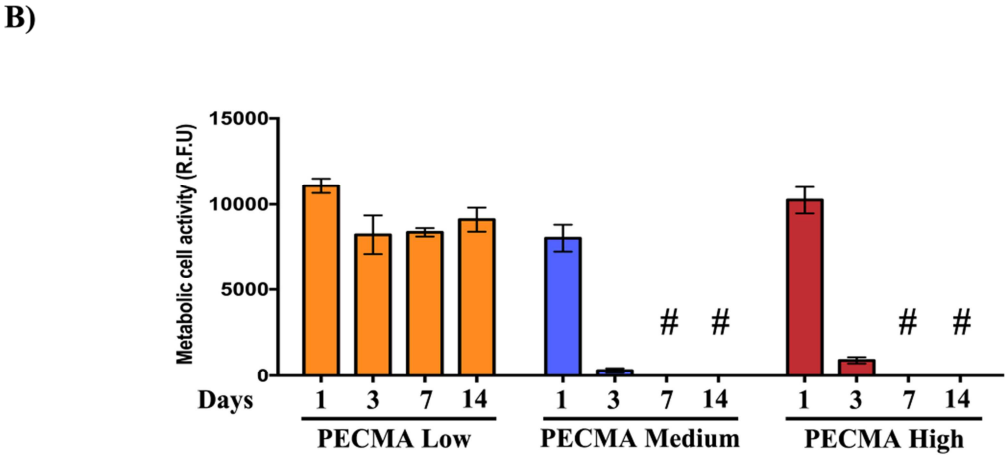
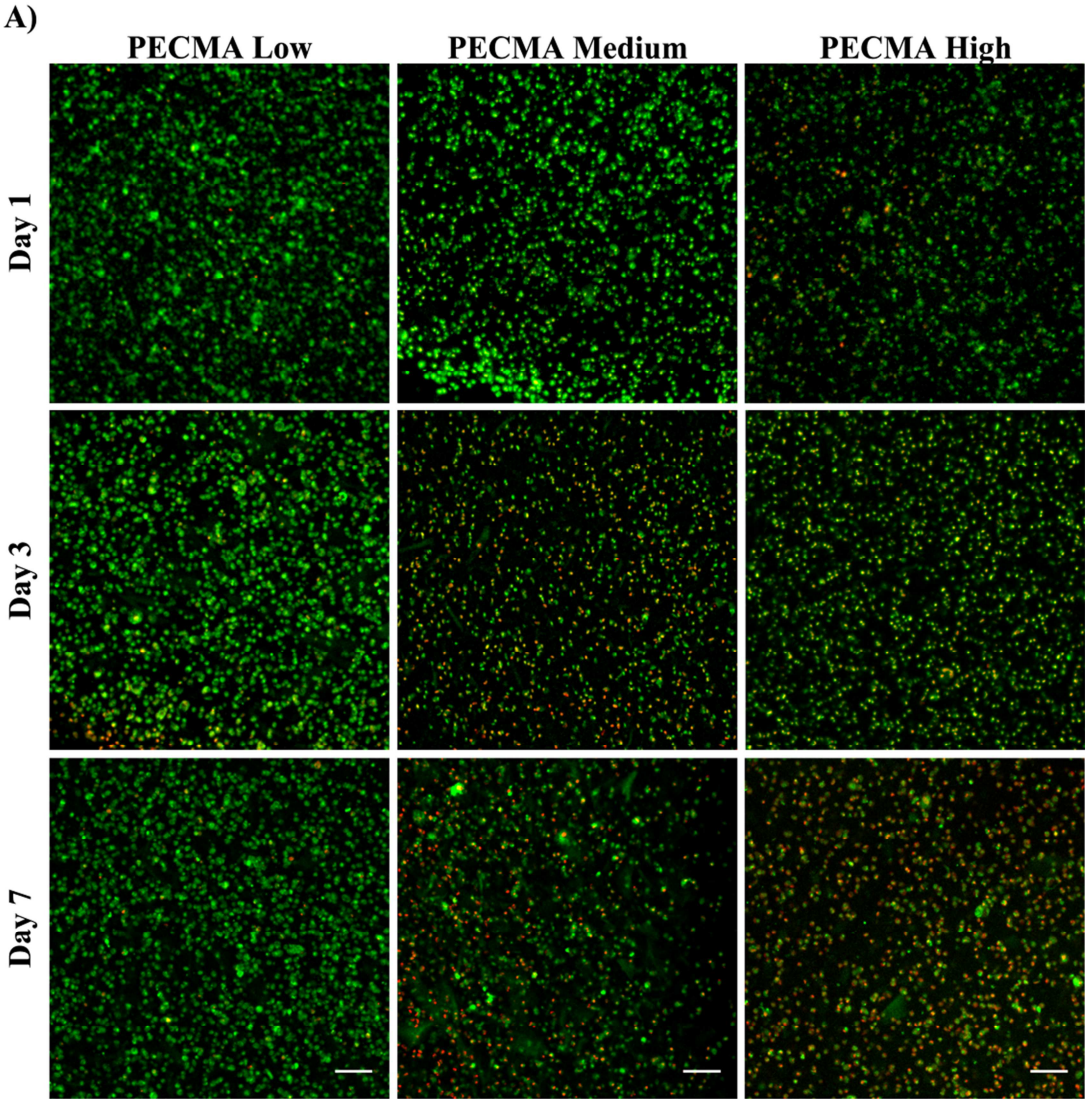


Figure S3.8. (A) Live/Dead staining confocal images of fibroblasts entrapped within RGD-functionalized, dual-crosslinked PECMA hydrogels (1.5 wt%, 160 s UV) with varying degrees of methacrylation throughout 7 days of culture. CyTRAK Orange™ is colored in green (live cells) and DRAQ7™ is colored in red (dead cells). Scale bars are 100 μm. **(B)** Metabolic activity of fibroblasts within the dual-crosslinked hydrogels (#represents residual levels of metabolic activity; RFU indicates

Random Fluorescence Units). Fibroblasts entrapped within PECMA low hydrogels remained metabolically active throughout 14 days of culture, while cells cultured within stiffer PECMA medium and PECMA high hydrogels displayed a significant reduction on the metabolic activity at day 3.

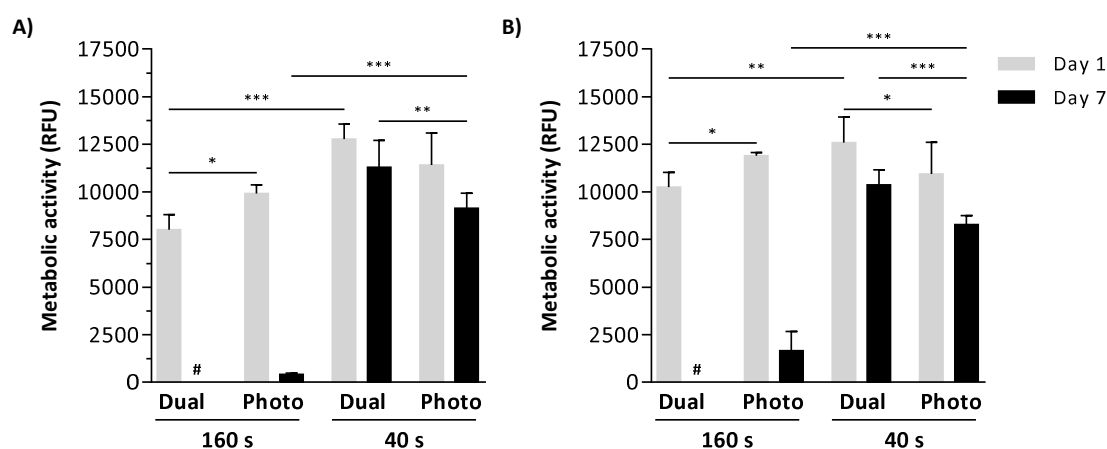


Figure S3.9. Metabolic activity of fibroblasts embedded within RGD-functionalized PECMA medium (A) and PECMA high (B) hydrogels (1.5 wt%) photocrosslinked for 80 s and 40 s, respectively. Both formulations were also photocrosslinked for 160 s for comparison. Chemical hydrogels were incubated in culture media containing calcium chloride (1.8 mM), yielding a dual crosslinked hydrogel (designated as “Dual”). Cell-laden hydrogels were also incubated in culture media without calcium chloride (designated as “Photo”). (# indicates residual levels of metabolic activity; (* $P < 0.05$; ** $P < 0.01$; *** $P < 0.001$).

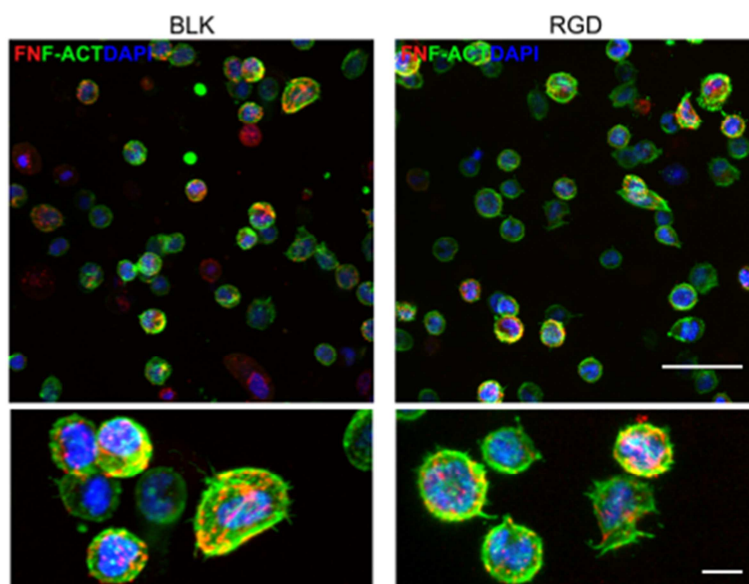


Figure S3.10. Morphology and spatial distribution of fibroblasts embedded within dual-crosslinked PECMA low hydrogels, with or without (BLK) tethered RGD-peptide, after 14 days of culture showing DNA (blue), F-actin (green) and fibronectin (red). Scale bars represent 50 μm on the top images and 10 μm on the bottom images with higher magnification.

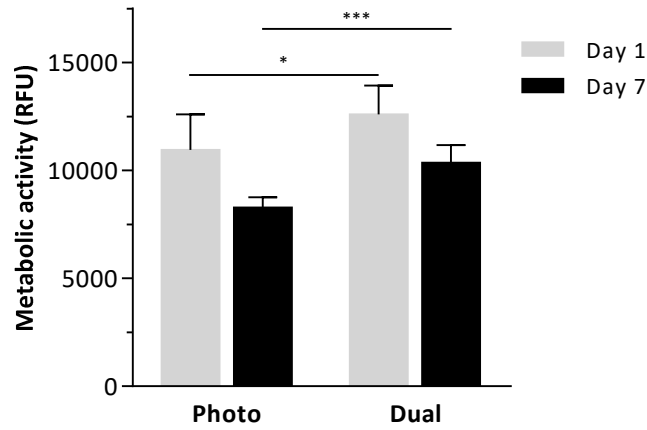


Figure S3.11. Metabolic activity of hNDFs embedded within photo- or dual-crosslinked RGD-PECMA high hydrogels (1.5 wt%, 40 s UV) for 7 days. * $P < 0.05$; *** $P < 0.001$.

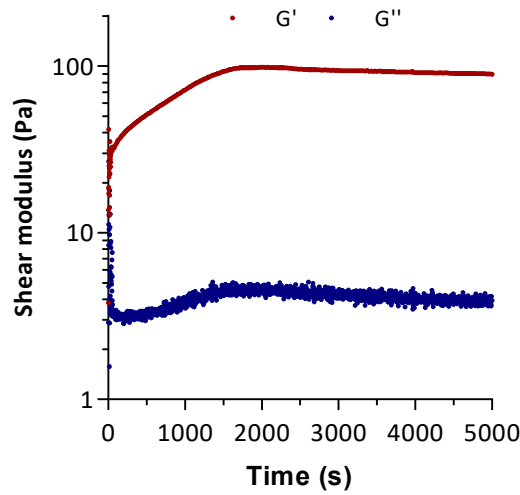


Figure S3.12. Gelation profile of PECMA low bioink at 1.5 wt% with 5 mM CaCl_2 . Gelation occurred within 1 h upon the addition of CaCl_2 . The elastic (G') and viscous (G'') modulus increased after the addition of CaCl_2 and remained stable after 1 h of reaction.

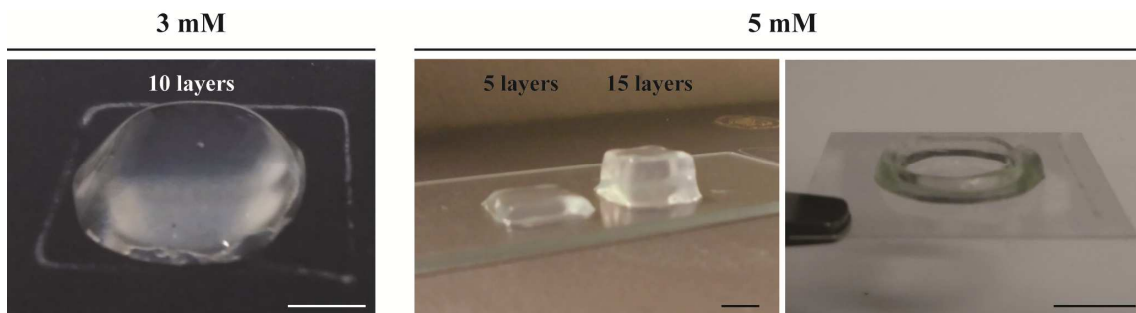


Figure S3.13. The effect of CaCl_2 concentration on the shape fidelity printed 3D constructs using PECMA low macromer solutions (1.5 wt%). Images of constructs (8 (L) \times 8 (W) mm^2) printed with

bioink solutions containing either 3 or 5 mM CaCl₂ (scale bar: 4 mm). Hollow tube construct (10 mm Ø, 10 layers) printed with the bioink solution containing 5 mM CaCl₂ (scale bar: 5 mm).

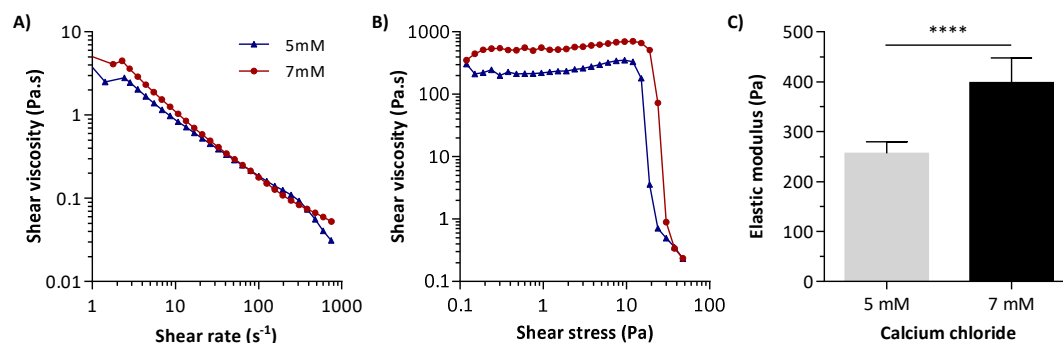


Figure S3.14. Effect of CaCl₂ concentration (5 mM and 7 mM) on the rheological and mechanical properties of printable bioinks prepared at 1.5 wt%: **(A)** viscosity, **(B)** yield stress curves, and **(C)** elastic modulus of 3D hydrogel constructs (1.5 wt%, 160 s UV) determined upon 24h of incubation in culture medium. Yield stress (5 mM: 9.16 Pa; 7 mM: 10.92 Pa) and elastic modulus (5 mM: 256.2 ± 23.8 Pa; 7 mM: 398 ± 49.6 Pa) increase as a function of CaCl₂ concentration. **** $P < 0.0001$.

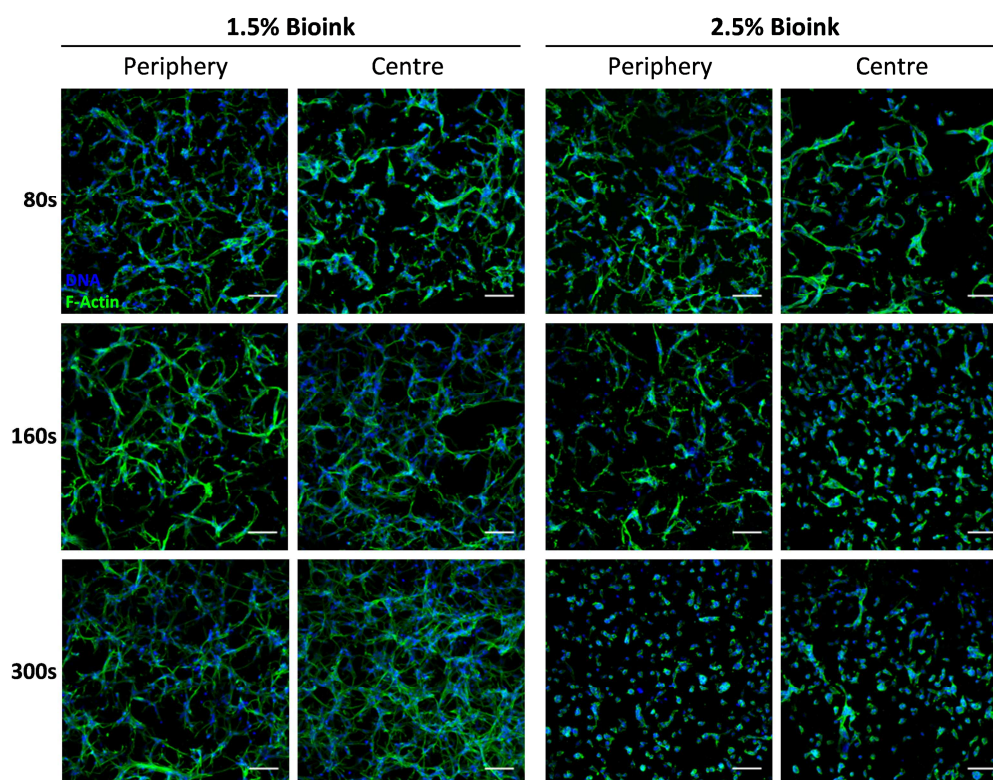


Figure S3.15. Effect of bioink concentration and UV photocrosslinking time on the morphology of dermal fibroblasts within bioprinted 3D constructs at day 7 of culture (scale bar: 100 μm).

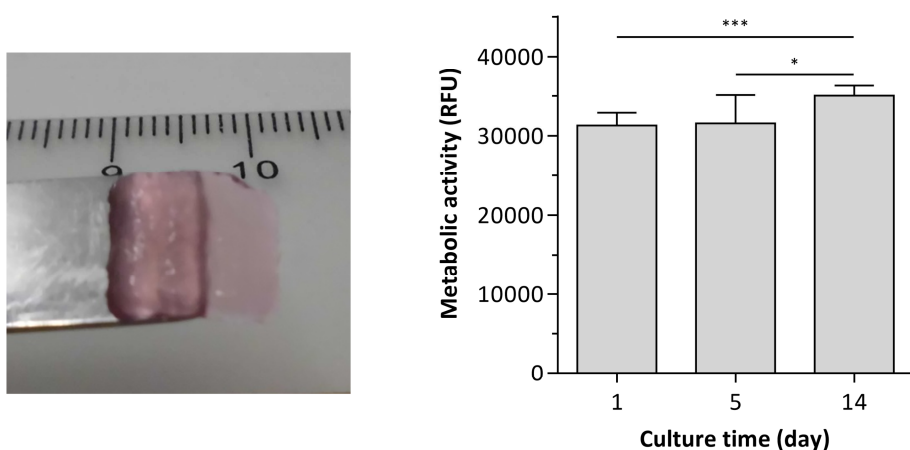


Figure S3.16. Photograph of printed the 3D construct (8 (L) × 8 (W) × 0.9 (H) mm³) at day 14 of culture and metabolic activity of dermal fibroblasts embedded within the printed construct throughout the culture period (n = 1, two independent experiments).

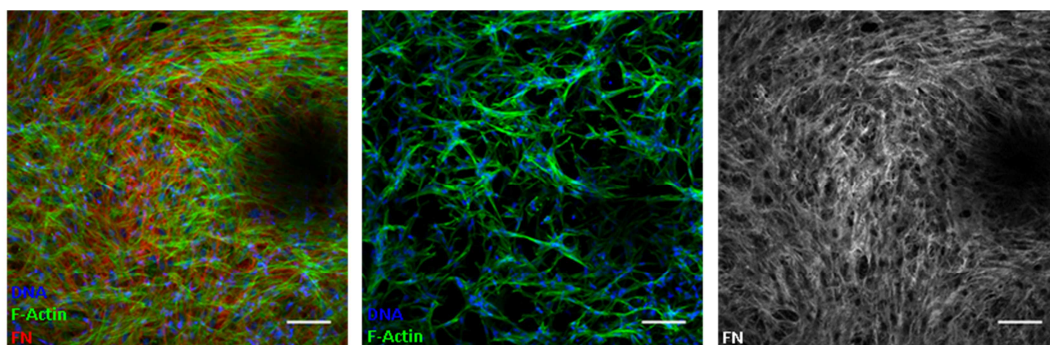


Figure S3.17. Morphology of embedded fibroblasts and fibronectin network within manually deposited hydrogels, stained for nuclei (blue), F-actin (green) and fibronectin (red). Scale bars represent 50 μ m.

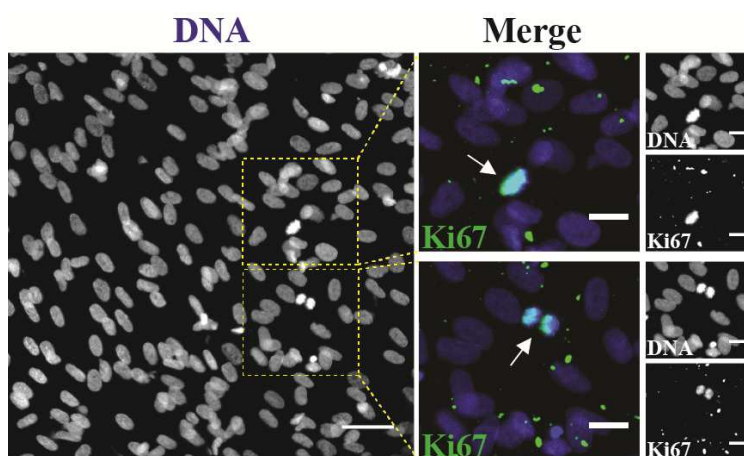


Figure S3.18. Confocal microscopy images showing the presence of proliferative fibroblasts (Ki67 positive, green) within the printed 3D constructs. The boxes mark the magnified areas in the panels on

the right stained for nuclei (blue) and Ki67 (green). Scale bars represent 50 μm for the left image and 10 μm for magnified images.

Table S3.1. Primary and secondary antibodies used for detection of cell morphology, proliferation and ECM protein deposition.

Target	Primary antibody	Dilution	Supplier and reference number	Secondary antibody	Dilution	Supplier and reference number
Fibronectin	Rabbit anti-fibronectin	1:400	Sigma-Aldrich f3648	Alexa Fluor 594 goat anti-rabbit	1:1000	Invitrogen A11072
Collagen-I	Rabbit anti-collagen type-I	1:200	Rockland 600-401-103-0.1	Alexa Fluor 594 goat anti-rabbit	1:500	Invitrogen A11072
Laminin	Rabbit anti-laminin	1:100	Sigma-Aldrich L9393	Alexa Fluor 594 goat anti-rabbit	1:500	Invitrogen A11072
Proliferation	Rabbit anti-Ki67	1:200	Abcam ab15580	Alexa Fluor 647 donkey anti-rabbit IgG	1:500	Invitrogen A31573
Keratinocytes	Rabbit anti-cytokeratin	1:100	Dako Z0622	Alexa Fluor 488 donkey anti-rabbit	1:1000	Invitrogen A21206
Fibroblasts	Mouse anti-vimentin	1:100	Santa-Cruz Biotechnology sc-6260	Alexa Fluor 488 donkey anti-mouse	1:1000	Invitrogen A21202

References

[1] H. Wining, N. Viereck, L. Nørgaard, J. Larsen, S.B. Engelsen, Quantification of the degree of blockiness in pectins using ^1H NMR spectroscopy and chemometrics, *Food Hydrocolloids* 21 (2007) 256-266.

CHAPTER IV

CELL-INSTRUCTIVE PECTIN HYDROGELS CROSSLINKED VIA THIOL-NORBORNENE PHOTO- CLICK CHEMISTRY FOR SKIN TISSUE ENGINEERING

This chapter was based on the following published paper:

Pereira, R.F., Barrias, C.C., Bártolo, P.J., Granja, P.L. "Cell-instructive pectin hydrogels crosslinked via thiol-norbornene photo-click chemistry for skin tissue engineering", *Acta Biomaterialia*, 66, 282-293, 2018.

Abstract

Cell-instructive hydrogels are attractive for skin repair and regeneration, serving as interactive matrices to promote cell adhesion, cell-driven remodelling and *de novo* deposition of extracellular matrix components. This paper describes the synthesis and photocrosslinking of cell-instructive pectin hydrogels using cell-degradable peptide crosslinkers and integrin-specific adhesive ligands. Protease-degradable hydrogels obtained by photoinitiated thiol-norbornene click chemistry are rapidly formed in the presence of dermal fibroblasts, exhibit tuneable properties and are capable of modulating the behaviour of embedded cells, including the cell spreading, hydrogel contraction and secretion of matrix metalloproteinases. Keratinocytes seeded on top of fibroblast-loaded hydrogels are able to adhere and form a compact and dense layer of epidermis, mimicking the architecture of the native skin. Thiol-ene photocrosslinkable pectin hydrogels support the *in vitro* formation of full-thickness skin and are thus a highly promising platform for skin tissue engineering applications, including wound healing and *in vitro* testing models.

Keywords: dermal fibroblasts; hydrogel; pectin; photocrosslinking; skin; thiol-norbornene chemistry.

4.1. Introduction

Skin wound healing is a complex, orchestrated cascade of biological processes that rely on the interaction between several mediators, such as extracellular matrix (ECM) molecules, cells, growth factors, cytokines and chemokines, towards the replacement of lost tissue [1]. Despite the variety of commercially available products and therapeutic strategies for skin wound healing (e.g., skin substitutes, wound dressings), the formation of functional skin remains a major challenge [1-3]. Hydrogels are widely explored as templates for skin wound healing due to their chemical versatility, hydrated nature, elasticity and ability to conform into complex-shaped defects. In addition, hydrogels can be designed to provide instructive environments for tissue formation as well as to deliver cells and growth factors in order to stimulate skin regeneration [4-6]. Cell-instructive hydrogels play a pivotal role in tissue engineering due to their biochemical and biophysical similarities with the native ECM, along with the ability to influence the behaviour of embedded cells [7, 8]. Synthetic materials have been widely explored to design such bioactive hydrogels as they provide greater control over the chemical composition and materials properties [9, 10]. However, materials derived from natural sources possess unique features (e.g., cell remodelling, biological recognition, biodegradation) that also make them suitable candidates to engineer ECM analogues [11, 12].

Pectin, a structural polysaccharide extracted from the primary cell wall of plants, is receiving increased attention for tissue engineering due to its water solubility, biocompatibility, biodegradability and anionic nature [13-15]. It is a branched polymer composed of multiple polysaccharide domains, providing a multitude of target sites for chemical modification. In addition, physical pectin hydrogels are susceptible to *in vitro* and *in vivo* degradation/dissolution [16, 17], which is useful for tissue engineering applications. A distinctive characteristic of pectin compared to other bioactive natural polymers (e.g., gelatin, fibrin) relies on the lack of endogenous cell-adhesive and cell-proteolytic sites. This feature allows for the precise introduction of specific biochemical moieties onto the otherwise bioinert polymer backbone [16] in order to control cell fate and to decouple their effect on cell behaviour.

The selection of suitable chemistries is of critical importance for the formation of cellularized ECM-inspired polymer hydrogels under cytocompatible conditions, without yielding toxic byproducts. Bio-orthogonal click chemistries assume a central role on the modular synthesis of advanced cell-laden hydrogels, as they can develop under mild conditions in the presence of cells, proceed with high yield and be easily controlled by selecting complementary chemical functionalities [18, 19]. Photoinitiated thiol-norbornene

chemistry is a click reaction between multifunctional norbornene-modified macromers and sulfhydryl-containing linkers (e.g., dithiothreitol, biscysteine peptides), triggered by UV or visible light in the presence of a low photoinitiator concentration [10]. In contrast to chain-growth hydrogels formed by radical-mediated polymerization, which often contain heterogeneous and high molecular weight crosslinks, light-mediated thiol-norbornene polymerization is non-oxygen inhibited and proceeds through a step-growth mechanism. Hydrogels formed by thiol-norbornene chemistry contain networks with less heterogeneities and lead to the formation of engineered tissues with improved overall quality [20, 21]. Furthermore, in thiol-norbornene reactions there is no homopolymerization or chain growth between strained norbornene groups and the gelation is much faster [22]. Norbornene end groups are widely used in the modification of both natural (e.g., hyaluronic acid, alginate) and synthetic (e.g., polyethylene glycol) polymers owing their fast reactivity and cytocompatibility. Norbornene-functionalized polymers can be rapidly converted into cell-laden hydrogels under physiologically relevant conditions and the crosslinking reaction did not affect the cell viability [10, 23, 24]. As the norbornene moieties are only reactive in the presence of active radical species, hydrogels bearing free norbornene groups can be explored to dynamically modulate the material properties and/or cell fate after hydrogel formation without cytotoxic effects for the embedded cells [25].

Recently, we reported on the development of photocrosslinkable methacrylate-modified pectin for the bioprinting of cell-responsive tissue constructs for skin applications [26]. Although bioprinted RGD-functionalized pectin hydrogels support the spreading of embedded dermal fibroblasts and *de novo* deposition of endogenously synthesized ECM, cell-mediated hydrogel remodelling is limited by the lack of protease degradable sites. This study describes for the first time the synthesis of norbornene-functionalized pectin (NorPEC) macromers for thiol-ene photopolymerization reactions. Macromers are rapidly converted into cell-instructive hydrogels through one-pot, photo-click reaction with a monocysteine RGD integrin binding peptide and a biscysteine matrix-metalloproteinase (MMP)-cleavable peptide as crosslinker. These new polymer-peptide conjugates are rapidly prepared in the presence of cells through an efficient thiol-norbornene reaction, providing sites for cell attachment and cellular-driven remodelling of the hydrogel network. This photo-click reaction also affords spatiotemporal control over the hydrogel formation and allows easy manipulation of biophysical and biochemical cues presented to the embedded cells. The proposed novel pectin hydrogel system allows the one-step formation of chemically defined cell-laden hydrogels capable of supporting the *in vitro* formation of full-thickness skin.

4.2. Materials and Methods

4.2.1. Synthesis of norbornene functionalized pectin

The norbornene-functionalized pectin (NorPEC) was synthesized through the reaction with carbic anhydride (CA, Acros Organics) in dimethyl sulfoxide (DMSO). Prior to synthesis, low methoxyl citrus pectin (Classic CU701, 86 % galacturonic acid unit content and 37 % degree of methylation, Herbstreith & Fox, Neuenbürg, Germany) was purified [16] and converted into tetrabutylammonium salt (PEC-TBA) for solubilization in organic solvents. Pectin was dissolved in ultrapure water at 1 wt%, the Dowex 50W proton exchange resin (Acros Organics) was added to the solution (3.5 g resin per 1 g polymer) and allowed to exchange under vigorous agitation for 3 h. The solution was centrifuged to remove the resin, filtered (0.20 μm) and neutralized to pH 6.50 with tetrabutylammonium (TBA, Sigma-Aldrich). The solution was subsequently frozen, lyophilized and stored at -20 °C. For the synthesis of NorPEC, PEC-TBA was dissolved in anhydrous DMSO at 1 wt% and CA added at 1-fold molar excess to hydroxyl groups in the polymer backbone. The solution reacted under vigorous agitation and inert (N_2) atmosphere at room temperature for 1 h. After this, the solution was immediately transferred to dialysis (MWCO 3500, Spectra/Por®, SpectrumLabs) with sodium chloride for 3 days, followed by purification with deionized water for additional 2 days. Then, the solution was treated with activated charcoal (1 g charcoal per 1 g of polymer, Sigma-Aldrich) for 1 h, centrifuged (60 000 rcf, Beckman Avanti J-26XP) and filtered (0.20 μm). Finally, the pH was adjusted to 7.00 with sodium hydroxide (0.1M), the solution frozen and the polymer recovered by lyophilization. The product was dissolved in deuterated water (D_2O , Euriso-top) containing 3-(trimethylsilyl)propionic-2,2,3,3- d_4 acid sodium salt (TSP- d_4 , Euriso-top) as internal standard ($\delta = 0$ ppm) and analyzed by ^1H NMR using a 400 MHz spectrometer AVANCE III (Bruker).

4.2.2. Formation and characterization of photocrosslinked hydrogels

For the fabrication of hydrogels, NorPEC macromer (2.5 wt%) was dissolved in 0.9% NaCl containing the photoinitiator VA-086 (0.25 wt%, Wako Chemicals), the peptide crosslinker CGPQG↓IWGQC (4–6 mM, arrow indicates enzymatically cleavable site, Genscript) and the cell-adhesive peptide ligand CGGGGRRGDSP (0–2 mM, underline indicates cell-adhesion motif, Genscript) at desired concentrations. After dissolution, the solution was pipetted on the top of a glass slide treated with SigmaCote (Sigma-Aldrich) to prevent attachment of the gel, covered by a treated glass side with 500 μm spacers and polymerized under UV light (365 nm, RoHS) at 7 mW/cm^2 for 20s.

To characterize the shear modulus, hydrogels were soaked in PBS at 37 °C for 24 h and the samples ($\varnothing = 4$ mm) tested in a humidified environment at physiological temperature (37 °C) using a strain-controlled Kinexus Pro rheometer (Malvern). Both frequency sweeps (0.01 to 10 Hz at 1% strain) and strain sweeps (0.1 to 100% at 0.1 Hz) were performed on swollen samples (30 % compression) to ensure that all measurements were representative of the linear viscoelastic regime.

The swelling ratio was determined by soaking freeze-dried hydrogel samples in PBS (0.5 mL) at 37 °C for 24 h. Hydrogel samples were collected, the superficial excess of water was gently removed with a tissue paper, and the swollen weight (W_S) determined. Swelling ratio (q) was determined by dividing the weight of hydrated hydrogel (W_S) by its initial dry weight (W_D).

The degradation of MMP-degradable NorPEC hydrogels was evaluated in the presence of Type II Collagenase (385 U/mg, Worthington Biochemical). Immediately after photopolymerization hydrogels were frozen and lyophilized to determine the initial weight (W_I). Dry samples were hydrated overnight in HBSS at 37 °C, followed by incubation in 0.5 mL HBSS containing Type II Collagenase at 2 U/mL, which corresponds to the collagenase concentration during the initial phase of the wound healing process [27]. At specific time periods, samples were removed from the solution, washed with ultrapure water, frozen and lyophilized to determine the final weight (W_F) after degradation. The degradation was expressed in percentage of the weight loss compared to the initial dry mass and determined using the following equation:

$$Degradation (\%) = \frac{W_I - W_F}{W_I} \times 100 \quad (1)$$

To determine the amount of non-bound RGD peptide during photopolymerization, hydrogels were incubated in 0.5 mL PBS at 37 °C for 24 h and the supernatant collected. The amount of released peptide in PBS was quantified by reversed phase chromatography (Merck-Hitachi HPLC) equipped with a detector at 220nm. Samples were run at 1 mL/min on a LiChroCART 250-4 C18 column, eluting with 0.065/0.05% trifluoroacetic acid in water/acetonitrile, respectively. The calibration curve for peptide quantification was obtained using the peptide dissolved in PBS at different concentrations (0–2 mM).

4.2.3. 3D cell embedding within hydrogels, cell viability and morphology analysis

Human neonatal dermal fibroblasts (hNDFs) isolated from human neonatal foreskin samples (Coriell Institute for Medical Research, USA) were cultured in DMEM supplemented with 10% fetal bovine serum (FBS, Gibco), antibiotics (100 U/mL penicillin and 100 µg/mL streptomycin, Sigma-Aldrich) and amphotericin B (2.5 mg/L, Sigma-Aldrich). Cells were cultured in 5% CO₂ at 37 °C in tissue culture polystyrene flasks. To characterize the behaviour of hNDFs within MMP-degradable NorPEC hydrogels, cells (passage 6 to 9) were trypsinized before reaching confluence (70–80%) using 0.05 wt% trypsin/ethylenediamine tetraacetic acid (EDTA) solution (Sigma-Aldrich) and centrifuged at 1200 rpm for 5 min. The cell pellet was suspended and added to the NorPEC gel precursor solution at a final density of 1×10^7 cells/mL. Cellular gel precursor solution (20 µL) was pipetted between SigmaCote-treated glass slides and cell-laden hydrogels obtained by UV photopolymerization. At predetermined time periods (day 1, 7 and 14), cell-laden hydrogels were collected and characterized for their metabolic activity, cell viability and cell morphology.

Metabolic activity of cells embedded with NorPEC hydrogels was assessed by the resazurin assay. Hydrogels were incubated in DMEM medium containing 20 v/v% resazurin sodium salt (Sigma-Aldrich) for 2 h at 37 °C. Samples were measured using a microplate reader (Synergy MX, Biotek) at 530 nm (excitation) and 590 nm (emission).

Cell viability was measured using the Live/Dead cytotoxicity kit (Life Technologies) according to the manufacturer instructions. Briefly, cell-laden hydrogels were incubated in phenol red-free DMEM media (Life Technologies) containing 1 µM calcein and 4 µM ethidium homodimer for 30 min. Cell-laden hydrogels were imaged on a laser scanning microscope (CLSM, Leica TCS-SP5 AOBS, Leica Microsystems).

The morphology of cells within NorPEC hydrogels was observed by immunofluorescence staining for F-actin and nuclei. Cell-laden hydrogels were fixed in 4 v/v% paraformaldehyde (PFA, Electron Microscopy Sciences) in HBSS (Life Technologies) for 20 min, followed by extensive washing with HBSS. Samples were incubated overnight with phalloidin/Alexa Fluor[®] 488 (1:40, Molecular Probes-Invitrogen) for F-actin staining, followed by incubation with Hoechst (Life Technologies) for nuclei staining for 45 min. Then, samples were extensively rinsed and imaged on a laser scanning microscope (CLSM, Leica TCS-SP5 AOBS, Leica Microsystems).

4.2.4. Matrix metalloproteinases secretion by gelatin zymography

To determine the expression of MMP-2 and MMP-9 from fibroblasts embedded within hydrogels of different stiffness, cell culture supernatants were collected at different time periods (day 1 and 3) and the levels compared to culture media in the absence of cell-laden hydrogels. After collection, conditioned media was centrifuged to remove cell debris and the total protein content in lysates of cells recovered from the hydrogels quantified by the DC protein assay (BioRad). Sample volumes were adjusted to yield equivalent total cell protein contents, loaded into gelatin-SDS polyacrylamide gels, and run in 1× Tris-Glycine SDS running buffer at 80 V (Mini Protean Tetra Cell system, BioRad). Following electrophoresis, gels were washed in 2% Triton X-100 to remove the SDS and incubated with MMP substrate buffer for 16 h at 37 °C. Then, gels were washed and stained with Coomassie Brilliant Blue R-250 (Sigma Aldrich). The activity of MMPs was visualized by clear bands in the stained gels and compared to molecular weight and standards. The gel was washed with distilled water, scanned using the GS-800 Calibrated Densitometer (Bio-Rad), and the activity of MMPs estimated by densitometric analysis (Quantity One, Bio-rad).

4.2.5. Formation of full-thickness skin using cell-instructive pectin hydrogels

The skin equivalent was constructed by the photopolymerization of MMP-degradable NorPEC gel precursor solution loaded with fibroblasts (1×10^7 cells/mL), as previously described. Cell-laden hydrogels were cultured submerged for 7 days. After this time period, cell line keratinocytes (HaCaT) were seeded onto the fibroblast-loaded hydrogel (5×10^5 cells/cm²), left to attach for 2 h and cultured submerged for 7 days. Then, the constructs were cultured at the air-liquid interface (ALI culture) for either 14 days or 28 days [28]. Culture medium was changed every two days in submerged culture and daily in ALI culture.

4.2.6. Histological and immunofluorescence analysis

Skin equivalents were rinsed with HBSS, fixed in 4 v/v% paraformaldehyde in HBSS for 30 min and extensively washed. Then, samples were embedded in paraffin, sectioned onto 6 µm slides and representative sections were stained for Hematoxylin and eosin (H&E) and Masson's Trichrome using routine protocols. The sections were mounted on coverslips and observed with an optical microscope. For immunofluorescence analysis, deparaffinized sections were subjected to heat-induced antigen retrieval, permeabilized with 0.25% Triton X-100 (Sigma-Aldrich) in PBS and rinsed with PBS, followed by blocking and overnight incubation with primary antibodies at 4 °C (Table S1). Then, sections were rinsed and incubated with secondary antibodies for 1 h at room temperature, following extensive

washing. After mounting, the sections were observed in a microscope (AxioImager Z1, Carl Zeiss). Negative controls were performed by replacing the primary antibody with blocking buffer.

4.2.7. Statistical analysis

Statistical analyses were performed in the GraphPad Prism 7.0 software. All experimental data are reported as the mean \pm standard deviation (SD) of at least three individual samples. Unless stated, the non-parametric Mann–Whitney test was applied with 95% confidence interval and statistically significant differences marked with $p < 0.05$ (*), $p < 0.01$ (**), $p < 0.001$ (***) and $p < 0.0001$ (****).

4.3. Results and Discussion

4.3.1. Synthesis of norbornene-functionalized pectin macromers for thiol-ene photopolymerization

In thiol-ene photopolymerization, the reaction kinetics, the extent of conversion and the structure of the polymer network are determined by the reactivity between thiols and carbon–carbon double bonds (referred to as alkenes), which in turn depends on both the reactivity in thiol–alkene reactions and the alkene chemical structure [29]. Among the variety of alkene functional groups capable of reacting with thiols, it is well-established that strained (norbornene) and electron-rich alkenes (e.g., vinyl ether) react faster than electron-poor alkenes [30]. Specifically, the strained norbornene functional group has received increased attention for thiol-ene reactions as it follows exclusively step-growth mechanism and displays extremely high reactivity, which can be explained by the relief of ring strain after thiol radical addition, absence of abstractable hydrogens and stereoelectronic effects [29, 31]. In this work, pectin was functionalized with norbornene functional groups for the fabrication of cell-laden hydrogels through thiol-ene click reaction in the presence of a low concentration type I photoinitiator and UV light. Norbornene-functionalized pectin was synthesized via an esterification reaction between pectin and CA in DMSO for 1h at room temperature (**Figure 4.1A**). Secondary hydroxyl groups of the polymer served as nucleophiles for reaction with CA, without compromising the water-solubility of modified polymer. The reaction was performed in organic solvents to overcome the limited solubility of CA in aqueous solutions and its pH dependence [32]. This strategy allows the neutralization of carboxylate groups with sodium ions, to improve the water-solubility of synthesized macromers and to prevent spontaneous ionic gelation of photocrosslinked hydrogels in culture medium mediated by

positively charged calcium ions (**Supplementary Figure S4.1**). Pectin was firstly converted to its tetrabutylammonium salt (PEC-TBA) for solubilization in organic solvents via reaction with the Dowex ion-exchange resin, followed by neutralization with tetrabutylammonium (TBA), as can be seen in the ^1H NMR spectra by the appearance of new peaks corresponding to the butyl groups (3.20, 1.66, 1.38, and 0.96 ppm) (**Figure 4.1B**, **Supplementary Figure S4.2**). Then, the lipophilic PEC-TBA was dissolved in anhydrous DMSO and reacted with CA under a N_2 atmosphere, yielding norbornene-functionalized pectin (NorPEC), as confirmed by ^1H NMR analysis through the appearance of new peaks (6.12–6.37 ppm) of vinyl protons on the norbornene functionality (**Figure 4.1B**, **Supplementary Figure S4.3**). The product was purified through dialysis against sodium chloride to ensure complete removal of the TBA via neutralization of the carboxylate groups into the sodium salt form. Further product purification was performed with activated charcoal and centrifugation to remove any unreacted CA and potential byproducts (**Supplementary Figure S4.4**). The extent of norbornene substitution was determined to be $20.0 \pm 0.6\%$ through ^1H NMR analysis by comparing the integral values corresponding to norbornene protons (6.12–6.37 ppm) and native protons in the polymer backbone (3.82–4.43 ppm). Higher substitution can be achieved by changing either the reaction time or the CA content (**Table S4.2**). The reproducibility and robustness of the chemical reaction was confirmed by performing independent synthesis of norbornene-functionalized pectin, followed by ^1H NMR analysis (**Supplementary Figure S4.5**). Compared to alternative strategies for norbornene-functionalization of natural polymers (*e.g.*, gelatin, hyaluronic acid), which are performed under aqueous alkaline buffers (pH 8, 6h, 50°C) to ensure CA dissolution [32] or using di-tert-butyl dicarbonate coupling chemistry in DMSO (20h, 45°C) [23], the modification procedure previously described presents several advantages, such as (i) prevents the addition of catalysts, (ii) precludes the pH adjustment during the reaction, (iii) proceeds at room temperature, and (iv) significantly reduces the reaction time.

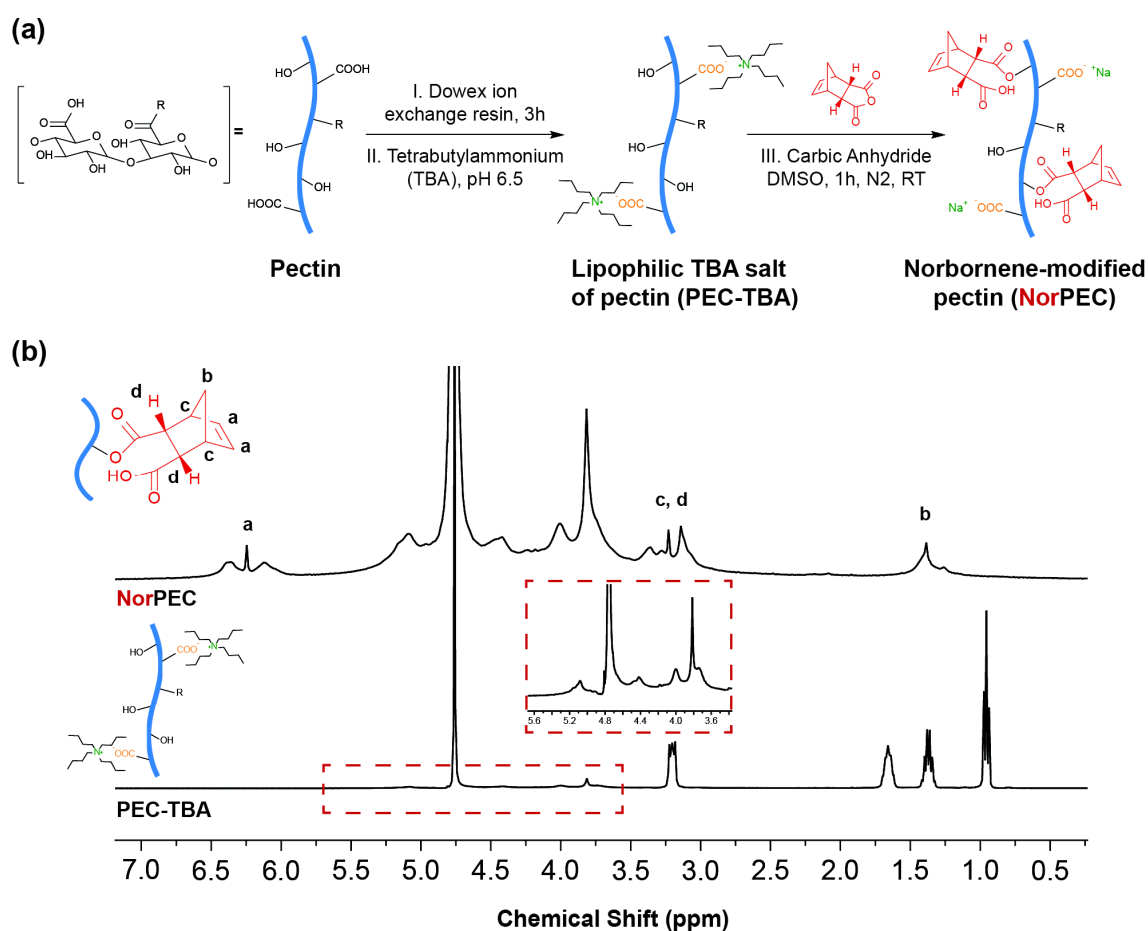


Figure 4.1. Synthesis and characterization of pectin derivatives for thiol-ene photopolymerization. (A) Synthesis of norbornene-functionalized pectin (NorPEC) macromer from PEC-TBA through the coupling of norbornene groups (shown in red) to secondary alcohols on pectin (R denotes substituting group on carboxylic acid moiety: NH_2 or OCH_3). **(B)** ^1H NMR spectra (D_2O , 400 MHz) of NorPEC after 1h reaction with carbic anhydride in DMSO and PEC-TBA after 3h treatment with Dowex ion exchange resin and neutralization with tetrabutylammonium. Insert shows the native protons in pectin backbone.

4.3.2. Formation and characterization of thiol-ene click pectin hydrogels

Biomimetic polymer-peptide hydrogels with MMP-cleavable peptide crosslinks are widely used as provisional matrices for tissue regeneration because they allow for localized cell-driven remodelling at the pericellular space, resembling the dynamic nature of ECM [7]. By simply altering the protease specific peptide crosslinker it was shown that engineered hydrogels differentially respond to MMPs secreted by distinct cell types, allowing for cell-specific invasion within the gel network and controllable cell responses [33, 34]. In this work, enzymatically degradable, cell-instructive pectin hydrogels were prepared via a fast UV photoinitiated thiol-ene reaction between a peptide crosslinker sensitive to cell-secreted proteases (CGPQGIWGQC) flanked with biscysteine and the norbornene groups of NorPEC

in the presence of VA-086 as a water-soluble photoinitiator (**Figure 4.2**). To mimic the cell-mediated remodelling of natural skin ECM, the protease sensitive sequence GPQG↓IWGQ, derived from the sequence GPQG↓IAGQ found in type I collagen, was covalently incorporated into the polymer backbone due to its susceptibility to cleavage by a wide range of MMPs (*e.g.*, 1, 2, 3 and 9) secreted by several cell types involved in skin wound healing, including fibroblasts and keratinocytes [35, 36], thus providing a substrate for cell degradation. After 20s of UV photopolymerization, the biscysteine MMP-degradable peptide become part of the crosslinked hydrogel, allowing for local network degradation and determining both biophysical and biochemical properties. The mono-cysteine peptide CGGGGRGDSP (fibronectin-derived adhesion ligand based on RGD sequence) was also incorporated within the hydrogels as a pendant moiety, via one-pot reaction during gel formation, to provide integrin-mediated cell adhesion and cell-matrix crosstalk [10]. Although the physical adsorption of native integrin-binding proteins and biomolecules onto biomaterials can contribute to a more robust signalling, the hydrophilic nature of hydrogels strongly reduces this phenomenon, limiting cell adhesion both *in vitro* and *in vivo* [37, 38]. A recent work with unmodified calcium-crosslinked pectin hydrogels prepared at different concentrations (1%, 2% and 4%) showed that macrophages seeded onto the hydrogel surfaces fail to adhere, though the hydrogels adsorbed blood plasma proteins in a polymer concentration dependent manner [39]. Therefore, the introduction of cell-adhesive peptides into the backbone of hydrogel precursors, including pectin, is recognized as an efficient strategy to promote cell adhesion. VA-086 was selected as photoinitiator owing to its strong absorbance at 365nm and enhanced biocompatibility compared to the commonly used Irgacure 2959 [40]. We took advantage of the orthogonality and ultrahigh reactivity of norbornene moiety toward thiol-ene reaction to reduce the concentration of photoinitiator to 0.25 wt%. This concentration is significantly lower than the ones typically applied in radical-mediated polymerization (1.0–1.5 wt%), preventing the formation of macroscopic air bubbles within the hydrogel due to the N₂ generation [41, 42].

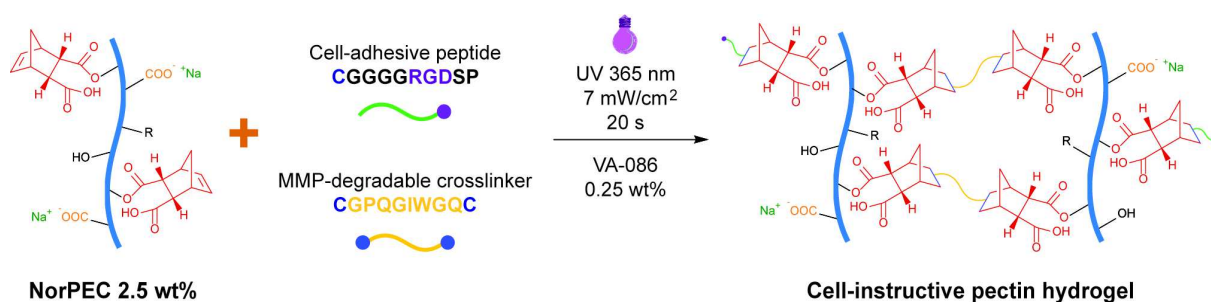


Figure 4.2. Schematic illustration of thiol-norbornene hydrogel preparation. Photocrosslinking and biofunctionalization of click NorPEC hydrogels via UV light photoinitiated thiol-ene reaction of di-thiol MMP-degradable peptide (CGPQG↓IWGQC, arrow indicates enzymatically cleavable site) and norbornene groups on NorPEC. Mono-thiol cell-adhesive peptide (CGGGGRGDSP, underline indicates cell-adhesion motif) is bond to the norbornene groups during the photopolymerization, providing pendant sites for cell-anchorage.

In order to closely mimic key features of the ECM, hydrogel mechanical properties and biological functions should be tailored on relevant time scales by the user or the cells. There are several approaches to tailor the rheological properties of photocrosslinkable hydrogels, such as varying the crosslinking time, light intensity, polymer fraction, crosslinker content or the degree of alkene substitution. Increasing the polymer fraction enhances the number of alkene groups available for reaction, potentially leading to increased RGD-peptide conjugation. Similarly, increasing the crosslinking time/light intensity could lead to a similar outcome as the UV dose to which hydrogels are subjected is higher. Both strategies often result in altered ligand density between hydrogels, influencing the hydrogel properties and cell fate [10, 43]. In this study, the crosslinking time, light intensity, polymer fraction and norbornene functionalization were maintained constant and the hydrogel crosslinking density was tailored by varying the content of MMP-peptide crosslinker. To evaluate the ability to precisely adjust the rheological properties, hydrogels were prepared with varying bulk concentration of MMP-peptide crosslinker (4, 5 and 6 mM), while maintaining constant the concentration of polymer (2.5 wt%) and RGD peptide (2 mM). As shown in **Figure 4.3A**, the rheological properties on the swollen state are dependent on the concentration of MMP-cleavable peptide used during the photopolymerization, with the shear elastic moduli varying between 70.03 ± 10.39 to 446.75 ± 35.66 Pa. Results show that higher MMP-cleavable peptide content increased the crosslink density and consequently the elastic modulus. To confirm such observations, the equilibrium mass swelling ratio of hydrogels was determined after 24h of incubation in PBS (**Figure 4.3B**). It was found that the swelling ratio decreases as the concentration of MMP-cleavable peptide increases, which correlates with the formation of a highly entangled and more crosslinked network. These data indicate that the

elastic modulus and swelling of low polymer fraction hydrogels can be tailored via modulation of MMP-degradable peptide content, which is in agreement with previous works [25].

Enzymatically degradable hydrogels sensitive to the action of MMPs are of particular interest for tissue regeneration because proteases play a key role in numerous biological processes during development and morphogenesis, including ECM remodelling, wound healing and angiogenesis [44, 45]. To confirm that thiol-ene hydrogels are susceptible to enzymatic degradation by collagenase type II, hydrogels with varying elastic moduli were incubated with the enzyme at a physiologically relevant concentration found during the wound healing [27] and their change in mass was determined as a function of time. It was found that all hydrogel formulations are sensitive to collagenase degradation and that the extent of degradation is dependent on the crosslinking density (**Figure 4.3C**). Hydrogels crosslinked with 4 mM of MMP-cleavable peptide were completely degraded after 3h of incubation, while hydrogels with 5 mM of MMP-cleavable peptide remained stable in solution for 5h of incubation. In contrast, highly crosslinked hydrogels (6 mM MMP-sensitive peptide) maintained structural integrity throughout the assay, clearly showing a crosslinking density-dependent degradation. Control hydrogels incubated in HBSS buffer alone exhibited minimal mass loss after 9h of incubation (**Supplementary Figure S4.6**), indicating that the degradation is specifically triggered by enzymatic stimuli. Due to the recent introduction of pectin-based hydrogels in the field of tissue engineering, evidence regarding the mechanisms underlying the clearance/degradation of pectin from the human body is still scarce. Since the degradation of pectin is mediated by several pectinases (e.g., pectate lyases, polygalacturonases) absent in the human body, the degradation of pectin hydrogels by collagenase could facilitate the polymer clearance upon implantation. As pectin polymer chains are crosslinked by the MMP-sensitive peptide, it is expected that the cleavage of the hydrogel network into soluble pectin chains facilitates the degradation/clearance of pectin via interaction with the complex proteolytic environment (e.g., physiological enzymes, cell-secreted proteases, pH and temperature) found *in vivo*.

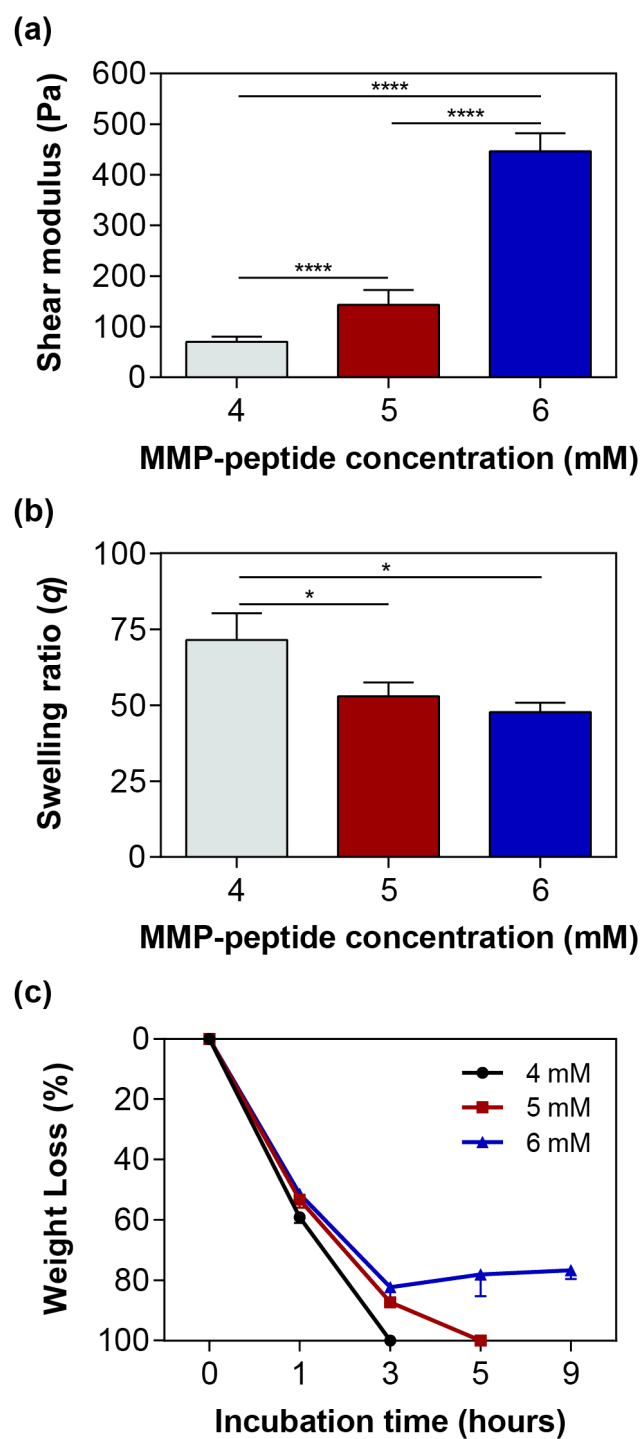


Figure 4.3. Physical and mechanical properties of MMP-degradable NorPEC hydrogels. (A) Influence of MMP-cleavable peptide concentration on the storage modulus (G') of photocrosslinked hydrogels. **(B)** Swelling of hydrogels upon overnight incubation in PBS. **(C)** *In vitro* degradation of hydrogels prepared with varying contents of MMP-degradable peptide in the presence of collagenase type II.

4.3.3. Chemically defined cell-instructive pectin hydrogels promote 3D cell attachment and spreading

A major challenge when using natural polymers as cellularized ECM-analogues relies on the difficulty of designing hydrogels with independently tuneable biochemical and biophysical properties, an important feature to precisely modulate cell functions [46, 47]. To decouple the influence of crosslinking density (MMP-cleavable peptide) from ligand density (RGD peptide) on the behaviour of embedded dermal fibroblasts, cell-laden hydrogels were produced with varying ligand density (0–2 mM), but using constant polymer concentration (2.5 wt%) and MMP-cleavable peptide content (5 mM). Live/Dead analysis showed that the majority of the cells remained alive after 7 days of culture, with marked differences on the morphology and distribution within the gel network (**Figure 4.4A**). The incorporation of RGD peptide conferred adhesiveness to the otherwise inert pectin network and was necessary to promote cell adhesion and spreading within the hydrogels. Fibroblasts cultured within RGD-functionalized hydrogels showed elongated morphology with major differences on the spreading and elongation as a function of the bulk RGD content. At day 7, cells within hydrogels containing 0.5 mM RGD displayed heterogeneous spreading at both the centre and periphery of the gels, while fibroblasts embedded within hydrogels with higher concentrations of RGD peptide (1 and 2 mM) were uniformly spread throughout the gel network (**Figure 4.4B**). In the absence of RGD, cells remained mostly round without spreading and lacking cell-cell contacts, though they remained metabolically active (**Supplementary Figure S4.7**). These results indicate that the peptide density determines the extent of cell spreading, which could be easily controlled by changing the bulk concentration of RGD peptide during the thiol-ene reaction. The influence of ligand density (RGD peptide) on cell spreading within thiol-ene 3D hydrogels has been investigated using several cell types [48-50]. For instance, Bott et al [49] showed that dermal fibroblasts embedded within MMP-degradable PEG hydrogels lacking cell-adhesion sites or containing the non-biologically active RDG peptide sequence remain round, while the tethering of RGD peptide promoted cell adhesion and spreading. In another work, Kyburz et al [48] reported that the adhesivity of MMP-degradable PEG hydrogels determines the spreading and migration of hMSCs in 3D. At 0 and 0.001 mM CRGDS concentrations embedded hMSCs remained round, while increasing the CRGDS concentration to 1.0 mM promoted a significant increase in cell spreading, elongation and migration. These authors hypothesized that increased network adhesivity facilitates cell attachment and spreading, providing the necessary traction for cells to migrate. In this work, RGD was used at a concentration of 2.0 mM in order to maximize the number of adhesion sites and promote uniform cell spreading within the hydrogel.

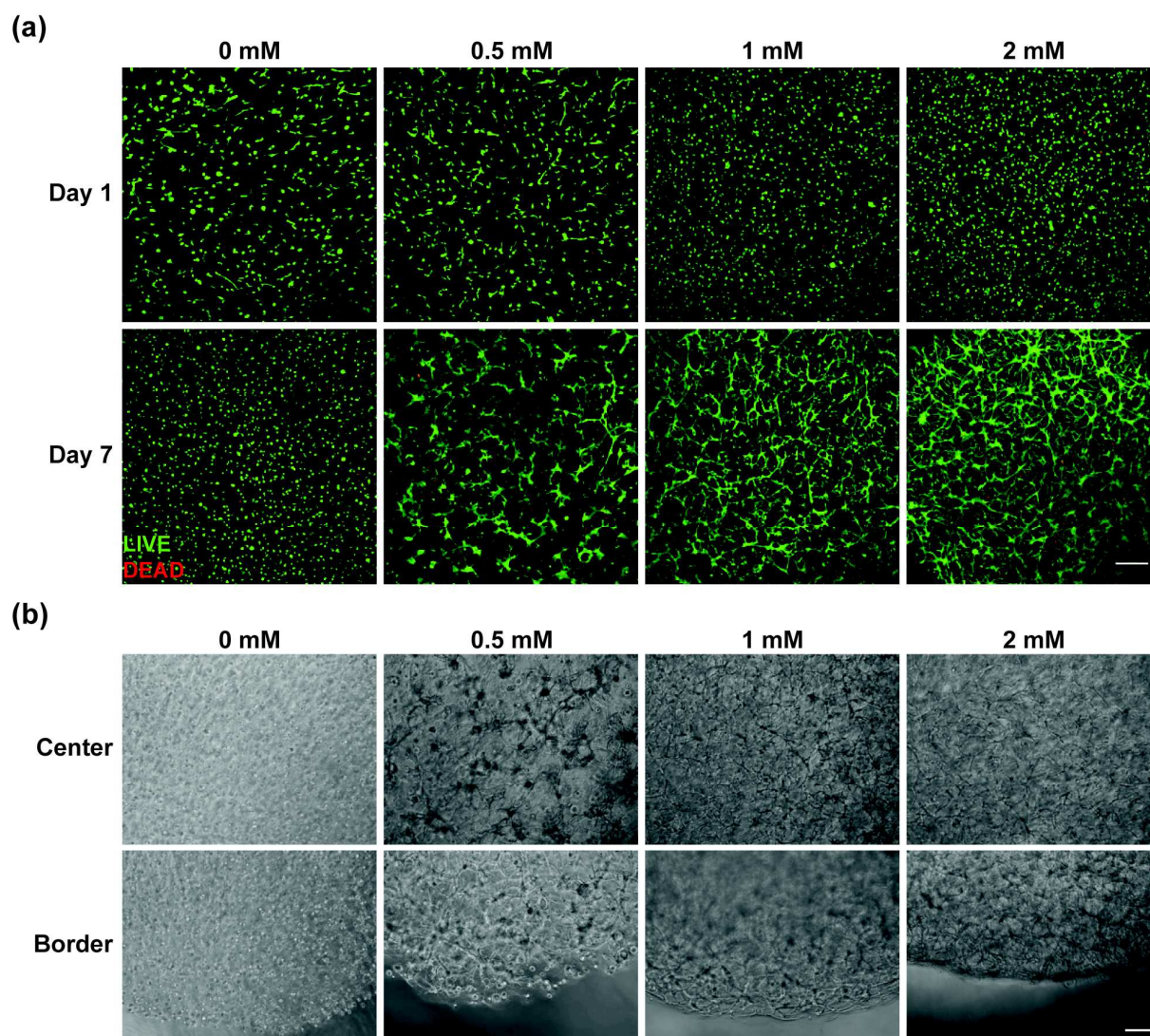


Figure 4.4. Influence of RGD peptide on dermal fibroblasts encapsulated within MMP-degradable NorPEC hydrogels. (A) Representative Live/dead images of fibroblasts embedded within 2.5 wt% NorPEC hydrogels (5 mM MMP peptide, 20s UV), showing the effect of bulk RGD concentration (0–2 mM) on cell viability and distribution within the hydrogels at day 7 (scale bar: 200 μ m). **(B)** Bright-field images showing the influence of RGD peptide content on the spreading of fibroblasts in the center and periphery of hydrogels at day 7 of culture (scale bar: 100 μ m).

To investigate the influence of matrix stiffness on cell behaviour, fibroblasts were embedded within MMP-degradable hydrogels (2.5 wt%, 2 mM RGD) of varying moduli. Adding the MMP-cleavable peptide at three different contents (4, 5 and 6 mM) resulted in the formation of hydrogels with low, medium and high crosslinking densities, respectively. Fibroblasts cultured within all hydrogel formulations remained metabolically active throughout 14 days of culture (**Supplementary Figure S4.8**) and extensively spread within the hydrogel network (**Figure 4.5A**). Major differences between the hydrogels were observed regarding

the time required for cells to spread, cell compaction and hydrogel contraction. At early time points (day 1), fibroblasts were round in stiffer hydrogels (5 and 6 mM MMP) and displayed elongated morphology in loosely crosslinked gels (4 mM MMP). At day 3, extensive cell spreading and elongation was observed in hydrogels with low and medium crosslinking density, while in hydrogels with high crosslinking density the majority of cells only start spreading, with few protrusions. At later time points (day 7), cells extensively spread within all hydrogels independently of the crosslinking density (**Supplementary Figure S4.9**). Fibroblasts embedded within MMP-degradable pectin hydrogels formed 3D interconnected multicellular networks and assumed a spindle-shaped morphology, characteristic of fibroblasts cultured within 3D environments [49]. Although MMP-degradable hydrogels supported extensive cell spreading, confocal images showed that cells cultured within stiffer hydrogels exhibit more pronounced compaction (**Supplementary Figure S4.9**), suggesting that the extent of cell compaction correlates with the hydrogel stiffness. To prove that differences in fibroblasts spreading and morphology were not a result of changes in the content of tethered RGD peptide during the thiol-ene photopolymerization, HPLC analysis was carried out to confirm that the conjugation efficiency was comparable between all hydrogel formulations (4 mM: $54.91 \pm 3.40\%$; 5 mM: $50.77 \pm 0.90\%$; 6 mM: $49.61 \pm 2.92\%$), as shown in **Figure 4.5B** and further confirmed using a fluorescently labelled RGD-peptide (**Supplementary Figure S4.10**). Results show that fibroblasts require more time to spread and remodel denser hydrogels, even in presence of MMP-cleavable peptide crosslinkers, due to the physical constraints imposed by the matrix. Our observations are in agreement with a previous work reporting a significant reduction on the percentage of hMSCs capable of elongate and migrate within thiol-ene MMP-degradable PEG hydrogels of increased crosslinking density [48].

As the rate of cell spreading, elongation and migration in 3D is dictated by both biochemical and biophysical cues [48], cell-laden hydrogels with varying crosslinking density were also cultured in the presence of a broad-spectrum MMP inhibitor (Marimastat) to assess whether cell spreading was exclusively dependent on MMP-mediated hydrogel degradation (**Supplementary Figure S4.11**). Fibroblasts displayed an elongated morphology within loosely crosslinked hydrogels throughout the 14 days of culture period, even in the presence of MMP inhibitor, suggesting that cells spread essentially by an MMP-independent mechanism (e.g., defects in the gel network). In contrast, cells embedded within medium or highly crosslinked hydrogels incubated with Marimastat failed to spread and remained mostly spherical with a few elongated cells located near the hydrogel surface. F-actin staining further confirmed that cells embedded within highly crosslinked hydrogels remained isolated and presented only minor protrusions (**Figure 4.5C**), indicating that cells are only able to

overcome the physical barrier of the matrix by enzymatic cleavage. Therefore, cell elongation within cell-degradable pectin hydrogels is determined not only by MMP-mediated degradation, but also by the hydrogel stiffness. For hydrogels with low crosslinking density ($G' = 70.03 \pm 10.39$ Pa), the stiffness was found to be a key parameter determining cell elongation, while in stiffer hydrogels ($G' > 143.09 \pm 29.70$ Pa) cell spreading was driven by MMP-mediated degradation. In a previous work using fully interpenetrating networks made of collagen-I and RGD-functionalized alginate with embedded dermal fibroblasts, it was found that cells fully spread within hydrogels of low storage modulus (50 Pa), but remained spherical when encapsulated in hydrogels of both intermediate (320 Pa) and high (1200 Pa) stiffness [51], which is in agreement to our observations regarding the effects of matrix stiffness on the response of dermal fibroblasts. The incorporation of MMP-cleavable peptides as part of the pectin hydrogel network allows embedded fibroblasts to locally degrade the surrounding matrix, which is essential to create space for spreading and elongation. Although cells require more time to degrade the matrix of highly crosslinked matrices, they are also able to fully spread in stiffer 3D hydrogels (446.80 ± 35.66 Pa), forming interconnected cellular networks throughout the hydrogel.

Fibroblasts play a key role during the healing of deep wounds, being involved in ECM synthesis, deposition and remodelling, while exerting forces towards wound contraction [52]. The contraction of cell-laden hydrogels was monitored during the culture period and assess whether the crosslinking density can be used to control dimensional changes of hydrogel network (**Figure 4.5D, E**). After three days of culture, only hydrogels crosslinked with 4 mM MMP-cleavable peptide shrank when compared to day 1, while at day 7 a significant reduction on the hydrogel's area was observed for all compositions. Loosely crosslinked hydrogels (4 mM) displayed the highest shrinkage degree, reaching 9.7% of their initial area at day 14. Hydrogels with medium and high crosslinking degree reached 24.3% and 36.4% of their initial area at the same culture time. Embedded fibroblasts were able to pull on the matrix and contract it in a matrix stiffness-dependent manner, as a result of contractile forces involved in cell attachment, elongation and migration [53]. These results showed that hydrogel contraction by dermal fibroblasts is linked to matrix stiffness, with higher stiffness correlating with both increased structural integrity and lower contraction degree. Thus, by using MMP-degradable pectin hydrogels of varying stiffness it's possible to modulate the contractility of embedded fibroblasts and associated matrix deformation.

During the healing of skin wounds, fibroblasts, keratinocytes, endothelial cells and inflammatory cells secrete a broad range of MMPs, which expression and activation is tightly regulated [54, 55]. MMPs play a pivotal role along the process, namely by changing the properties of the wound matrix to allow cell migration and new ECM deposition. In order to

evaluate whether fibroblasts embedded within MMP-degradable hydrogels secrete relevant MMPs for remodelling, the activity levels of two ubiquitous gelatinases (MMP-2 and MMP-9) involved in skin wound healing [54], were determined in culture medium by gelatin zymography at different culture times (**Figure 4.5F**). Zymography analysis clearly showed that cells produced MMP-2 (72 kDa) and MMP-9 (92 kDa), with higher expression of MMP-2. It was also found that the activity of MMP-2 increased from day 1 to day 3 of culture, which corresponds to the time period that fibroblasts start spreading within the gel network. Characteristic bands of MMP-9 were detected at low levels in conditioned media, indicating that embedded fibroblasts mostly express MMP-2, which is in agreement to previous works with dermal fibroblasts cultured in 3D hydrogels [49].

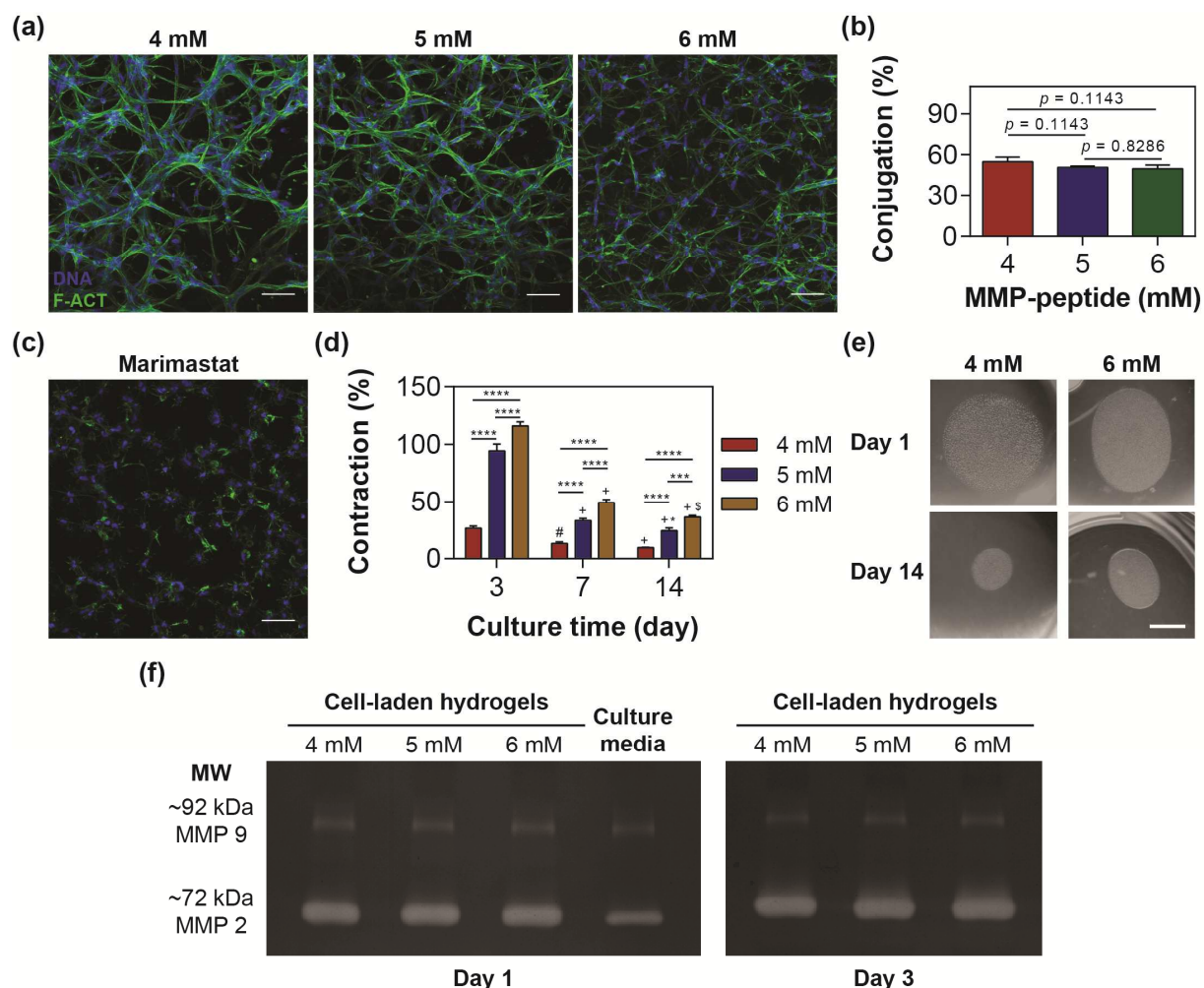


Figure 4.5. Cell encapsulation of dermal fibroblasts within MMP-degradable NorPEC hydrogels. (A) Representative confocal microscopy images detailing the influence of MMP-peptide content (4, 5 and 6 mM MMP-cleavable peptide, 2.5 wt% NorPEC, 2 mM RGD peptide, 20s UV) on the morphology and spatial distribution of fibroblasts stained for DAPI (blue) and F-actin (green) at day 14 (scale bar: 50 μm). (B) Influence of bulk MMP-degradable peptide content on the conjugation efficiency of RGD-

peptide during photopolymerization. **(C)** Representative confocal microscopy images of fibroblasts cultured within NorPEC hydrogels (2.5 wt%, 6 mM MMP, 2 mM RGD) in medium containing 50 μM of MMP-inhibitor Marimastat at day 7 (scale bar: 50 μm). **(D)** Effect of MMP-peptide content on the contraction of hydrogels during the culture period. Results are expressed as a percentage of area reduction compared to day 1. **(E)** Photographs showing the appearance of low and highly crosslinked hydrogels at day 1 and 14 of culture (scale bar: 2.5 mm). **(F)** Gelatin-zymograms of conditioned media collected at day 1 and 3. Data from contraction assays were analyzed using two-way ANOVA with Tukey's multiple comparisons test ($***p < 0.001$, $****p < 0.0001$); compared to day 3: $^+p < 0.0001$, $^\#p < 0.001$; compared to day 7: $*p < 0.01$, $^\$p < 0.001$.

4.3.4. Thiol-ene click pectin hydrogels support full-thickness skin formation

To demonstrate the potential of the MMP-degradable pectin hydrogels for skin repair and regeneration, dermal fibroblasts were embedded within pectin hydrogels of medium crosslinking density (2.5% NorPEC, 2 mM RGD, 5 mM MMP), cultured for 1 week and subsequently seeded with keratinocytes. After submerged culture for additional 1 week, cell-laden hydrogels were exposed to the air-liquid interface to promote the stratification of epidermis and characterized by histological and immunofluorescence analysis. Histological analyses depicted in **Figure 4.6A** clearly show that cell-instructive pectin hydrogels supported the *in vitro* formation of full-thickness skin, with morphological resemblance to the human skin. H&E staining showed that the dermal compartment is uniformly populated with elongated dermal fibroblasts, while a well-defined epidermis was formed on the top of the fibroblast-laden hydrogel. Keratinocytes formed a dense epidermal tissue after 14 days of ALI culture with marked differences on cell morphology as a function of their location in the epidermis. Basal keratinocytes in the close proximity to the dermal-like layer display a cuboidal shape, while most of the cells at the epidermis-air interface present a flattened morphology, which is characteristic of the differentiation and stratification of keratinocytes [56]. A higher number of flattened keratinocytes at the surface of the constructs could be observed at day 28 of ALI culture compared to day 14 (**Supplementary Figure S4.12a**). Notably, the thickness of the epidermis-like layer ($\sim 120 \mu\text{m}$) is within the range of native human epidermis, which is in the range of 60–150 μm , depending on the location in the human body [57]. Masson's trichrome staining (**Figure 4.6B**) revealed that fibroblasts were secreting collagen, a key ECM component of skin tissue, with more intense blue staining (increased deposition) from day 14 to day 28 of ALI culture (**Supplementary Figure S4.12b**). Immunohistological analysis also showed the presence of specific markers associated to epidermal differentiation and proliferation, including cytokeratin (**Figure 4.6C**) and Ki67 (**Supplementary Figure S4.13**), respectively. The presence of Ki67 proliferation marker mainly in the suprabasal layers of epidermis correlates with the differentiation state of the

keratinocytes, as in native skin only keratinocytes in the *stratum basale* maintain proliferative activity [56]. To confirm that the presence of fibroblasts is limited to the dermal compartment, sections were stained against vimentin, a cytoskeletal protein characteristic of fibroblasts (**Figure 4.6D**). No cell invasion across dermal and epidermal layers was observed, since the presence of cytokeratin- and vimentin-positive cells was limited to the epidermal and dermal layers, respectively. Key characteristic markers of ECM production in dermal compartment were also identified such as collagen type-I (**Figure 4.6E**) and fibronectin (**Figure 4.6F**), indicating that fibroblasts were secreting essential ECM components for new dermal tissue formation. Although these results clearly demonstrate that protease-degradable pectin hydrogels support the *in vitro* formation of skin equivalents, a limitation of the present study relies on the use of immortalized keratinocyte cell line (HaCaT) to generate the epidermal layer instead of primary keratinocytes. It is well recognized that immortalized keratinocytes undergo gradual loss of cell phenotype and function throughout passaging and culture, which can delay or even compromise the stratification and terminal differentiation [58]. However, we anticipate that the use of primary keratinocytes can potentially address this issue.

In a future work we will focus on the detailed characterization of the performance of MMP-sensitive pectin hydrogels in skin formation and adhesion to biological tissues. The ability of MMP-degradable pectin hydrogels to support the *in vitro* skin formation will be compared to MMP-insensitive pectin hydrogels (e.g., DTT, non-degradable CGDQGIAGFC peptide crosslinker) and standard constructs for skin tissue engineering (e.g., collagen, alginate) to elucidate the benefits of the proposed hydrogel. The adhesion of hydrogels to the surrounding biological tissues is challenging in wound healing as it requires the establishment of chemical bonds between the hydrogel and the tissue surface for sufficient bonding strength. *In situ* photopolymerizable hydrogels are particularly advantageous for wound healing as they can be formed under clinically safe 365 nm light irradiation, conform to the wound bed, and depending on the chemical composition, can enhance the interaction with the tissue surface promoting better integration [59]. The developed MMP-sensitive pectin hydrogel exhibits key properties for wound healing such as fast gelation (**Supplementary Figure S14**) and the ability to promote cell spreading, ECM deposition and *in vitro* skin formation. Pectin hydrogel also contains multiple domains that bind to cell-surface receptors, with potential to promote subsequent cell attachment and tissue integration. In addition, the carboxylic groups present in the pectin backbone can also contribute for tissue adhesion through interaction with amino groups [39]. In case of poor hydrogel adhesion and integration, the chemical versatility of pectin allows for easy modification with functional groups (e.g., aldehydes) capable of reacting with the amino groups present on the tissue surface. Alternative biomimetic strategies to improve the tissue

adhesion can also be translated to pectin hydrogels, including the functionalization with mussel adhesive proteins (MAPs) containing the amino acid 3,4-dihydroxyphenylalanine (DOPA). Through oxidative crosslinking or metal chelation, the catechol moiety in DOPA amino acid chain covalently crosslinks both to itself and to biologically relevant nucleophiles (e.g., primary amines and thiols), allowing better tissue adhesion and improving haemostasis [60]. Due to the poor yield in the isolation and purification of MAPs, nature-inspired adhesive hydrogels have been mostly designed by incorporating DOPA-based peptides and simplified DOPA alternatives such as dopamine and catechol functional groups [61-63]. Mussel-inspired functionalization represents an attractive strategy to improve the wet adhesion of hydrogels with particular interest for *in situ* skin tissue engineering.

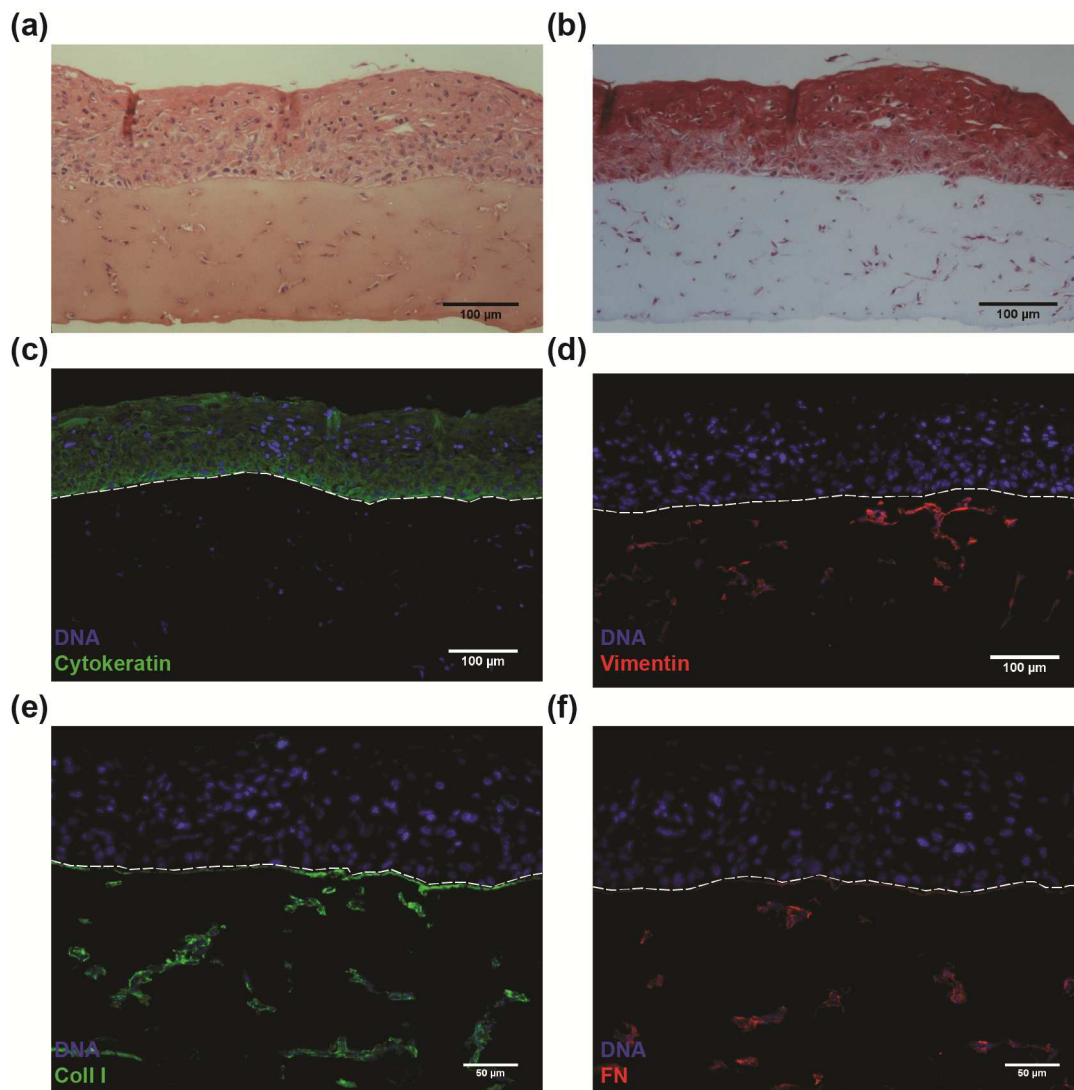


Figure 4.6. Histological and morphological characterization of skin equivalents formed using the protease-degradable pectin hydrogels after 14 days of differentiation at the ALI culture. (A) Haematoxylin & eosin and (B) Masson trichrome staining's showing the histology of skin equivalents.

Immunostaining of paraffin embedded samples using antibodies directed against **(C)** cytokeratin (keratinocytes), **(D)** vimentin (fibroblasts), **(E)** collagen type-I (Coll I) and **(F)** fibronectin (FN). Dash line delineates the interface between the dermal and epidermal layers.

4.4. Conclusions

A simple, fast and robust method for the synthesis of norbornene-functionalized pectin was developed and applied for the fabrication of cell-laden MMP-cleavable hydrogels through photoinitiated thiol-ene reaction. Step-growth pectin hydrogels were rapidly formed upon exposure to UV light for very short irradiation times, without compromising the viability of embedded dermal fibroblasts. By selecting suitable MMP-degradable peptide crosslinkers and pendant cell-adhesive peptides, biofunctional hydrogels were engineered with varying levels of crosslinking density, resulting in distinct biological responses. Embedded fibroblasts displayed elongated morphology and less compaction in more permissive hydrogels, contracting the matrix in a higher extent. Cell-instructive hydrogels with embedded dermal fibroblasts and seeded with keratinocytes supported the *in vitro* formation of full-thickness skin resembling the architecture and morphology of human skin. Two distinct regions corresponding to the dermal and epidermal layers were formed, showing the presence of specific markers associated to proliferation and ECM deposition. This versatile hydrogel system allows for independent tuning of biochemical and biophysical cues of the gel network, allowing the fabrication of chemically defined 3D matrices from pectin as a natural polymer. Overall, this study demonstrates the potential of novel biofunctionalized, click pectin hydrogels for skin tissue engineering applications.

4.5. Acknowledgements

This work was supported by the European Regional Development Fund (ERDF) through the COMPETE 2020 - Operational Programme for Competitiveness and Internationalization (POCI), Norte Portugal Regional Operational Programme (NORTE 2020), under the PORTUGAL 2020 Partnership Agreement, and by Portuguese funds through Portuguese Foundation for Science and Technology (FCT) in the framework of the project Ref. PTDC/BBB-ECT/2145/2014. R.P. and C.B. thank FCT for the doctoral grant SFRH/BD/91151/2012 and the FCT Investigator research position IF/00296/2015 (FCT and POPH/ESF), respectively. The authors acknowledge Mariana Andrade from CEMUP (Centro de Materiais da Universidade do Porto) for the ¹H NMR analyses, Dr Frederico Silva from B2Tech (Biochemical and Biophysical Technologies, i3S) for the support with HPLC

analyses, and Dr Silvia Bidarra from Biomaterials for Multistage Drug & Cell Delivery Group (i3S) for the support with gelatin zymography.

4.6. References

- [1] S.A. Eming, P. Martin, M. Tomic-Canic, Wound repair and regeneration: mechanisms, signaling, and translation, *Sci Transl Med* 6 (2014) 265sr6.
- [2] R.F. Pereira, C.C. Barrias, P.L. Granja, P.J. Bartolo, Advanced biofabrication strategies for skin regeneration and repair, *Nanomedicine (Lond)* 8 (2013) 603-21.
- [3] R.F. Pereira, P.J. Bartolo, Traditional Therapies for Skin Wound Healing, *Adv Wound Care (New Rochelle)* 5 (2016) 208-229.
- [4] A.S. Klar, S. Guven, T. Biedermann, J. Luginbuhl, S. Bottcher-Haberzeth, C. Meuli-Simmen, M. Meuli, I. Martin, A. Scherberich, E. Reichmann, Tissue-engineered dermo-epidermal skin grafts prevascularized with adipose-derived cells, *Biomaterials* 35 (2014) 5065-78.
- [5] G. Sun, X. Zhang, Y.I. Shen, R. Sebastian, L.E. Dickinson, K. Fox-Talbot, M. Reinblatt, C. Steenbergen, J.W. Harmon, S. Gerecht, Dextran hydrogel scaffolds enhance angiogenic responses and promote complete skin regeneration during burn wound healing, *Proc Natl Acad Sci U S A* 108 (2011) 20976-81.
- [6] C. Huang, H. Orbay, M. Tobita, M. Miyamoto, Y. Tabata, H. Hyakusoku, H. Mizuno, Proapoptotic effect of control-released basic fibroblast growth factor on skin wound healing in a diabetic mouse model, *Wound Repair Regen* 24 (2016) 65-74.
- [7] K.B. Fonseca, P.L. Granja, C.C. Barrias, Engineering proteolytically-degradable artificial extracellular matrices, *Prog. Polym. Sci.* 39 (2014) 2010-2029.
- [8] E. Jabbari, J. Leijten, Q. Xu, A. Khademhosseini, The matrix reloaded: the evolution of regenerative hydrogels, *Mater. Today* 19 (2016) 190-196.
- [9] M.V. Tsurkan, K. Chwalek, S. Prokoph, A. Zieris, K.R. Levental, U. Freudenberg, C. Werner, Defined polymer-peptide conjugates to form cell-instructive starPEG-heparin matrices in situ, *Adv. Mater.* 25 (2013) 2606-10.
- [10] B.D. Fairbanks, M.P. Schwartz, A.E. Halevi, C.R. Nuttelman, C.N. Bowman, K.S. Anseth, A Versatile Synthetic Extracellular Matrix Mimic via Thiol-Norbornene Photopolymerization, *Adv. Mater.* 21 (2009) 5005-5010.
- [11] K.B. Fonseca, D.B. Gomes, K. Lee, S.G. Santos, A. Sousa, E.A. Silva, D.J. Mooney, P.L. Granja, C.C. Barrias, Injectable MMP-sensitive alginate hydrogels as hMSC delivery systems, *Biomacromolecules* 15 (2014) 380-90.

- [12] T. Tokatlian, C. Cam, T. Segura, Porous hyaluronic acid hydrogels for localized nonviral DNA delivery in a diabetic wound healing model, *Adv Healthc Mater* 4 (2015) 1084-91.
- [13] F. Munarin, M.C. Tanzi, P. Petrini, Advances in biomedical applications of pectin gels, *Int. J. Biol. Macromol.* 51 (2012) 681-9.
- [14] F. Munarin, S.G. Guerreiro, M.A. Grellier, M.C. Tanzi, M.A. Barbosa, P. Petrini, P.L. Granja, Pectin-based injectable biomaterials for bone tissue engineering, *Biomacromolecules* 12 (2011) 568-77.
- [15] P. Coimbra, P. Ferreira, H.C. de Sousa, P. Batista, M.A. Rodrigues, I.J. Correia, M.H. Gil, Preparation and chemical and biological characterization of a pectin/chitosan polyelectrolyte complex scaffold for possible bone tissue engineering applications, *Int. J. Biol. Macromol.* 48 (2011) 112-8.
- [16] S.C. Neves, D.B. Gomes, A. Sousa, S.J. Bidarra, P. Petrini, L. Moroni, C.C. Barrias, P.L. Granja, Biofunctionalized pectin hydrogels as 3D cellular microenvironments, *J. Mater. Chem. B* 3 (2015) 2096-2108.
- [17] F. Munarin, P. Petrini, M.C. Tanzi, M.A. Barbosa, P.L. Granja, Biofunctional chemically modified pectin for cell delivery, *Soft Matter* 8 (2012) 4731.
- [18] P.M. Kharkar, K.L. Kiick, A.M. Kloxin, Designing degradable hydrogels for orthogonal control of cell microenvironments, *Chem. Soc. Rev.* 42 (2013) 7335-72.
- [19] R.F. Pereira, P.J. Bártolo, 3D Photo-Fabrication for Tissue Engineering and Drug Delivery, *Engineering* 1 (2015) 90-112.
- [20] M.W. Tibbitt, A.M. Kloxin, L. Sawicki, K.S. Anseth, Mechanical Properties and Degradation of Chain and Step Polymerized Photodegradable Hydrogels, *Macromolecules* 46 (2013) 2785-2792.
- [21] J.J. Roberts, S.J. Bryant, Comparison of photopolymerizable thiol-ene PEG and acrylate-based PEG hydrogels for cartilage development, *Biomaterials* 34 (2013) 9969-79.
- [22] C.C. Lin, C.S. Ki, H. Shih, Thiol-norbornene photo-click hydrogels for tissue engineering applications, *J. Appl. Polym. Sci.* 132 (2015) 41563.
- [23] W.M. Gramlich, I.L. Kim, J.A. Burdick, Synthesis and orthogonal photopatterning of hyaluronic acid hydrogels with thiol-norbornene chemistry, *Biomaterials* 34 (2013) 9803-11.
- [24] R.M. Desai, S.T. Koshy, S.A. Hilderbrand, D.J. Mooney, N.S. Joshi, Versatile click alginate hydrogels crosslinked via tetrazine–norbornene chemistry, *Biomaterials* 50 (2015) 30-37.
- [25] K.M. Mabry, R.L. Lawrence, K.S. Anseth, Dynamic stiffening of poly(ethylene glycol)-based hydrogels to direct valvular interstitial cell phenotype in a three-dimensional environment, *Biomaterials* 49 (2015) 47-56.

- [26] R.F. Pereira, A. Sousa, C.C. Barrias, P.J. Bártolo, P.L. Granja, R.F. Pereira, A. Sousa, C.C. Barrias, P.J. Bártolo, P.L. Granja, A single-component hydrogel bioink for bioprinting of bioengineered 3D constructs for dermal tissue engineering, *Mater Horiz* 5 (2018) 1100-1111.
- [27] M.S. Agren, C.J. Taplin, J.F. Woessner, Jr., W.H. Eaglstein, P.M. Mertz, Collagenase in wound healing: effect of wound age and type, *J Invest Dermatol* 99 (1992) 709-14.
- [28] P. Gangatirkar, S. Paquet-Fifield, A. Li, R. Rossi, P. Kaur, Establishment of 3D organotypic cultures using human neonatal epidermal cells, *Nat. Protocols* 2 (2007) 178-186.
- [29] T.M. Roper, C.A. Guymon, E.S. Jönsson, C.E. Hoyle, Influence of the alkene structure on the mechanism and kinetics of thiol-alkene photopolymerizations with real-time infrared spectroscopy, *J. Polym. Sci., Part A: Polym. Chem.* 42 (2004) 6283-6298.
- [30] C.E. Hoyle, C.N. Bowman, Thiol-ene click chemistry, *Angew. Chem. Int. Ed. Engl.* 49 (2010) 1540-73.
- [31] B.H. Northrop, R.N. Coffey, Thiol-ene click chemistry: computational and kinetic analysis of the influence of alkene functionality, *J. Am. Chem. Soc.* 134 (2012) 13804-17.
- [32] Z. Muñoz, H. Shih, C.-C. Lin, Gelatin hydrogels formed by orthogonal thiol–norbornene photochemistry for cell encapsulation, *Biomater. Sci.* 2 (2014) 1063-1072.
- [33] M. Bracher, D. Bezuidenhout, M.P. Lutolf, T. Franz, M. Sun, P. Zilla, N.H. Davies, Cell specific ingrowth hydrogels, *Biomaterials* 34 (2013) 6797-803.
- [34] A.K. Jha, K.M. Tharp, S. Browne, J. Ye, A. Stahl, Y. Yeghiazarians, K.E. Healy, Matrix metalloproteinase-13 mediated degradation of hyaluronic acid-based matrices orchestrates stem cell engraftment through vascular integration, *Biomaterials* 89 (2016) 136-47.
- [35] J. Patterson, J.A. Hubbell, Enhanced proteolytic degradation of molecularly engineered PEG hydrogels in response to MMP-1 and MMP-2, *Biomaterials* 31 (2010) 7836-45.
- [36] A.A. Tandara, T.A. Mustoe, MMP- and TIMP-secretion by human cutaneous keratinocytes and fibroblasts--impact of coculture and hydration, *J Plast Reconstr Aesthet Surg* 64 (2011) 108-16.
- [37] J.A. Rowley, G. Madlambayan, D.J. Mooney, Alginate hydrogels as synthetic extracellular matrix materials, *Biomaterials* 20 (1999) 45-53.
- [38] T.T. Lee, J.R. García, J.I. Paez, A. Singh, E.A. Phelps, S. Weis, Z. Shafiq, A. Shekaran, A. del Campo, A.J. García, Light-triggered in vivo activation of adhesive peptides regulates cell adhesion, inflammation and vascularization of biomaterials, *Nat Mater* 14 (2015) 352-360.
- [39] P.A. Markov, N.S. Krachkovsky, E.A. Durnev, E.A. Martinson, S.G. Litvinets, S.V. Popov, Mechanical properties, structure, bioadhesion, and biocompatibility of pectin hydrogels, *J Biomed Mater Res A* 105 (2017) 2572-2581.

- [40] A.D. Rouillard, C.M. Berglund, J.Y. Lee, W.J. Polacheck, Y. Tsui, L.J. Bonassar, B.J. Kirby, Methods for photocrosslinking alginate hydrogel scaffolds with high cell viability, *Tissue Eng Part C Methods* 17 (2011) 173-9.
- [41] P. Occhetta, R. Visone, L. Russo, L. Cipolla, M. Moretti, M. Rasponi, VA-086 methacrylate gelatine photopolymerizable hydrogels: A parametric study for highly biocompatible 3D cell embedding, *J Biomed Mater Res A* 103 (2015) 2109-17.
- [42] E.E. Coates, C.N. Riggan, J.P. Fisher, Photocrosslinked alginate with hyaluronic acid hydrogels as vehicles for mesenchymal stem cell encapsulation and chondrogenesis, *J Biomed Mater Res A* 101 (2013) 1962-70.
- [43] S.P. Zustiak, R. Durbal, J.B. Leach, Influence of cell-adhesive peptide ligands on poly(ethylene glycol) hydrogel physical, mechanical and transport properties, *Acta Biomaterialia* 6 (2010) 3404-3414.
- [44] C. Bonnans, J. Chou, Z. Werb, Remodelling the extracellular matrix in development and disease, *Nat Rev Mol Cell Biol* 15 (2014) 786-801.
- [45] A. Page-McCaw, A.J. Ewald, Z. Werb, Matrix metalloproteinases and the regulation of tissue remodelling, *Nat Rev Mol Cell Biol* 8 (2007) 221-33.
- [46] R. Cruz-Acuna, A.J. Garcia, Synthetic hydrogels mimicking basement membrane matrices to promote cell-matrix interactions, *Matrix Biol.* 57-58 (2017) 324-333.
- [47] J. Patterson, M.M. Martino, J.A. Hubbell, Biomimetic materials in tissue engineering, *Mater. Today* 13 (2010) 14-22.
- [48] K.A. Kyburz, K.S. Anseth, Three-dimensional hMSC motility within peptide-functionalized PEG-based hydrogels of varying adhesivity and crosslinking density, *Acta Biomater* 9 (2013) 6381-92.
- [49] K. Bott, Z. Upton, K. Schrobback, M. Ehrbar, J.A. Hubbell, M.P. Lutolf, S.C. Rizzi, The effect of matrix characteristics on fibroblast proliferation in 3D gels, *Biomaterials* 31 (2010) 8454-64.
- [50] M.P. Schwartz, B.D. Fairbanks, R.E. Rogers, R. Rangarajan, M.H. Zaman, K.S. Anseth, A synthetic strategy for mimicking the extracellular matrix provides new insight about tumor cell migration, *Integr Biol (Camb)* 2 (2010) 32-40.
- [51] C. Branco da Cunha, D.D. Klumpers, W.A. Li, S.T. Koshy, J.C. Weaver, O. Chaudhuri, P.L. Granja, D.J. Mooney, Influence of the stiffness of three-dimensional alginate/collagen-I interpenetrating networks on fibroblast biology, *Biomaterials* 35 (2014) 8927-36.
- [52] P. Bainbridge, Wound healing and the role of fibroblasts, *J Wound Care* 22 (2013) 407-8, 410-12.
- [53] M. Eastwood, R. Porter, U. Khan, G. McGrouther, R. Brown, Quantitative analysis of collagen gel contractile forces generated by dermal fibroblasts and the relationship to cell morphology, *J. Cell. Physiol.* 166 (1996) 33-42.

- [54] M.P. Caley, V.L. Martins, E.A. O'Toole, Metalloproteinases and Wound Healing, *Adv Wound Care (New Rochelle)* 4 (2015) 225-234.
- [55] R. Lobmann, A. Ambrosch, G. Schultz, K. Waldmann, S. Schiweck, H. Lehnert, Expression of matrix-metalloproteinases and their inhibitors in the wounds of diabetic and non-diabetic patients, *Diabetologia* 45 (2002) 1011-6.
- [56] A. Baroni, E. Buommino, V. De Gregorio, E. Ruocco, V. Ruocco, R. Wolf, Structure and function of the epidermis related to barrier properties, *Clin Dermatol* 30 (2012) 257-62.
- [57] M.J. Koehler, T. Vogel, P. Elsner, K. Konig, R. Buckle, M. Kaatz, In vivo measurement of the human epidermal thickness in different localizations by multiphoton laser tomography, *Skin Res Technol* 16 (2010) 259-64.
- [58] N. Maas-Szabowski, A. Starker, N.E. Fusenig, Epidermal tissue regeneration and stromal interaction in HaCaT cells is initiated by TGF- α , *J. Cell Sci.* 116 (2003) 2937-48.
- [59] Y. Yang, J. Zhang, Z. Liu, Q. Lin, X. Liu, C. Bao, Y. Wang, L. Zhu, Tissue-Integratable and Biocompatible Photogelation by the Imine Crosslinking Reaction, *Adv. Mater.* 28 (2016) 2724-2730.
- [60] M. Shin, S.-G. Park, B.-C. Oh, K. Kim, S. Jo, M.S. Lee, S.S. Oh, S.-H. Hong, E.-C. Shin, K.-S. Kim, S.-W. Kang, H. Lee, Complete prevention of blood loss with self-sealing haemostatic needles, *Nat Mater* 16 (2017) 147-152.
- [61] R. Wang, J. Li, W. Chen, T. Xu, S. Yun, Z. Xu, Z. Xu, T. Sato, B. Chi, H. Xu, A Biomimetic Mussel-Inspired ϵ -Poly-L-lysine Hydrogel with Robust Tissue-Anchor and Anti-Infection Capacity, *Adv. Funct. Mater.* 27 (2017) 1604894.
- [62] C. Fan, J. Fu, W. Zhu, D.-A. Wang, A mussel-inspired double-crosslinked tissue adhesive intended for internal medical use, *Acta Biomater* 33 (2016) 51-63.
- [63] B.P. Lee, C.-Y. Chao, F.N. Nunalee, E. Motan, K.R. Shull, P.B. Messersmith, Rapid Gel Formation and Adhesion in Photocurable and Biodegradable Block Copolymers with High DOPA Content, *Macromolecules* 39 (2006) 1740-1748.

4.7. Supplementary Information

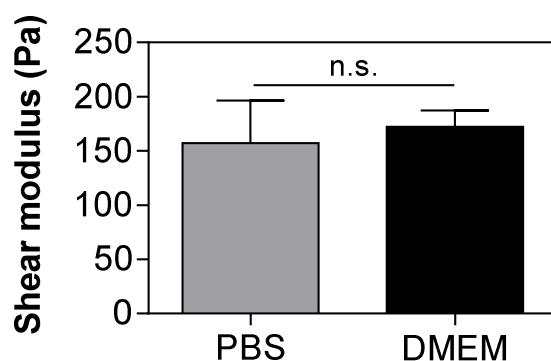


Figure S4.1. Effect of calcium ions on the shear elastic moduli (G') of NorPEC hydrogels (2.5wt%, 5 mM MMP, 2 mM RGD) prepared with 20s of UV exposure (7 mW/cm^2). Hydrogels were incubated in PBS (no calcium) and DMEM (31966-021, Gibco, $1.8 \text{ mM CaCl}_2 \cdot 2\text{H}_2\text{O}$) culture medium supplemented with 10% FBS for 24h and the mechanical properties tested through rheological analysis. No statistically significant changes were observed in the G' of hydrogels incubated in both the presence and absence of calcium (Mann-Whitney test $p = 0.1059$). These data suggests that the neutralization of carboxylate groups with sodium ions precludes the occurrence of secondary ionic gelation between the carboxylic groups on pectin and calcium ions, at tested concentration of calcium.

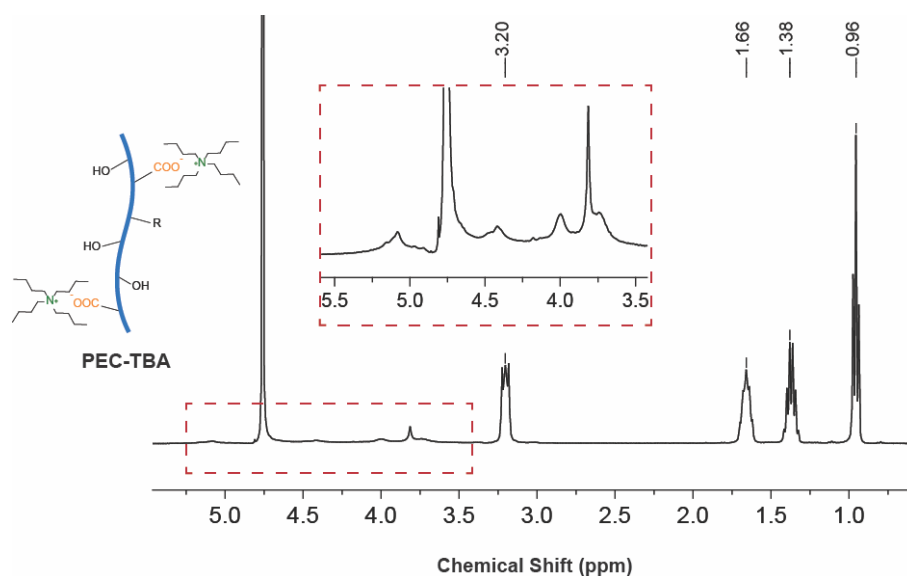


Figure S4.2. Representative ^1H NMR spectrum (D_2O , 400 MHz) of lipophilic TBA salt of pectin (PEC-TBA) after 3h treatment with Dowex ion exchange resin and neutralization with tetrabutylammonium, resulting in four new peaks that correspond to the butyl groups (3.20, 1.66, 1.38, and 0.96 ppm). Insert shows the native protons on pectin backbone.

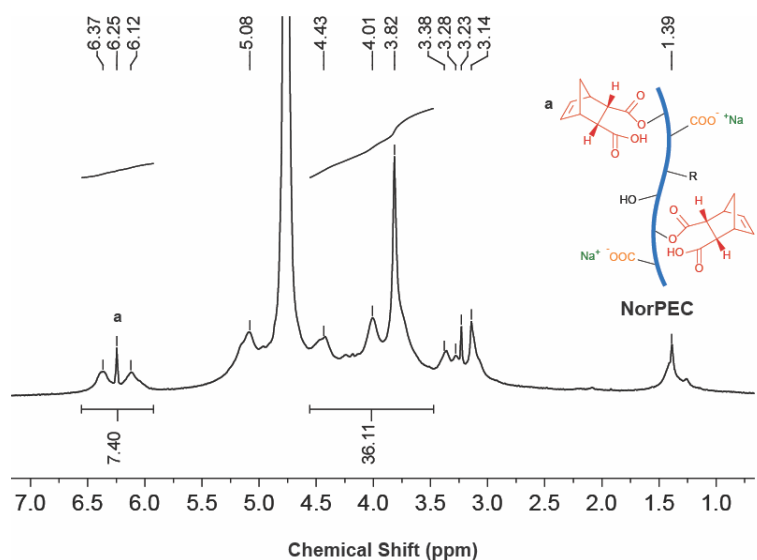


Figure S4.3. Representative ^1H NMR spectrum (D_2O , 400 MHz) of norbornene-functionalized pectin (NorPEC) after 1h reaction in DMSO. Substitution of pectin is calculated from the ratio of norbornene integrals (6.12–6.37 ppm) to native protons in pectin (4.56–3.47 ppm).

Macromer purification

Several purification steps were carried out to ensure the removal of unreacted reagent and/or by-products, including (i) dialysis, (ii) activated charcoal and (iii) sterile filtration ($0.20\mu\text{m}$). Dialysis was performed using MWCO 3.5 kDa dialysis membrane to ensure the removal of carbic anhydride (CA), which Mw is 164.16 Da. After dialysis, the polymer solution was treated with activated charcoal to adsorb potential by-products, followed by centrifugation and sterile filtration. Since CA has poor solubility in aqueous solutions at physiological pH (e.g., PBS, pH 7.4), the chemical modification was performed in DMSO with two major objectives: (1) reduce the amount of CA needed for chemical modification and increase the reaction efficiency; (2) facilitate the removal of unreacted reagent through water precipitation during the dialysis step, followed by centrifugation. Thus, based on the solubility of CA and purification procedures carried out, it is expected complete removal of unreacted CA. This was further confirmed by ^1H NMR analysis of both pure CA and norbornene-modified pectin. Deuterated methanol (CD_3OD) was added to pure CA to ensure complete dissolution and confirm the presence of characteristic peaks of native protons (peak attribution was done based on published data [1]). After chemical reaction, the spectrum of norbornene-functionalized pectin was recorded and several alterations were observed regarding the multiplicity of CA characteristic peaks and chemical shift of protons in the vicinity of reactive centre, indicating the occurrence of chemical reaction with consumption of CA.

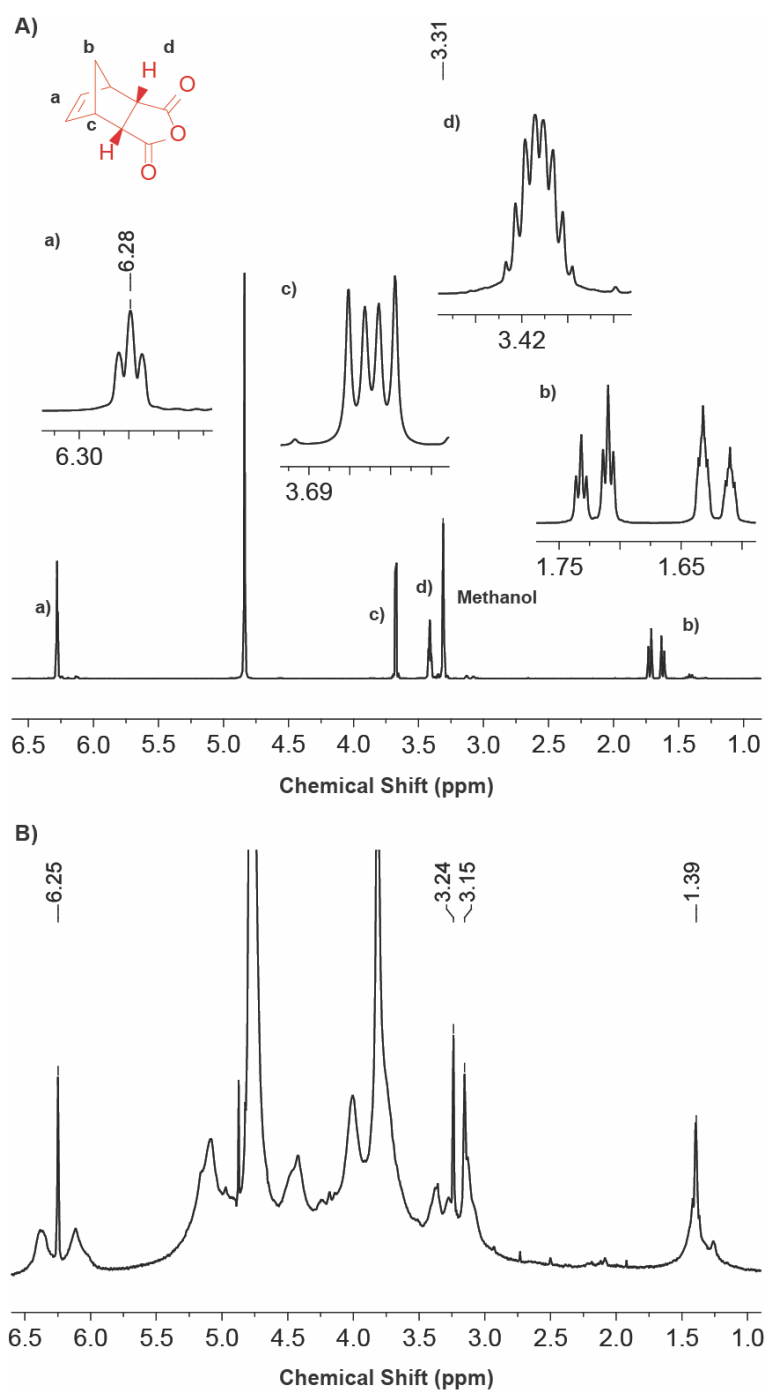


Figure S4.4. Representative ^1H NMR spectra of both **(A)** pure carbic anhydride (CD_3OD , 400 MHz) and **(B)** norbornene-functionalized pectin (D_2O , 400 MHz).

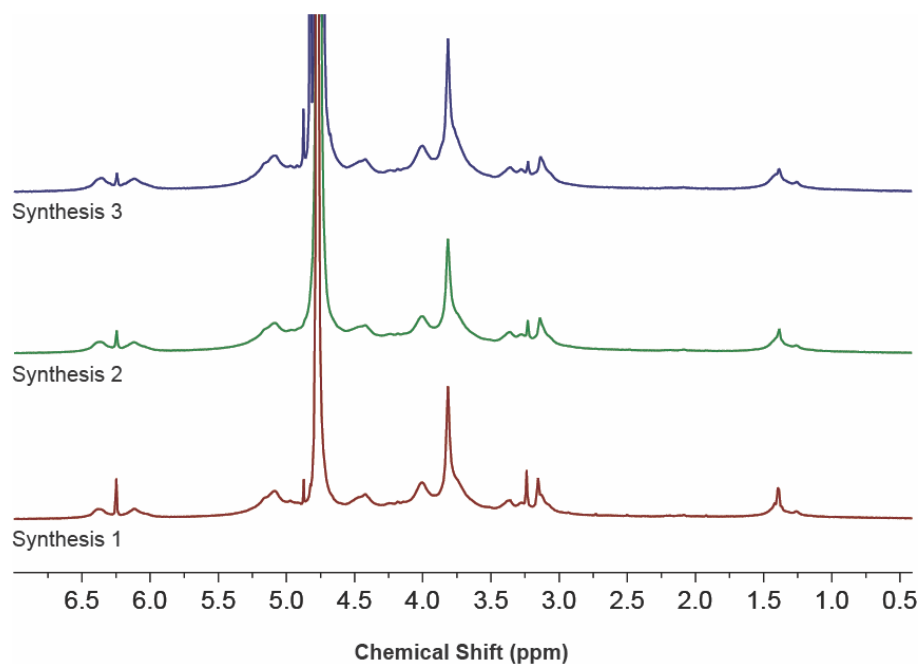


Figure S4.5. Representative ^1H NMR spectrum (D_2O , 400 MHz) of norbornene-functionalized pectin (NorPEC). Macromers were obtained through three independent syntheses to confirm the reproducibility and robustness of chemical reaction. No significant alterations between NorPEC macromers were verified regarding both the degree of substitution (synthesis 1: 20.5%; synthesis 2: 20.1%; synthesis 3: 19.4%) and chemical shift of carbon-carbon double bond (synthesis 1: 6.12–6.37 ppm; synthesis 2: 6.12–6.36 ppm; synthesis 3: 6.11–6.37 ppm).

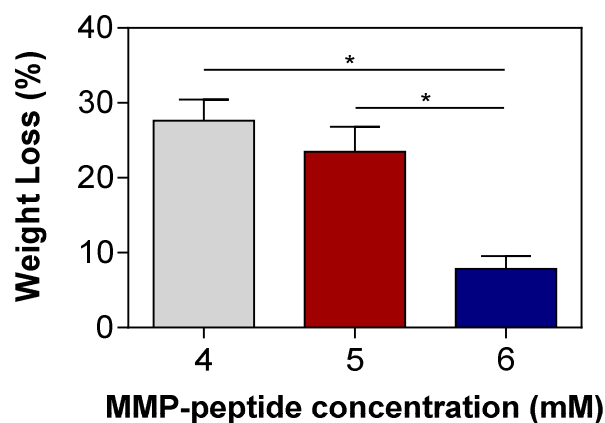


Figure S4.6. Weight loss of photocrosslinked pectin hydrogels incubated in HBSS for 9h at 37°C. Data were analysed using Mann-Whitney test (* $p < 0.05$).

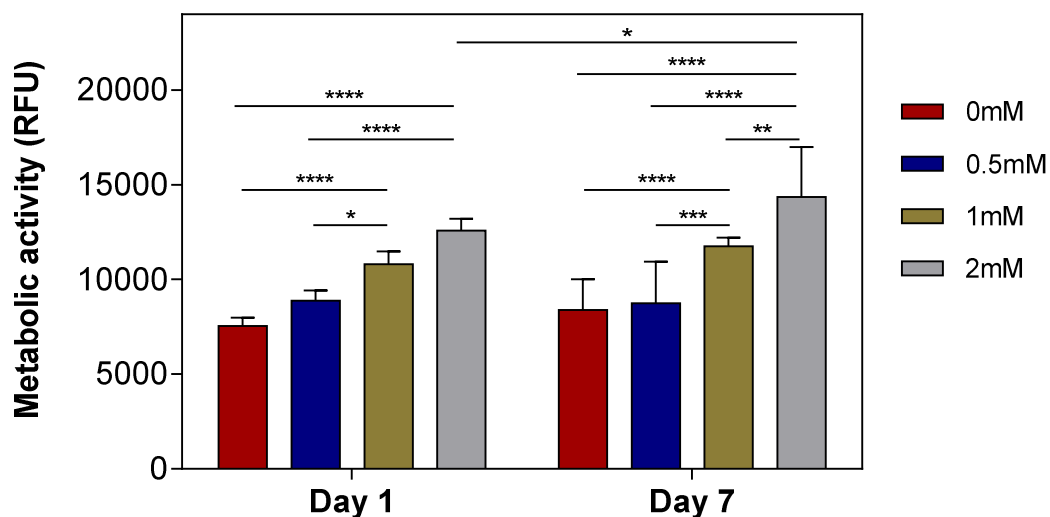


Figure S4.7. Metabolic activity of dermal fibroblasts embedded in NorPEC hydrogels containing varying concentrations of RGD peptide. Data were analysed using two-way ANOVA with Bonferroni's multiple comparisons test ($*p < 0.05$, $**p < 0.01$, $***p < 0.001$, $****p < 0.0001$).

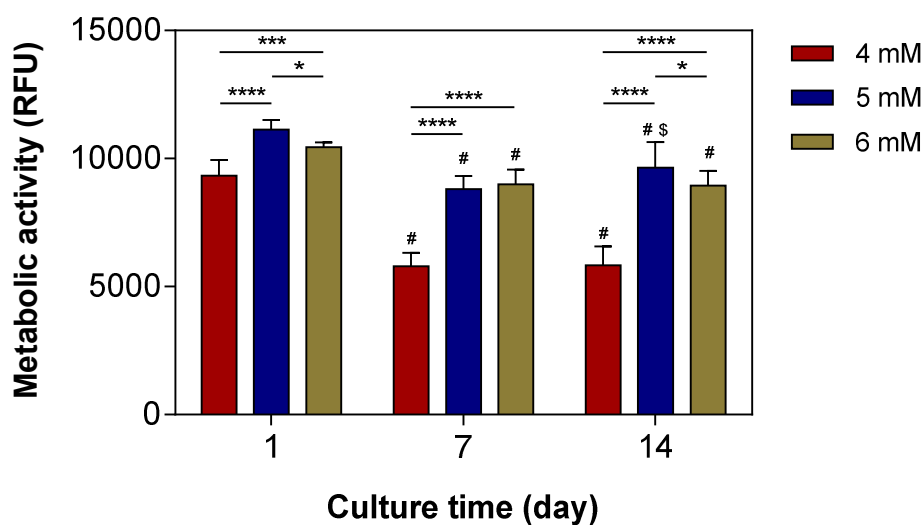


Figure S4.8. Metabolic activity of dermal fibroblasts embedded in NorPEC hydrogels containing varying concentrations of MMP-peptide. Data were analysed using two-way ANOVA with Tukey's multiple comparisons test ($*p < 0.05$, $***p < 0.001$, $****p < 0.0001$); compared to day 1: $\#p < 0.0001$; compared to day 7: $\$p < 0.01$.

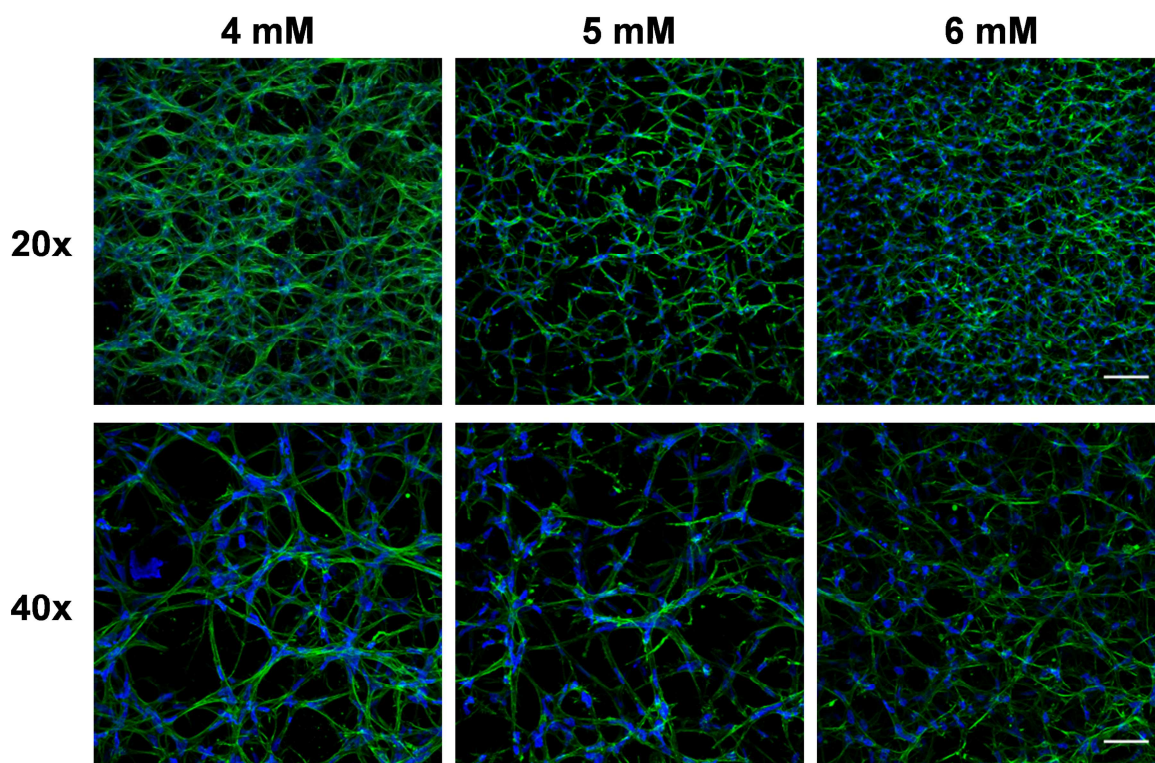


Figure S4.9. Representative confocal microscopy images of dermal fibroblasts cultured within MMP-degradable pectin hydrogels (2.5% NorPEC, 20s UV) prepared with different contents of MMP-sensitive peptide (4, 5 and 6 mM) showing the morphology and spatial distribution of fibroblasts stained for DAPI (blue) and F-actin (green) at day 7 (scale bar: 100 μ m for 20x objective and 50 μ m for 40x objective).

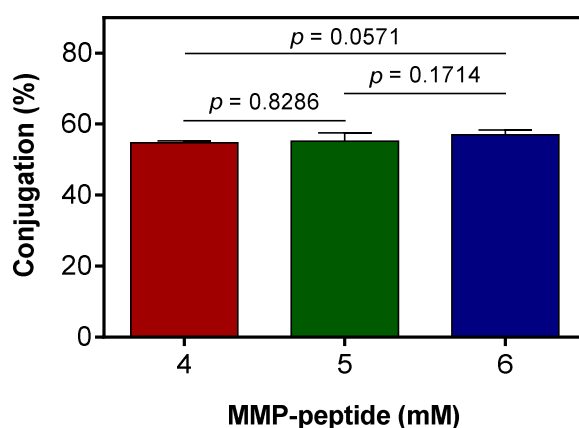


Figure S4.10. Influence of bulk MMP-degradable peptide content on the conjugation efficiency of RGD-peptide during photopolymerization (4 mM: 54.77 ± 0.56%; 5 mM: 55.15 ± 2.40%; 6 mM: 57.00 ± 1.35%). A fluorescently labelled RGD-peptide (CGGGGRGDSP{LYS(FITC)}), Genscript) was added to the hydrogel precursor solution, photocrosslinked and incubated in PBS for 24h. Then, the supernatant was collected and the amount of released peptide quantified by measuring the supernatant

fluorescence ($\lambda_{\text{ex}} = 494 \text{ nm}$, $\lambda_{\text{em}} = 521 \text{ nm}$) in comparison to a calibration curve using a microplate reader. Data were analysed using Mann-Whitney test.

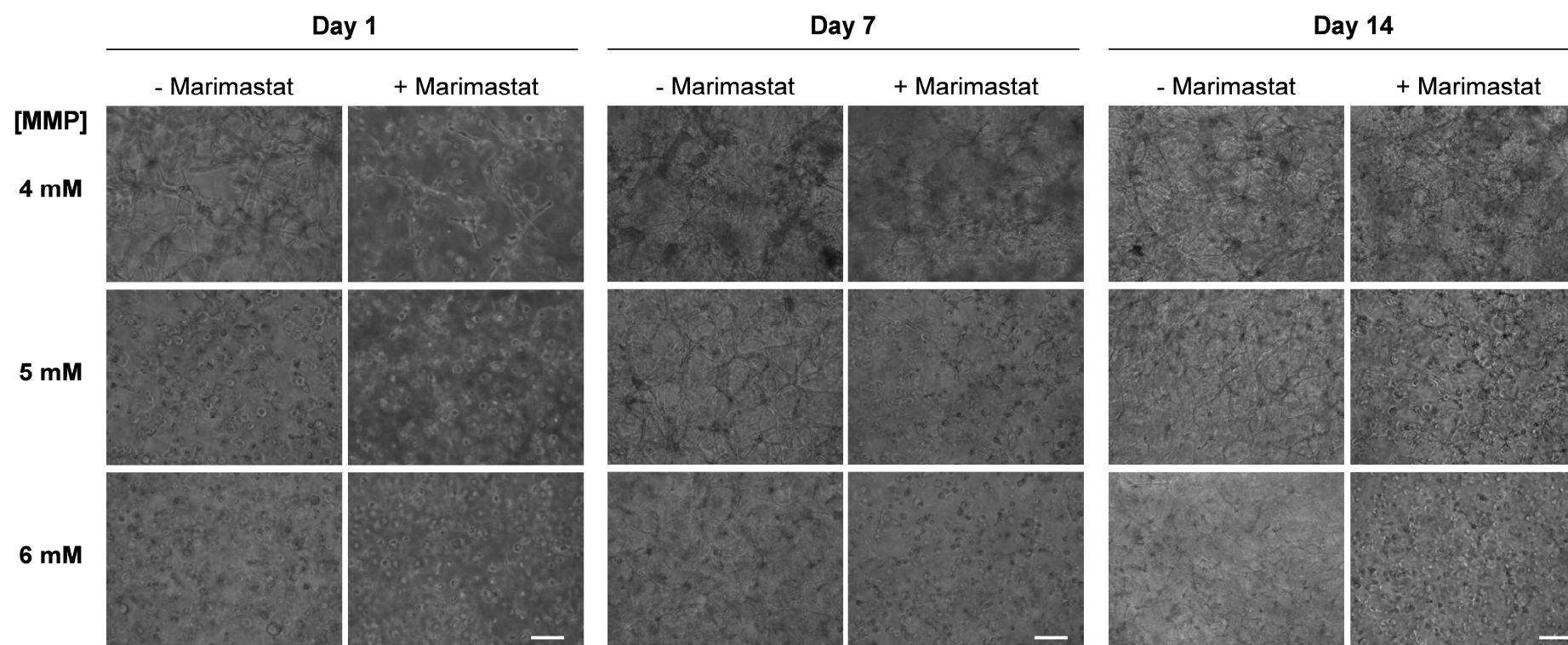


Figure S4.11. Bright-field images showing the influence of MMP-mediated degradation on cell spreading of dermal fibroblasts embedded within 2.5% NorPEC hydrogels of varying crosslinking densities prepared with different content of MMP-sensitive peptide (4, 5 and 6 mM). Cell-laden hydrogels were incubated in control medium and medium containing the MMP inhibitor (Marimastat) for 1, 7 and 14 days of culture (scale bar represents 100 μ m).

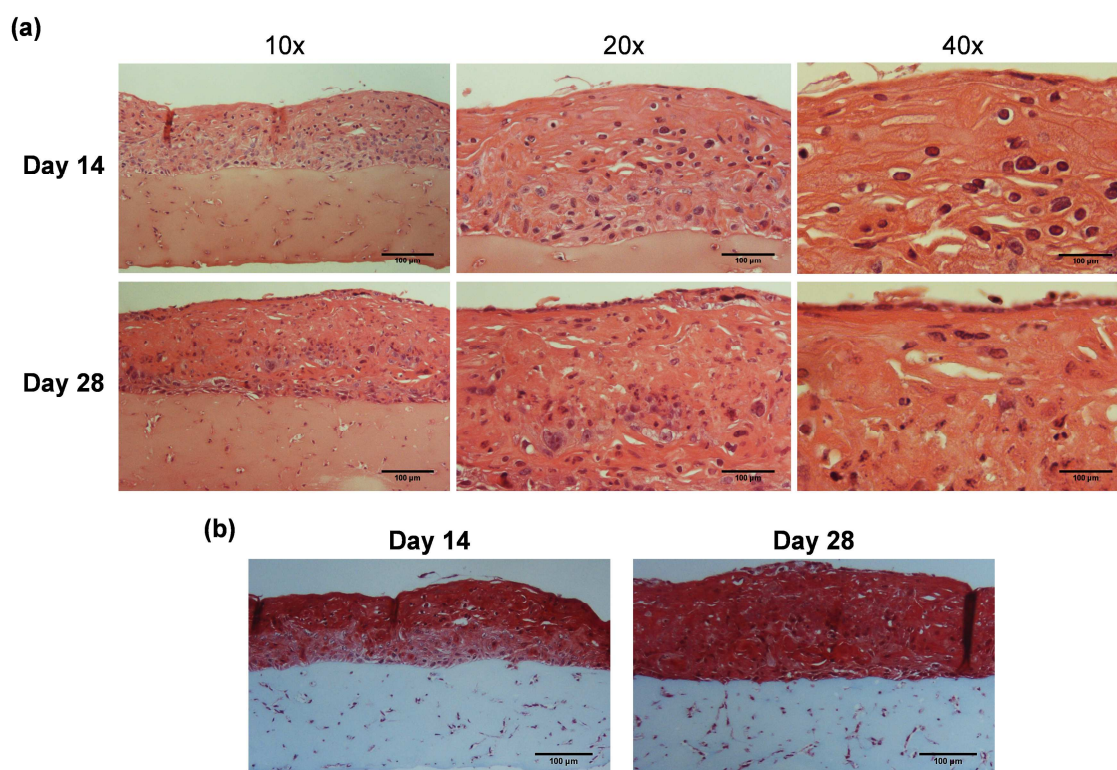


Figure S4.12. Histological and morphological characterization of skin equivalents formed after 14 and 28 days of differentiation at the air-liquid interface. **(A)** Hematoxylin & eosin and **(B)** Masson trichrome staining showing the histology of skin equivalents (scale bars represent 100 μm).

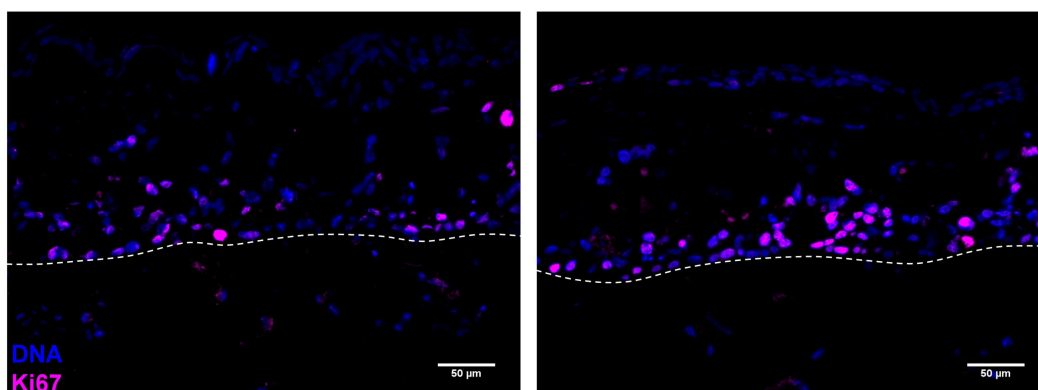


Figure S4.13. Immunostaining of paraffin embedded samples cultured at ALI interface for 28 days, using antibody directed against Ki67 (proliferation marker). Proliferative cells are mostly located at the basal region of the epidermal layer. Dash line indicates the interface between the dermal and epidermal layers (scale bars represent 50 μm).

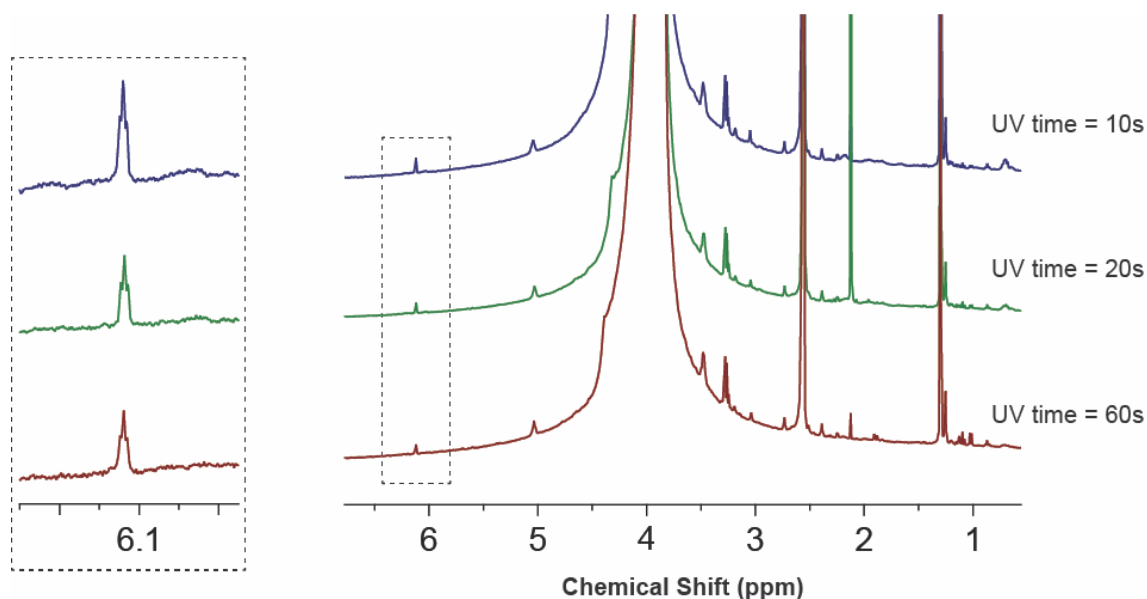


Figure S4.14. Consumption of vinyl protons on the norbornene functionality of NorPEC hydrogels (2.5 wt%, 2mM RGD, 5mM MMP) determined as a function of UV irradiation time. Representative ^1H NMR spectra of NorPEC hydrogels prepared by varying the UV exposure time. After photopolymerization, deuterated dimethyl sulfoxide (500 μl) was added to the hydrogel (100 μl) to partially dissolve the network prior ^1H NMR analysis [2]. For quantification of the double bond (6.12 ppm) consumption, all spectra were normalized to 3-(trimethylsilyl)propionic-2,2,3,3-d₄ acid sodium salt (TSP-d₄, Euriso-top) as internal standard ($\delta = 0$ ppm). Based on ^1H NMR data, crosslinking degree was calculated according to the following equation [2]:

$$\text{Crosslinking degree (\%)} = \left(1 - \frac{I_{\text{carbon-carbon double bonds}}}{I_{\text{internal standard}}}\right) \times 100$$

The crosslinking degree was 82% and 92% after 10s and 20s of UV irradiation, respectively, indicating the fast kinetics of thiol-norbornene reaction of the developed hydrogel system. After 60s of UV irradiation the crosslinking degree was 99%, which indicates that the hydrogel crosslinking was completed. Interestingly, the crosslinking degree between 20s and 60s of photopolymerization is similar, suggesting that the reaction rate is stabilizing due to the consumption of vinyl bonds and the formation of a crosslinked gel network.

Table S4.1. Antibodies used for immunofluorescence staining.

Primary Antibody	Company	Antigene Retrieval	Secondary antibody
Cytokeratin (1:100)	Dako (Wide Spectrum Screening)	Citrate buffer pH 6.0	Alexa Fluor 488 donkey anti-rabbit
Fibronectin (1:200)	Sigma-Aldrich	Citrate buffer pH 6.0	Alexa Fluor 488 donkey anti-rabbit
Collagen type I (1:100)	Rockland	Citrate buffer pH 6.0	Alexa Fluor 488 donkey anti-rabbit
Ki67 (1:800)	Abcam	Citrate buffer pH 6.0	Alexa Fluor 488 donkey anti-rabbit
Vimentin (1:100)	Santa-Cruz Biotechnology	Citrate buffer pH 6.0	Alexa Fluor 488 donkey anti-mouse

Table S4.2. Influence of reaction conditions on the norbornene functionalization of pectin. Percentage of norbornene functionalization as a function of reaction time (1, 3, 6 and 12h) and carbic anhydride content (1, 2.5, and 5-fold excess of CA relatively to the hydroxyl groups in pectin backbone).

Carbic anhydride fold excess	Reaction time (h)	Functionalization (%)
1	1	20.0
	3	30.3
	6	35.7
5	3	43.8
	12	41.2
1	6	35.7
2.5		29.8
5		32.7

References

- [1] D. Dakshinamoorthy, S.P. Lewis, M.P. Cavazza, A.M. Hoover, D.F. Iwig, K. Damodaran, R.T. Mathers, Streamlining the conversion of biomass to polyesters: bicyclic monomers with continuous flow, *Green Chemistry* 16 (2014) 1774-1783.
- [2] A. Assmann, A. Vegh, M. Ghasemi-Rad, S. Bagherifard, G. Cheng, E.S. Sani, G.U. Ruiz-Esparza, I. Noshadi, A.D. Lassaletta, S. Gangadharan, A. Tamayol, A. Khademhosseini, N. Annabi, A highly adhesive and naturally derived sealant, *Biomaterials* 140 (2017) 115-127.

CHAPTER V

BIOORTHOGONAL PECTIN BIOINK FOR BIOPRINTING OF PROTEASE-DEGRADABLE 3D CELLULAR MICROENVIRONMENTS

This chapter was based on the following publication:

- **R.F. Pereira**, B.N. Lourenço, P.J. Bártolo, P.L. Granja, “Bioorthogonal pectin bioink for bioprinting of protease-degradable 3D cellular microenvironments”. (in preparation)

Abstract

Bioinks are an essential tool for bioprinting functional tissue constructs for tissue engineering and regenerative medicine applications. The design of cell-instructive bioinks for extrusion bioprinting is demanding as they must exhibit suitable rheological behaviour, fast post-printing crosslinking, and provide a cell-responsive microenvironment that supports and directs cell functions. In this work, a novel photocrosslinkable bioink was designed for the bioprinting of 3D ECM-like microenvironments with tuneable biochemical and biophysical properties. The bioink was developed using norbornene-modified pectin, living cells, and peptide crosslinkers and ligands as basic building compounds. Ionic gelation was employed to achieve suitable yield stress point and bioink printability using a lower concentration of CaCl_2 (13 mM) compared to BaCl_2 (15 mM). Bioinks with similar rheological behaviour loaded with dermal fibroblasts were printed into 3D constructs and rapidly crosslinked via UV thiol-norbornene click chemistry. Stiffer constructs were created by simply increasing the photopolymerization time from 30 s to 90 s, allowing a significant increase in the elastic moduli of Ca^{2+} - (294.3 Pa to 869.9 Pa) and Ba^{2+} -crosslinked (391.0 to 1098.5 Pa) hydrogels. By selecting suitable thiolated protease-degradable peptide crosslinkers (CGPQGIWGQC) and thiolated cell-adhesive peptide pendant moieties (CGGGGRGDSP), printed 3D constructs supported the adhesion of embedded cells, allowed cell-driven gel network remodelling, supported extensive spreading of dermal fibroblasts, and stimulated the deposition of fibronectin. Overall, this bioink provides a new platform to generate biomimetic and customized cell- and tissue-specific 3D constructs with controllable tethering of biochemical cues and tuneable mechanical properties.

Keywords: bioink; bioprinting; pectin norbornene; photocrosslinking; thiol-norbornene chemistry.

5.1. Introduction

Biofabrication is a multidisciplinary field that employs bioassembly or bioprinting approaches to generate biologically functional tissue constructs [1]. Extrusion bioprinting allows the automated layer-by-layer production of 3D constructs with precise control over the positioning of living cells and functional components (e.g., biomolecules and biomaterials), providing a promising strategy to create tissue constructs mimicking key features of the native extracellular matrix (ECM) [2]. The ability to print 3D cell-biomaterial constructs that resemble the complex hierarchical architecture of human tissues and organs depends on the design of bioink formulations that meet both processing and biological requirements. Advanced bioinks must ensure not only high shape fidelity and allow fast crosslinking, but also provide a cell-specific and dynamic microenvironment that directs cell fate [3]. The design of bioinks resembling key features of the ECM, including cell-adhesion and cell-remodelling capabilities, hydrated nature, and fibrillar structure, is challenging due to the tissue-specificity of the biochemical and biophysical features of native ECM, and narrow processing window.

Hydrogels are the most explored bioink materials as they resemble many features of the ECM and can be crosslinked using a broad range of cytocompatible chemistries. They can also be functionalized with specific reactive end groups and bioactive ligands to further control the network formation and cell interactions [4, 5]. A variety of natural and synthetic hydrogel materials have been adopted for bioprinting, including alginate, gelatin, hyaluronic acid, and poly(ethylene glycol) [6]. Traditionally, these materials are formulated as either highly viscous single-component bioinks or hybrid multimaterial bioinks to achieve enough viscosity for bioprinting and allow subsequent construct consolidation. However, suitable printability of these bioinks is often associated to increased shear stress during the printing process, which reduces cell viability and might compromise the overall quality of newly formed tissue [7]. In order to address these limitations, elegant approaches based on physical crosslinking mechanisms have been developed to modulate the bioink viscosity prior printing, including ionic crosslinking [8], thermal gelation [9], and dynamic covalent bonds [10]. These approaches allow the design of physically crosslinked hydrogel bioinks with suitable rheological properties that can be directly printed into 3D constructs without additional materials for viscosity modulation. Nevertheless, secondary crosslinking postprinting is often required to consolidate the construct and eventually modulate the stiffness of the gel network.

Photopolymerization reactions are widely explored in bioprinting for the crosslinking of hydrogel constructs post-deposition, independently on whether the bioink was subjected to physical or chemical crosslinking before printing. Free-radical polymerization of meth(acrylate)-functionalized hydrogels is the most common approach, enabling the cytocompatible formation of chemically crosslinked constructs [11]. However, the homopolymerization of vinyl bonds on meth(acrylate) groups is associated to the generation of network heterogeneities due to the random chain polymerization, which negatively impacts the hydrogel mechanical properties [12]. Thiol-ene click reaction represents an alternative crosslinking scheme that was recently adopted for bioprinting [13, 14]. It is characterized by orthogonal reactivity and proceeds via step-growth mechanism, yielding structurally uniform hydrogels with minimal network defects. Importantly, thiol-ene reaction is insensitive to oxygen, requires lower concentration of initiator, and develops with faster kinetics when compared to free-radical polymerization. Photoinitiated thiol-norbornene reaction is one example of thiol-ene chemistry with tremendous potential for bioprinting due to the faster rate of thiol-ene conjugation of norbornene end groups compared to other alkenes (norbornene > vinyl ether > alkene > vinyl ester > allyl ether > acrylate > N-substituted maleimide > methacrylate > conjugated dienes) [15]. It involves light-mediated orthogonal reactions between multifunctionalized macromers end-capped with norbornene groups and sulfhydryl-containing linkers in the presence of an initiator, yielding water-stable thioether bonds. Thiol-norbornene reaction has been successfully used to encapsulate cells within manually casted hydrogels using both natural and synthetic polymers [16, 17], but a very limited number of works have explored this reaction in the context of bioprinting. In a recent study thiol-norbornene was employed as a secondary crosslinking reaction to control the functionality of bioprinted hydrogel constructs via photostiffening and photopatterning [10], while other work demonstrated its applicability for the in situ photocrosslinking of hyaluronic acid bioinks using a more complex bioprinting setup [13].

In this work, a new approach is reported to design a modular, protease-degradable bioink for the bioprinting of 3D hydrogel constructs mimicking fundamental aspects of the native ECM, including the ability to promote integrin-mediated cell-adhesion, allow protease-mediated network degradation, and provide a surrounding microenvironment of biologically relevant stiffness to the embedded cells. A single-component bioink was designed based on norbornene-modified pectin (NorPEC), enabling dual crosslinking via ionic gelation and photoinitiated thiol-norbornene click chemistry. Ionic gelation was explored to finely tune the rheological behaviour of the bioink for extrusion bioprinting, while the norbornene end groups enabled fast post-printing secondary crosslinking. By exploring the thiol-norbornene click chemistry, it was possible to rapidly introduce a myriad of biochemical cues (e.g., pendant

cell-adhesive ligands and protease-degradable peptides) during hydrogel formation, and simultaneously control the mechanical properties of the printed construct. This strategy provides the possibility to design ECM-like bioinks displaying the ability to control and direct the functions of embedded cells, which is essential in many bioprinting applications.

5.2. Materials and Methods

5.2.1. Bioink synthesis and preparation

Norbornene-modified pectin (NorPEC) with $20.0 \pm 0.6\%$ of functionalization degree was synthesized using a method previously developed [18]. Briefly, purified low methoxyl citrus pectin (Classic CU701, 86 % galacturonic acid unit content and 37 % degree of methylation, Herbstreith & Fox, Neuenbürg, Germany) was firstly converted to its tetrabutylammonium salt (PEC-TBA) through 3h of reaction with Dowex 50 W (3.5 g resin per 1 g polymer) proton exchange resin (Acros Organics) and neutralized to pH 6.50 with tetrabutylammonium (TBA, Sigma-Aldrich). Lyophilized PEC-TBA was dissolved in anhydrous dimethyl sulfoxide (DMSO) at 1 wt% and carbic anhydride (CA, Acros Organics) added at 1-fold molar excess to hydroxyl groups in the polymer backbone. After 1h of reaction at room temperature under vigorous agitation and inert (N_2) atmosphere, the solution was dialyzed (MWCO 3500, Spectra/Por®, SpectrumLabs) for 5 days, washed with activated charcoal (1 g charcoal per 1 g of polymer, Sigma-Aldrich) for 1 h, centrifuged (60 000 g, Beckman Avanti J-26XP), and filtered (0.20 μ m). Finally, the pH was adjusted to 7.00 with sodium hydroxide (0.1 M) and the modified polymer was recovered by lyophilization.

For the bioink preparation, NorPEC (final concentration 2.5 wt%) was dissolved in 25 mM of 4-(2-hydroxyethyl)-1-piperazineethanesulfonic acid (HEPES, Sigma Aldrich) containing 0.9 wt% sodium chloride (NaCl) and VA-086 (0.25 wt%, Wako Chemicals) as a photoinitiator. To this solution, the peptide crosslinker CGPQG↓IWGQC (arrow indicates enzymatically cleavable site, Genscript) and the cell-adhesive peptide ligand CGGGGRGDSP (underline indicates cell-adhesion motif, Genscript) were added to achieve a final concentration of 2 mM and 5 mM, respectively. After solubilization, desired concentrations of either calcium chloride ($CaCl_2$) dihydrate or barium chloride ($BaCl_2$) dihydrate (10 v/v% of the total bioink volume) were added dropwise under vigorous agitation as ionic crosslinking agent, and the solution incubated at 25 °C and 900 rpm for 180 min. Final concentrations of ionic crosslinking agents were in a range of 11–25 mM. The bioink was maintained at 25 °C before use.

5.2.2. Rheological measurements

The rheological properties of bioinks containing different concentrations of ionic crosslinking agents were analysed with a Kinexus Pro rheometer (Malvern) at 25 °C in a humidified environment. To determine the yield stress, bioinks were subjected to a shear stress ramp, ranging from 1 to 100 Pa (2 min) with plate–plate geometry (0.5 mm distance). The yield point, which indicates the point at which the material first started to flow, was defined as the intersection between two linear regressions at the plateau-region and viscosity-drop regions of the viscosity-shear stress diagrams. The viscosity rotational shear-viscosity measurements were performed using a shear ramp test (1 to 1000 s⁻¹ shear rate, 2 min) after applying one loading cycle with 2 min intervals before the rheological data acquisition. Rotational recovery measurements were performed to characterise the bioink recovery behaviour by applying a low shear rate of 1 s⁻¹ for 100 s, following by a high shear rate of 100 s⁻¹ for 100 s, and finally a low shear rate of 1 s⁻¹ for 100 s. The gelation kinetics of bioinks was determined by measuring the evolution of storage (G') and loss modulus (G'') at a constant strain of 2 % and frequency of 0.1 Hz

5.2.3. Mechanical properties of hydrogels

The mechanical properties of hydrogels were analysed in a Kinexus Pro rheometer using 4 mm diameter hydrogel samples (n = 4) in a humidified environment at 37 °C. Hydrogel samples were compressed at 30 % of their initial height and strain amplitude sweeps were conducted from 0.1 to 100% at 0.1 Hz, while frequency sweeps were carried out from 0.01 to 10 Hz at 2 % strain, after determining the linear viscoelastic region. Bioink solutions were manually casted between 1 mm spaced glass slides treated with SigmaCote (Sigma-Aldrich) to prevent gel attachment and photopolymerized under UV light (365 nm, UV-LED spot light source L11921, Hamamatsu) at 7 mW/cm² for desired time periods (30 s, 60 s, and 90 s). Hydrogels were incubated in culture medium Dulbecco's Modified Eagle's Medium (DMEM, Gibco) without fetal bovine serum (FBS) for 24 h before testing.

5.2.4. Bioprinting of cellularized 3D constructs

Bioprinting was performed in a commercial bioprinter Regemat 3D V1 (Regemat 3D, Spain) at 25 °C using physically crosslinked bioinks containing either 13 mM CaCl₂ or 15 mM BaCl₂ loaded with human neonatal dermal fibroblasts (Coriell Institute for Medical Research). Cells were cultured in DMEM supplemented with 10% FBS, antibiotics (100 U/mL penicillin, 100 µg/mL streptomycin, Sigma Aldrich), and amphotericin B (2.5 mg/L, Sigma Aldrich) in 5 % CO₂ at 37 °C in tissue culture polystyrene flasks. Cells (passage 7) were trypsinized using

a 0.05 wt% trypsin/ethylenediamine tetraacetic acid (EDTA) solution before reaching 80 % confluency, centrifuged (1200 rpm, 5 min), and the cell pellet was suspended in the bioink at a final density of 1×10^7 cells/mL, corresponding to 10 % of the final bioink volume. Cell-laden bioinks were loaded in sterile syringes with a 25 G tapered tip (7018391, Nordson EFD), and printed into 3D constructs ($8 \times 8 \times 1$ mm³). Proprietary software was used to define the operating parameters (deposition speed 3 mm/s), construct attributes (4 printed layers, pore size 0.6 mm), and generate G-code to control the bioprinter. After deposition, 3D constructs were photocrosslinked using UV light irradiation (30 s, 60 s, and 90 s), and incubated in culture media for 14 days. After predetermined time points, constructs were fixed in 4 %v/v paraformaldehyde (PFA, Electron Microscopy Sciences) in Hank's Balanced Salt Solution (HBSS, Life Technologies) for 20 min, washed with HBSS, and stored at 4 °C.

5.2.5. Characterization of bioprinted 3D constructs

The metabolic activity of printed cells was determined by the resazurin assay. 3D constructs were incubated in DMEM medium containing 20 %v/v resazurin sodium salt (Sigma-Aldrich) for 2 h at 37 °C, and sample fluorescence was measured using a microplate reader (Synergy MX, Biotek) at 530 nm (excitation) and 590 nm (emission). The morphology of the cells within the printed constructs was visualized by immunofluorescence staining of F-actin and nuclei staining. Samples were incubated overnight with phalloidin/Alexa Fluor® 488 (Molecular Probes-Invitrogen) for F-actin staining, followed by incubation with Hoechst (Life Technologies) for nuclei staining for 45 min. Samples were rinsed and imaged on a confocal laser scanning microscope (CLSM, Leica TCS-SP5 AOBS, Leica Microsystems). The deposition of ECM was analysed by immunofluorescence staining of fibronectin. Briefly, samples were permeabilized for 10 min with 0.2 %v/v Triton X-100 (Sigma) in HBSS, washed, incubated in blocking solution (1 %w/v bovine serum albumin in HBSS) for 1 h at room temperature, and left overnight at 4 °C with rabbit anti-fibronectin antibody (F3648, Sigma-Aldrich) and phalloidin/Alexa Fluor® 488. Then, samples were rinsed with HBSS and incubated for 45 min with Alexa Fluor 594 goat anti-rabbit secondary antibody (Molecular Probes-Invitrogen) and Hoechst for nuclei staining. Samples were rinsed and imaged on CLSM. For double-stranded DNA (dsDNA) quantification, cells were recovered from the printed 3D constructs by enzymatic degradation with a pectinase (Sigma Aldrich)/type II collagenase (Worthington Biochemical) cocktail (37 °C, 30 min), centrifuged (10 000 rpm, 5 min), washed twice with 1X phosphate buffered saline (PBS) and stored at -20°C until quantification. Cells were lysed in 1 %v/v Triton X-100 for 1 h at 4 °C, diluted 1:10 in 1X PBS, and dsDNA quantification was performed using the Quant-iT PicoGreen dsDNA kit (Thermo Scientific), according to manufacturers' instructions.

5.2.6. Statistical analysis

Statistical analyses were performed in the GraphPad Prism 7.0 software and the results presented as the mean \pm standard deviation (SD). The non-parametric Mann–Whitney test was applied with 95 % confidence interval and statistically significant differences marked with $p < 0.05$ (*), $p < 0.01$ (**), $p < 0.001$ (***) and $p < 0.0001$ (****).

5.3. Results and discussion

5.3.1. Design of a modular bioink crosslinked by thiol-norbornene click chemistry

The design of bioinks that recapitulate many of the structural and functional characteristics of the ECM in target tissue is essential for the bioprinting of biomimetic tissue constructs. In this work, a single-component bioink was designed to meet the processing criteria for extrusion bioprinting and simultaneously provide a modular platform where a broad range of crosslinkers (e.g., non-degradable DTT, MMP-degradable peptide sequences), pendant ligands (e.g., growth factors, cell-specific adhesion moieties), and cells can be used as basic building blocks to create customized cell- and tissue-specific 3D constructs. The design principle for the bioink synthesis and bioprinting strategy is illustrated in **Figures 5.1A** and **5.1B**, respectively. Bioink formulation is crucial to ensure the viability and functionality of cells in printed constructs as well as to enable the user-controlled bioink functionalization for a target application. The developed bioink consisted of a multicomponent system based on norbornene-modified pectin as a sole material, VA-086 as initiator, a biscysteine protease-degradable crosslinker, a thiolated cell-adhesive peptide ligand, and living cells. The components were selected to serve different purposes in the bioink: (i) norbornene-modified pectin allows the formation of a physically crosslinked hydrogel via ionic gelation with divalent ions before printing to provide ideal rheological behaviour, while norbornene end groups enable both the formation of crosslinks between polymer chains and the tethering of pendant moieties via a fast thiol-norbornene photoclick reaction; (ii) VA-086 as a photoinitiator allows the photocrosslinking and/or photopatterning of printed constructs after printing; (iii) biscysteine protease-degradable crosslinker (CGPQG↓IWGQC) performs a dual function by forming a chemically crosslinked hydrogel post-printing upon UV light exposure and providing a protease sensitive sequence for cell-mediated remodelling of the gel network, similarly to what happens in native ECM; (iv) thiolated cell-adhesive peptide ligand (CGGGGRGDSP) confers anchorage sites to the hydrogel, allowing integrin-mediated cell-adhesion and cell-matrix crosstalk, which mimics the cell-adhesive nature of ECM; (v)

dermal fibroblasts are used as cell component of the bioink due to their key role in skin wound healing and ability to sense and respond to the biochemical and biophysical cues from the surrounding microenvironment.

The bioprinting strategy consists of three steps: (i) ionic crosslinking of the bioink in the absence of living cells via reaction with divalent ions, (ii) extrusion bioprinting of the cell-laden bioink, and (iii) fast UV thiol-norbornene polymerization of printed 3D constructs. Since NorPEC solutions cannot be printed due to the low viscosity, two cations, namely Ca^{2+} and Ba^{2+} , were selected for ionic crosslinking of the polymer solution before printing and to compare their effects on both rheological behaviour and cell response. By optimizing the final concentrations, both cations allowed the formation of consistent filaments at the nozzle and the direct printing of tubular 3D hollow structures without the need for support structures or photocrosslinking during the printing process. After printing, the structures were exposed to very short UV light irradiation time periods at cytocompatible light intensity (7 mW/cm^2), which is essential for preclude cell dead and DNA damage. Since the thiol-norbornene reaction is non-oxygen inhibited, photopolymerization was carried out immediately postprinting at room conditions, yielding water-stable thioether bonds via reaction between the alkene groups in norbornene function and thiol group in peptides. The resultant 3D structures were mechanically robust and stretchable, as shown in **Figure 5.1C**.

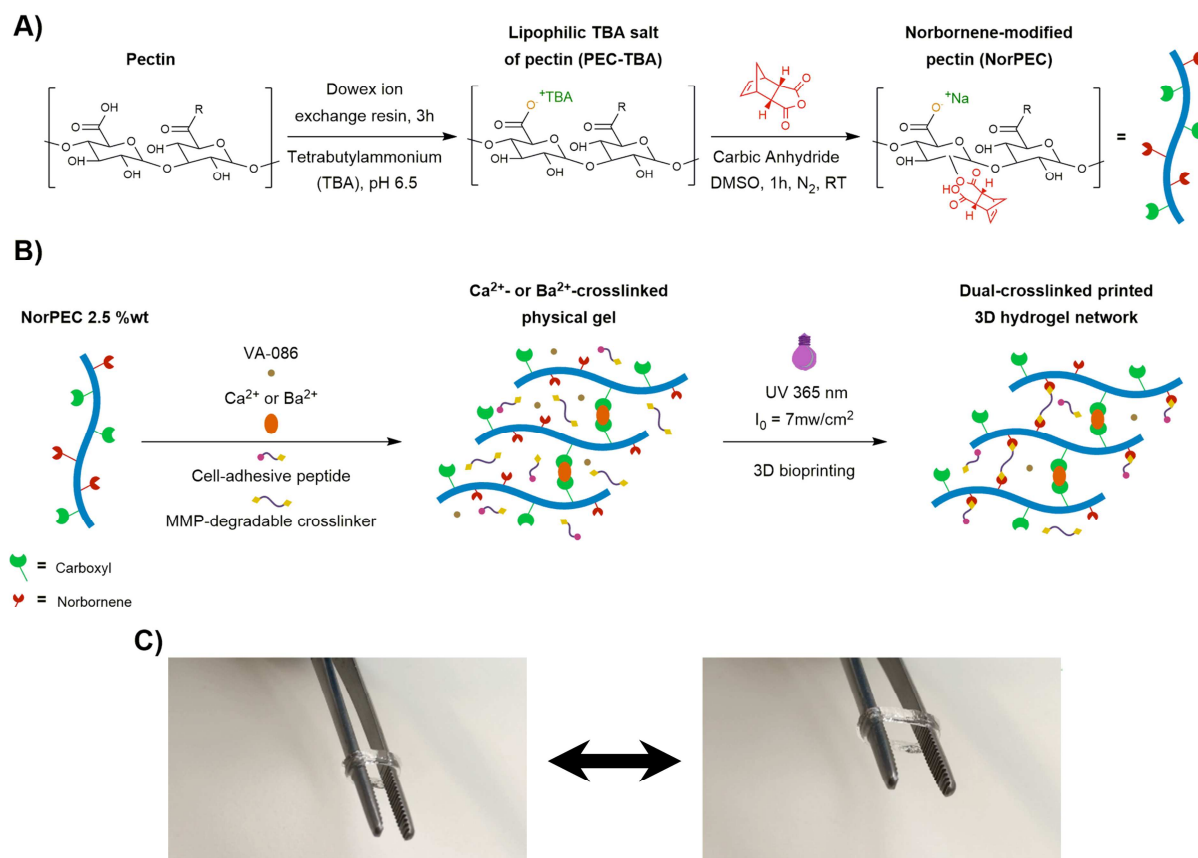


Figure 5.1. Design, synthesis and bioprinting of the thiol-norbornene photoclickable pectin bioink. (A) Synthesis of norbornene-modified pectin through reaction with carbic anhydride. **(B)** Schematic illustration of bioprinting strategy and crosslinking chemistries involved during the bioprinting process. **(C)** Photograph of the printed hollow tube structure before (left) and during (right) stretching.

A variety of natural polymers have been explored as hydrogel bioinks for extrusion bioprinting due to their biocompatibility, biodegradability and bioactive properties. Contrary to unmodified synthetic polymers, which lack of bioactive properties, many natural polymers such as collagen and gelatin intrinsically contain arginine–glycine–aspartate (RGD) sequences and cell-remodelling sites, conferring superior biological properties. Protein-derived materials are the first choice for the design of cell-responsive bioinks either individually or combined with other materials owing their fibrillar structure and cell-interactive domains [9, 19]. Although these characteristics resemble key features of the native ECM, alterations in macromer concentration inevitably change the content of biochemical cues in the surrounding cell microenvironment, making difficult to decouple both biophysical and biochemical properties from macromer concentration. One alternative to tackle these limitations consists on the chemical functionalization of protein-derived materials (e.g.,

gelatin) with vinyl bonds for photopolymerization reactions to control the hydrogel stiffness independently on the macromer concentration [20]. Despite useful, the major bottleneck of this strategy is the poor control over the biochemical composition of the bioink towards a specific application. As a result, a great deal of interest has been focused on alternative natural materials which biochemical composition and biophysical properties can be controlled independently on the macromer concentration or crosslinking chemistry, allowing the design of customized bioinks that mimic cell- and tissue-specific features. In this work, pectin was proposed as an alternative biomaterial for the formulation of advanced bioinks for 3D bioprinting due to its biocompatibility, gelation properties, and lack of cell-adhesion moieties and cell-remodelling sites [21]. The absence of cell-responsive moieties was a fundamental criterion in polymer selection, enabling the user-specific functionalization of the bioink for a desired application. A second criterion for the selection of pectin consisted on its ionic crosslinking ability under cytocompatible conditions, which was explored for the formation of weakly crosslinked physical hydrogels with adjustable rheological properties. Finally, pectin has a rich chemical composition that provides a multitude of functional groups for chemical modification, which is fundamental in the synthesis of photosensitive pectin derivatives for thiol-norbornene polymerization.

5.3.2. Tuning the bioink printability via ionic crosslinking

One fundamental requisite of bioinks for extrusion bioprinting is the ability to form mechanically stable filaments capable of maintaining the predesigned shape after deposition and supporting the subsequent printed filaments without collapsing. This is a major challenge as the bioink must exhibit enough structural integrity both during and postprinting without compromising the mixing with the cells and simultaneously precluding mechanically induced cell membrane damage. The ability of NorPEC solutions to form physical gels in the presence of divalent ions was explored as a straightforward strategy to adjust the rheological behaviour of the developed bioink. To this end, two cations widely used in the formation of ionically crosslinking hydrogels were selected namely Ca^{2+} and Ba^{2+} . These cations have been applied to induce the crosslinking of printed 3D constructs through immersion in gelation baths [22], while Ca^{2+} has also been employed to crosslink alginate-containing bioinks during the printing process [23]. In order to explore the ability of Ba^{2+} to form stronger physical alginate microbeads when compared to Ca^{2+} [24], in this work we evaluated the effect of cation type and concentration on the rheological behaviour and printability of bioinks, while fixing the bioink composition (2.5 wt% NorPEC, 5 mM peptide crosslinker, 2 mM cell-adhesion peptide, and 0.25 wt% VA-086 initiator) and nozzle diameter (250 μm). The

concentrations of polymer precursor, peptide crosslinker, cell-adhesion peptide, and initiator were selected based on our previous work [18].

To systematically compare the influence of Ca^{2+} and Ba^{2+} on the rheological properties of bioinks, the concentration of both cations was varied in a range of 11–20 mM and the yield stress point determined by rheological analysis. The yield stress is intimately related to the flow initiation of the bioink and was selected to determine the required stress to induce the material flow as a function of both cation source and concentration. A shear stress ramp was applied to each bioink formulation containing different cation concentrations to test whether the material exhibits yield stress behaviour. In parallel, the printability of each bioink was manually assessed by dispensing the material through a printing nozzle to verify whether a continuous filament or droplets are formed during deposition (**Figure 5.2A**). It was observed that Ca^{2+} -crosslinked bioinks exhibit suitable printability when Ca^{2+} concentration is in the range of 13–15 mM. At lower concentrations, the degree of ionic crosslinking is too low, leading to the formation of droplets rather than a consistent filament. On contrary, for Ca^{2+} concentration in a range of 17.5–20 mM, the bioink is too crosslinked, which results in the formation of irregular filaments that easily fracture during deposition. Ba^{2+} -crosslinked bioinks required higher concentration to form stable filaments compared to Ca^{2+} . Suitable gelation for Ba^{2+} -crosslinked bioinks was obtained using concentrations in a range of 15–17.5 mM. Using optimal concentrations of Ca^{2+} and Ba^{2+} , smooth and uniform filaments were continuously extruded, which is fundamental for the bioprinting of 3D constructs. To quantitatively determine the yield stress of bioinks, below which the material behaves like a solid rather than a liquid, a shear stress ramp was applied to the physically crosslinked bioinks and the results summarized in **Table 5.1** and **Figure 5.2B**. Consistent with data from the manual deposition, the bioink yield stress point increased with higher concentrations of Ca^{2+} - and Ba^{2+} due to the formation of a more crosslinked gel network. For the same cation concentration, the yield stress point of Ca^{2+} -crosslinked bioink is higher than the Ba^{2+} -crosslinked bioink, except for the concentration of 20 mM, suggesting a more efficient crosslinking reaction of the NorPEC in the presence of calcium ions. From **Figures 5.2C** and **5.2D** it is possible to observe that all formulations displayed a clear drop in viscosity upon flow initiation, which is indicative of the yield stress behaviour. Printable bioinks presented higher yield stress point and viscosity compared to unprintable low crosslinked bioinks. For the developed bioinks, yield stress values around 25 Pa result in highly crosslinked materials that form irregular filaments, difficult the mixing with the cell pellet, and can eventually reduce the viability of printed cells due to high shear stresses generated during the printing process.

Table 5.1. Influence of cation source and concentration of the yield stress point of calcium (Ca^{2+})- and barium (Ba^{2+})-crosslinked pectin bioinks.

Cation concentration (mM)	Ca^{2+} -crosslinked bioink Yield stress (Pa)	Ba^{2+} -crosslinked bioink Yield stress (Pa)
11	11.92 ± 2.39	5.19 ± 1.57
13	16.60 ± 0.87	11.23 ± 0.57
15	20.23 ± 1.07	16.97 ± 0.43
17.5	26.20 ± 3.15	24.38 ± 3.71
20	31.77 ± 5.23	36.17 ± 7.86

As recent works have demonstrated that the printability of bioinks is highly dependent on the crosslinking degree and yield stress point [25, 26], the selection of printable Ca^{2+} and Ba^{2+} concentrations was done based on the yield stress data. Theoretically, if bioinks can be printed using the same operating conditions and photocrosslinked upon exposure to equal doses of UV light, effects on cell behaviour can be almost exclusively attributed to the microenvironment provided by the 3D construct rather than to the printing process. To ensure that both Ca^{2+} - and Ba^{2+} -crosslinked bioinks can be printed using the same processing parameters (e.g., dispensing rate, printing speed), optimal cation concentrations of 13 mM and 15 mM were selected, respectively. These concentrations fall in the suitable crosslinking region on the printability window diagram and result in no statistical significant differences on the yield stress point (Ca^{2+} : 16.60 ± 0.87; Ba^{2+} : 16.97 ± 0.43), as observed in **Figure 5.2E**. Although the viscosity at the yield stress point of Ba^{2+} -crosslinked bioink is slightly higher when compared to the Ca^{2+} -crosslinked bioink, this difference is not statistical significant (**Figure 5.2F**) and does not compromised the mixing with the cell pellet. In order to determine the gelation kinetics, Ca^{2+} and Ba^{2+} were individually added to the bioink solution and the evolution on the elastic (G') and viscous (G'') moduli determined by rheometry. From **Figure 5.2G** it is possible to observe that both G' and G'' increased drastically in the beginning of the test, followed by a slow increase until achieving the plateau. Ca^{2+} -crosslinked bioink showed a faster increase of G' and G'' immediately after mixing, followed by a slow crosslinking until became constant (>139.7 min). On the other hand, the Ba^{2+} -crosslinked bioink exhibited a slower increase of G' and G'' after mixing, suggesting a slower reaction kinetics. Both bioinks required similar reaction times to achieve the plateau, with the Ba^{2+} -crosslinked bioink exhibiting higher G' at the plateau (Ca^{2+} : G' 73.3 ± 2.3 Pa, G'' 4.07 ± 0.1 Pa, gelation time 139.7 min; Ba^{2+} : G' 102.4 ± 3.0 Pa, G'' 4.88 ± 0.1 Pa, gelation time 133.4 min). This data

indicate that Ba^{2+} resulted in stiffer physically crosslinked bioinks, which could be attributed to its higher concentration in solution rather than the superior affinity of barium ions to the carboxyl groups in the pectin backbone. Contrary to the expected, a higher content of Ba^{2+} was needed to obtain a similar yield stress value of bioinks compared to Ca^{2+} . We hypothesize that this outcome can be related with constraints in the accessibility of carboxyl groups by the cations in solution imposed by the introduction of norbornene end groups. However, further investigation is needed to elucidate these effects.

After determining the effect of cations and their concentration on the flow initiation of bioinks, shear viscosity tests were performed to characterise the shear thinning properties of developed bioinks during the extrusion. Both Ca^{2+} - and Ba^{2+} -crosslinked bioinks present a shear thinning behaviour, characterised by a decrease in viscosity as a function of increased shear rate (**Figure 5.2H**). This behaviour is essential to allow the bioink extrusion at low levels of viscosity, precluding cell death during the printing process. Bioinks exhibited a similar shear thinning behaviour over the applied shear rate range ($1\text{--}1000\text{ s}^{-1}$), allowing one to predict that bioinks would have similar printability independently on the cation source.

A key characteristic of advanced bioinks is the ability to retain the predesigned shape after printing, allowing high shape fidelity and eventually secondary crosslinking without structure deformation. The behaviour of developed bioinks postprinting was characterised using recovery tests. During the test, regimes of high and low shear rates are applied to analyse the bioink recovery after printing. To simulate the shear conditions that the bioink is subjected during the printing, a low shear rate of 1 s^{-1} was firstly applied for 100 s to simulate at-rest conditions before extrusion, analogous to being held in the syringe without extrusion. Then, a high shear rate of 100 s^{-1} for additional 100 s was applied to simulate the shear forces in the nozzle tip during the extrusion, followed by a low shear rate of 1 s^{-1} for 100 s to determine the recovery ability of the bioinks. **Figure 5.2I** shows that bioinks exhibited a fast recovery after exposure to high shear stress, indicating their ability to rapidly increase the viscosity after printing. This behaviour is essential to ensure high shape fidelity and shape maintenance of the printed structure. If bioinks do not rapidly recover their initial viscosity after deposition, permanent changes in the material can be induced due to the application of a high shear rate, which often leads to poor shape fidelity.

Multiple strategies have been explored to control the rheological properties of bioinks towards suitable printability. Most common approaches rely on highly viscous bioinks obtained by either increased macromer content or addition of high molecular weight polymers (e.g., alginate, hyaluronic acid) [27]. Despite these approaches improve the viscosity and consequently the rheological properties of bioinks, cell viability and function is often

compromised due to the high shear stress during printing. In this work, a simple yet efficient ionic crosslinking strategy was employed to control the rheological properties of pectin bioinks. In addition to the commonly used calcium ion, we introduced barium as an alternative ionic crosslinker of bioinks for extrusion bioprinting. Although barium has been applied to crosslink alginate constructs after printing, this is the first work reporting its ability to generate physically crosslinked bioinks with suitable printability for extrusion bioprinting. Rheological data indicated that higher concentration of Ba^{2+} compared to Ca^{2+} is needed to achieve similar printability and yield stress point, though Ba^{2+} forms a slightly more viscous bioink solution when the same cation concentration is used. Importantly, both Ca^{2+} - and Ba^{2+} -crosslinked bioinks exhibited shear thinning behaviour and fast recovery regardless cation source, indicating that bioinks with optimal rheological properties for extrusion bioprinting can be designed by both Ca^{2+} - and Ba^{2+} -mediated ionic crosslinking.

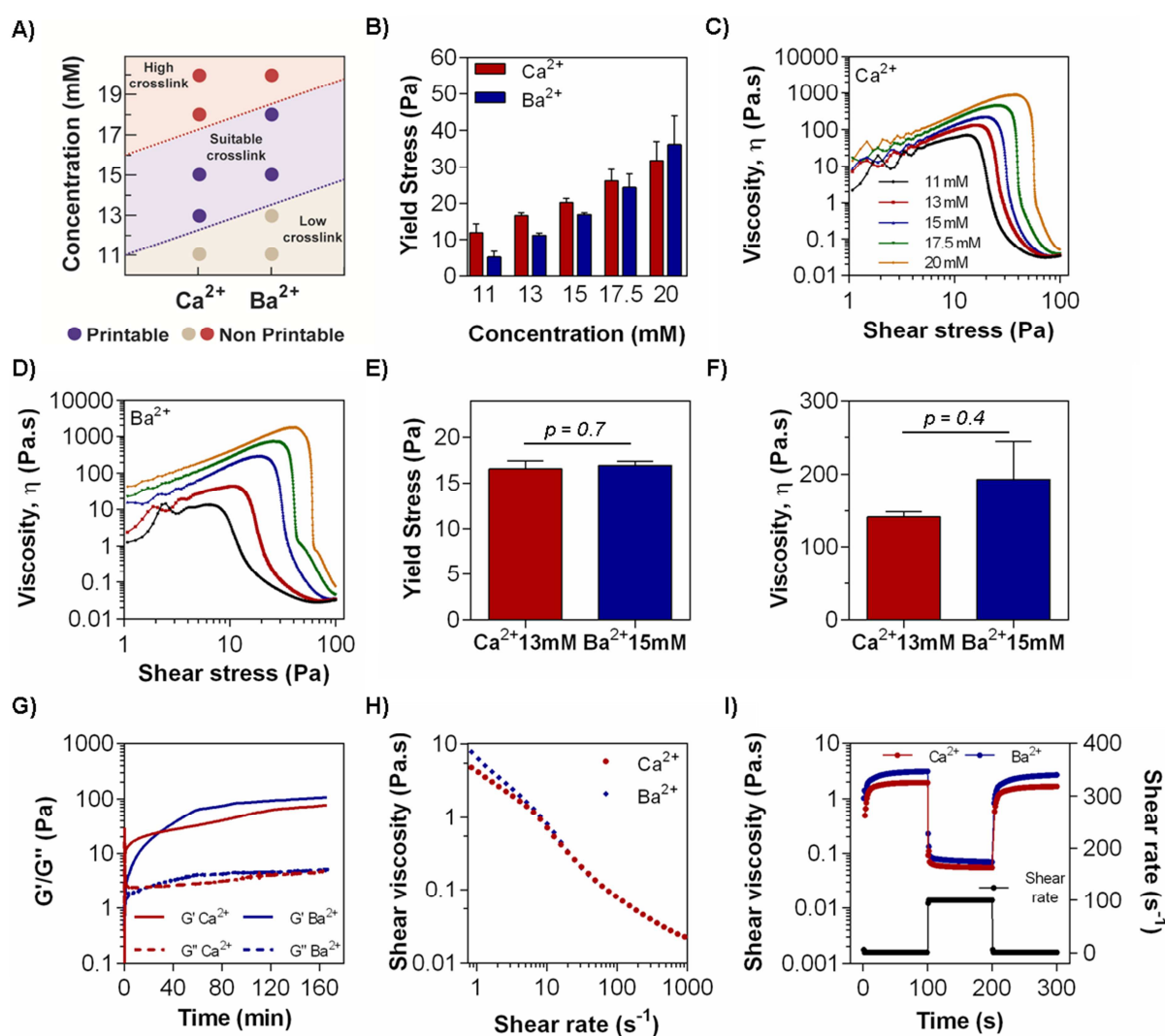


Figure 5.2. Rheological behaviour of thiol-norbornene photocrosslinkable pectin bioinks. (A) Phase diagram for the printability window of Ca^{2+} - and Ba^{2+} -crosslinked bioinks. The bioinks can be

printed when the cation concentration is located in the suitable crosslinking region. **(B)** Effect of cation source and concentration on the yield stress value of bioinks. **(C)** Shear stress ramp data for a Ca^{2+} -crosslinked bioinks. **(D)** Shear stress ramp data for a Ba^{2+} -crosslinked bioinks. **(E)** Yield stress point for bioinks crosslinked with 13 mM Ca^{2+} and 15 mM Ba^{2+} . **(F)** Viscosity at the yield stress point for bioinks crosslinked with 13 mM Ca^{2+} and 15 mM Ba^{2+} . **(G)** Gelation of Ca^{2+} - and Ba^{2+} -crosslinked bioinks with evolution of elastic (G') and viscous (G'') moduli as a function of time. **(H)** Viscosity of 13 mM Ca^{2+} - and 15 mM Ba^{2+} -crosslinked bioinks as function of shear rate. **(I)** Recovery tests of 13 mM Ca^{2+} - and 15 mM Ba^{2+} -crosslinked bioinks.

5.3.3. Modulating the viscoelastic properties of thiol-ene bioinks

One important advantage of the developed NorPEC bioink is the fast curing kinetics of the photoinitiated thiol-norbornene reaction, enabling the rapid formation of chemical hydrogels postprinting. Another important benefit of the bioink is the ability to decouple biochemical composition and mechanical properties from polymer content as the hydrogel stiffness exclusively depends on the crosslinker (type and content) and photopolymerization conditions. Thus, defined biochemical cues can be tethered to the polymer backbone at a fixed macromer concentration either before or during photocrosslinking independently on the final hydrogel stiffness. The ability to precisely control the biochemical and biophysical properties of bioinks in an independent manner is of outstanding importance to print ECM-like microenvironment for a desired application.

Contrary to other photocrosslinkable hydrogel systems, in which increasing the polymer weight percentage represents the unique possibility to significantly improve the mechanical properties, in the developed bioink and bioprinting strategy the hydrogel stiffness can be modulated independently on the polymer content using different approaches. Previously, we showed that varying the concentration of the protease-degradable peptide crosslinker (4–6 mM) enables to tailor the mechanical properties of non-printable NorPEC hydrogels in a physiologically relevant range [18]. In this study, the photopolymerization time was explored to control the stiffness of hydrogels prepared from the developed bioink. Since the application of UV irradiation for cell encapsulation raises concerns about potential light-induced cellular DNA damage [28], the bioink composition, crosslinking chemistry, and cytocompatible UV curing conditions ($\lambda = 365 \text{ nm}$, light intensity of 7 mW/cm^2) were carefully selected and optimized to minimize the crosslinking time, and thereby mitigate potential harmful effects to embedded cells. Mechanically stable hydrogels were formed after 30 s of UV irradiation, resulting in dual-crosslinked hydrogel networks containing physical crosslinks from either Ca^{2+} - or Ba^{2+} -mediated ionic gelation and thioether chemical crosslinks of thiol-norbornene polymerization. From **Figure 5.3A** it is observed that the G' of hydrogels

increased with increasing photopolymerization time regardless the cation source used for ionic crosslinking. Soft hydrogels (< 400 Pa) were obtained after 30 s of UV curing, while stiffer (> 850 Pa) hydrogels were produced by increasing the photocrosslinking time to 90 s. In all tested conditions, Ba²⁺-crosslinked hydrogels presented statistically significant higher G' than Ca²⁺-crosslinked hydrogels, independently on the photopolymerization time. For example, Ca²⁺-crosslinked hydrogels prepared with 30 s of UV curing exhibited G' of 294.3 ± 40.7 Pa, while in Ba²⁺-crosslinked hydrogels the G' was 391.0 ± 37.1 Pa. The same trend was verified for the stiffer hydrogel networks obtained with 90 s of photopolymerization (Ca²⁺: G' = 869.9 ± 121.5 Pa; Ba²⁺: G' = 1098.0 ± 159.7 Pa), while intermediate stiffness was achieved with 60 s of UV curing. The differences on the mechanical properties as a function of the ionic crosslinker agent can be attributed to the higher concentration of Ba²⁺ (15 mM Ba²⁺ versus 13 mM Ca²⁺) required to obtain comparable rheological behaviour between both bioinks. This observation is corroborated by the gelation tests that indicated the formation of stiffer networks in physically Ba²⁺-crosslinked hydrogels. One possible solution to mitigate potential effects of different hydrogel stiffness on cell behaviour that arises from the concentration of ionic crosslinking agents can be the optimization of the photocrosslinking time in order to obtain hydrogels with similar stiffness. As shown in **Figure 5.3B**, decreasing the photocrosslinking time of 15 mM Ba²⁺-crosslinked bioinks to 20 s instead of 30 s led to a significant reduction of the G' of hydrogels from 391.0 ± 37.1 Pa to 307.5 ± 47.6 Pa, which is comparable to the G' of 13 mM Ca²⁺-crosslinked hydrogels prepared with 30 s photopolymerization (294.3 ± 40.7 Pa).

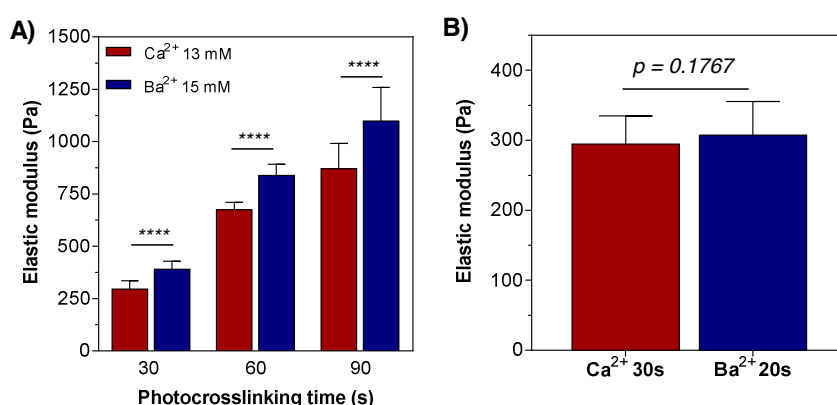


Figure 5.3. Tuneable mechanical properties of dual-crosslinked pectin hydrogels obtained by thiol-norbornene photopolymerization. Hydrogels were prepared from either 13 mM Ca²⁺- or 15 mM Ba²⁺-crosslinked bioink solutions containing 2.5 wt% norbornene-modified pectin, 2 mM cell-adhesion peptide, 5 mM protease-degradable peptide crosslinker, and 0.25 wt% VA-086. **(A)** Influence of photocrosslinking time on the elastic modulus of hydrogels. **(B)** Hydrogel networks prepared from 13

mM Ca²⁺- or 15 mM Ba²⁺-crosslinked bioinks with equivalent elastic modulus obtained by changing the photocrosslinking time (13 mM Ca²⁺: 30 s; 15 mM Ba²⁺: 20s).

5.3.4. Bioprinted cell-responsive 3D microenvironments support cell spreading and ECM deposition

A distinctive characteristic of the developed bioink compared to existing bioinks is the ability to precisely control the biochemical composition and mechanical properties of printed 3D constructs with the ultimate goal of creating cell-specific microenvironments that support and direct cell behaviour. In this work, individual peptide sequences to promote cell-adhesion or cell-driven network remodelling were included in the bioink formulation enabling the printing of biochemical defined hydrogel microenvironments that stimulate cell-cell and cell-ECM interactions, mimicking these features of native ECM. To validate these features, the single-component NorPEC bioink was printed into cell-laden 3D constructs (8 × 8 mm², 4 layers) and their biological performance evaluated throughout 14 days of culture. Human neonatal dermal fibroblasts were selected due to its key role on cutaneous wound healing. Cells were carefully added to either Ca²⁺- or Ba²⁺-crosslinked bioink solutions containing both protease-degradable peptide (5 mM) and cell-adhesion peptide (2 mM), printed into 3D constructs with 1 mm thickness, and subjected to photocrosslinking. Two different UV irradiation times (30 s and 90 s) were selected to demonstrate the ability to tune the mechanical properties of printed hydrogels and evaluate its effect on cell response.

Immunofluorescence analysis of printed 3D constructs at day 3 of culture clearly showed the influence of mechanical properties on cell behaviour (**Figure 5.4**). Cells embedded within soft hydrogel networks photocrosslinked for 30 s displayed elongated morphology and formed interconnected multicellular networks regardless the cation source used in ionic crosslinking. Notably, deposition of fibronectin was observed in UV photopolymerized Ca²⁺-crosslinked 3D constructs (Ca²⁺/UV) as soon as day 3, while residual amounts of fibronectin were identified in UV photopolymerized Ba²⁺-crosslinked 3D constructs (Ba²⁺/UV). On the other hand, stiffer hydrogel constructs photocrosslinked for 90 s almost inhibited cell spreading with a low number of detectable cells start spreading with few protrusions. Fibronectin was present in residual amounts and limited to the vicinity of the cells. Together, these data indicated that, at early time points, the microenvironment provided by the printed constructs determines cell function either by stimulating or restricting cell spreading and fibronectin deposition via hydrogel stiffness. Although the hydrogel provides both cell-adhesion moieties and protease-degradable sites to enable cell adhesion and localized cell-mediated matrix remodelling, the density of crosslinks and the mechanical

constrains imposed by the stiffer constructs severely restricted cell spreading and ECM deposition.

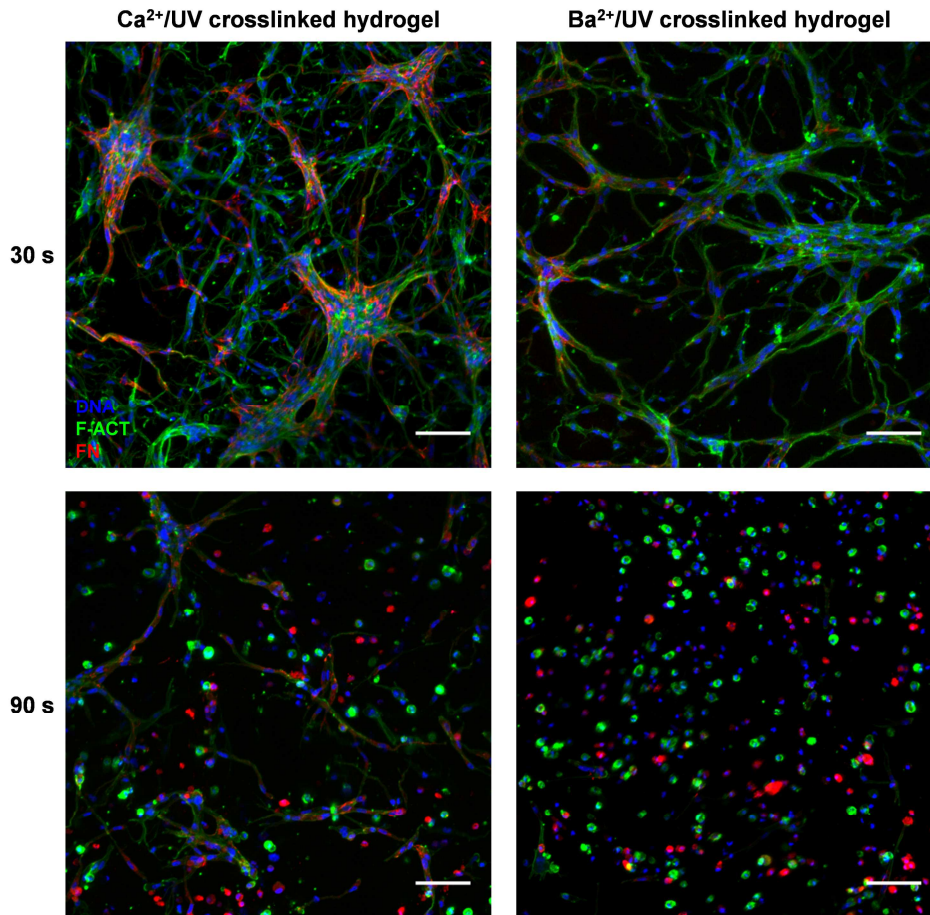


Figure 5.4. Immunofluorescence images showing the influence of hydrogel stiffness on dermal fibroblast behaviour within printed 3D constructs at day 3 of culture. After printing, 3D constructs prepared from either 13 mM Ca²⁺- or 15 mM Ba²⁺-crosslinked bioinks were photocrosslinked for 30 s or 90 s to produce soft or stiff constructs, respectively. Dermal fibroblasts were stained for DAPI (blue), F-actin (green), and fibronectin (FN, red) (scale bar: 100µm).

To demonstrate that printed 3D constructs are capable of supporting the functions of embedded cells for long time periods, the metabolic activity and DNA content were evaluated after 14 days of culture. Results showed that printed cells were metabolically active within all constructs without statistically significant differences between cells embedded within Ca²⁺- and Ba²⁺-crosslinked soft hydrogels (30 s UV) (**Figure 5.5A**). However, in Ba²⁺-crosslinked stiff hydrogels (90 s UV) cell metabolic activity was significantly lower compared to the other tested groups, suggesting that a more restrictive microenvironment is provided to the cells limiting their functions, which is corroborated by the lowest DNA content (**Figure 5.5B**).

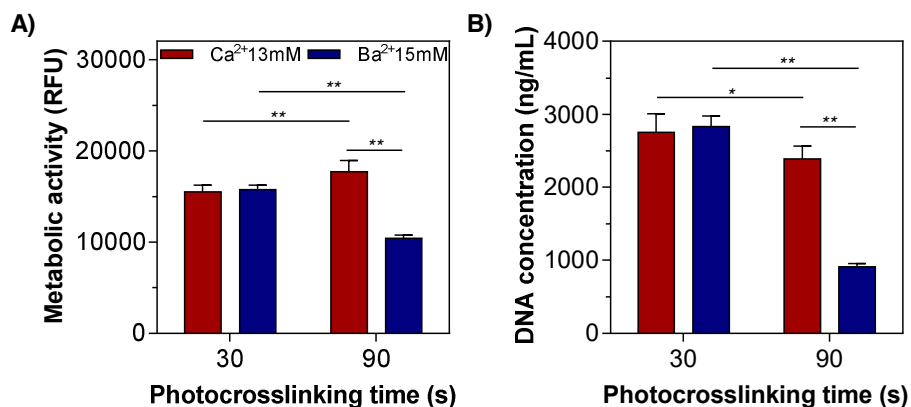


Figure 5.5. Biological characterization of cells within printed 3D hydrogel constructs. (A) Metabolic activity and **(B)** DNA content of dermal fibroblasts within soft (30 s UV photocrosslinking) and stiff (90 s UV photocrosslinking) printed 3D constructs at day 14 of culture.

An essential function of artificial ECM-like matrices is the ability to establish reciprocal and dynamic cell-cell and cell-ECM interactions to guide cell functions similarly to what occurs *in vivo* [29]. Bioprinted 3D constructs for cutaneous wound healing must not only support viable cells, but also stimulate the cell-mediated production of new ECM components to replace the lost tissue. During this process, the artificial microenvironment provided by the printed 3D construct should be gradually degraded via hydrolysis and/or enzymatic degradation, providing free space for new tissue growth and integration within the host. To demonstrate that the developed bioinks are capable of direct cell functions, we firstly evaluated whether printed cells display spread morphology throughout the construct thickness rather than limited to the proximity of the hydrogel surface. To this end, each construct was cut and the cross section corresponding to its thickness (**view A, Figure 5.6**) was imaged through confocal microscopy with cells stained for DNA and F-actin. Cells within printed soft constructs (both Ca²⁺- and Ba²⁺-crosslinked) and Ca²⁺-crosslinked stiff constructs assumed a characteristic spindle-shaped morphology, established extensive cell-cell interactions, and formed interconnected multicellular networks along the gel thickness. Contrary, Ba²⁺-crosslinked stiff constructs were sparsely populated with cells and exhibited limited spreading, which indicates that these hydrogels restrict cell spreading in 3D.

To evaluate the ability of the developed bioink to stimulate the production of new ECM by embedded dermal fibroblasts, *de novo* deposition of fibronectin, a prominent protein of the dermal tissue, was analysed by immunofluorescence staining from the surface of the construct towards its centre (**view B, Figure 5.6**). At day 14, printed cells extensively spread throughout the hydrogel, forming interconnected multicellular networks embedded by a fibronectin-rich network, except in the Ba²⁺-crosslinked stiff construct. In addition to the cell

spreading observed at day 3, soft hydrogels constructs also provided a suitable microenvironment that stimulated printed cells to secrete a continuous network of fibronectin. In Ca^{2+} -crosslinked stiff constructs, it was found that cells displayed an elongated morphology along with the deposition of fibronectin. As the majority of cells were round at day 3, this data indicated the ability of cells to locally degrade the hydrogel network to enable cell spreading and ECM deposition. Although in Ba^{2+} -crosslinked stiff constructs the majority of embedded cells also present spread morphology compared to day 3, a significant reduction of cell number can be observed with almost nonexistent fibronectin. Consistently with data from cell metabolic activity and DNA content, Ba^{2+} -crosslinked stiff constructs imposed severe restrictions to cell functions by limiting their spreading and ECM deposition, probably due to the higher stiffness. Together, these results demonstrate how the biochemical and biophysical properties of printed 3D constructs can be separately modulated to influence the behaviour of dermal fibroblasts.

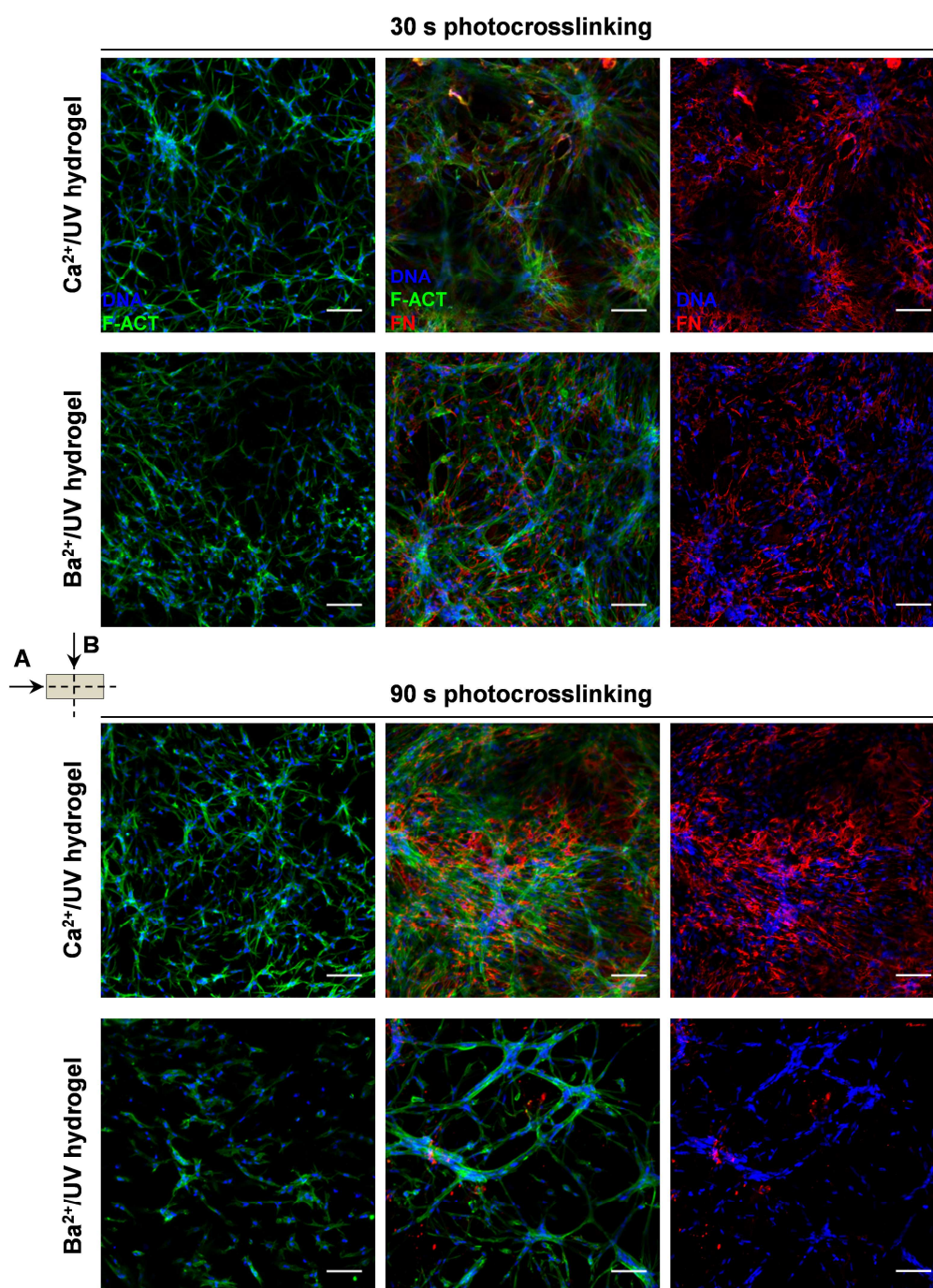


Figure 5.6. Representative confocal microscopy images of the morphology of dermal fibroblasts and fibronectin deposition within printed dual-crosslinked pectin hydrogel constructs. Hydrogels were obtained by thiol-norbornene photopolymerization of either 13 mM Ca^{2+} - or 15 mM Ba^{2+} -crosslinked bioink solutions containing 2.5 wt% norbornene-modified pectin, 2 mM cell-adhesion peptide, 5 mM protease-degradable peptide crosslinker, and 0.25 wt% VA-086 (scale bar: 100 μm). Left images: cross section of the construct to depict the morphology of cells stained for DAPI (blue) and F-actin (green) throughout its thickness (view A). Middle images: immunofluorescence staining from the surface of the construct towards its centre (view B) with cells stained for DAPI (blue), F-actin (green), and fibronectin (FN, red). Right images: immunofluorescence staining from the surface of the construct towards its centre (view B) with cells stained for DAPI (blue) and fibronectin (FN, red).

5.4. Conclusions

In this study, a cell-instructive bioink was designed for the extrusion bioprinting of protease-degradable hydrogel constructs from a norbornene-modified pectin precursor photocrosslinked via thiol-norbornene click reaction. The developed bioink, consisting of modified pectin macromers, cell-degradable peptide crosslinkers, and integrin-specific adhesive ligands, allowed the printing of complex and elastic 3D constructs that hold the shape after deposition for subsequent fast photocrosslinking upon exposure to UV light. The bioink rheological properties were precisely adjusted via ionic gelation using either Ca^{2+} or Ba^{2+} , while the construct stiffness was controlled by varying the photocrosslinking time. Bioprinted 3D constructs supported metabolically active cells throughout 14 days of culture and extensive spreading of embedded dermal fibroblasts in a stiffness-dependent manner. The modular nature of the bioink allowed precise adjustment of the rheological properties, and facile functionalization with a multitude of peptide crosslinkers and pendant ligands through an ultrafast thiol-norbornene photoclick chemistry. Furthermore, the biochemical, biophysical, and rheological properties of the modular norbornene-functionalized pectin bioink can be easily controlled by changing the type of crosslinker, peptide ligands or ionic- and photo-crosslinking conditions, providing a versatile bioink for the bioprinting of tissue constructs mimicking key features of the native ECM.

5.5. Acknowledgements

This work was supported by the European Regional Development Fund (ERDF) through the COMPETE 2020 - Operational Programme for Competitiveness and Internationalization (POCI), Norte Portugal Regional Operational Programme (NORTE 2020), under the PORTUGAL 2020 Partnership Agreement, and by Portuguese funds through Portuguese Foundation for Science and Technology (FCT) in the framework of the project Ref. PTDC/BBB-ECT/2145/2014. R.F.P. and B.N.L. thank FCT for the doctoral grants SFRH/BD/91151/2012 and SFRH/BD/87400/2012, respectively.

5.6. References

[1] L. Moroni, T. Boland, J.A. Burdick, C. De Maria, B. Derby, G. Forgacs, J. Groll, Q. Li, J. Malda, V.A. Mironov, C. Mota, M. Nakamura, W. Shu, S. Takeuchi, T.B.F. Woodfield, T. Xu, J.J. Yoo, G. Vozzi, *Biofabrication: A Guide to Technology and Terminology*, Trends Biotechnol. 36 (2018) 384-402.

- [2] I.T. Ozbolat, M. Hospodiuk, Current advances and future perspectives in extrusion-based bioprinting, *Biomaterials* 76 (2016) 321-43.
- [3] D. Williams, P. Thayer, H. Martinez, E. Gatenholm, A. Khademhosseini, A perspective on the physical, mechanical and biological specifications of bioinks and the development of functional tissues in 3D bioprinting, *Bioprinting* 9 (2018) 19-36.
- [4] Y.S. Zhang, A. Khademhosseini, Advances in engineering hydrogels, *Science* 356 (2017).
- [5] D.D. McKinnon, D.W. Domaille, J.N. Cha, K.S. Anseth, Biophysically Defined and Cytocompatible Covalently Adaptable Networks as Viscoelastic 3D Cell Culture Systems, *Adv. Mater.* 26 (2014) 865-872.
- [6] M. Hospodiuk, M. Dey, D. Sosnoski, I.T. Ozbolat, The bioink: A comprehensive review on bioprintable materials, *Biotechnol. Adv.* 35 (2017) 217-239.
- [7] O. Liliang, Y. Rui, Z. Yu, S. Wei, Effect of bioink properties on printability and cell viability for 3D bioplotting of embryonic stem cells, *Biofabrication* 8 (2016) 035020.
- [8] W. Jia, P.S. Gungor-Ozkerim, Y.S. Zhang, K. Yue, K. Zhu, W. Liu, Q. Pi, B. Byambaa, M.R. Dokmeci, S.R. Shin, A. Khademhosseini, Direct 3D bioprinting of perfusable vascular constructs using a blend bioink, *Biomaterials* 106 (2016) 58-68.
- [9] W. Liu, M.A. Heinrich, Y. Zhou, A. Akpek, N. Hu, X. Liu, X. Guan, Z. Zhong, X. Jin, A. Khademhosseini, Y.S. Zhang, Extrusion Bioprinting of Shear-Thinning Gelatin Methacryloyl Bioinks, *Adv Healthc Mater* 6 (2017) 1601451.
- [10] L.L. Wang, C.B. Highley, Y.C. Yeh, J.H. Galarraga, S. Uman, J.A. Burdick, Three-dimensional extrusion bioprinting of single- and double-network hydrogels containing dynamic covalent crosslinks, *J Biomed Mater Res A* (2018) 865-875.
- [11] R.F. Pereira, P.J. Bártolo, 3D bioprinting of photocrosslinkable hydrogel constructs, *J. Appl. Polym. Sci.* 132 (2015) 42458.
- [12] M.W. Tibbitt, A.M. Kloxin, L. Sawicki, K.S. Anseth, Mechanical Properties and Degradation of Chain and Step Polymerized Photodegradable Hydrogels, *Macromolecules* 46 (2013) 2785-2792.
- [13] L. Ouyang, C.B. Highley, W. Sun, J.A. Burdick, A Generalizable Strategy for the 3D Bioprinting of Hydrogels from Nonviscous Photo-crosslinkable Inks, *Adv. Mater.* 29 (2017) 1604983.
- [14] S. Bertlein, G. Brown, K.S. Lim, T. Jungst, T. Boeck, T. Blunk, J. Tessmar, G.J. Hooper, T.B.F. Woodfield, J. Groll, Thiol-Ene Clickable Gelatin: A Platform Bioink for Multiple 3D Biofabrication Technologies, *Adv. Mater.* (2017) 1703404.
- [15] M.A. Tasdelen, Y. Yagci, Light-Induced Click Reactions, *Angew. Chem. Int. Ed.* 52 (2013) 5930-5938.
- [16] Z. Muñoz, H. Shih, C.-C. Lin, Gelatin hydrogels formed by orthogonal thiol–norbornene photochemistry for cell encapsulation, *Biomater. Sci.* 2 (2014) 1063-1072.

- [17] K.M. Mabry, R.L. Lawrence, K.S. Anseth, Dynamic stiffening of poly(ethylene glycol)-based hydrogels to direct valvular interstitial cell phenotype in a three-dimensional environment, *Biomaterials* 49 (2015) 47-56.
- [18] R.F. Pereira, C.C. Barrias, P.J. Bartolo, P.L. Granja, Cell-instructive pectin hydrogels crosslinked via thiol-norbornene photo-click chemistry for skin tissue engineering, *Acta Biomater* 66 (2018) 282-293.
- [19] E.B. Luiz, C.C. Juliana, M. Vijayan, L.C. Ana, S.B. Nupura, A.A. Wesleyan, Z. Pinar, E.V. Nihal, M.G. Amir, R.D. Mehmet, K. Ali, Direct-write bioprinting of cell-laden methacrylated gelatin hydrogels, *Biofabrication* 6 (2014) 024105.
- [20] J.W. Nichol, S.T. Koshy, H. Bae, C.M. Hwang, S. Yamanlar, A. Khademhosseini, Cell-laden microengineered gelatin methacrylate hydrogels, *Biomaterials* 31 (2010) 5536-44.
- [21] F. Munarin, M.C. Tanzi, P. Petrini, Advances in biomedical applications of pectin gels, *Int. J. Biol. Macromol.* 51 (2012) 681-9.
- [22] T. Atabak Ghanizadeh, A.H. Miguel, R.L. Nicholas, S. Wenmiao, Three-dimensional bioprinting of complex cell laden alginate hydrogel structures, *Biofabrication* 7 (2015) 045012.
- [23] C. Colosi, S.R. Shin, V. Manoharan, S. Massa, M. Costantini, A. Barbetta, M.R. Dokmeci, M. Dentini, A. Khademhosseini, Microfluidic Bioprinting of Heterogeneous 3D Tissue Constructs Using Low-Viscosity Bioink, *Adv. Mater.* 28 (2016) 677-84.
- [24] Ý.A. Mørch, I. Donati, B.L. Strand, Effect of Ca²⁺, Ba²⁺, and Sr²⁺ on Alginate Microbeads, *Biomacromolecules* 7 (2006) 1471-1480.
- [25] H.M.M. Vivian, P.W.M. Ferry, V. Jetze, J.A.D. Wouter, G. Debby, M. Jos, Yield stress determines bioprintability of hydrogels based on gelatin-methacryloyl and gellan gum for cartilage bioprinting, *Biofabrication* 8 (2016) 035003.
- [26] P. Naomi, S. Willi, B. Thomas, M. Ferry, G. Jürgen, J. Tomasz, Proposal to assess printability of bioinks for extrusion-based bioprinting and evaluation of rheological properties governing bioprintability, *Biofabrication* 9 (2017) 044107.
- [27] S. Stichler, T. Jungst, M. Schamel, I. Zilkowski, M. Kuhlmann, T. Böck, T. Blunk, J. Teßmar, J. Groll, Thiol-ene Clickable Poly(glycidol) Hydrogels for Biofabrication, *Ann Biomed Eng* 45 (2017) 273-285.
- [28] I. Mironi-Harpaz, D.Y. Wang, S. Venkatraman, D. Seliktar, Photopolymerization of cell-encapsulating hydrogels: Crosslinking efficiency versus cytotoxicity, *Acta Biomater* 8 (2012) 1838-1848.
- [29] G. Huang, F. Li, X. Zhao, Y. Ma, Y. Li, M. Lin, G. Jin, T.J. Lu, G.M. Genin, F. Xu, Functional and Biomimetic Materials for Engineering of the Three-Dimensional Cell Microenvironment, *Chem. Rev.* 117 (2017) 12764-12850.

CHAPTER VI

GENERAL DISCUSSION AND FUTURE PERSPECTIVES

6.1. General discussion

The clinical requirement for cost-effective skin substitutes that promote the repair of acute and chronic wounds continues growing mostly due to the low level of compositional and architectural biomimicry of available products, which results in limited functional and aesthetic outcomes. In an attempt to closely resemble the composition and, in part, the architecture of the native skin ECM, most of the commercial wound care products both acellular and cellular (i.e., modern dressings and bioengineered skin substitutes) are based on ECM-derived materials such as collagen. Acellular products are easy to use and less expensive, but do not deliver either autologous or allogeneic skin cells to the injured site, which has been demonstrated to be beneficial for the wound healing by providing cell-secreted factors to the host cells [1]. On the other hand, cellularized products are expensive and characterized by key limitations like the poor engraftment, adhesion to the wound bed, limited cell-recruitment, and poor vascularization [2, 3]. As cellularized products are manufactured using traditional fabrication methods (e.g., manual cell seeding), which fail in controlling the position of skin cells throughout the construct, the level of architectural and composition skin biomimicry is still low. In addition, the inability to precisely control the position of cells in a 3D microenvironment and consequently cell-cell and cell-ECM interactions precludes the integration of skin pigmentation, vasculature and skin appendages (e.g., sweat glands) in bioengineered products.

In this research work, the ability of extrusion bioprinting to automatically control the deposition of bioinks composed of materials, cells and/or biochemicals in predesigned 3D locations in a layer-by-layer procedure was explored to create 3D constructs resembling the anatomy of the native skin. Although extrusion bioprinting holds the promise to solve the limitations of manual fabrication methods, it faces major challenges on the design of suitable bioinks that can be printed into complex structures with high shape fidelity and simultaneous provide control over the biochemical and biophysical composition of printed microenvironments. As discussed in the **Chapter II**, bioinks for skin bioprinting are based on a limited number of materials including alginate, collagen, fibrin, gelatin, and hyaluronic acid. Importantly, the majority of these bioinks have been processed through inkjet bioprinting [1, 4], which precludes the fabrication of 3D constructs resembling the complex architecture of the skin due to the need for printing low-viscous bioink formulations to preclude nozzle clogging [5]. Bioinks were also processed using other bioprinting modalities, including LAB [6, 7] and extrusion bioprinting [8, 9]. Extrusion bioprinting is regarded as the most affordable due to its low cost and ability to print highly viscous bioinks containing high cellular densities

[10], which is fundamental to generate complex 3D structures that mimic the cell-cell and cell-ECM interactions in the skin tissue. However, bioinks for extrusion bioprinting of skin substitutes are limited to collagen, gelatin, and alginate-based materials, which restrict the range of processable materials. Recently, decellularized skin tissue was also explored for extrusion bioprinting of skin, improving the range of printable materials [9]. Despite these advances, available bioinks still offer limited control over the biochemical and biophysical properties as they are usually based on protein-derived materials (e.g., collagen, gelatin) that inherently contain biochemical cues in the native composition. Over the last years, several works have demonstrated the importance of chemically defined microenvironments in controlling the cell fate and guide new tissue formation [11-14], highlighting the need to translate these concepts to develop a new generation of advanced bioinks with cell-instructive properties.

To explore alternative materials and expand the range of printable bioinks, in **Chapter III**, a simple and efficient strategy was described to design dual-crosslinked pectin hydrogels that could be explored for both fundamental cell studies and extrusion bioprinting of skin constructs. Pectin, a polysaccharide used in wounds dressings and hydrogels for cell entrapment, was selected mostly due to its biocompatibility, ionic gelation ability, and the presence of multiple functional groups amenable to chemical modification. Photocrosslinkable pectin macromers were synthesized by the introduction of methacrylate functional groups via reaction with MA under aqueous conditions. The degree of methacrylate substitution was optimized considering the water solubility of the synthesized macromers and the hydrogel formation. Three methacrylate-modified pectin macromers (PECMA) were produced to provide a low, medium, and high number of methacrylate groups for photopolymerization. All macromers allowed the formation of chemically crosslinked hydrogels at low polymer concentration (1–2.5 wt%) through UV photopolymerization in presence of I2959 as a photoinitiator. Several formulations containing variable PECMA concentration and methacrylate substitution were photocrosslinked for different UV curing times (80 s to 300 s) and tested for their gel fraction, mechanical properties, and swelling behaviour. All the properties were dependent on the crosslinking degree of the hydrogel network and could be easily controlled by changing the photopolymerization conditions, PECMA concentration or degree of methacrylate substitution. The biofunctionalization of methacrylated pectin with a thiolated cell-adhesive peptide via a base-catalysed thiol-Michael reaction demonstrated to be an efficient strategy to promote the attachment of dermal fibroblasts to the otherwise biologically inert hydrogel network. This conjugation strategy provided a facile approach to control the biochemical cues in the PECMA backbone. Taking advantage of the ionic gelation ability of PECMA, a dual-crosslinking strategy was designed

to develop a single-component methacrylated pectin bioink for bioprinting. Ionic gelation was explored to adjust the rheological properties of a low concentration (1.5 wt%) pectin solution via ionic interaction with calcium ions, yielding an extrudable, physically crosslinked bioink. Different calcium chloride concentrations (0–5 mM) were optimized to allow the formation of stable filaments that could be printed into 3D constructs and to study their effect on the bioink rheological properties. The bioink printability was dependent on the calcium content and consequently degree of physical crosslinking. An optimized bioink formulation functionalized with a cell-adhesive peptide and loaded with dermal fibroblasts was applied for the bioprinting of 3D dermal constructs. Printed constructs supported viable cells during the culture period and promoted extensive cell spreading throughout the constructs. More importantly, dermal fibroblasts within printed constructs secreted several ECM components of the dermal tissue including fibronectin, type-I collagen, and laminin. These data showed that the developed bioink and printing strategy enable the bioprinting of cellularized 3D constructs that stimulate *de novo* deposition of key ECM components of dermis, proposing PECMA as an alternative bioink for skin bioprinting.

In view of a clinical application and *in vivo* implantation of bioprinted pectin 3D constructs, the degradation of dual-crosslinked hydrogels must be taken in consideration. Pectin is inherently non-degradable in mammals due to the lack of the enzyme (i.e., pectinase) that can cleave the polymer chains, but ionically crosslinked pectin gels can dissolve and disintegrate upon implantation by the release of the divalent ions that participate in the hydrogel crosslinking [15]. Although *in vivo* biodegradation studies were not performed using the PECMA bioink described in **Chapter III**, the formation of chemical bonds during photopolymerization resulted in gel networks with higher resistance to *in vitro* degradation by pectinase. Covalent crosslinks were introduced to preclude the dissolution of the physically crosslinked hydrogel bioink postprinting, providing long term stability and superior mechanical properties. As a result of both non-degradable nature of chemical bonds resulting from the homopolymerization of methacrylates and the absence of cell-degradable sites in the hydrogel network, potential limitations of the PECMA bioink consisted on its *in vivo* biodegradation and inability of embedded cells to locally degrade the surrounding microenvironment to create space for spreading and migration. To address these limitations, in **Chapter IV**, a new class of norbornene-modified pectin (NorPEC) was synthesized to allow the formation of protease-degradable hydrogels through UV photoinitiated thiol-norbornene chemistry using a cell-degradable peptide sequence as crosslinker. A fast and robust chemical modification strategy was developed for the modification of pectin with norbornene end groups via reaction with CA in organic solvents, improving the reaction efficiency and reducing the reaction time compared to published protocols [16, 17]. Enzymatically

degradable hydrogels were prepared by a fast UV photoinitiated thiol-ene reaction between a peptide crosslinker sensitive to cell-secreted proteases flanked with biscysteine and the norbornene groups in pectin using VA-086 as a photoinitiator. During the photopolymerization, the biscysteine protease-degradable peptide becomes part of the crosslinked hydrogel, allowing for gel network degradation as demonstrated by the enzymatic digestion using the enzyme collagenase, which is present in wound healing process [18]. Contrary to the free-radical polymerization of PECMA hydrogels, which proceeds via a chain-growth mechanism, the thiol-norbornene polymerization develops through a step-growth mechanism resulting in less network heterogeneities. Importantly, in thiol-norbornene polymerization there is no homopolymerization or chain growth between strained norbornene groups and the reaction is non-oxygen inhibited which increases the reaction kinetics and reduces the UV photocrosslinking time [19]. We took advantage of these characteristics to develop photoclickable pectin hydrogels that mimic key functions of the native ECM, including the cell-adhesion and cell-driven matrix remodelling. The behaviour of dermal fibroblasts embedded within thiol-ene NorPEC hydrogels was controlled by altering the density of cell-adhesive peptide ligand and/or the hydrogel crosslinking degree via adjusting the concentration of protease-degradable peptide. Through the pharmacological inhibition of the action of cell-secreted proteases, it was demonstrated that both matrix stiffness and protease-degradable peptide determine cell spreading and hydrogel remodelling. The ability of the developed NorPEC hydrogels to support the formation of full-thickness skin was also demonstrated *in vitro*. Skin models showed morphological resemblance to the human skin with a well-defined epidermis formed on the top of the fibroblast-laden hydrogel. Specific markers associated to epidermal differentiation and proliferation, including cytokeratin and Ki67 were detected in the epidermal compartment, while characteristic ECM markers for type-I collagen and fibronectin were observed in the dermal compartment. These results demonstrated that by selecting suitable protease-degradable peptide crosslinkers and pendant cell-adhesive peptides, biomimetic NorPEC hydrogels can be designed to induce distinct biological responses and support the *in vitro* formation of skin equivalents.

One critical limitation of current bioinks relies on the difficulty to precisely define and control the biochemical composition and biophysical properties without compromising the printability and cell response. In parallel, another important drawback in the design of advanced bioinks consists on the need for modular strategies that enable the customization of the bioink composition for a desired application. In **Chapter V**, a modular bioink was designed for the extrusion bioprinting of 3D ECM-like microenvironments using NorPEC, living cells, peptide crosslinkers and peptide ligands as basic building blocks. A major advantage of this bioink compared to existing ones resides on its versatility as a general

platform where a range of user-defined thiolated crosslinkers and thiolated ligands can be chemically bond to the NorPEC backbone and loaded in desired cells to engineer cell- and tissue-specific 3D constructs with controllable biochemical and mechanical properties. Based on the ionic gelation mechanism described in **Chapter III**, one additional cation (Ba^{2+}) was selected to modulate the rheological properties of the NorPEC bioink which composition was optimized to allow *in vitro* skin formation in **Chapter IV**. An extensive rheological study was carried out to compare the effects of Ca^{2+} and Ba^{2+} on the printability of physically crosslinked bioinks. Suitable printability was achieved for Ca^{2+} concentrations in a range of 13–15 mM and Ba^{2+} concentrations in a range of 15–17.5 mM. Printable formulations (13 mM Ca^{2+} and 15 mM Ba^{2+}), selected based on the yield stress data, allowed the formation of smooth and continuous filaments that enable the printing of elastic 3D structures. Both bioink formulations exhibited proper rheological properties for extrusion bioprinting namely shear thinning behaviour and fast recovery after exposure to high shear stress. The mechanical properties of hydrogels were precisely controlled by changing the photopolymerization time, while keeping fixed the bioink composition, demonstrating the ability to independently modulate the hydrogel stiffness without altering the biochemical properties. Dermal fibroblasts printed using either Ca^{2+} - or Ba^{2+} -crosslinked bioinks photocrosslinked into soft or stiff hydrogel networks showed distinct cell spreading and fibronectin as a function of the matrix stiffness. Together, these results demonstrated that the developed modular strategy for the design of advanced bioinks based on NorPEC provides a cutting-edge natural-derived bioink which biochemical and biophysical properties can be independently controlled and decoupled from the NorPEC concentration to induce distinct cell responses.

Overall, this thesis ended up with novel cell-responsive pectin-based bioinks designed to meet the printability criteria for extrusion bioprinting and to provide ECM-like microenvironments that instruct and guide the cell behaviour. The designed single-component bioinks, crosslinking chemistries and bioprinting strategies were successfully applied to generate 3D skin constructs that hold promising properties for several skin tissue engineering applications including bioengineered skin substitutes for cutaneous repair and *in vitro* testing models.

6.2. Future perspectives

Although the work developed in this thesis addressed important limitations in skin bioprinting, the proposed bioinks, crosslinking chemistries and their application also have some limitations that have to be surpassed in the future.

The most obvious limitation is the need for *in vivo* studies devoted to evaluate the biodegradation behaviour of developed bioinks both subcutaneously and applied as a topical skin substitute. In this thesis, pectin was proposed as a promising biomaterial to design cell-responsive bioinks for 3D bioprinting by exploring ionic gelation and photopolymerization crosslinking reactions. As previously discussed, pectin is inherently non-degradable in mammals, but ionically crosslinked pectin hydrogels disintegrate upon subcutaneous *in vivo* implantation. However, the formation of chemical bonds in the hydrogel network resulted in stable dual-crosslinked hydrogels with increased resistance to enzymatic degradation *in vitro*. The *in vivo* evaluation of the degradation profile of bioprinted dual-crosslinked 3D hydrogels constructs constitutes an important topic of research for future work. This study will provide valuable information regarding the contribution of chemical bonds on the *in vivo* hydrogel degradation. These data could be used to correlate the mechanical properties of printed constructs, ECM deposition, and *in vivo* degradation profiles in order to design constructs with proper degradation rates. Although NorPEC enabled the formation of cell-degradable hydrogels through UV photoinitiated thiol-ene reaction with biscysteine protease-degradable peptide crosslinkers, the *in vivo* degradation kinetics of such hydrogels remains unknown. As these hydrogels as susceptible to remodelling through embedded cells, the characterization of biodegradation profiles using cell-laden hydrogels should also be considered in futures studies.

Other limitation refers to use of UV photopolymerization reactions to induce the chemical crosslinking of developed bioinks. Although hydrogels were formed under cytocompatible conditions and the photopolymerization parameters were optimized to preclude UV light-mediated cell damage, one alternative is to explore visible light photopolymerization schemes for hydrogel crosslinking. Preliminary work using NorPEC hydrogels photocrosslinked in the presence of Eosin Y as a sole photoinitiator and visible light showed promising results regarding the structural integrity of prepared hydrogel networks.

Another limitation consists in studies focusing on the ability of printed 3D constructs to stimulate *in vivo* skin formation. Although *in vitro* skin formation was demonstrated in this work, animal experimentation is required to test whether the constructs either cellular or acellular can be used for the repair of cutaneous wounds. In addition, the adhesion properties of hydrogel constructs to the wound bed must be also considered in a future work.

An alternative proposed application of bioprinted 3D skin constructs is *in vitro* testing models. In this context, the cellular composition of printed constructs must be further complexed by the inclusion of additional cells present in the skin. Endothelial and immune

cells could be explored to better mimic the dermis, while pigmentation should be considered in the epidermal layer by the printing of melanocytes. Novel strategies to integrate skin appendages such as sweat glands and hair follicles in printed skin models also constitute an important topic of future research.

Finally, the developed bioinks display ideal properties for *in situ* bioprinting, by providing a modular platform with controlled properties, suitable printability and fast gelation. The concept of *in situ* skin bioprinting was proposed few years ago by researchers from the Wake Forest Institute (US) using an inkjet bioprinting device specifically developed to dispense cell-laden solutions onto the wound bed [20]. As previously discussed, inkjet bioprinting has limitations on the fabrication of 3D constructs with complex architecture similar to the skin due to the processing of low viscosity bioinks. As the bioinks developed in this thesis present many of the ideal properties of advanced bioinks such as (1) allow the printing of complex 3D constructs with high shape fidelity, (2) undergo fast crosslinking postprinting, (3) permit cell-adhesion and cell-mediated remodelling, (4) exhibit tuneable mechanical properties, (5) provide control over the biochemical composition, and (6) support the deposition of ECM components by embedded cells, they can also be explored for *in situ* skin bioprinting. Furthermore, the developed bioinks can be processed through extrusion bioprinting, allowing the generation of 3D constructs with high levels of skin biomimicry at clinically relevant dimensions.

6.3. References

- [1] A. Skardal, S.V. Murphy, K. Crowell, D. Mack, A. Atala, S. Soker, A tunable hydrogel system for long-term release of cell-secreted cytokines and bioprinted *in situ* wound cell delivery, *J Biomed Mater Res B Appl Biomater* 105 (2017) 1986-2000.
- [2] S.T. Boyce, A.L. Lalley, Tissue engineering of skin and regenerative medicine for wound care, *Burns & Trauma* 6 (2018) 4.
- [3] A.G. Haddad, G. Giatsidis, D.P. Orgill, E.G. Halvorson, Skin Substitutes and Bioscaffolds: Temporary and Permanent Coverage, *Clin Plast Surg* 44 (2017) 627-634.
- [4] A. Skardal, D. Mack, E. Kapetanovic, A. Atala, J.D. Jackson, J. Yoo, S. Soker, Bioprinted amniotic fluid-derived stem cells accelerate healing of large skin wounds, *Stem Cells Transl Med* 1 (2012) 792-802.
- [5] S.V. Murphy, A. Atala, 3D bioprinting of tissues and organs, *Nat. Biotechnol.* 32 (2014) 773-85.

- [6] S. Michael, H. Sorg, C.T. Peck, L. Koch, A. Deiwick, B. Chichkov, P.M. Vogt, K. Reimers, Tissue engineered skin substitutes created by laser-assisted bioprinting form skin-like structures in the dorsal skin fold chamber in mice, *PLoS One* 8 (2013) e57741.
- [7] L. Koch, A. Deiwick, S. Schlie, S. Michael, M. Gruene, V. Coger, D. Zychlinski, A. Schambach, K. Reimers, P.M. Vogt, B. Chichkov, Skin tissue generation by laser cell printing, *Biotechnol. Bioeng.* 109 (2012) 1855-63.
- [8] W. Lee, J.C. Debasitis, V.K. Lee, J.H. Lee, K. Fischer, K. Edminster, J.K. Park, S.S. Yoo, Multi-layered culture of human skin fibroblasts and keratinocytes through three-dimensional freeform fabrication, *Biomaterials* 30 (2009) 1587-95.
- [9] B.S. Kim, Y.W. Kwon, J.S. Kong, G.T. Park, G. Gao, W. Han, M.B. Kim, H. Lee, J.H. Kim, D.W. Cho, 3D cell printing of in vitro stabilized skin model and in vivo pre-vascularized skin patch using tissue-specific extracellular matrix bioink: A step towards advanced skin tissue engineering, *Biomaterials* 168 (2018) 38-53.
- [10] I.T. Ozbolat, M. Hospodiuk, Current advances and future perspectives in extrusion-based bioprinting, *Biomaterials* 76 (2016) 321-43.
- [11] M.P. Lutolf, J.A. Hubbell, Synthetic biomaterials as instructive extracellular microenvironments for morphogenesis in tissue engineering, *Nat. Biotechnol.* 23 (2005) 47-55.
- [12] M.P. Lutolf, J.L. Lauer-Fields, H.G. Schmoekel, A.T. Metters, F.E. Weber, G.B. Fields, J.A. Hubbell, Synthetic matrix metalloproteinase-sensitive hydrogels for the conduction of tissue regeneration: Engineering cell-invasion characteristics, *Proc Natl Acad Sci USA* 100 (2003) 5413-5418.
- [13] B.V. Sridhar, J.L. Brock, J.S. Silver, J.L. Leight, M.A. Randolph, K.S. Anseth, Development of a Cellularly Degradable PEG Hydrogel to Promote Articular Cartilage Extracellular Matrix Deposition, *Adv Healthc Mater* 4 (2015) 702-713.
- [14] E.Y. Tokuda, J.L. Leight, K.S. Anseth, Modulation of matrix elasticity with PEG hydrogels to study melanoma drug responsiveness, *Biomaterials* 35 (2014) 4310-4318.
- [15] S.C. Neves, D.B. Gomes, A. Sousa, S.J. Bidarra, P. Petrini, L. Moroni, C.C. Barrias, P.L. Granja, Biofunctionalized pectin hydrogels as 3D cellular microenvironments, *J Mater Chem B* 3 (2015) 2096-2108.
- [16] W.M. Gramlich, I.L. Kim, J.A. Burdick, Synthesis and orthogonal photopatterning of hyaluronic acid hydrogels with thiol-norbornene chemistry, *Biomaterials* 34 (2013) 9803-11.
- [17] Z. Muñoz, H. Shih, C.-C. Lin, Gelatin hydrogels formed by orthogonal thiol–norbornene photochemistry for cell encapsulation, *Biomater. Sci.* 2 (2014) 1063-1072.
- [18] M.S. Agren, C.J. Taplin, J.F. Woessner, Jr., W.H. Eaglstein, P.M. Mertz, Collagenase in wound healing: effect of wound age and type, *J Invest Dermatol* 99 (1992) 709-14.

[19] M.W. Tibbitt, A.M. Kloxin, L. Sawicki, K.S. Anseth, Mechanical Properties and Degradation of Chain and Step Polymerized Photodegradable Hydrogels, *Macromolecules* 46 (2013) 2785-2792.

[20] K.W. Binder, W. Zhao, T. Aboushwareb, D. Dice, A. Atala, J.J. Yoo, In situ bioprinting of the skin for burns, *Journal of the American College of Surgeons* 211 (2010) S76.